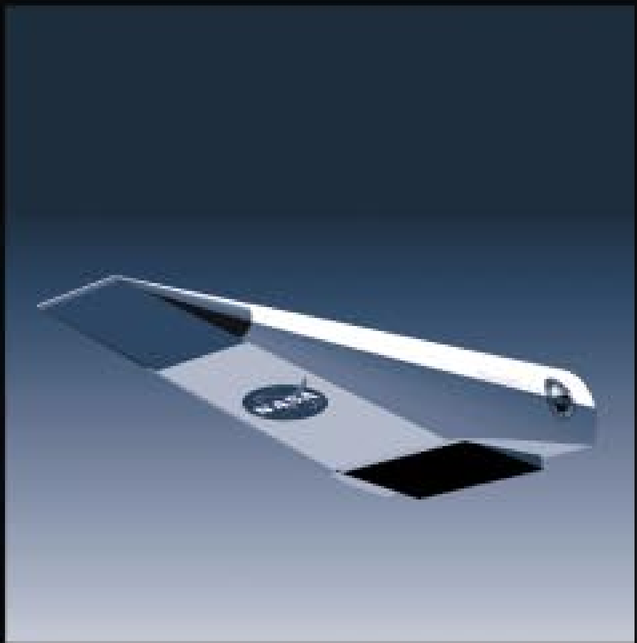

RESEARCH & TECHNOLOGY 1998

NASA AMES RESEARCH CENTER

Notice

The use of trade names and manufacturers in this document does not constitute an official endorsement of such products or manufacturers, either expressed or implied, by the National Aeronautics and Space Administration.

Available from:

NASA Center for AeroSpace Information
7121 Standard Drive
Hanover, MD 21076-1320
(301) 621-0390

National Technical Information Service
5285 Port Royal Road
Springfield, VA 22161
(703) 487-4650

Foreword

This report highlights the research accomplished during fiscal year 1998 by Ames Research Center scientists and engineers. The work is divided into accomplishments that support NASA's four Strategic Enterprises: Aero-Space Technology, Space Science, Office of Earth Science, and Human Exploration and Development of Space (HEDS). The key purpose of this report is to communicate information to our stakeholders, customers, and the people of the United States about the scope and diversity of Ames' mission and the nature of Ames' research and technology activities.

Ames Research Center is making significant contributions to the Aero-Space Technology Enterprise mission to pioneer the identification, development, and commercialization of high-payoff aeronautics and space transportation technologies. Ames has the Agency's lead role for basic research in Aviation Operations Systems, Information Systems Technology, and Rotorcraft. Ames is also the Lead Center for focused programs in Aviation System Capacity and High-Performance Computing and Communications. The Center's key core competencies include human factors, air traffic management, information systems, rotorcraft, vertical/short takeoff and landing technology, and thermal protection systems technology.

Ames is recognized as a world leader in Astrobiology, the study of life in the Universe and of the chemical and physical forces and adaptations that influence life's origin, evolution, and destiny. This endeavor pulls together Ames' core competencies in exobiology, planetary science, atmospheric chemistry, and astrophysics. Ames supports the Office of Earth Science by conducting research in such areas as biogeochemical cycling, ecosystem dynamics, and the chemical and transport processes that determine atmospheric composition, dynamics and climate. Support for the HEDS Enterprise includes conducting research, managing spaceflight projects, and developing technologies. The key areas of research include astronaut health, fundamental science, progress in improving space travel, and technology transfer.

Ames has also been designated the Agency's Center of Excellence for Information Technology. The three cornerstones of Information Technology research at Ames are automated reasoning, human-centered computing, and high performance computing and networking. The mission critical capabilities enabled by NASA's three cornerstones of Information Technology span all four of NASA's strategic enterprises. They include the Design and Fabrication in the Virtual Environment, Human Exploration of Space, Robotic Exploration of Space, Aircraft Operations, and Science Understanding. State-of-the-art capability in Information Technology is essential to realizing Dan Goldin's challenge to do it "faster, better, and cheaper."

For further information on Ames' research and technology projects, please contact the person designated as the point of contact at the end of each article. For further information about the report itself, contact Dr. Stephanie Langhoff, Chief Scientist, Mail Stop 230-3, NASA Ames Research Center, Moffett Field, CA 94035. An electronic version of this report is available on the Ames home page.

W. E. Berry

William E. Berry
Acting Director
Ames Research Center

Aero-Space Technology Enterprise

GLOBAL CIVIL AVIATION/AFFORDABILITY

Revolutionary Technology

Access to Space

Space Science Enterprise

EXOBIOLOGY

PLANETARY SCIENCE

Astrophysics

Space Technology

Human Exploration and Development of Space Enterprise

Progress in Improving Space Travel

Technology Transfer

Earth Science Enterprise

Atmospheric Chemistry and Dynamics

Atmospheric Physics

Aero-Space Technology Enterprise

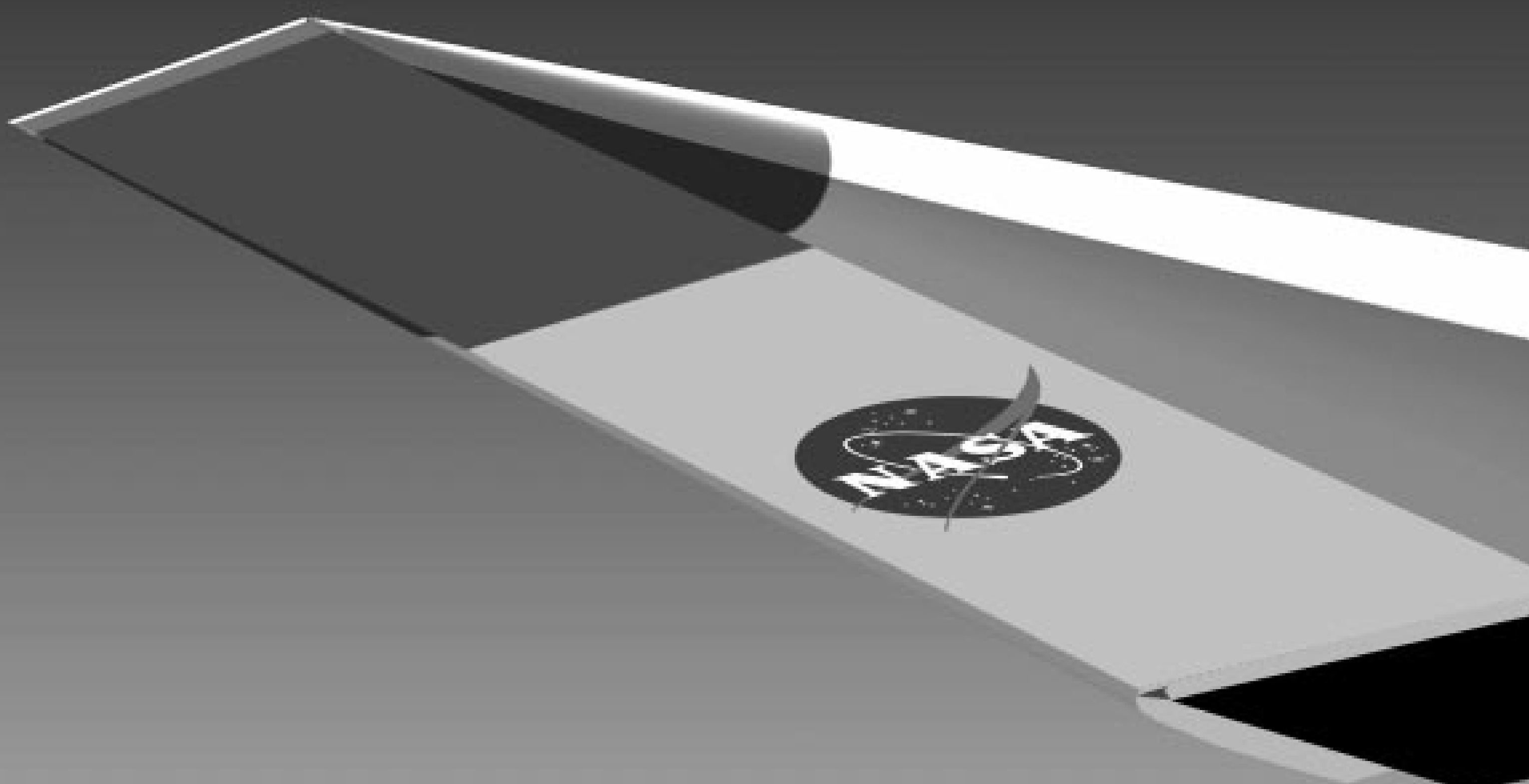

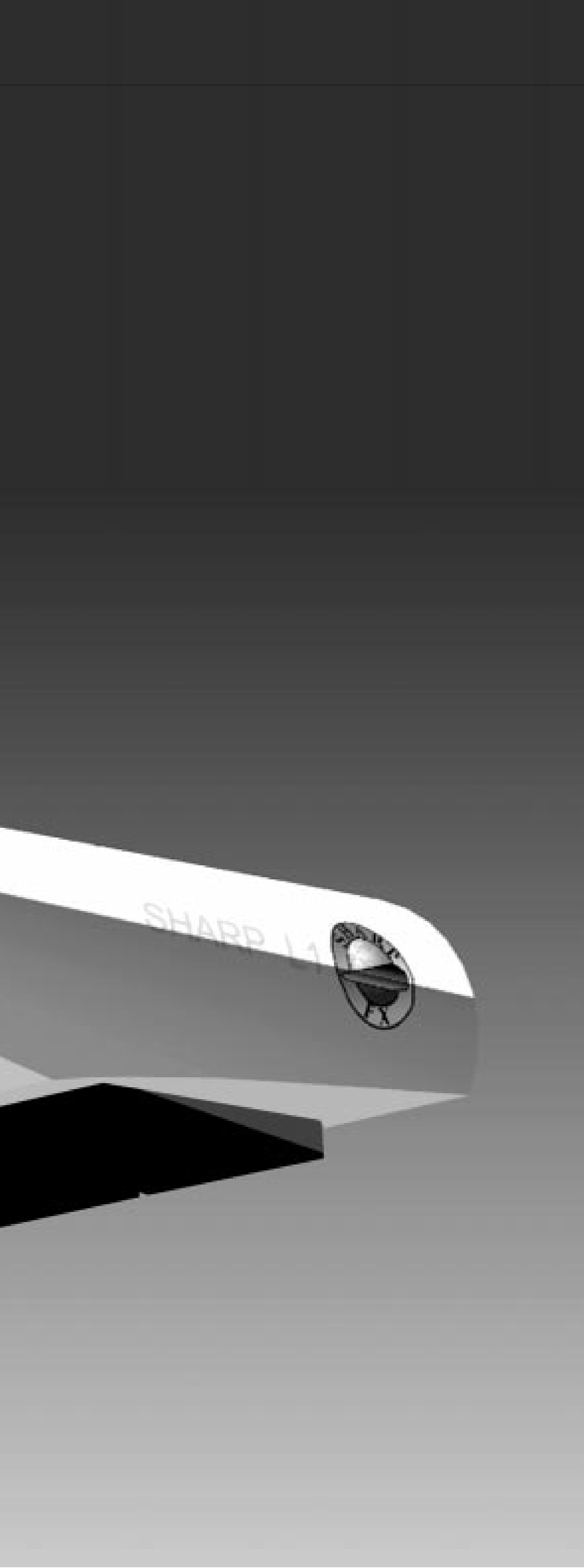

Overview

NASA’s mission for the Aero-Space Technology (AST) Enterprise is to pioneer the identification, development, application, and commercialization of high-payoff aeronautics and space transportation technologies. The Enterprise’s research and technology programs promote economic growth and contribute to national security through advances that will lead to a safe and efficient national aviation system, affordable and reliable space transportation, and improved information management systems.

The Agency manages principally through Enterprises. The AST Enterprise manages through a carefully defined set of technology areas that are aligned with designated Center Missions. Lead Centers have the responsibility to manage the implementation and execution phases of technology programs. To achieve this mission, NASA has designated Ames Research Center as the Center of Excellence for Information Technology and has delegated to Ames the lead role for basic research in Aviation Operations Systems, Information Systems Technology, and Rotorcraft. Ames is also the NASA Lead Center for focused programs in Aviation System Capacity and High-Performance Computing and Communications. Ames also leads the Enterprise in the core competency areas of human factors research, air-traffic management, information systems technologies, rotorcraft, vertical/short takeoff and landing technology, and thermal protection systems technology.

The Slender Hypersonic Aerothermodynamic Research Probe—Lifting #1 (SHARP-L1) is an example of a revolutionary lifting body concept designed to maximize hypersonic aerodynamic performance. The reusable ultra-high-temperature ceramic composite (UHTC) material on the sharp leading edge will allow this new shape to survive the nearly 5000°F temperatures of reentry into the atmosphere while providing dramatically improved spacecraft flight performance and safety.

The plans and goals of the AST Enterprise directly support national policy in both aeronautics and space, which are documented in "Goals for a National Partnership in Aeronautics Research and Technology" and the "National Space Transportation Policy," respectively. The Aero-Space Technology Enterprise has three major technology goals, or pillars. The first pillar, Global Civil Aviation, enables the Nation's leadership in global civil aviation through safer, cleaner, quieter and more affordable air travel. The second, Revolutionary Technology Leaps, revolutionizes air travel and the way in which aircraft are designed, built, and operated. And the third, Access to Space, enables the full commercial potential of space research and exploration. The following paragraphs highlight Ames Research Center's accomplishments in FY98 toward achieving the goals of the Enterprise.

Global Civil Aviation

Air transportation has become an essential component of the economic progress of the United States. Efficient aviation operations assist in domestic industrial progress and help U.S. businesses to compete in the increasingly global marketplace. Aviation products are also a major contributor to a positive U.S. industrial balance of trade. Projections linked to world economic growth suggest air travel demand will triple over the next twenty years. To preserve the Nation's economic health and the welfare of the traveling public, NASA must provide technology advances for safer, cleaner, quieter, and more affordable air travel. Ames has unsurpassed expertise in key disciplines that are requisite to addressing these challenges. These include human-centered air traffic management automation tools, innovative rotorcraft and short takeoff vehicles, integrated design-automation tools, and technologies for managing and communicating information on every level. Ames maintains key national facilities that are crucial for performing the basic and applied research needed to support the U.S. aerospace industry. These efforts are all part of Ames' contribution to safety, capacity, and affordability goals.

Airlines and businesses lose billions of dollars annually from delays and lost productivity owing to weather and traffic congestion in the current airspace system. Under Aviation System Capacity goals, Ames has developed air traffic management decision-support tools such as the Active Final Approach Spacing Tool (aFAST) component of the Center/TRACON Automation System (CTAS). The success of the CTAS system has led to widespread FAA acceptance of the system including plans to field CTAS at numerous major airports across the country. Ames also leads in the development of innovative vehicles such as the Civil Tiltrotor transport that lay the foundation for changes in airport operations to help decrease aviation congestion.

While increasing aviation system capacity and affordability, Ames is improving safety with innovative research in new aircraft crew station designs and display systems and human centered air traffic controller station design. In addition, advanced neural network control systems promise the ability to autonomously reconfigure a vehicle so that it can survive the failure of virtually any of its systems.

A major challenge in deploying rotorcraft vehicles to alleviate air traffic congestion is noise abatement. Ames projects are providing revolutionary technology advances in aeroacoustics including phased microphone array technology, development of a Tilt Rotor Aeroacoustic Model (TRAM), and blade-vortex interaction noise reduction.

Revolutionary Technology Leaps

NASA's charter is to explore high-risk technology areas that can revolutionize air travel and create new markets for U.S. industry. The technology challenges for NASA include eliminating the barriers to affordable and environmentally friendly high-speed travel, expanding general aviation, and accelerating the application of technology advances to increase design confidence and decrease design cycle time.

Next-generation design tools will revolutionize the aviation industry. The impact will be felt across the three AST Enterprise pillars, contributing to every technology goal. Ames' information technology research programs are developing aerospace-vehicle design tools that integrate the design system with performance analysis and high-accuracy computational and wind tunnel performance testing. These Ames-developed systems have demonstrated order-of-magnitude improvements in the time required to develop and validate a successful design. The

OVERGRID technology developed at Ames is now a dominant computational fluid dynamics (CFD) tool in both government and industry. Additional research at Ames in information technology will elevate the power of these computing tools to artificial domain experts through application of fuzzy logic, neural networks, and other new artificial intelligence methods. These tools will integrate multidisciplinary product teams, linking design, operations, and training databases to dramatically cut design cycle times and improve operational efficiency. Ames' accomplishments include applying neural networks and genetic algorithms to aerodynamic optimization, pressure-sensitive paint, particle image velocimetry, revolutionary grid-generation tools for CFD design, CFD analysis of an entire high-lift aircraft, and the Environmental Research Aircraft and Sensor Technology (ERAST) flight program.

Access to Space

Low-cost space access is key to realizing the commercial potential of space and to greatly expanding space research and exploration. Through integration of aviation technologies and flight operations principles with commercial launch vehicles, a tenfold reduction in the cost of placing payloads in low-Earth orbit is anticipated within the next decade. High reliability and rapid turn-around are the first steps to increased confidence in delivering payloads on time with fewer ground crews. NASA has initiated research on a broad spectrum of technology advancements that have the potential to reduce costs well beyond the initial reusable launch vehicle goals. This involves new technologies and integrating aeronautical principles such as air-breathing propulsion and advanced structures. This will enable a cost-to-orbit measured in hundreds, not thousands, of dollars per pound. Additional innovative work in interplanetary spacecraft thermal protection and autonomous vehicle systems promises to decrease the mass of interplanetary spacecraft while dramatically improving their reliability and performance.

Ames is developing new thermal protection systems that will enable radical improvements in vehicle entry performance. If forced to de-orbit in an emergency, current spacecraft, such as the space shuttle, have very limited cross-range capability; as a result, the crew has very few available landing sites. Dramatic improvements in thermal protection technology, such as the SHARP (Slender Hypervelocity Aerothermodynamic Research Probe), will allow radically different aerodynamic shapes that will lead to dramatic improvements in cross-range capability. Advanced sensor technology and intelligent vehicle health management research will provide order-of-magnitude decreases in the cost and time required to inspect and refurbish reusable launch vehicles. These Ames technologies are at the heart of system-wide improvements in the launch-to-low-Earth-orbit space transportation market.

Aviation and space transportation have been exciting and challenging areas of scientific and engineering endeavor since their inception. The basic aerospace paradigm is shifting from large hardware developments to information-based design and data system management. As NASA's Center of Excellence for Information Technology, Ames Research Center's contribution will continue to grow throughout the remainder of this century and into the next.

Improving Pilots' Understanding of Vertical Guidance

Everett Palmer, Michael Feary

The objective of this project was to integrate the design of the system, interface, procedures, and training of flight deck automation, focusing on the vertical guidance portion of the Flight Management System (FMS) by using a formal model referred to as the Operational Procedure Model (OPM).

In the latest generation of vertical guidance systems, increasing complexity has been dealt with by integrating the autopilot and the autothrottle and by dealing with the desired aircraft behavior as opposed to the behavior of individual autopilot and autothrottle control systems. The pilots on the design team specified how they wanted the vertical guidance system to behave in order to cope with all of the different situations that could occur during flight.

A project team was created that was composed of representatives from the design community, Lance Sherry, Daniel McCrobie (Honeywell), and Noreen McQuinn (Boeing); operators, Martin Alkin (Federal Express); and the research community, Peter Polson (Univ. of Colorado) and researchers from Ames. The team designed a simplified vertical guidance display and computer-based training package that is compatible with the philosophy used to design the vertical guidance automation behavior.

The experimental design displays a unique and meaningful label for each of the automation behaviors. The first figure shows the current *control-based* display and the proposed *behavior-based* display for three descent behaviors: (1) a normal descent with the aircraft on the descent path and on speed, (2) a case in which the aircraft is more than 500 feet above the descent path, and (3) a case in which the aircraft is on the descent path but fast.

A flight simulation experiment was designed to evaluate the hypothesis that the display of the vertical guidance operational procedures on the flight mode annunciator (FMA) would significantly improve pilot situation awareness and improve operation in the modern glass cockpit. Twenty-seven airline pilots participated in an experiment on a modified MD-11 simulator at Long Beach and at Honeywell.

	Current "Control-Based" display		Experimental "Guidance-Based" display
1	355 PITCH | NAV1 | IDLE 23ooo	→	355 | NAV1 | Early descent 23ooo
2	355 PITCH | NAV1 | IDLE 23ooo	→	355 | NAV1 | Late descent 23ooo
3	340 PITCH | NAV1 | IDLE 23ooo	→	340 | NAV1 | Descent overspeed 23ooo

Fig. 1. Comparison of current and experimental display for three aircraft behaviors.

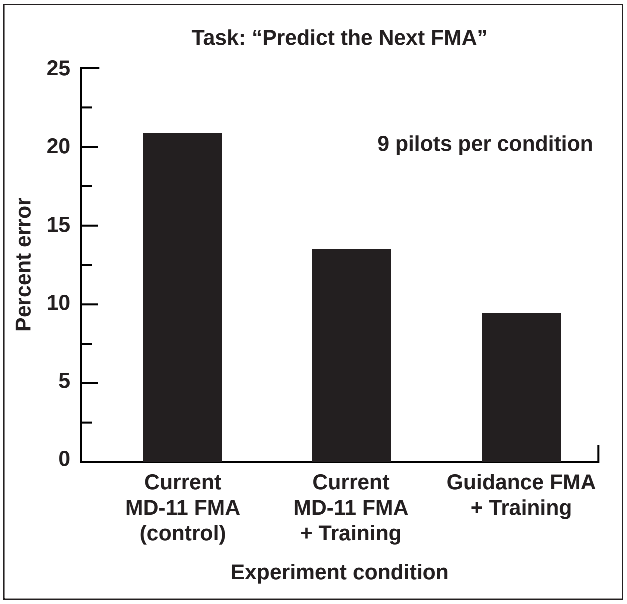

Fig. 2. Results of the flight simulation experimental conditions represented in terms of percentage of errors per condition.

The experiment tested the effects of training and performance on different levels of knowledge using the new display and descriptions of the vertical guidance logic.

Pilots who were given the new guidance FMA display could describe the current and future vertical guidance system situations significantly better than pilots using the current FMA display. The results, as shown in the second figure, suggest that pilots have better situation awareness with the guidance FMA display and a better understanding of the avionics.

Point of Contact: E. Palmer
(650) 604-6073
epalmer@mail.arc.nasa.gov

Detecting and Correcting Errors in Flight

Judith Orasanu

National Transportation Safety Board analyses of commercial aviation accidents, in which crew performance was a factor, found that in almost three-fourths of them, one crewmember made an error and that the other crewmember failed to detect or correct it (called *monitoring and challenging* errors). These errors are significant because they often represent the last opportunity to break a chain of events that may lead to an accident. Monitoring and challenging errors may reflect three different sources: (1) the original error was not detected; (2) the error was detected, but the detecting pilot chose not to say anything; or (3) the error was detected, but the communication was not effective in changing the course of events.

A simulator study was conducted to gain a better understanding of the factors that contribute to monitoring and challenging errors. This study examined two potential causal factors: (1) level of risk in a developing situation and (2) degree of "face-threat" involved in challenging an error. Face-threat refers to a challenge to a person's skill, judgment, or other flight-related competency. Errors were scripted into full-mission flight scenarios which were then flown by two Boeing 747-400 pilots. In each crew a study subject pilot flew with a pilot trained to act as a research confederate who flew either in the role of captain or first officer, depending on the actual status of the subject pilot. Scripted errors varied in their threat to flight safety (high or low risk) and in degree of face-threat. The level of face-threat was determined by the source of the errors: Errors committed by the confederate pilot were high face-threat because the subject had to directly confront the other pilot to correct the mistake; errors originating in a source outside the flight deck, such as Air Traffic Control, were low face-threat. This design permitted the first two hypotheses concerning sources of monitoring/challenging errors to be addressed.

Error detection was based on a verbalization by the subject referring to the error or to an attempt to correct it. As shown in the first figure, not all errors

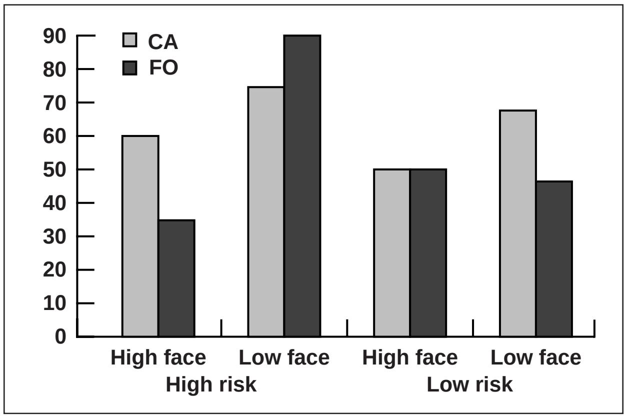

Fig. 1. Percent of error catches by condition and crew position.

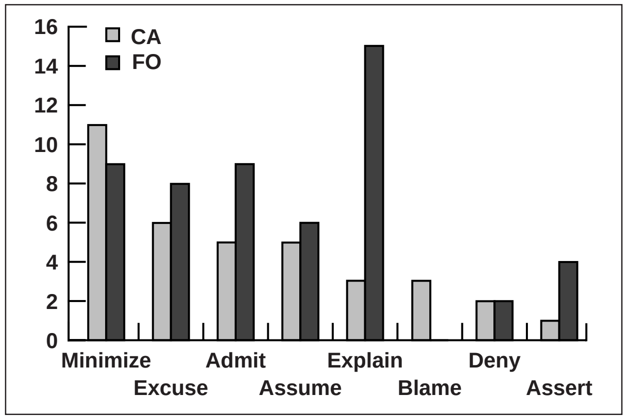

Fig. 2. Frequency of reasons cited for failure to detect in-flight errors.

were caught. The overall catch rate was approximately 62%. Captains were more likely than first officers to detect and correct errors. Captains tended to be very proactive in high-risk situations and often prevented these situations from developing through preemptive actions. First officers were sensitive to the social dynamic of challenging the captain (face-threat). They were most likely to intervene in situations involving external errors when risk levels were high. Overall, no significant difference was found in error detection as a function of risk level, although there was a tendency for more errors to be caught in high-risk than in low-risk situations.

The relatively low error-catch rate suggests that monitoring and challenging errors originate in failures to detect an error. To explore this hypothesis further, post-simulation interviews probed the pilots' understanding of those cases in which they said nothing to correct the situation. As shown in the second figure, captains were most likely to report that they noticed the problem, but minimized its severity and thus said nothing. First officers were most likely to explain company procedures that led to their decisions not to respond. They were also more likely than captains to admit that they had made a mistake, particularly in high face-threat situations. The lowest detection rate by first officers was in the high-face-threat/high-risk situations. These scenarios involved direct challenges to the captain's skill and judgment. As such, they would constitute the greatest social risk to the first officers.

This study identified situations that might occur during real flights and that might pose a threat to safety if not corrected. Based on this information, training programs can develop intervention skills, especially in first officers, that are most effective in producing corrective actions, thus enhancing flight safety.

Point of Contact: J. Orasanu
(650) 604-3404
jorasanu@mail.arc.nasa.gov

Intelligent Flight Controller

Charles Jorgensen

The Intelligent Flight Control (IFC) program is a joint technology development effort that addresses the needs of NASA and the U.S. aerospace industry for aircraft control systems that can be produced and tested at lower cost, and for flight systems that can adapt to damaged control surfaces resulting from failures or severe accidents.

The objective of the program is to develop next-generation neural flight controllers that exhibit higher levels of adaptivity and autonomy than state-of-the-art systems. These next-generation flight controllers will be capable of automatically compensating for a broader spectrum of damaged or malfunctioning aircraft, controlling remote or autonomous vehicles, and further reducing costs associated with flight-control law development.

A major IFC team technical milestone was reached in February 1998 when the Ames Research Center's NeuroEngineering Group formally delivered the final version of the real-time Dynamic Cell Structure neural network learning software to Boeing.

Preliminary F-15 performance evaluations of the software by Boeing were described as excellent, and installation of the software into a newly redesigned F-15 flight processor board has begun. Achieving this software performance represents the culmination of the most challenging technical goal for the NASA side of the project and is a definite advance in neural flight-control technologies.

Final Phase I/III flight tests have been delayed because of unforeseen issues related to the F-15 ACTIVE aircraft. Phase I/III flight tests will be conducted as soon as the aircraft is available under NASA Dryden Work Order 23. Discussions are under way regarding additional cost and aircraft availability required to complete the Phase II flight tests.

Aerodynamic and inertial data on the LoFLYTE unmanned aerial vehicle was received from Accurate Automation Corporation (AAC) and integrated into the NeuroLab real-time simulation environment. Initial testing of the longitudinal open-loop dynamic characteristics produced results that correlate well with AAC's predicted behavior (see figure 1). Testing of the lateral-directional open-loop characteristics, as well as synthesis of the neural flight control architecture and the autopilot control laws, are under way.

The success of IFC paves the way for the development of safer aircraft control systems that are capable of recovering from serious accidents or failures. In addition, the fast-adaptive nature of these controls will reduce the design cycles of aircraft control systems in terms of cost and time to certification. IFC will thus help the aeronautics industry attain

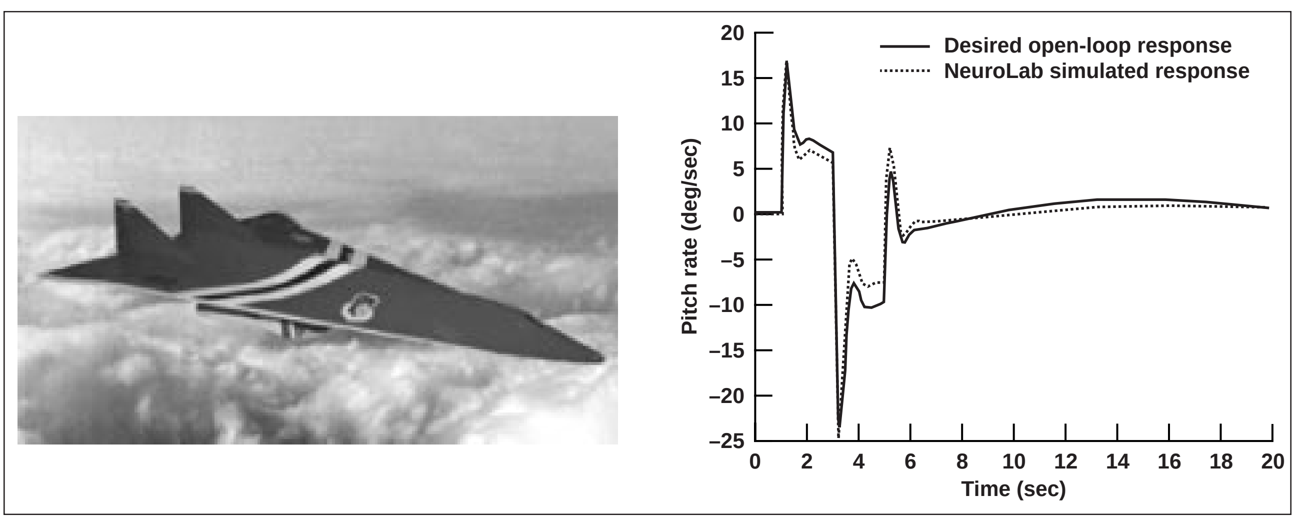

Fig. 1. LoFLYTE open-loop pitch-rate response resulting from an elevated doublet.

its goal of a 50% decrease in the time required to develop aircraft software in the next 5 years.

This capability was recently demonstrated by developing a Mars Airplane concept, starting with two-dimensional drawings and ending with a fully actuated flight simulation over texture-mapped ground data in the Valles Marineris area of Mars, in a period of just 4 days. The Mars Airplane simulation was demonstrated for NASA Administrator Dan Goldin in December 1998, and at the Administrator's request, a sample of the simulation was provided to him to be included as part of a future presentation to Congress.

Point of Contact: C. Jorgensen
(650) 604-3594
cjorgensen @mail.arc.nasa.gov

Visualization and Analysis of Flight Crew Procedure Performance

Todd J. Callantine

Activity tracking—a way of inferring operator intent—was conceived to support technology that detects errors and provides operators with context-sensitive advice and reminders. The activity tracking method embodied in the Crew Activity Tracking System (CATS) has been validated using line pilots. Full-mission Boeing 747-400 simulation data have also been used to demonstrate how CATS can automatically identify deviations from expected crew actions and capture the context in which the deviations occur; such information is useful in refining new procedures to improve error-tolerance. The objective of this research is to enhance CATS to support visualization and analysis of flight crew performance on proposed terminal-area procedures as part of the NASA Terminal Area Productivity (TAP) research program.

The first figure depicts the elements of the CATS procedure performance visualization and analysis project. Full-mission, pilot-in-the-loop simulation studies using the proposed procedures were conducted in the Ames Advanced Concepts Flight Simulator (ACFS). The CATS Data Server filters crew actions and key events from the binary ACFS data and supplies them to CATS in real time. CATS processes these data to (1) detect deviations from expected crew actions, and (2) simultaneously allow researchers to visualize the information presented on the ACFS displays.

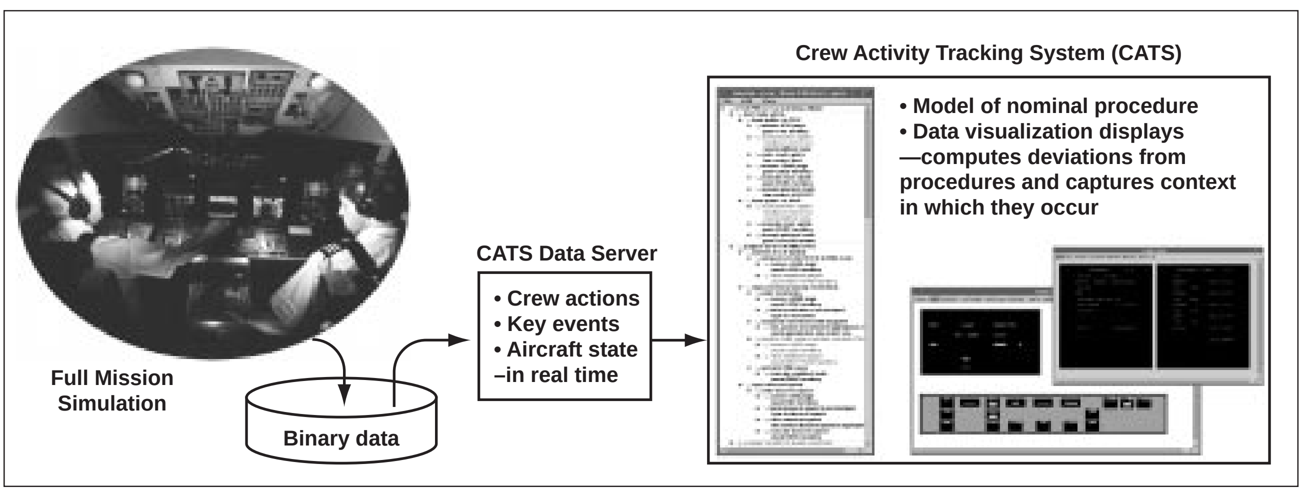

Fig. 1. Crew Activity Tracking System (CATS) with full-mission simulation data server.

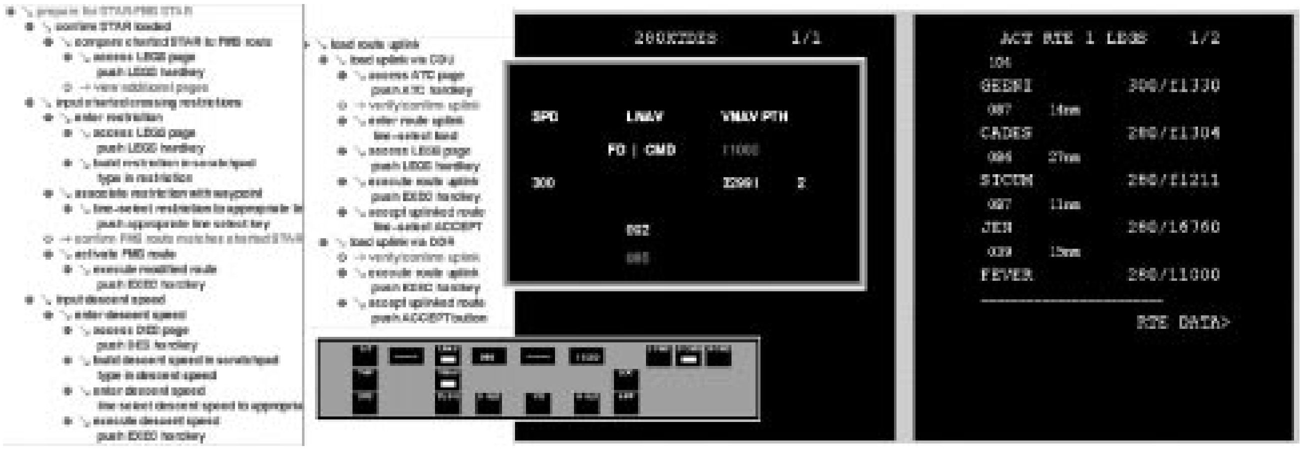

Fig. 2. Collected portions of the CATS model of crew procedures and visualization displays.

To detect deviations from expected crew actions, CATS uses a computational model of the nominal procedure, portions of which are shown in the second figure. The CATS model decomposes functions essential to correct performance of the procedure, and includes conditions that specify when crew actions should be performed. The figure also shows some of the displays developed for visualizing the appearance of flight deck interfaces.

Contributions of this research include an automated system for effectively utilizing full-mission ACFS data, and a means of replaying and visualizing those data in real time to examine crew procedure performance and possible errors. Errors may be attributed, for example, to apparent deficiencies in the information available to the flight crew.

CATS will be evaluated as an integral part of a model-based design method. The CATS model will be examined for possible enhancements that will enable it to act as an online "sketchbook" for documenting concepts and outlining procedures for new systems. CATS will thereby serve as a tool to support all aspects of the development and evaluation of new crew procedures.

Point of Contact: T. Callantine
(650) 604-2631
tcallantine@mail.arc.nasa.gov

Virtual Acoustic Enhancement of Traffic Collision Avoidance System Advisories

Elizabeth Wenzel, Durand R. Begault

Research has been ongoing at the Spatial Auditory Display Laboratory at Ames Research Center in the use of head-up auditory displays for enhancing commercial aviation safety. Similar to a head-up visual display, the use of three-dimensional (3-D) audio cues allows a pilot to keep his line of sight out-the-window "head-up" while simultaneously receiving situational awareness information of a spatial nature. The 3-D audio cues are imposed on speech signal messages that are delivered to each pilot via active noise-cancellation headphones.

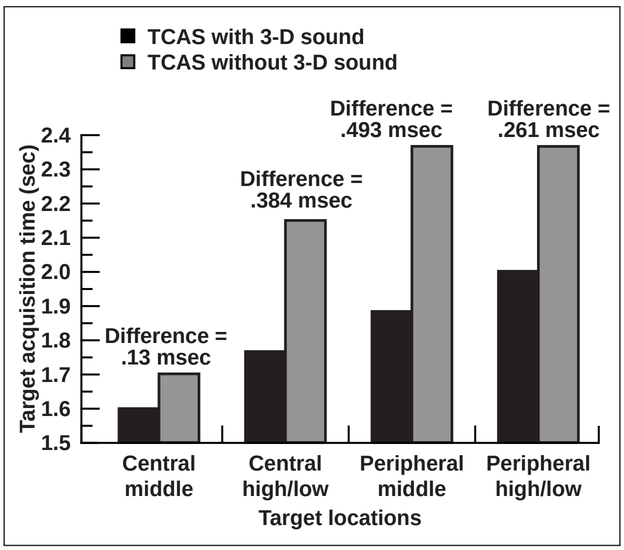

Fig. 1. Results from an experiment that demonstrates the advantage of enhancing TCAS displays with 3-D audio. Central targets were located at ±35 degrees azimuth relative to forward position; peripheral targets were at ±48 degrees azimuth. Middle targets were at an elevation of ±1000 feet; high/low targets were at the edge of the field of view at elevations of +4000 and −2500 feet, respectively.

Ten commercial airline crews were evaluated in a flight simulator study to determine whether the existing Traffic Alert and Collision Avoidance System (TCAS) could be improved by including 3-D audio cues with the head-down map display system currently in use. The experimental condition had the verbal "traffic traffic" alert for the TCAS advisory processed so that its perceived lateral spatial location corresponded to the location of aircraft traffic ("targets") seen out of the windshield; a control condition used the standard TCAS system. Ten crews participated in a within-subjects design, flying a route from San Francisco to Los Angeles with 49 targets.

The results indicated a significant difference for target-acquisition time favoring the 3-D audio TCAS condition by 307 milliseconds on average. The maximum advantage for 3-D audio was 493 milliseconds on average for peripheral targets at ±48 degrees relative azimuth. There was no significant difference in the number of targets acquired. The figure gives a summary of the data as a function of target location.

Overall, the advantages of implementing a 3-D audio display to augment existing TCAS systems can be seen. The idea of augmenting the existing TCAS system with 3-D audio cues, rather than building a new display system from the ground up, is unique and would probably be inexpensive to implement. It appears that the integration of two-channel binaural sound into the cockpit would offer safety benefits to the aviation community in line with other mechanisms for enhancing situational awareness.

Point of Contact: E. Wenzel
(650) 604-6290
bwenzel@mail.arc.nasa.gov

Analysis of Rotorcraft Accidents

Laura E. Iseler

A study was conducted to analyze the causes of recent rotorcraft accidents for the purpose of determining how best to decrease their number and severity. All U.S. civil rotorcraft accidents that occurred in the period 1990–1997 as documented by the National Transportation Safety Board (NTSB) were examined.

During the 7-year period from 1990 through 1996, there were 1396 civil rotorcraft accidents in the United States as documented by the NTSB. A total of 491 people were killed. This is an average of 199 rotorcraft accidents and 70 fatalities per year.

An accident is defined by the NTSB as an occurrence associated with the operation of an aircraft that takes place between the time any person boards the aircraft with the intention of flight and the time all such persons have disembarked, and in which any person suffers death or serious injury, or in which the aircraft is substantially damaged.

Aircraft were categorized based on purchase price in 1994 dollars, and placed into one of four cost categories: low, less than $600,000; medium, $600,000 or more, but less than $1.5 million; high, $1.5 million or more, but less than $4 million; and very high, $4 million or more. There were 10 cause categories: pilot impairment, experience, preflight preparation, in-flight decision and judgment, interpretation, high-risk operations, aircraft defects, environment, wire strike, and other. Both first-event and cause were examined.

The first figure shows that the common first-events resulting in the most fatalities are collision-with-obstacle, system-failure, collision-with-ground, and loss-of-engine-power, in that order. Collision-with-obstacle and collision-with-ground both require some sort of low-cost obstacle-detection system or proximity warning system to alleviate the problem. System failures might be mitigated by more vigilant maintenance programs and by more stringent pre-flight inspections. System-failures and loss-of-engine-power accidents could be reduced through increased training in emergency procedures.

The second figure shows that the most common cause of accidents and the second most common cause of fatal accidents was aircraft problems. The most likely solutions for this cause category are health and use monitoring systems and more vigilant maintenance programs. The third most common cause of fatal accidents is imprudent in-flight decisions. Decision making can be addressed through training. Although infrequent, flight into Instrument Meteorological Conditions, interpretation, and pilot impairment are particularly deadly. Promoting safety is a potential solution to all of these problems.

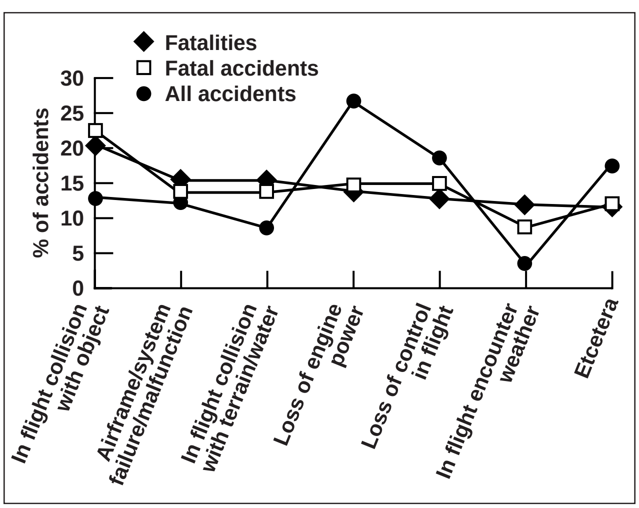

Fig. 1. First events in rotorcraft accidents.

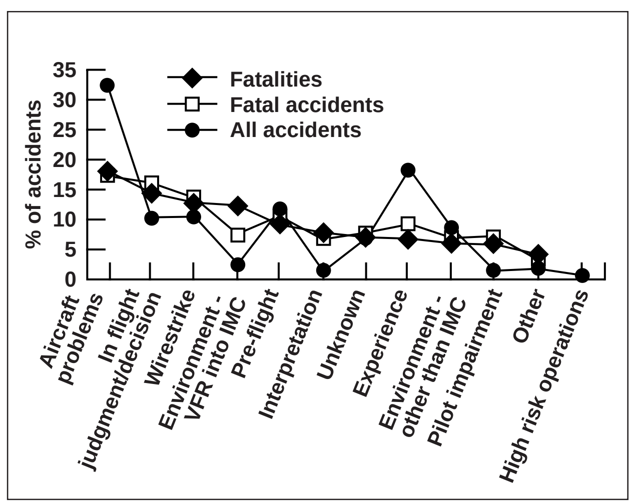

Fig. 2. Accident causes.

The top three first-events in serious injury accidents were loss-of-engine-power, loss-of-control, and system-failure. Improved training and pilot aids might reduce the number of serious injuries incurred in these accidents. Half of the nonmechanical loss-of-engine-power accidents were caused by lack of fuel or improper fuel.

System-failure and in-flight-collision-with-object were the most common first-events for the very-high-cost helicopters. Wires were the objects most often struck. A low-cost obstacle-detection system or proximity warning system would help prevent collisions with such obstacles as wires.

Point of Contact: L. Iseler
(650) 604-0872
liseler@mail.arc.nasa.gov

Rotorcraft Accident Analysis

Eugene F. Kasper

The National Transportation Safety Board (NTSB) database of accidents involving U.S. civil registered rotorcraft from mid-1963 through 1997 was obtained and analyzed. The NTSB database included 8,436 rotorcraft accidents, each of which was assigned to one of 21 "first-event" categories. The accident summaries included data such as engine type, flight phase, mission type, and a brief narrative of the accident sequence; these data permitted deeper characterization of accidents to determine underlying common events. Because of the limitations in determining rotorcraft fleet activity in terms of annual flight hours, the analyses used the annual number of registered aircraft as reported by the Federal Aviation Administration (FAA) as the rate basis (that is, rates were calculated per 1,000 registered aircraft).

In examining the entire database, it was determined that over 70% of the accidents involved one of four first-events: loss of engine power (2,408 events, 28.5% of all mishaps), in-flight collision with objects (1,322 events, 15.7%), loss of control (1,114 events, 13.2%), and airframe/component/system failure or malfunction (1,083 events, 12.8%). This distribution held also for single-piston-engine and single-turbine-engine-powered helicopters; for twin-turbine-engine helicopters, airframe failure was the most common first-event. Piston-engine helicopters accounted for 63.7% of the accidents.

The rate of accidents per 1,000 aircraft has steadily decreased and appears to be approaching a limit of 20 per 1,000 aircraft per year. The trend is the same for single-piston and single-turbine rotorcraft; the limit for twin-turbine aircraft is approximately 10. For fatal accidents, the average is approximately 35 per year, which translates to a fatal accident rate of 5 per 1,000 aircraft per year. This rate has remained essentially constant since the mid-1970s.

Considering the number of accidents (fatal and nonfatal) per year, the NTSB has recorded approximately 250 accidents per year with a decreasing trend since 1980. Rates for single-piston and single-turbine types are approximately equal to the overall fleet rate and equal to each other; the rate for twin-turbine types is lower. Overall, fuel system-related incidents accounted for 40% of the loss-of-engine-power accidents. The rate for in-flight collisions with objects has remained essentially constant since 1980. The total number of loss-of-control accidents increased during the 1980s and early 1990s and has shown a decrease only since 1994. The number of airframe-failure accidents per year showed a distinct "bubble" from 1975 through 1984.

Point of Contact: E. Kasper
(650) 604-6881
ekasper@mail.arc.nasa.gov

Partial Authority Flight Control Augmentation

Matt Whalley

The goal of partial-authority flight-control augmentation (PAFCA) is to achieve a functionality similar to that of highly augmented fly-by-wire systems within the constraints of existing flight-control-system architectures. The rotorcraft handling-qualities specification, ADS-33D, mandates an attitude-command, attitude-hold (ACAH) response type as the minimum necessary control mode for Level 1 handling qualities in degraded visual environment (DVE) operations. Unfortunately, the implementation of an ACAH response type requires significant stability augmentation system (SAS) servo authority, since—given a rate-command response type for the unaugmented aircraft—the SAS servo displacement must exactly cancel the pilot control input in the steady state in order to command a zero angular rate and hold a nonzero attitude. The level of SAS servo authority is typically limited to ±10% (with respect to total boost servo displacement) and hence significant saturation will be encountered, even at the low levels of aggression typically encountered in DVE operations. This can be offset by distributing the augmentation to both SAS and trim servos simultaneously, but the resulting trim follow-up of the cockpit controls can have a detrimental effect on the handling qualities.

The PAFCA studies have taken the novel approach of tailoring the flight-control system to "frequency-match" the gain and phase of the closed-loop response to the unaugmented aircraft dynamics in the region of the pilot/vehicle crossover (1–10 radians per second). This helps mitigate unpredictable transients in aircraft dynamic behavior upon saturation and focuses available control effort on stabilization of the low-frequency modes and inter-axis decoupling.

A simulation trial was conducted on the Vertical Motion Simulator (VMS) at Ames Research Center to test the frequency-matching concept. A PAFCA ACAH-response type was developed within the constraints of the UH-60A Black Hawk helicopter control-system architecture. Two control-law gainsets were synthesized—one that minimized the potential for series actuator saturation (termed "frequency-matched"), and a second that met all ADS-33D Level 1 criteria (termed "performance optimized"). The trial consisted of four tasks flown using a simulated nighttime scene, and ANVIS-6 night vision goggles to ensure a DVE. For each ACAH gainset there were three levels of SAS servo authority limit, ±10%, ±15%, and full authority.

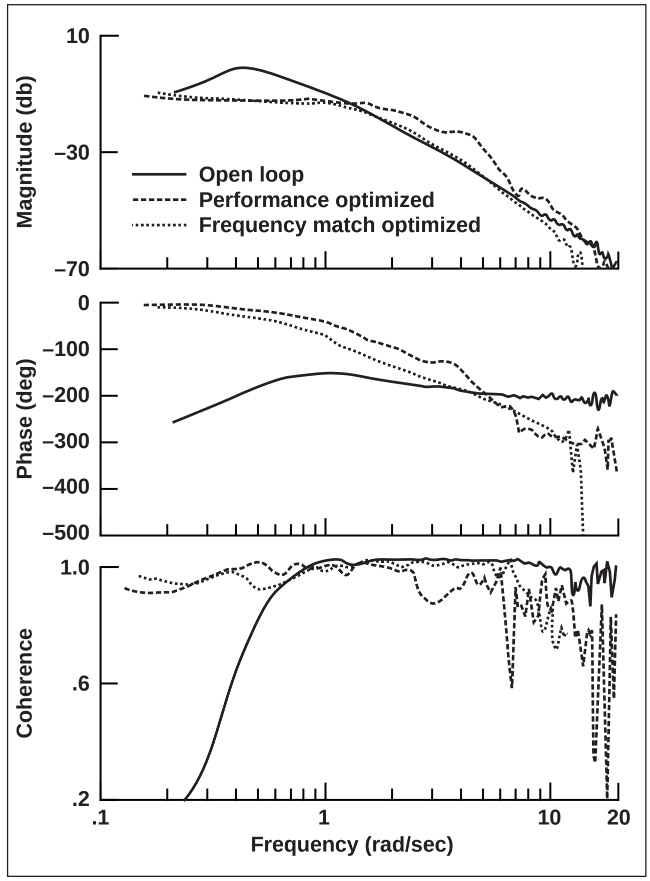

Fig. 1. Pitch-axis frequency response of the configurations evaluated in the VMS trial.

The two ACAH configurations were preferred to the production UH-60 Black Hawk, with the frequency-matched configuration always one-half to one Handling-Quality Rating (HQR) better (on the Cooper-Harper Handling Qualities Rating Scale). Pilot commentary for the frequency-matched configurations was nearly always positive. In addition, it was found that a ±15% SAS servo authority always

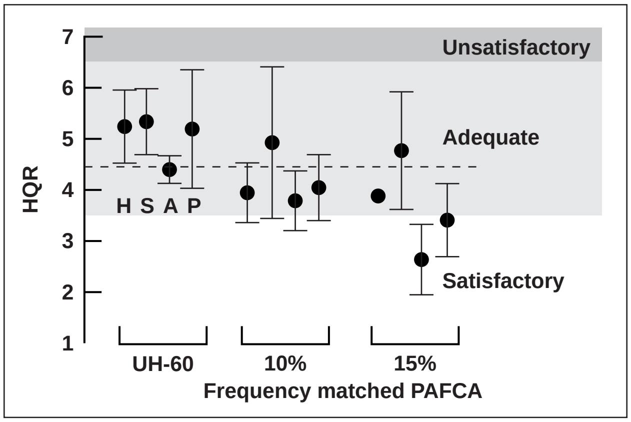

Fig. 2. Subjective handling-qualities ratings assigned for the hover (H), side-step (S), acceleration/ deceleration (A), and pirouette (P) tasks.

resulted in ratings one-half to one HQR better than a ±10% authority configuration, and that Level 1 handling qualities were possible. In summary, frequency-matching made the difference between desired (HQR ≤ 4.5) and adequate (HQR > 4.5) task performance, and ±15% SAS servo authority reduced the workload further still such that it could make the difference between overall Level 1 (HQR ≤ 3.5) and Level 2 (HQR > 3.5) handling qualities.

The work described was conducted as a collaborative study between the U.S. Army Aeroflightdynamics Directorate (AFDD) and the UK Defence and Evaluation Research Agency (DERA) under the auspices of Technical Co-operation Panel (TTCP) AER-TP-2, KTA 2B.1.

Point of Contact: M. Whalley
(650) 604-3505
mwhalley@mail.arc.nasa.gov

Ship Air-Wake Characteristics

Greg Zilliac, Kurt Long

To evaluate the ability of helicopters to operate aboard various ship classes, and to determine any limitations that might be associated with such operations, the U.S. Navy conducts shipboard Dynamic Interface (DI) test programs. DI test programs require large outlays of money, personnel, equipment, and time resources, but they are also subject to atmospheric and other factors that often significantly limit the information collected during each test. As a result, the Naval Air Systems Command and other groups within the U.S. military are attempting to develop a capability to predict shipboard helicopter performance with reduced dependence on actual shipboard test data. An essential element of such an analytic capability is the prediction of air-wake conditions near the flight deck, using limited full-scale test data. In an attempt to characterize the air-flow patterns around U.S. Navy amphibious assault ships, a wind-tunnel research effort was initiated at Stanford University in 1997 and has been ongoing at Ames Research Center since June 1998. The ultimate goal of the work is to produce ship air-wake information and data that can be used in conjunction with computational fluid dynamics (CFD) air-wake predictions to determine rotorcraft shipboard operating limits with a minimum of full-scale testing. Corollary ship air-wake information gained during the effort will prove useful in the ship design-optimization process, as well as being a source of data that can be used for both flight simulations and accident prevention.

The experimental portion of the effort, conducted in the Ames 32- by 48-Foot Wind Tunnel at the Fluid Mechanics Laboratory (FML), has focused on obtaining quantitative and qualitative air-wake data for the USS WASP (LHD 1) and USS TARAWA (LHA 1) amphibious assault ship classes. The FML wind-tunnel effort has employed a variety of innovative flow-visualization techniques (pressure-sensitive paint, deck tufts, helium-filled soap bubbles, smoke, and oil-flow visualization) to provide information about basic shipboard (bluff-body) air-wake characteristics (location of streamlines, bow-separation bubble, deck-edge vortices, areas of extreme turbulence). Significant findings to date include the identification of a strong recirculating flow region at

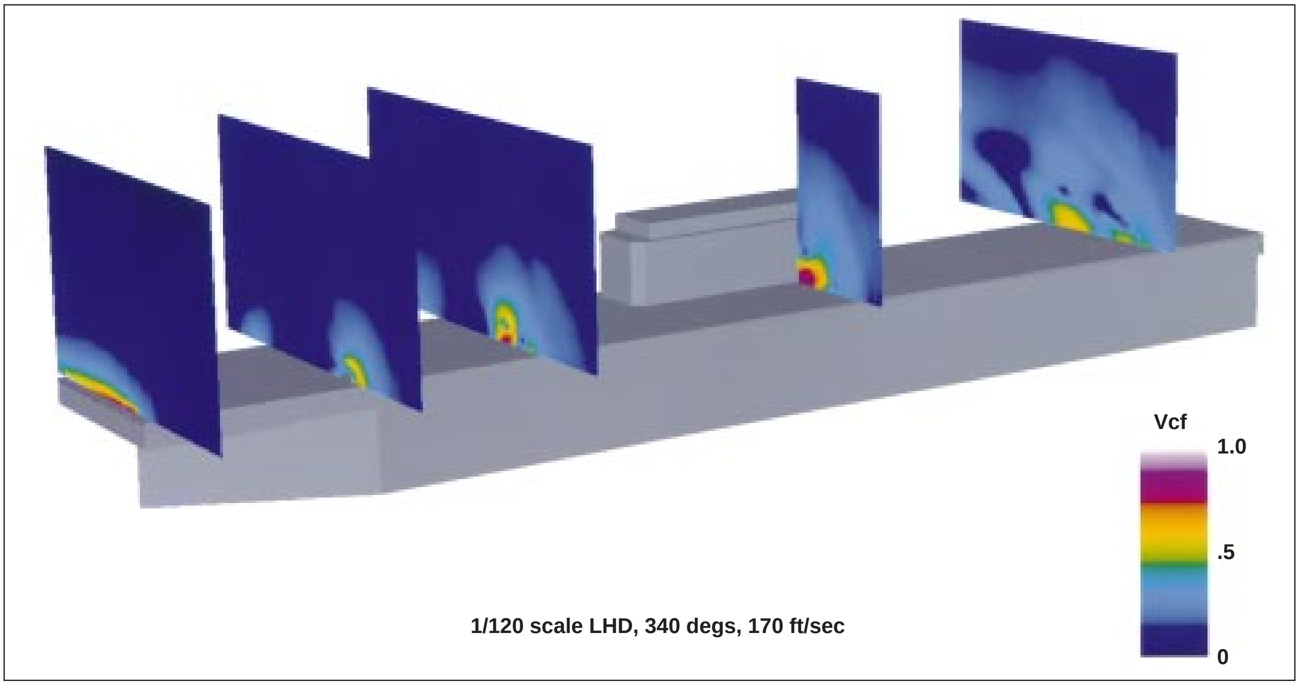

Fig. 1. Measured cross-flow velocity on an LHD amphibious assault ship.

the flight deck leading edge for bow-wind conditions, and significant island/deck flow interactions for all wind conditions. Perhaps the most significant finding to date is the presence of a strong “delta wing” type longitudinal vortex (located inboard of the upwind edge of the flight deck) that forms under beam-wind conditions and spans the length of the 800-foot-long flight deck. Experimental measurements suggest that the mean cross-flow velocities in this vortex can easily exceed 50% of the free-stream flow velocity. The figure shows the distribution of measured dimensionless cross-flow velocities (nominal tunnel speed of 170 feet per second), for winds from 20 degrees to port of the ship centerline. These values, and the location of the vortex core, correlate well with full-scale shipboard helicopter accidents known as tunnel strikes, which can occur during main-rotor startup sequences whenever the rotor blades flap excessively, striking and damaging other portions of the helicopter. Supplemental ship/rotor interaction tests conducted in the Ames 7- by 10-Foot Wind Tunnel in August confirmed the vortex strength trends identified at the FML.

The experimental effort has also demonstrated the potential aerodynamic benefits (which can be directly translated to enhanced piloted and unmanned aircraft operational safety) associated with slight changes in ship geometry. Measurements confirm that the installation of a small bow flap can dramatically reduce the size of the leading-edge separated flow region, in turn improving the downstream air-wake characteristics.

Currently in its second year, this project has already obtained a variety of previously unknown information about the air-wake of U.S. Navy amphibious assault ships. The next milestone for the effort is to obtain fluctuating velocity data at various locations around the deck. Ultimately, project goals include the combination of wind-tunnel and CFD data to develop analytic operational envelopes for various rotorcraft operating from the candidate ships, with extensions to other rotorcraft and ship classes as appropriate.

Point of Contact: G. Zilliac
(650) 604-3904
gzilliac@mail.arc.nasa.gov

Human Performance in Multitask Settings

Roger W. Remington, James C. Johnston, Eric Ruthruff

The safety of aerospace systems depends critically on various characteristics of human performance. It is important therefore to determine factors that may affect performance, especially the probability of human error. One of the features of domains of interest is the prevalence of human multitasking. Operators frequently are required to switch from one task to another, and often it can be several minutes before they revisit a specific task. There is a question whether such switching entails a performance cost. If so, it is important to know how this cost is related to the length of time since the task was last performed (recency), as well as the degree to which the task was anticipated (expectancy).

These questions were investigated by measuring response time as a function of whether the task was expected and noting how many trials had intervened since the last presentation (recency). One task required subjects to identify which of four letters had been presented, the other task, which of four colors. Tasks were presented in a clockwise sequence in a 2 x 2 matrix. On expected trials (p = 0.8) a stimulus from the letter task was presented in the top row of the matrix, or one from the color task in the bottom. On unexpected trials (p = 0.2) this was reversed.

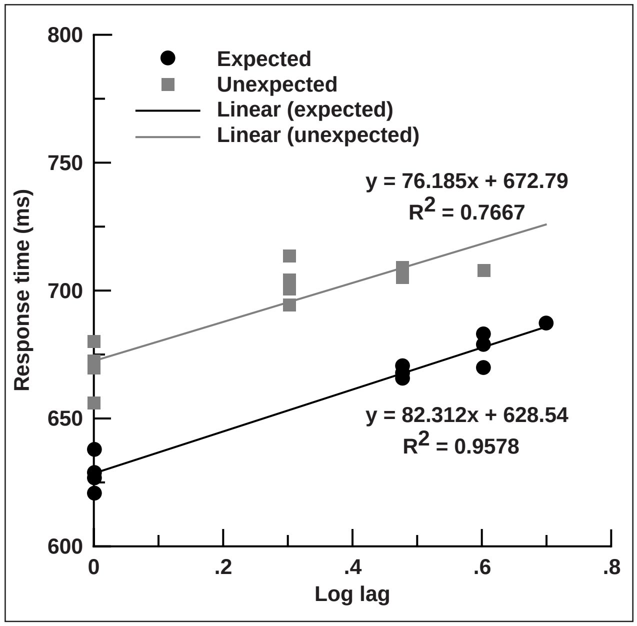

Fig. 1. Response time for expected and unexpected tasks as a function of recency (log lag).

As shown in the figure, the results suggest a pronounced switching cost affected by both recency and expectancy. The experiments demonstrate that for even the simplest tasks there is a fundamental cost in processing when one switches to another task that cannot be eliminated. Moreover, this cost increased with increases in the time since the task was last performed.

The observed switching costs were well fitted by a dual-locus bottleneck model in which task expectancy and task recency affect separate stages of processing. According to the model, expectancy affects task set configuration (TSC), which is responsible for activating task rules. TSC must be completed for processing to proceed. For expected switches, TSC can be done prior to task onset. For unexpected switches, the time required for TSC produces additional response-time cost since it could not be done in advance.

According to the model, recency affects stimulus-response mapping (SRM), which is responsible for retrieving the appropriate response from memory. Retrieval is more efficient for tasks that have been done more recently. Recency could affect other processes, but in simple tasks such as these, SRM presents the main cognitive difficulty. The additive effects of expectancy and recency suggest that they affect distinct, separate underlying mental operations.

The results have implications for performance in operationally relevant settings. The effects of expectancy suggest that performance will degrade when operators are confronted with unpredictable task sequences. The effects of recency suggest that the cost of interruptions that suspend task performance will increase as the time away from the task increases. The small costs observed for these two simple tasks may well be magnified in more complex environments with multiple challenging tasks. For example, as the number of tasks increases it will take longer to return to any one task. The decreased recency will adversely affect task performance. Our dual-locus model predicts that the time required for TSC should increase with the complexity of the task rules. This suggests greater costs for complex operationally relevant tasks.

Point of Contact: R. Remington
(650) 604-6243
rremington@mail.arc.nasa.gov

Perceptual Effect of System Latency on Localization of Virtual Sounds

Elizabeth Wenzel

Surprisingly little is known regarding the effect of introducing latency during dynamic auditory localization, although it is clearly a critical issue for virtual environments. Excessive latencies may degrade basic perceptual skills such as the ability to localize a sound source in three-dimensional space. The effect of latency on performance may be even more critical in multi-modal displays, such as a virtual environment that combines visual and auditory information. For example, recent research in visual virtual displays indicates that latencies of 31 milliseconds or more can increase errors in distance judgments for virtual targets when observers are allowed to move their heads, although performance remains superior compared to that of stationary observers. Delays of this magnitude or greater are typical in many virtual display systems.

In a virtual acoustic environment, the total system latency (TSL) refers to the time elapsed from the transduction of an action, such as head movement, until the consequences of that action cause the equivalent change in the virtual sound source. The effect of increasing TSL on localization accuracy when head motion is enabled is presented here. Five subjects estimated the location of 12 virtual sound sources (individualized head-related transfer functions (HRTFs)) with latencies of 33.8, 100.4, 250.4, or 500.3 milliseconds in an absolute judgment paradigm. The task was to indicate the apparent azimuth, elevation, and distance of a virtual source using a graphical response method. Subjects also rated the perceived latency on each trial. Localization performance measures included plots of the estimated versus target locations, azimuth and elevation confusion rates, externalization rates, and average error angles. In an effort to characterize the listeners' localization strategies, their head motions were also recorded and summarized in terms of the maximum deviations of pitch, roll, and yaw on each localization trial.

Previous studies have produced baseline performance data for localization of spatialized sound using static (non-head-coupled) virtual sounds. Such stimuli tend to produce increased localization errors (relative to real sound sources) including increased confusion rates (sound heard with a front-back or up-down error), decreased elevation accuracy, and failures of externalization (sound heard inside the head). Enabling head motion typically improves localization performance, particularly by reducing front-back confusions. Here, the data indicated that localization was generally accurate, even with a latency as great as 500.3 milliseconds. Front-back confusions were minimal, and almost all stimuli were externalized by all subjects. Both azimuth confusions and externalization were unaffected by latency. Elevation confusions and error angles increased with latency, although the increases were significant only for the largest latency tested (500.3 milliseconds). Mean latency ratings, on the other hand, indicated that a latency of 250.4 milliseconds was noticeable to the subjects.

Overall, subjects' localization strategies were only moderately affected by latency. Yawing motions, a method for disambiguating front from rear locations, remained the primary strategy for the listeners in all conditions. Pitching and rolling motions appear to be moderately inhibited by increased latency in the stimuli. Although the individual head-motion traces have not yet been examined in detail, it appears that the maximum angular velocities of the head motions (in particular, yaw) are similar to those observed in previous studies, for example, about 175 degrees per second.

Together with the results of previous studies, these data suggest that head motion provides powerful cues for localization of virtual sounds. These dynamic cues counteract many disrupting factors in the stimulus, including non-individualized HRTFs, conflicting interaural cues, and increased latency. The fact that accuracy was generally comparable for the shortest and longest latencies tested here suggests that listeners are largely able to ignore latency during active localization. Apparently, this is possible even though latencies of this magnitude produce an obvious spatial "slewing" of the sound source such that it is no longer stabilized in space as the head is reoriented. It may be that the localization task per se is not the most sensitive test of the effect of latency in a virtual audio system. Other tasks that are more directly dependent on temporal synchrony, such as tracking an auditory-visual virtual object, may be much more sensitive to latency effects. The latency rating data suggest that a discrimination paradigm, such as that used to measure minimum audible movement angles, may also be more likely to indicate changes in listeners behavior at lower latencies.

Point of Contact: E. Wenzel
(650) 604-6290
bwenzel@mail.arc.nasa.gov

Visual-Cue Use in Perspective Scenes During Manual Control

Barbara T. Sweet

Little is known about how humans extract information from a perspective scene, particularly for performing closed-loop manual control tasks. Examples of perspective scenes include computer-generated imagery (commonly used in simulators), camera images, and natural viewing of a scene (such as out the window of an aircraft). Manual control refers to activities in which the human makes nearly continuous adjustments to a controlled element (for example, aircraft) through a control inceptor (for example, joystick), in order to produce some desired outcome (for example, tracking or regulation).

A better understanding of how humans use information in a perspective scene can be important for several reasons. The content of a perspective scene is often a design choice. Airport and heliport markings constitute manipulation of perspective-scene content for real-world applications. Designers of simulators and associated databases for out-the-window scene generation make choices concerning scene content, complexity, and update rate. And designers of control systems for unmanned aerospace vehicles (UAVs) have choices to make concerning the field of view, resolution, dynamic range, and update rates of imaging technologies. Currently, decisions related to perspective-scene content are frequently made using an empirical approach in which multiple potential configurations are tested. Very little theoretical framework exists to enable designers to make informed a priori decisions in these types of applications.

The purpose of the research described herein was to advance the fundamental knowledge of this subject, and from there to develop a basic new tool to aid in the design of the most cogent perspective-scene content. The effort consisted of the development of a model of perspective-scene viewing in a manual control task. Several models were developed and validated in a series of experiments. In these experiments, participants were required to "hover" over ground planes with varying types of features present. The first figure shows an example scene used in the task. Various scene elements were manipulated, such as the number and layout of the lines, and the random placement of dots in some scenes. The control activity data of the operator performing the task were collected, and the results used to develop a model combined of perspective-scene viewing and manual control. This very simple model was shown

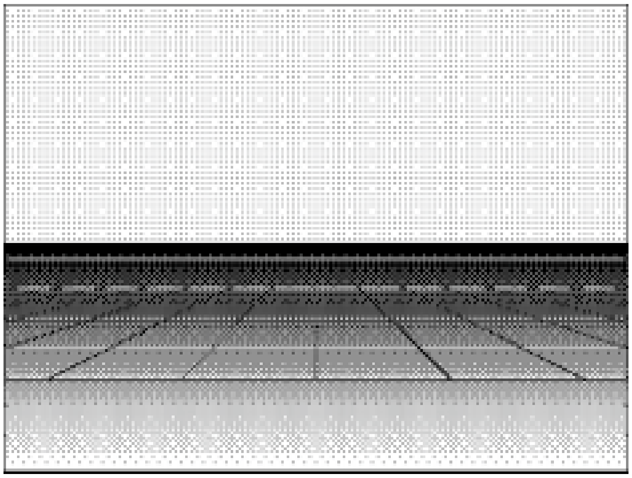

Fig. 1. Example of a scene used in task. Other scenes showed parts of this scene; for example, longitudinal lines only, or lateral lines only.

to accurately characterize the output of the human operator in most of the cases. The model is based on the assumption that two sources of visually derived information are used to formulate the control strategy: one source is related to position sensing and the other is related to direct sensing of velocity. The velocity-sensing capability is enhanced with more detailed picture elements, particularly when those elements are in the lower periphery of the display. The velocity sensing is also associated with better differentiation between pitch and longitudinal motion of the operators. An example of the model quality for one operator and condition is shown in the second figure.

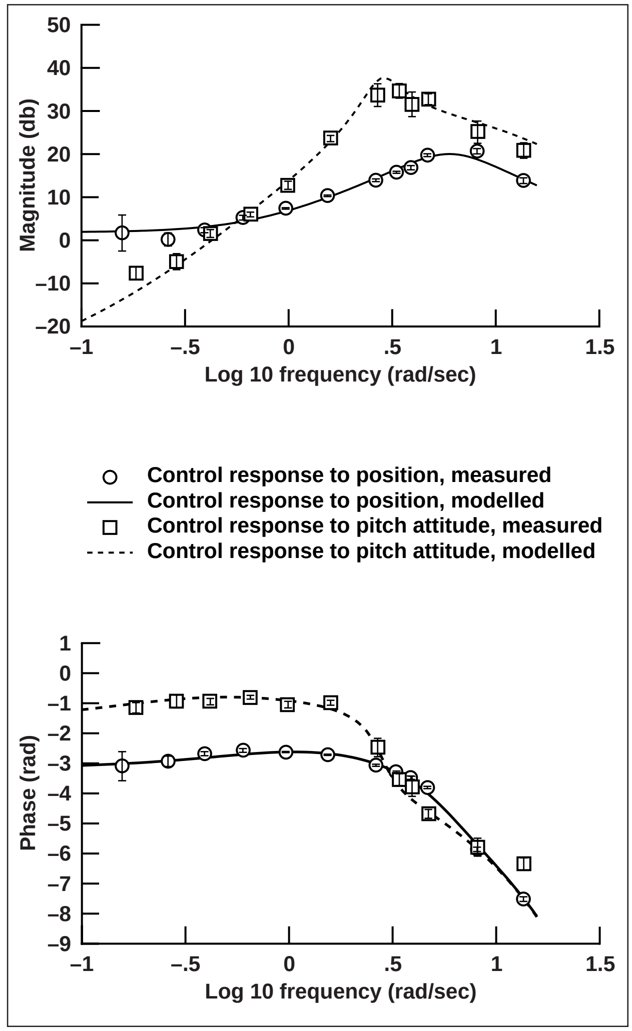

Fig. 2. Comparison of measurements and model for one operator and condition. Display used was similar to that shown in figure 1. Data points show the magnitude and phase of the operator's control response to longitudinal position (o) and pitch attitude (x); lines show the modelled response.

Point of Contact: B. Sweet
(650) 604-0006
bsweet@mail.arc.nasa.gov

A Neural Network Learning Model for Visual Discrimination

Albert J. Ahumada, Jr., Bettina L. Beard

As part of NASA's goal to improve aircraft safety and performance, Ames Research Center is developing models to predict a human observer's ability to detect visual targets. To detect a target in an unpredictable background, there must be a representation of the target in the observer's memory. In the models used here the memory representation consists of one or more templates, that is, visual system representations of the target. The observer must then compare the visual images with the templates to estimate the likelihood that a target is present in the image. Previous models of visual detection have assumed that these target templates do not change as the detection task proceeds. Here, a mathematical model of target detection has been developed in which the observer is assumed to learn, or refine, the target templates during the detection task.

A diagram of the detection model is shown in the figure. An image is presented to the observer, who forms a noisy visual representation of the image. That noisy representation is correlated with the memory templates, and the correlations form the basis of the observer's decision. Feedback about the correctness of the decision is then sent to the perceptual learning module to update the templates. The learning rules are essentially the same as those used in neural-network-supervised learning algorithms such as back propagation. The learning model developed here was able to predict the improved detection of targets in fixed pattern noise as compared with random noise. It also predicts the extremely poor performance of observers asked to detect targets at very low signal-to-noise ratios.

Point of Contact: A. Ahumada, Jr.
(650) 604-6257
aahumada@mail.arc.nasa.gov

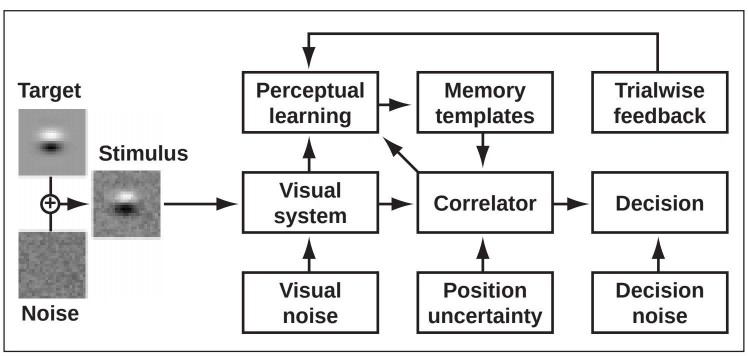

Fig. 1. Diagram of a visual target detection model with template learning.

GLOBAL CIVIL AVIATION / ENVIRONMENTAL COMPATIBILITY

Civil Tilt-Rotor Guidance Development for Noise Abatement

William A. Decker

Civil tilt-rotor transports have the potential to relieve the growing congestion around the nation's conventional airport runways. Operating as regional transports, civil tilt rotors can operate from airport vertipads, from short, unused runway segments, or directly from urban vertiports located near population and business centers. Safe, all-weather, low-noise terminal-area operations are needed to realize the tilt rotor's potential for improving the capacity of the air transportation system. Low-noise terminal-area operations that minimize airspace effects on conventional fixed-wing transport operations are expected to require complex flightpaths in order to work around runway airspace, obstructions, and noise sensitive areas.

Cockpit guidance for complex approach and landing operations has been under development for civil tilt-rotor transports in a series of flight simulation experiments. As shown in the central display area of the first figure, flightpath guidance is provided by a stylized "leader aircraft" symbol (winged diamond) that the pilot pursues with his own aircraft flightpath (shown with winged circle). Excellent tracking of the commanded flightpath has been achieved with this path-guidance design. Recent efforts have concentrated on speed guidance, crucial to the decelerating approach profile needed for steep final approaches and noise abatement. Speed guidance is provided via the command airspeed reference tab on the airspeed drum (left side of the display in the figure) and flight director symbols arrayed around the own-ship flightpath symbol for low-speed operation. A cue for movement of the thrust control lever was provided on the left "wing," and a pitch attitude director was provided on the right "wing." This pair of flight director elements was intended to guide a pilot through the control strategy shift required between airplane cruise operations and powered-lift, slow-speed approach operations.

In addition to developing appropriate guidance for the pilot "on-controls" for a tilt-rotor transport, second crewmember duties have been defined. The development of a large, side-by-side transport simulator cockpit, shown in the second figure, has made crew interactions more natural and typical of transport operations.

Fig. 1. Civil tilt-rotor primary flight display with flightpath vector path guidance.

Fig. 2. Two-seat transport simulator cockpit. Pilot's perspective on approach to an urban vertiport is shown.

Point of Contact: W. Decker
(650) 604-5362
bdecker@mail.arc.nasa.gov

Correlation Results of Blade-Vortex Interaction Noise

Cahit Kitaplioglu

An important source of rotorcraft noise is blade-vortex interaction (BVI) noise arising from unsteady pressure fluctuations on rotor-blade surfaces during encounters of the individual blades with the tip-vortex system of the rotor in forward flight. The objective of this work was to compare methods for predicting parallel BVI noise by using data from a specialized rotor test performed in the Ames 80- by 120-Foot Wind Tunnel. The test, illustrated in the figure, utilized a small-scale rotor interacting with a vortex generated by an upstream-mounted wing. This test configuration allowed independent control of the major parameters determining BVI noise.

An informal working group, with participants from industry, academia, and government, as well as from foreign countries, contributed a broad range of state-of-the-art results to compare with the experimental data. The aerodynamic models included computational fluid dynamics, as well as simpler analytical and boundary element methods to predict the unsteady rotor surface-pressure distributions. These were combined with several Acoustic Analogy and Kirchhoff methods to predict the far-field acoustics.

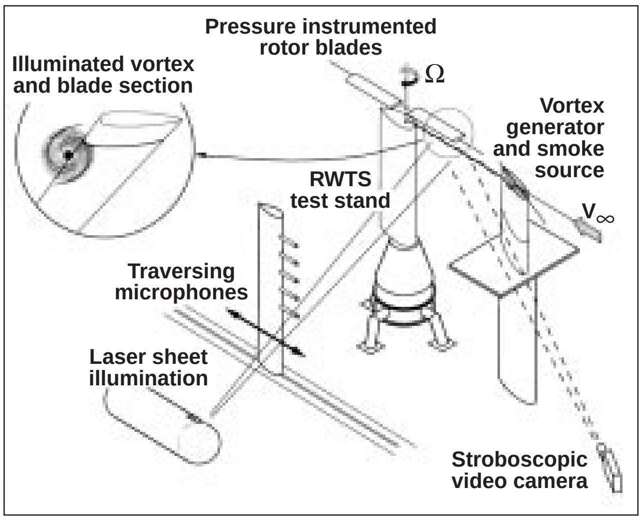

Fig. 1. Schematic of the blade-vortex interaction test in the Ames 80- by 120-Foot Wind Tunnel.

All methods predicted quite well the main aerodynamic feature of primary acoustic importance, namely, a large pressure jump as the vortex is encountered by the blade leading edge. Therefore, it is reasonable to expect good correlations with the acoustics as well. Nevertheless, important differences were observed between the various acoustic computations. Generally, excellent results were obtained with the Acoustic Analogy methods; a greater variability was noted among the Kirchhoff techniques. However, it should be emphasized that these observations relate to a situation in which there were no important nonlinearities, where the Acoustic Analogy is the method of choice. In cases with significant flow phenomena (higher speeds and the presence of surface shocks, for example), the Acoustic Analogy approach may reasonably be expected to break down and the Kirchhoff methods reveal a clear advantage.

Point of Contact: C. Kitaplioglu
(650) 604-6679
ckitaplioglu@mail.arc.nasa.gov

Aeroelastic Response of an Active Rotor

Mark V. Fulton, Robert A. Ormiston

High levels of fuselage vibration in rotorcraft cause various problems, including structural fatigue, increased maintenance costs, and passenger discomfort. Modern "smart" materials provide an opportunity for active, on-blade control to reduce vibration. A small-scale, two-bladed rotor with on-blade control surfaces (elevons) was previously tested in hover and in forward flight. That test demonstrated a significant reduction in the vibratory flap-bending moment harmonics. The objective of the current project was to study the acquired data for physical understanding through further data analysis and comparison with a simplified two-degree-of-freedom (2-DOF) analytical model and with the Second Generation Comprehensive Helicopter Analysis System (2GCHAS).

In the first figure, the active rotor is shown in the Ames 7- by 10-Foot Wind Tunnel. The model is a two-bladed, 7.5-foot-diameter rotor which was operated at reduced tip speeds. Each blade has one elevon which is actuated by two lead zirconate titanate (PZT) piezoceramic bimorphs. The effectiveness of the elevons was measured by performing both elevon frequency sweeps and elevon phase sweeps

Fig. 1. Rotor with on-blade elevons in the Ames 7- by 10-Foot Wind Tunnel.

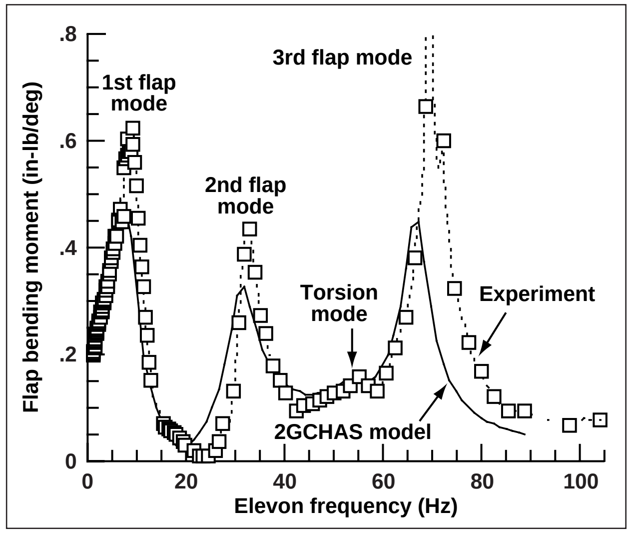

Fig. 2. Comparison of analytical results with experimental data, flap-bending moment frequency response function (FRF) magnitude in hover (425 rpm).

for five harmonics of the rotor speed (1/rev–5/rev) while recording the vibratory bending and torsion moments at the root of each blade. These tests were performed at various flight conditions, including low to moderate thrust levels, rotor speeds between 200 and 760 revolutions per minute (rpm), and several tunnel speeds. The experimental data showed a number of aeroelastic effects, including elevon reversal, which occurs when the lift due to elastic twist cancels the elevon direct lift.

Data analysis revealed a significant variation in elevon effectiveness with frequency, as well as significant differences between 450 and 760 rpm, both in hover and in forward flight. These variations in elevon effectiveness were principally caused by structural dynamics and dynamic pressure effects and were successfully captured by the 2GCHAS (for example, see the second figure). Besides the structural dynamic amplification effects apparent in figure 2, elevon reversal was also shown to play an important role at low frequencies. The 2-DOF model and the 2GCHAS verified, however, that the elevon remains effective at the higher frequencies typically associated with vibration control. It was also shown that wind-speed effects tend to be small except at low frequencies, where these effects can be understood in terms of elevon reversal. In summary, this project has provided an improved understanding of the physical mechanisms of on-blade rotor control and verified the validity of 2GCHAS.

Point of Contact: M. Fulton
(650) 604-0102
mfulton@mail.arc.nasa.gov

Prediction of Blade-Vortex Interaction for the HART Rotor

Joon W. Lim, Chee Tung, Yung H. Yu

Analytical predictions of blade-vortex interaction (BVI) air loads were compared with experimental data obtained from the Higher-harmonic-control Aeroacoustic Rotor Test (HART) program. Earlier studies had demonstrated poor correlation when information about the measured data was not used in the analysis. The same conclusion was reached in the present study. Since the experimental data supplies key information on the blade-vortex interaction wake data, an understanding of the source of this discrepancy was necessary. The ability to obtain good predictions with this HART model may produce significant progress in the ability to predict helicopter vibration and noise.

The HART model is a 40%, Mach-scaled wind-tunnel model of the hingeless BO-105 main rotor. The data included measurements of blade-surface-pressure distribution, blade deformation, acoustic signatures, and vortex-wake data during blade-vortex interactions with higher-harmonic pitch controls. Since blade air loads and noise are closely interrelated with wake geometry and blade aeroelastic deformation, this comprehensive database is extremely valuable for validating analytical prediction methods and for understanding noise and vibration characteristics with active blade pitch controls.

In this study, the HART data were analyzed using the Second Generation Comprehensive Helicopter Analysis System (2GCHAS). The 2GCHAS is an interdisciplinary comprehensive code that has been developed to integrate various analyses to provide analytical capabilities for rotorcraft analyses. Its structural analysis capability is based on a library of finite elements which includes nonlinear beam,

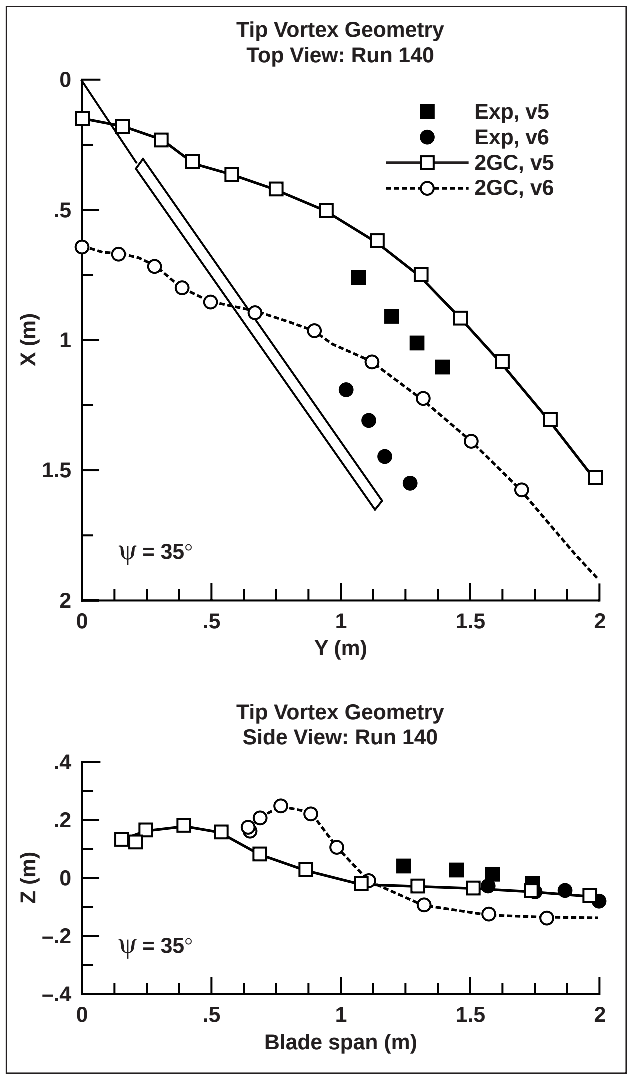

Fig. 1. The 2GCHAS prediction of tip-vortex geometry for HART rotor baseline case at an advance ratio of 0.15.

linear beam, and rigid-body mass elements. The figure shows the predicted and measured tip-vortex geometry (top and side views) at 35-degree azimuth. A significant blade-vortex interaction was anticipated around this azimuth angle. The tip-vortex geometries selected were those considered to be most influential on the rotor air load at the given azimuth. The 2GCHAS predictions were consistently located upstream by roughly 2 chords (top view), relative to the measured data. The predicted miss distances (side view) are larger than the measured data by about 1 chord length. A better understanding of this discrepancy and an improvement in the prediction will be pursued. In order to examine blade-vortex interaction more accurately, the FPX computational fluid dynamics code coupled with 2GCHAS will be used.

Point of Contact: J. Lim
(650) 604-5891
jwlim@mail.arc.nasa.gov

V-22 Tilt Rotor Aeroacoustics

Gloria K. Yamauchi, Larry A. Young, Jeffrey L. Johnson

The Tilt Rotor Aeroacoustic Model (TRAM) is composed of two hardware-compatible test rigs: an isolated rotor test stand and a full-span model (dual 0.25-scale V-22 rotors with a complete V-22 airframe representation). Both the isolated and full-span TRAM are key to NASA's Short Haul (Civil Tilt Rotor) program. The TRAM program is a joint effort between NASA, the U.S. Army, and industry. The isolated TRAM configuration was tested in the Duits-Nederlandse Windtunnel (DNW) during April-May 1998 by a team consisting of personnel from Ames, NASA Langley, and Boeing Helicopters (Mesa). The objectives of this test were to measure blade-vortex interaction (BVI) and broadband noise directivity, to measure blade surface pressures, to acquire wake geometry data and vortex strength data, and to measure tilt-rotor performance. A Short Haul (Civil Tilt Rotor) Level II milestone was achieved with the successful completion of the TRAM-DNW test.

The first figure shows the TRAM installed in the DNW open-jet test section. The TRAM rotor is three-bladed with a diameter of 9.5 feet. The rotor was operated at nominal tip speeds of 704 and 659 feet per second for operating conditions simulating helicopter mode and airplane mode, respectively.

Fig. 1. Isolated TRAM installed in the DNW; microphone array in foreground.

Fig. 2. Laser light sheet image of vortices.

The rotor angle of attack was changed by DNW sting actuation. Thus the rotor, rotor shaft, and nacelle were fixed relative to each other. The rotor was trimmed to nominal zero 1/rev flapping. Acoustic measurements were acquired using the DNW's microphone array which was traversed beneath the rotor. Blade air-loads data were acquired from 150 dynamic pressure transducers distributed between two of the three blades. Rotor performance was measured using a six-component rotor balance and an instrumented flex-coupling. Wake-geometry measurements were acquired using the laser light sheet technique; the vortex velocity field measurements were acquired using the particle image velocimetry technique. All flow measurements were acquired by the DNW. The second figure shows a cross section of several vortex filaments.

The data will primarily be used for code validation by NASA (for example, Langley's Tilt Rotor Aeroacoustic Code or TRAC) and U.S. industry. In addition, this data set is critical for the on-going preparations of the full-span TRAM program.

Point of Contact: G. Yamauchi
(650) 604-6719
gyamauchi@mail.arc.nasa.gov

Closed-Loop Optimal Neural-Network Controller to Optimize Rotorcraft Aeromechanical Behavior

Jane Anne Leyland

The predicted growth in air transportation has the potential to create significant market niches for rotary-wing subsonic vehicles. Technological advances that optimize rotorcraft aeromechanical behavior can contribute significantly to the commercial and military development of rotorcraft, and to their acceptance and sales. Examples of the optimization of rotorcraft aeromechanical behavior which are of interest include the minimization of vibration and the minimization of loads. The reduction of rotorcraft vibration and loads is important in extending the useful life of the vehicle and in improving its ride quality. Although vibration reduction can be accomplished by using passive dampers or tuned masses, active closed-loop control has the potential to reduce vibration and loads throughout a wider flight regime while imposing less additional weight on the aircraft than do passive methods.

Previous development and design of closed-loop controllers focused on the simple "standard" closed-loop controller which employed a linear plant model (that is, a single system matrix) to model the rotorcraft and simplified pseudo-optimal methods to determine the control. In a recent development, actual constrained optimization techniques were used rather than the commonly used pseudo-optimal methods to determine the optimal control subject to constraints for a linear plant model. The closed-loop optimal neural-network controller (first figure) which was developed during this research employs a nonlinear neural-network function (second figure) rather than a linear function to model the plant. Actual constrained optimization methods are used to determine or update the constants in the neural-network plant model, as well as in the determination of the optimal control vector.

Current data are read, weighted, and added to a sliding data window. When the specified maximum data window length (that is, the number of data sets allowed in the data window) is exceeded, the oldest data set is purged and the remaining data sets are re-weighted. This procedure provides at least four additional degrees of freedom in addition to the size and geometry of the neural-network itself with which to optimize the overall operation of the controller

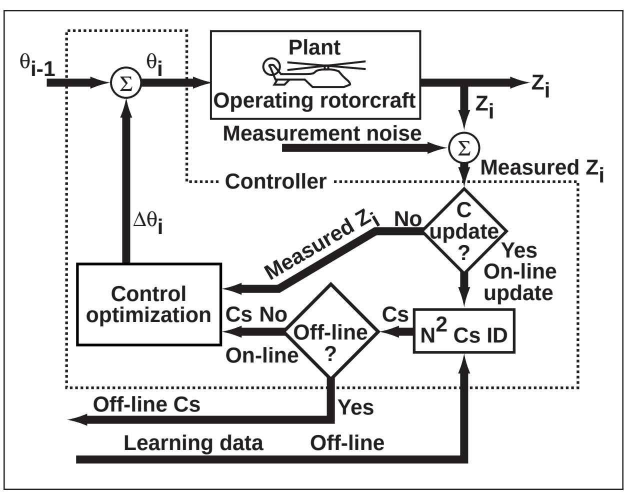

Fig. 1. Optimal closed-loop neural-network (N^2) controller.

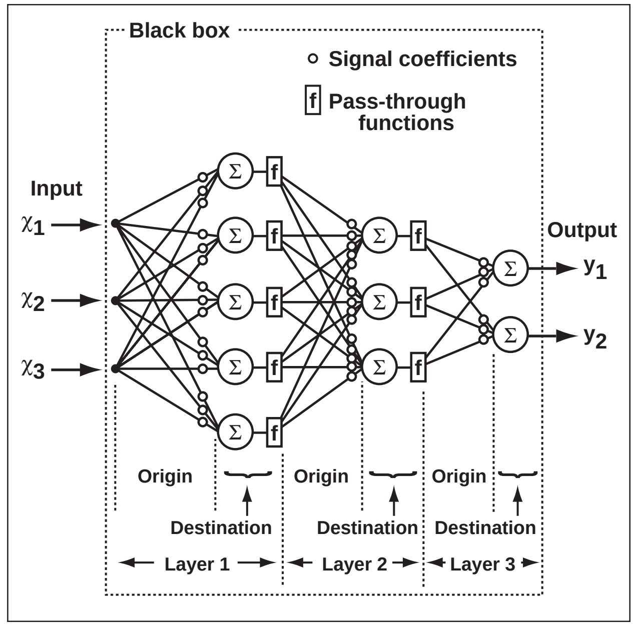

Fig. 2. Nonlinear neural-network function.

(that is, the update of the nonlinear neural-network function plant model and the determination of the optimal control). These four additional degrees of freedom are (1) the maximum length of the sliding data window, (2) the frequency of the neural-network updates, (3) the weighting of the individual data sets within the sliding window, and (4) the maximum number of optimization iterations used for the neural-network updates.

Point of Contact: K. Nguyen/W. Warmbrodt
(650) 604-5043/5642
knguyen@mail.arc.nasa.gov
wwarmbrodt@mail.arc.nasa.gov

Phased Microphone Array Technology: Flap Edge III Results

Paul Soderman, Bruce Storms

Phased microphone array technology (PMAT) is a high-speed, robust, single-axis 100-channel phased microphone array system for nonintrusive operation in wind tunnels. It is designed to provide calibrated noise source locations and levels generated by aircraft model components and assemblies during simultaneous aerodynamic and acoustic testing. Sound is transformed into color maps, and acoustic spectra are created for analysis.

The Flap Edge III program involved a wind-tunnel test in the Ames 7- by 10-Foot Wind Tunnel for the purpose of simulating and studying airframe noise. Airframe noise is an important component of landing noise, particularly for heavy aircraft operating at low engine power. The model used in the 7- by 10-foot tunnel is a small-scale, idealized section of a transport aircraft high-lift system. The objectives of program phases I and II were to investigate flap-edge noise, including source characterization, noise generation, and flow physics. Phase III (reported here) was actually designed to investigate slat noise on the same two-dimensional wing/flap/slat model mounted in the 7- by 10-foot tunnel as shown in the first figure. Also shown in the photo is the PMAT array microphone system mounted flush in the test-section sidewall. The array was designed to focus on the slat gap noise sources as various model parameters, such as Mach number, slat deflection angle (δ_s), and wing angle of attack (α), were varied. Slat noise control devices were also evaluated, and various flow diagnostic tools were used to measure the unsteady flow field in the slat region.

Fig. 1. Three-element high-lift system in the Ames 7- by 10-Foot Wind Tunnel between floor and ceiling end plates. The PMAT array is mounted in the sidewall.

The results of the slat noise experiment were as follows.

1. Tones were identified that scale to tones measured by Boeing from full-scale Boeing 777 transport aircraft flyovers.

2. The slat noise varied with Mach number to the fifth power as expected. Acoustic and fluid mechanic diagnostics suggest that the distributed source regions were located at the slat trailing edge.

3. A reduction in slat deflection caused a gradual reduction in slat noise.

4. Variation of slat noise with slat loading is nonlinear and does not have a simple dependence on trailing-edge velocity (see the second figure). It appears that the unsteady flow in the slat cove changes with loading in a complex way to generate noise. The data suggest that an aeroacoustic feedback mechanism between the slat trailing edge and unsteady cove flow or cusp separation or both is important.

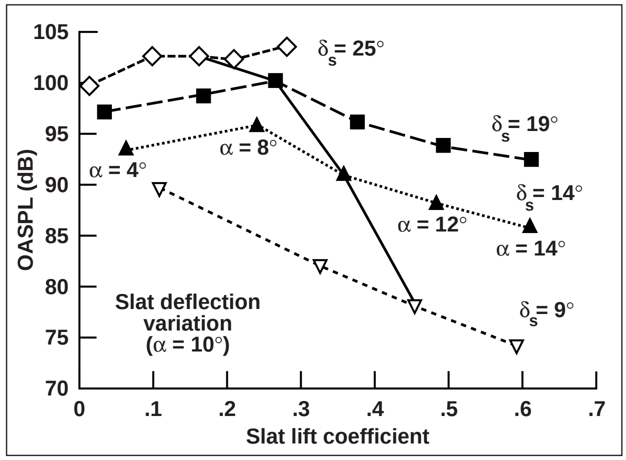

Fig. 2. Slat noise versus loading.

Point of Contact: P. Soderman
(650) 604-6675
psoderman@mail.arc.nasa.gov

Airline-Influenced Arrival Sequencing and Scheduling

Greg Carr, Heinz Erzberger, Frank Neuman

Air traffic control automation tools are used in arrival-flow management to assist controllers in efficiently matching traffic demand and airport capacity while minimizing delays. These tools use sequencing and scheduling algorithms to automatically plan the most efficient landing order (sequence) and landing times (schedule) for arriving aircraft. NASA and the Federal Aviation Administration (FAA) have designed and developed a suite of software decision-support tools (DSTs) for use in arrival flow management which is collectively known as the Center/TRACON Automation System (CTAS). The principle underlying the CTAS sequencing and scheduling algorithms is referred to as first-come-first served (FCFS). Although this principle generates fair schedules when delays must be absorbed, it does not take into account airline priorities among individual flights. The development of new arrival-flow management techniques that consider priorities expressed by air carriers will reduce the economic effect of Air Traffic Management (ATM) restrictions on the airlines, and will lead to increased airline economic efficiency by allowing airlines to have greater control over their individual arrival banks of aircraft. As part of the Collaborative Arrival Planning (CAP) research and development program, the Terminal Area ATM Branch is exploring the possibility of allowing airlines to express relative arrival priorities to ATM through the development of new CTAS sequencing and scheduling algorithms that take into account airline arrival preferences.

Two studies of airline-influenced sequencing and scheduling algorithms have been completed. Fast-time simulations were developed to evaluate the feasibility of new sequencing and scheduling algorithms that consider airline arrival preferences. The first study introduced the concept of a "delay exchange" as a fair method of accommodating an airline request for an earlier arrival for one of its aircraft when arrival traffic is being restricted using sequencing and scheduling algorithms. A delay exchange is performed by advancing the landing time of one aircraft while simultaneously delaying the landing time of another aircraft belonging to the same airline (see first figure). By requiring that any time gained by the advanced aircraft be offset by an equivalent amount of additional delay, a delay

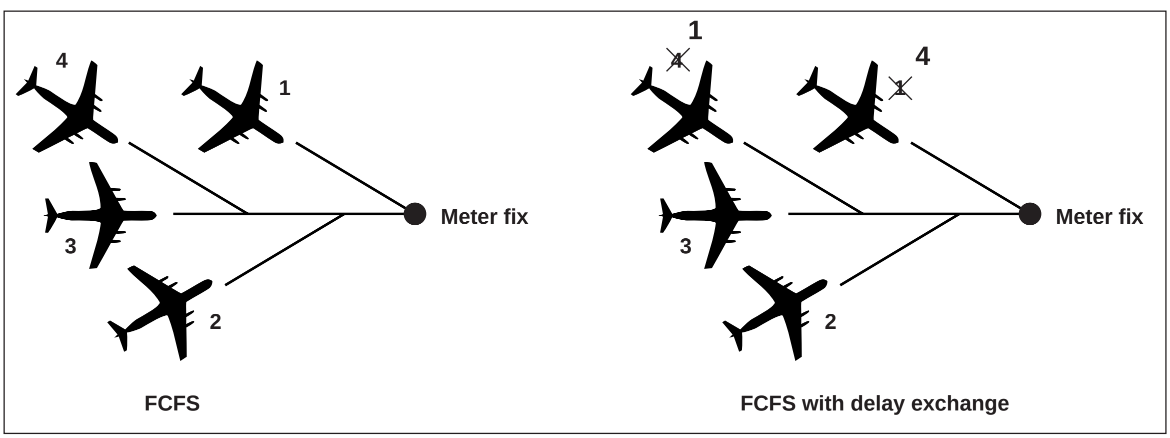

Fig. 1. Notional depiction of a delay exchange.

Preferred Order	FCFS Schedule	Priority Schedule
AAL1150 (1)	AAL1150 (1)	AAL1150 (1)
EGF628 (2)	AAL1934 (3)	AAL1934 (3)
AAL1934 (3)	AAL1428 (4)	EGF628 (2)
AAL1428 (4)	AAL1554 (5)	AAL1428 (4)
AAL1554 (5)	EGF628 (2)	AAL1554 (5)

Fig. 2. Priority scheduling example.

exchange does not affect the scheduled delays of any other arriving aircraft. Three different delay-exchange algorithms were implemented to evaluate the feasibility of performing delay exchanges in arrival sequencing and scheduling. Results showed that the most successful of the three delay-exchange algorithms yields an earlier time of arrival of 5 minutes or more approximately 25% of the time. Given that the delay-exchange algorithms were highly constrained to ensure fairness and scheduling efficiency, this is a conservative estimate of the success rate of a delay-exchange scheme.

Although the delay-exchange study focused on a method of accommodating an airline request for early arrival for a single aircraft, many airlines would like to be able to specify the arrival order of a group or "bank" of aircraft. The ability to specify the preferred arrival order within the user's own arrival bank is useful for maximizing bank integrity and minimizing bank time, that is, exchange of passengers/cargo, and aircraft servicing. The second study introduced the concept of "priority scheduling," a method of scheduling a bank of arrival aircraft according to a preferred order of arrival instead of according to an FCFS sequence based on estimated time of arrival at the runway. In order to minimize the effect on scheduling efficiency, only the bank aircraft are scheduled according to the preferred order of arrival; all remaining aircraft in an arrival rush are scheduled according to an FCFS sequence. A fast-time simulation was developed to evaluate the feasibility of this scheduling method in terms of scheduling efficiency. Results show that for the simulated traffic conditions, the priority scheduling algorithm results in a scheduled bank order that closely matches the preferred order of arrival (second figure). Results also show that when compared with FCFS scheduling, priority scheduling will, for certain traffic conditions, substantially reduce deviations from the preferred bank order while causing little or no decrease in scheduling efficiency.

These studies provide a starting point for evaluating the potential benefit of airline-influenced sequencing and scheduling algorithms.

Point of Contact: G. Carr
(650) 604-2545
gcarr@mail.arc.nasa.gov

Active Final Approach Spacing Tool

John E. Robinson

Today, in many highly congested terminal areas, air traffic controllers are forced to provide sub-optimal aircraft sequencing and spacing in order to maintain prescribed levels of flight safety. At Ames Research Center, NASA and the Federal Aviation Administration (FAA) are continuing to design, develop, and deploy a software-based decision-support tool (DST), called the Final Approach Spacing Tool (FAST), for terminal-area air traffic management and control of arriving aircraft. FAST incorporates advanced-knowledge engineering algorithms, accurate trajectory predictions, and specialized graphical user interfaces to provide detailed schedule and spacing information to air traffic managers and radar controllers. An early version of this DST, known as *Passive* FAST (pFAST), represented its minimal set of usable functionality. pFAST provides strategic (that is, passive) advisory information, namely runway assignments and relative landing orders. This information helps controllers to consistently balance the runway use of a congested, and otherwise unbalanced, airport. A future version of this DST, known as *Active* FAST (aFAST) will, in addition, provide tactical (that is, active) advisory information, namely heading, speed, and altitude commands. This research includes the development of advanced scheduling algorithms, the formulation of automated conflict-resolution schemes, and the definition of computer human interface requirements. This information will be used to further reduce excess in-trail separation between aircraft at touchdown to the runway.

The figure represents a mock-up of a proposed aFAST display. In this example, passive and active advisories are shown for two aircraft, AAL123 and UAL456. Both aircraft have runway assignment and sequence number advisories presented as blue flight datablock text. AAL123 is No. 3 to runway 17L, and UAL456 is No. 2 to runway 18R. In addition, both aircraft have heading and speed advisories presented as green flight datablock text and map graphics. AAL123 is instructed to turn to a heading of 270 degrees along the arc, and UAL456 is instructed to reduce its indicated airspeed to 190 knots at the splat.

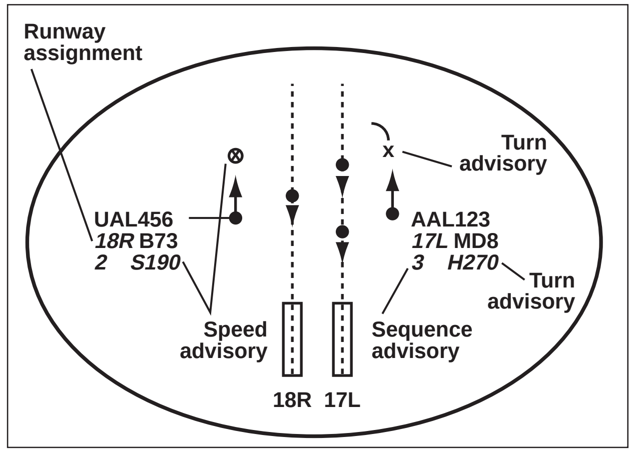

Fig. 1. Illustration of an aFAST display.

During FY98, a significant amount of the software infrastructure of aFAST's scheduling algorithm was redesigned and re-engineered. The new design addresses several key improvements noted during the deployment of pFAST and allows easier rapid prototyping of the scheduling and conflict-resolution algorithms of aFAST. Also, a method for determining the controller interface requirements for aFAST has been developed. This approach provides test subjects with active advisory information extracted from recorded traffic scenarios. Although these advisories represent the actual maneuvers executed by the aircraft during the scenario, the test subjects are instructed to respond as if the advisories were actually generated by aFAST. Thus, the real-time presentation of the recorded advisory data allows salient information about the controller interface requirements of aFAST to be gathered without requiring mature scheduling or conflict-resolution algorithms. As the first step in a series of controller interface experiments, this approach will be used to investigate the presentation attributes (that is, color, size, shape, and timing) of active advisory information for the terminal-area radar controller. The baseline traffic scenarios to be used for these human factors simulations were collected in December 1998.

Point of Contact: J. Robinson
(650) 604-0873
jrobinson@mail.arc.nasa.gov

Integration of Conflict Probe with Arrival Metering

Dave McNally

A common traffic scenario in transition airspace near major airports involves the merging of two or three streams of arrivals descending from cruise altitude and speed and to an en route-to-terminal-area transition point at an altitude of 10,000 feet and at a speed of 250 knots. Overflight traffic in cruise and climbing departure traffic pass through the same airspace. If the airport is capacity-constrained, as is typical during arrival rush periods or adverse weather conditions, controllers must meter the arrival flow so airport capacity is approximately utilized but not exceeded. The combined separation and metering problem in transition airspace can be very workload intensive and the automation aides are limited. Aircraft are often descended early for conflict-resolution and then given large vectors or put into holding patterns to meet metering constraints.

The Center/TRACON Automation System (CTAS) is an integrated set of tools that provide information and advisories to assist in the planning and control of traffic within several hundred miles of the airport. CTAS tools are based on accurate prediction of aircraft four-dimensional trajectory (space and time) using aircraft flight plans and radar data, wind predictions, and aircraft performance models. The Traffic Management Advisor (TMA) computes arrival sequence and metering information that helps controllers maintain efficient traffic flow during periods when arrival metering is required. The Descent Advisor (DA), originally developed in the 1992–1995 period, assists controllers by providing fuel-efficient, conflict-free descent clearance advisories that conform to TMA metering constraints. However, the DA was not fully developed, because only arrival data were available from the Federal Aviation Administration (FAA) host computer during initial development and testing. All-track (arrival, overflight, departure) data became available in 1996; and the DA trajectory prediction, conflict prediction, and trial planning capabilities were enhanced for all-track analysis and field tested at Denver Center in 1997. The trial planning capability was well accepted by controllers and provided measurable user (aircraft operator) benefit in en route airspace. The trial planner allows the controller to interactively build and conflict-check a “what if” trajectory through point and click, menu-based manipulation of the flight data tag on the traffic display. The goal of this research was to evaluate the trial planning capability integrated with conflict and metering information to assist controllers in transition airspace where there is a mix of climbing, descending, and overflight aircraft in cruise flight.

The trial planner was integrated with the TMA allowing the controller to simultaneously evaluate the separation and metering status of a trial plan trajectory. Controller-in-the-loop simulations were conducted in April and July 1998. Ft. Worth Center traffic scenarios were developed that combined metered arrivals with overflight and departure traffic. The trial planner was well accepted as a strategic tool for routing climbing and overflight traffic around arrival airspace but was not usable for the arrival-metering problem that is typical during an arrival rush at Ft. Worth Center. Controllers are too busy to operate the trial planner during metering. The first figure shows a predicted conflict between a metered arrival (AAL1059) and an overflight aircraft in cruise (N650KC). Using the trial planner, the user quickly determines that a direct route to Tulsa (yellow route) for N650KC solves the conflict, gives N650KC a short cut, and keeps AAL1059 on a fuel-efficient descent profile. The graphic display also shows the top-of-descent point for a 280-knot minimum-fuel descent to the meter fix for AAL1059. Results suggest that automatic advisories could benefit arrival metering and other transition traffic problems. The following comment characterizes controller feedback: "You (CTAS) know the solution, just give it to me, don't make me try all the options." Altitude advisories were integrated into the altitude trial planning function to give immediate feedback on separation status for a climb or descent to any altitude. The system was tested in shadow mode on the operational floor at

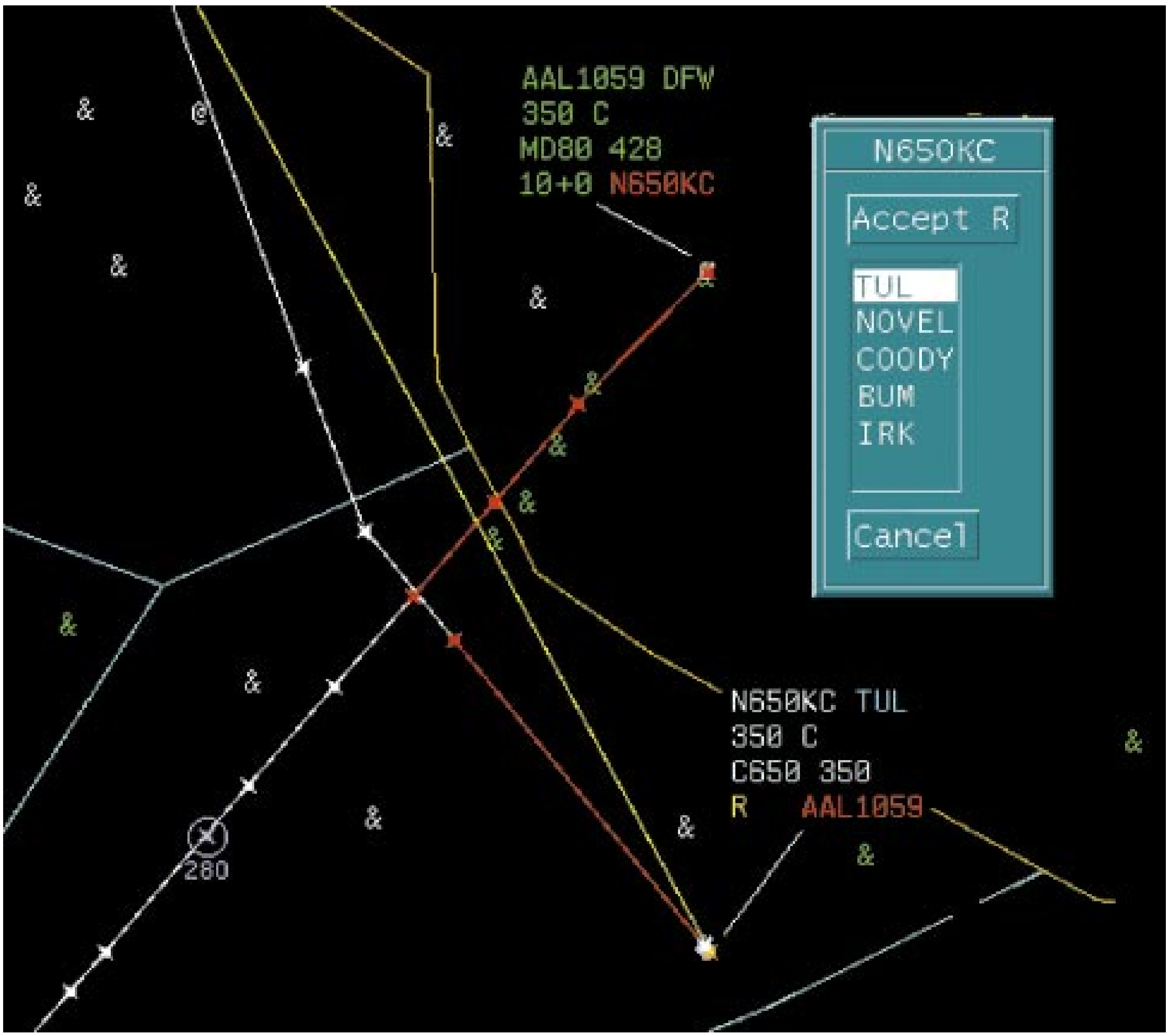

Fig. 1. Trial planner facilitates direct routing for overflight and minimum-fuel descent for arrival.

Fig. 2. Integrated conflict probe, trial planner, TMA system during Ft. Worth Center Field Evaluation, November 1998.

Ft. Worth Center in November 1998 (second figure). Six full-performance-level controllers participated in the evaluation. It was found that trajectory prediction for climbing aircraft needs to be improved. Field results confirm that manual trial planning, that is, without advisories, is not workable for arrival metering. Clearance advisory information needs to be fully integrated into the radar controller's display for usability in transition airspace traffic management.

Point of Contact: D. McNally
(650) 604-5440
dmcnally@mail.arc.nasa.gov

Empirical Test of Conflict Probability Estimation

Russell A. Paielli

The efficiency of air traffic management (ATM) is enhanced by a conflict-probe that predicts future conflicts as early as possible. Early prediction of a potential conflict enables its more efficient resolution; however, early prediction also lessens the certainty that the conflict will actually occur. In earlier work, a stochastic method called conflict probability estimation (CPE) was developed to help determine the best time to alert air traffic controllers of a potential conflict. In that earlier work, the CPE algorithm was successfully tested by simulation. It was then integrated into the Center/TRACON Automation System (CTAS), but it is general enough to be used in any other ATM decision-support system with a conflict probe. The primary objective of the current work was to empirically test the accuracy of the CPE procedure with real air traffic data for level flight.

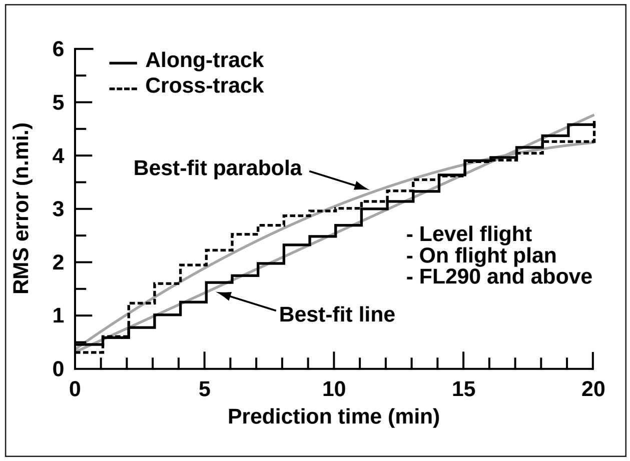

Fig. 1. Prediction error vs. prediction time.

A preliminary step in testing the accuracy of the CPE procedure was to test the accuracy of the trajectory-prediction error model on which it is based. The trajectory predictions for this study came from CTAS. The figure is a plot of the empirically determined root-mean-square (rms) errors for the along-track and cross-track axes in 1-minute increments of prediction time from 0 to 20 minutes. The along-track rms error grew linearly with prediction time for the first 20 minutes, as expected; the cross-track rms error grew roughly as the square root of prediction time for the first 20 minutes. Although not shown here, the distribution of the trajectory prediction errors was found to be remarkably close to Gaussian, hence the Gaussian error model was validated.

The overall accuracy of the CPE procedure is summarized in the table for three equal ranges of conflict probability above 40%. The second column shows the statistically expected conflict rate based on the CPE algorithm itself (it is simply the average of the computed conflict probabilities). The third column

Table 1. Summary of CPE test results based on real air traffic data.

Probability range, %	Expected, %	Actual, %	Difference, %
40–60	49	44	–5
60–80	70	70	0
80–100	89	93	4

shows the actual conflict rate, and the last column gives the difference. The largest magnitude of the three differences is only 5%, which is more than adequate. Although not shown here, the results were also categorized according to prediction time and path-crossing angle. As expected, the accuracy degrades with increasing prediction time and with smaller path-crossing angle.

The CPE algorithm has been generalized to nonlevel flight; it will eventually be tested empirically for nonlevel flight. Conflict-probability estimation is currently being applied to the problem of optimal conflict resolution, to help determine both when and how to optimally resolve conflicts.

Point of Contact: R. Paielli
(650) 604-5454
rpaielli@mail.arc.nasa.gov

Method for Conflict Probe-Performance Evaluation

Karl D. Bilimoria

A conflict probe is an air traffic management tool that can predict conflicts well in advance, using information about aircraft position, speed, and flight plans, along with forecasts of wind and temperature profiles. Strategic (early) resolution of conflicts has the potential to reduce the cost associated with conflict-resolution maneuvers. Such a tool would be especially useful in a “free flight” environment, which is expected to have a less structured traffic flow than the current operating environment.

The objective of this research is to develop a comprehensive method for quantitatively evaluating the performance of any conflict probe, and to apply it to the Center/TRACON Automation System (CTAS) Conflict Probe Tool developed at the Ames Research Center.

Such a method has been developed over the course of this work. The method is generic, and can be applied to any conflict probe. It can therefore provide a framework for a comparative study of conflict probes. A key feature of this method is the use of real traffic data and expanded separation criteria. It has been established that the characteristic properties of vertically offset pseudoconflicts approximate those of operational conflicts. Therefore, the performance of a conflict probe using a vertically offset pseudoconflict window is indicative of its performance using an operational conflict window. Rates of missed alerts and false alerts (first figure) are

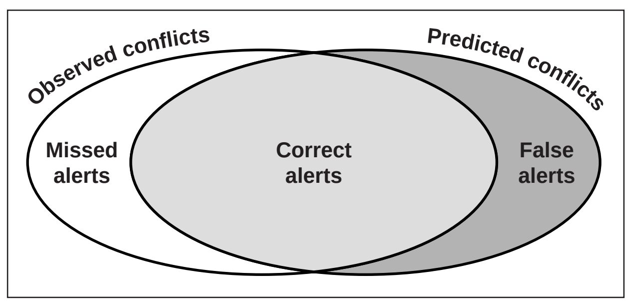

Fig. 1. Conceptual definition of missed alerts and false alerts.

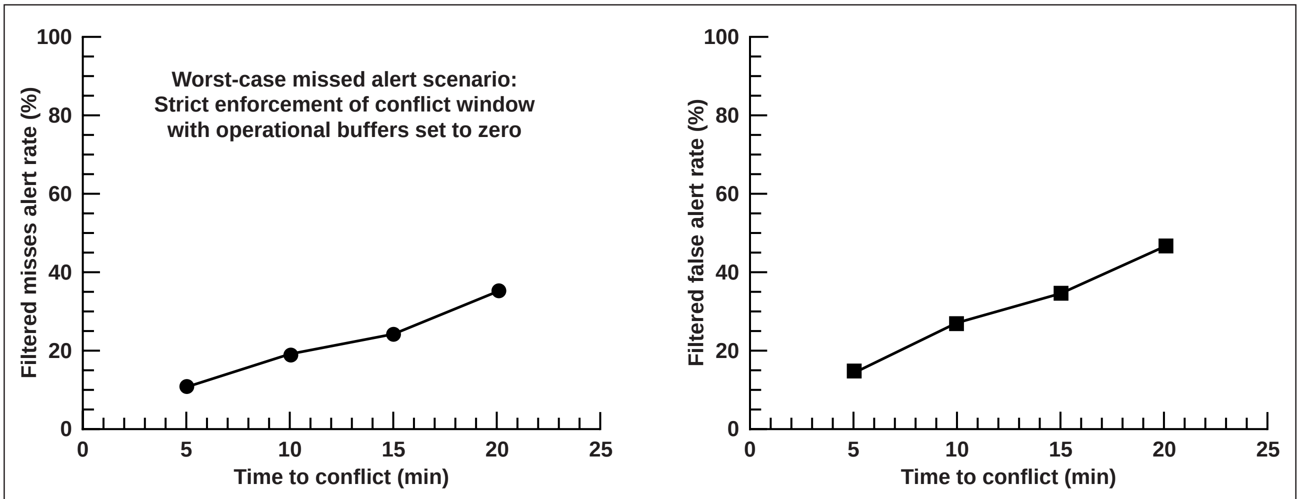

Fig. 2. Example of filtered (good flight-intent information) rates of missed and false alerts for the CTAS conflict probe tool.

primary metrics of conflict probe performance. Work is under way to validate the evaluation method developed in this work by applying it to the CTAS Conflict Probe Tool, using real traffic data from the Denver Center. The second figure shows preliminary results on missed and false alert rates for the "filtered" category of conflicts, that is, for conflicts characterized by good flight-intent information.

Point of Contact: K. Bilimoria
(650) 604-1638
kbilimoria@mail.arc.nasa.gov

En Route Wind Prediction for Conflict Probe and Airline Flight Planning

Steven M. Green

Air Traffic Management (ATM) Decision Support Tools (DSTs), such as the Center/TRACON Automation System (CTAS), help controllers reduce delays and fuel consumption. The quality of ATM/DST advisories, and airline flight planning, depend on the accuracy of flight-path (trajectory) predictions. Flight testing of CTAS predictions has revealed that wind-prediction errors are a major source of trajectory-prediction error and that they can exceed 20–50 knots along individual trajectories. ATM/DST functions, for conflict prediction and resolution, are not only sensitive to the "aggregate" wind accuracy, but also to "large" errors (that is, errors greater than 20 knots) that may occur over regions of airspace. Past wind-prediction accuracy studies have focused primarily on metrics that are of interest to the meteorologists, metrics such as "aggregate" root-mean-square error over a large airspace and time period. Little information has been gathered on other metrics of importance to ATM, particularly with respect to large errors. The objectives of this effort are to develop methods to improve wind-prediction accuracy (such as near real-time use of the latest aircraft-measured winds); and to conduct a statistically significant measurement of wind-prediction accuracy based on key metrics for ATM (for example, large errors).

To combine ATM and meteorological research expertise, Ames coordinated a joint study with the National Oceanographic and Atmospheric Administration (NOAA) and the MIT Lincoln Laboratories (MITLL). Winds-aloft data (predicted and measured) were collected for a 13-month period over Denver Center airspace. United Airlines voluntarily increased automatic reports of aircraft-measured winds for this test.

NOAA evaluated its experimental upgrade to the Rapid Update Cycle (RUC), with improved modeling and update rate compared with the operational RUC I. RUC II reduced the overall root-mean-square wind error by 22% (2.4 knots) and significantly reduced large errors. The first figure illustrates the percentage reduction in large errors over the test period. The performance varied greatly with season, but on average, RUC II reduced the percentage of large errors from 8% (RUC I) to 5%.

The MITLL developed and evaluated an experimental algorithm to correct RUC predictions (in near-real time) based on the latest aircraft-measured winds between RUC cycles (3 hours for RUC I). Compared with RUC I, the MITLL system reduced the overall root-mean-square wind error by about 25% while also reducing the large errors. The MITLL evaluated large errors with a slightly different metric, namely, the percentage of hours (over the test period) for which the hourly root-mean-square error exceeded 20 knots. Compared with RUC I, the MITLL system reduced the percentage of large-error hours from 11% to 4%. In the second figure, the entire set of data is combined to illustrate the cumulative probability of the 75th percentile (that is, the probability that 75% of the wind errors, over any given hour, are less than a certain speed). For example, RUC I had an 88% probability that its hourly errors were less than 20 knots, whereas the MITLL system (noted as TW) had a 97% probability.

Other analyses were also conducted to determine how the wind-prediction accuracy varied with the weather regime (for example, thunderstorms), wind speed, altitude, and the density of aircraft reports. Detailed results of the studies were published in technical reports by each laboratory and are available through NASA.

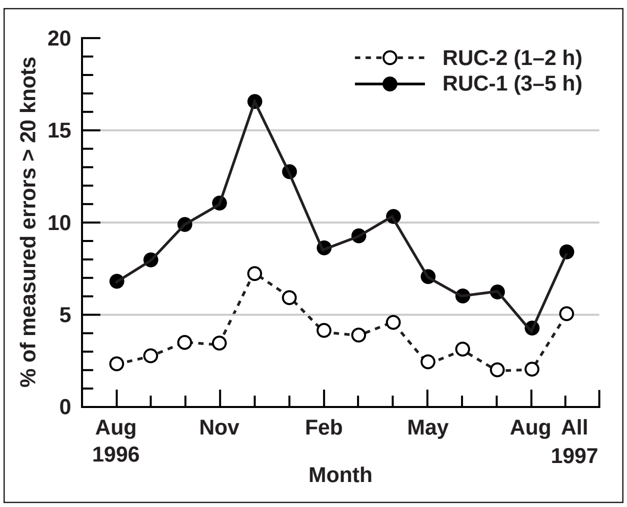

Fig. 1. Large errors for each month.

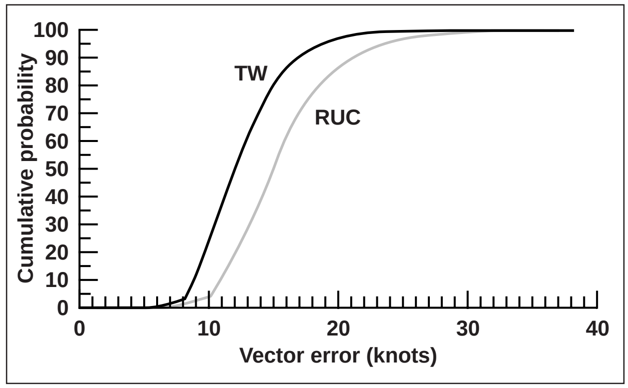

Fig. 2. Cumulative probability of hourly 75% error.

Point of Contact: S. Green
(650) 604-5431
sgreen@mail.arc.nasa.gov

Integration of CTAS and ETMS

Ronald J. Reisman, James R. Murphy

The FAA Traffic Management Units (TMUs) use the Enhanced Traffic Management Systems (ETMS) developed by the Volpe Transportation Laboratory. Air traffic control (ATC) data from all U.S. and Canadian Air Route Traffic Control Centers (ARTCCs), as well as British transatlantic radar-track data are transmitted to the Volpe laboratory. The data are processed and redistributed to approximately 85 ATC facilities throughout the United States, Canada, and Great Britain. The ETMS provides near-real-time position information of almost all aircraft in U.S. and transatlantic airspace. The TMUs visualize the data on aircraft situation displays which provide a number of predictive tools (for example, monitoring en route flow, sector overloading). The Center TRACON Automation System (CTAS) currently relies on aircraft position data from a single ARTCC and TRACON enabling its time and spatial conflict-free scheduling, visualization, and control capability. Though this is acceptable for the deployment of the CTAS tools for the FAA's Free Flight Phase 1 effort, the development of a multifacility (multiple ARTCC) CTAS has long been requested as a major enhancement to CTAS.

The goals of the CTAS- ETMS integration are (1) to analyze the benefits of a CTAS system driven by ETM-derived radar track data, and (2) to provide researchers the capability to use radar track data for aircraft that are physically outside a single ARTCC for the Advanced Air Transportation Technologies project extensions to CTAS.

During FY98, substantial integration of ETMS data with CTAS has been accomplished, enabling researchers to use track data for aircraft that are physically outside the area covered by a single ARTCC. CTAS has used the ETMS data to generate estimated times of arrival (ETAs) for aircraft untracked by an ARTCC, and presents clear benefits over the current reliance on ETA predictions derived from the current ARTCC flight-plan coordination-fix/time fields. The analysis shows an average decrease in ETA uncertainty of 2 minutes for these external ARTCC aircraft. Recently, the system has been used to demonstrate the capability to provide CTAS with aircraft arriving at Philadelphia International Airport, providing a virtual multicenter TMA.

The current method is to transfer ETMS Map and Route files to a CTAS Sun workstation via a shell script (first figure). These files are then processed by the ETMS Data Acquisition Router (EDR) process, which parses the ETMS files, formats the information into CTAS data-structures, and transmits the data to a standard CTAS suite. Radar data from the host may be mosaiced with the ETMS data, such that aircraft positions outside the ARTCC are supplied by ETMS, and positions inside are provided by the higher-resolution host radar (second figure).

CTAS is capable of generating ETAs for both ETMS and host tracks, displaying the derived data on standard TMA timeline and plan view displays. A variety of analyses performed on the data demonstrate the integrity and robustness of this method.

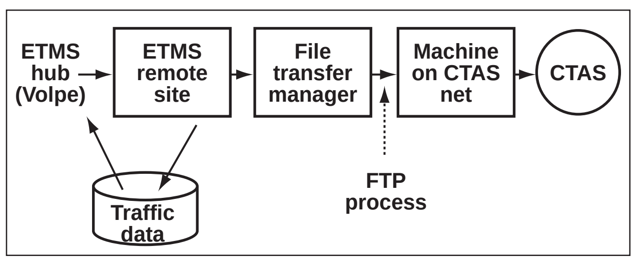

Fig. 1. ETMS to CTAS data flow: The ETMS hub at Volpe Transportation Laboratory sends air traffic data to the ETMS remote site, which creates data files. These files are transferred via FTP to workstations on the CTAS network. These files are parsed, and the filtered data are sent to a CTAS system.

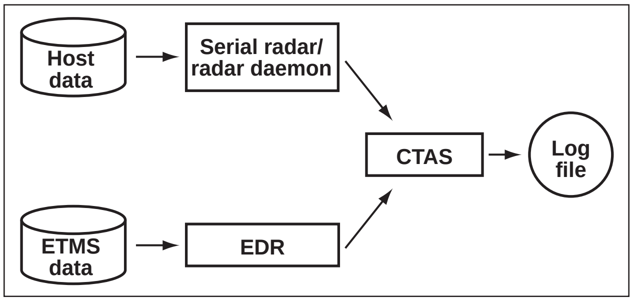

Fig. 2. Air traffic mosaic scheme: Radar data from an Air Route Traffic Control Center (ARTCC) host computer (12-second updates) are processed by the CTAS radar processing software. The ETMS traffic data (1-minute updates) are processed by the ETMS Data Acquisition Router (EDR). CTAS mosaics these two sources, so that data outside the ARTCC boundary are supplied by ETMS, whereas the host supplies data for aircraft under ARTCC radar coverage.

In addition to this demonstrable quantitative advantage, there are several qualitative improvements, such as the ability to visualize the stream of arrival traffic outside the center-boundaries on CTAS tools. Although the current method of integration suffers from data transfer and robustness problems, work is proceeding with Volpe, the MIT Lincoln Laboratories, and Computer Science Corp. to address those problems.

Point of Contact: R. Reisman
(650) 604-1459
rreisman@mail.arc.nasa.gov

CTAS Technology Transfer at NTX

Shawn A. Engelland

The NASA/Federal Aviation Administration (FAA) North Texas Research Station (NTX) was established to support the evaluation of advanced air traffic management decision-support tools, such as the Center/TRACON Automation System (CTAS), in an operational environment. As illustrated in the figure, NTX currently has CTAS installations at the Fort Worth Air Route Traffic Control Center (ARTCC), Dallas/Fort Worth (DFW) Terminal Radar Approach Control (TRACON), DFW Air Traffic Control Towers, and American Airlines System Operations Control. Successful field evaluations of the Traffic Management Advisor (TMA) and passive Final Approach Spacing Tool (pFAST) led the FAA to place these CTAS prototype tools into regular daily use at Fort Worth ARTCC and DFW TRACON.

Operational use of the TMA and pFAST prototypes at NTX provides Ames Research Center with a unique opportunity to collect long-term data on these tools in one of the world's busiest and most complex airspace environments. Additionally, TMA and pFAST prototype operations provide the FAA with the experience essential to successful national deployment of CTAS. A primary objective of these prototype operations was for the FAA to assume full responsibility for the maintenance and technical support of the daily-use TMA and pFAST systems.

Responsibility for TMA and pFAST daily-use operations has been transferred from NASA to the FAA following a three-phased strategy. In the initial phase (10/96–9/97), daily-use support was provided entirely by NASA researchers, software developers, and NTX personnel. In the second phase (10/97–4/98), support was provided by a NASA-directed team of engineers at NTX reporting to the FAA Liaison Office at Ames. Now in the third and final phase, the NTX daily-use support team is self-directed and reports to the FAA's Free Flight Phase 1 Program Office.

Ames personnel at NTX continue to collect data on the operational performance of the TMA and

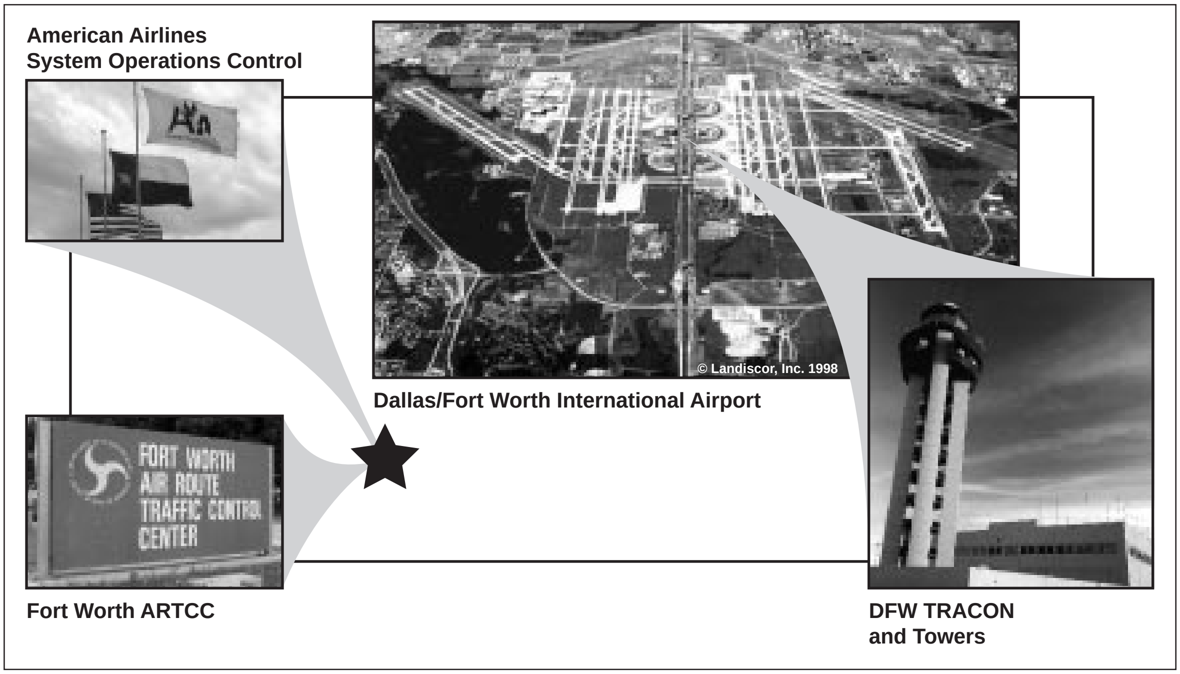

Fig. 1. CTAS installations at the NASA/FAA North Texas Research Station.

pFAST tools. Of particular interest is the performance of these tools in off-nominal environmental conditions. Additionally, NTX continues to be the focal point for field evaluations of CTAS follow-on tools. A long-term evaluation of the Collaborative Arrival Planning display system is under way at American Airlines, and field evaluations of the En Route/Descent Advisor tool were recently conducted at Fort Worth ARTCC.

Point of Contact: S. Engelland
(650) 604-7634
sengelland@mail.arc.nasa.gov

Human Factors Evaluation of An Advanced Decision-Aid for Air Traffic Control

Nancy Smith, Larry Arend, Shon Grabbe, Thomas Prevot, Stephen Shelden

A field evaluation of the En Route/Descent Advisor (E/DA) component of the Center/TRACON Automation System (CTAS) was conducted at the Fort Worth Air Traffic Control Center (ZFW). The E/DA provides predictive and advisory information to assist the Center controller in maintaining separation between aircraft-pairs, and in managing arrival and departure traffic. An example of the E/DA's display of conflict-prediction, arrival metering, and trial planning information is shown in the figure. The two primary human factors objectives of the E/DA field evaluation were (1) to evaluate the usability and suitability of its interface to the task environment, and (2) to explore how the information it provides might affect communication and coordination among controllers.

During the field evaluation, the E/DA was used in "shadow mode" by sector-qualified air traffic controllers at three different sector positions on the control room floor at ZFW, providing controllers and researchers an excellent opportunity to assess its potential value and its suitability to the task environment.

Results from the study indicated that test controllers benefited from the predictive information provided by the E/DA, frequently using it with the radar display to improve their understanding of current traffic. This, coupled with other observations of the controllers' use of trial planning and advisory information, suggests that the E/DA should be an integrated part of the radar controller's display. For example, the E/DA was often used by controllers to monitor predicted separation between aircraft; if readily available to the radar controller, this information could reduce the number of traffic-related route-deviation clearances.

Future integration of E/DA into the radar controller's workstation will require significant modifications in three different areas: (1) information must be appropriately integrated into the traffic display, (2) user interactions must be streamlined, and (3) functionality must be compatible with the FAA's new Display System Replacement hardware upgrade. A review of the E/DA interface is under way, along with research into radar controller use of currently displayed information. Interface modifications will then be made and tested in a simulation that emulates as closely as possible the target system configuration.

Point of Contact: N. Smith
(650) 604-3744
nsmith@mail.arc.nasa.gov

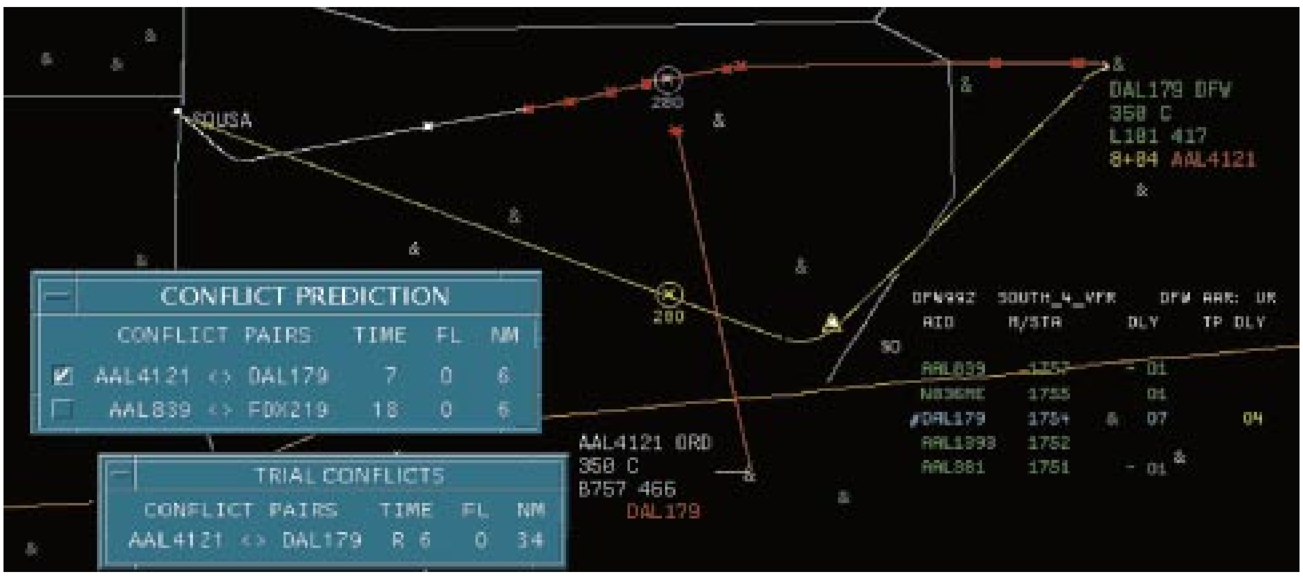

Fig. 1. Sample E/DA display. DAL179's trial planned route (shown in yellow) absorbs 3 minutes of a metered 7-minute delay, and resolves predicted conflict with ASL4121. Conflict resolution is indicated by "Trial Conflicts" list display of 35-nautical-mile predicted minimum separation.

A New Flight Management System Capability

Matthew Blake

In order to accommodate advanced research in cockpit systems, the Advanced Concepts Flight Simulator (ACFS) utilizes a software-programmable Flight Management System (FMS) rather than aircraft hardware. A 2-year project to significantly improve the FMS was completed this year. The system is believed to be unique in the world in terms of the data-link capabilities and the programmable flexibility required for advanced airspace operations and automation research.

Modern commercial transport aircraft are equipped with an on-board FMS, an extremely complex computational system. The FMS can be programmed to fly complete routes anywhere in the world. Because of the extreme complexity of these systems, most commercial transport aircraft simulators use actual FMS hardware from the aircraft, and that hardware cannot be modified for research purposes. Nonetheless, the complexity of a modern FMS and its often cumbersome interface give rise to many human-factors research issues that pertain to efficient and safe operations.

To address these problems, the ACFS was fitted with a software-programmable FMS that was originally developed by Boeing for its engineering flight simulator. To meet Ames's requirements, the system was modified by an integrated product team of personnel from the simulation facilities and from the primary research organization. The modified FMS was integrated into the ACFS this year and is being used for the CTAS-FMS Datalink experiment. This same system is available to the Ames research community for use in a desktop environment called the Mini-ACFS.

Fig. 1. An enhanced, software-programmable FMS was integrated into the Advanced Concepts Flight Simulator. This type of system enables an integration between ground and airborne air traffic management systems.

Most of the basic functions available in a state-of-the-art commercial FMS are also available in this research version. Most of the advanced features relate to airborne data link and its interface with ground-based air traffic management systems, specifically the Center/TRACON Automation System (CTAS). The system provides the capability to transmit a descent clearance from CTAS directly into the FMS, which then automatically modifies the flight plan with the clearance route. This capability to link directly into the FMS and modify the flight plan is unique in the world. An additional benefit of the software-programmable FMS is the ability to collect data on how the FMS performs internally and how the crew interacts with it. Much of this information cannot be collected from experiments utilizing flight hardware for the FMS function. In the future, the FMS will continue to be enhanced as needed to support the specific research goals of the airspace capacity, safety, and base research efforts at Ames.

Point of Contact: M. Blake
(650) 604-1795
mblake@mail.arc.nasa.gov

Civil Tilt-Rotor Procedures Study in MIDAS

Adolph Atencio, Jr.

The civil tilt rotor is moving toward its introduction into the national airspace. The civil tilt rotor has the unique capability to deliver passengers along current traffic lanes as a turboprop and to then convert to rotorcraft mode by tilting the nacelles in the terminal area allowing for noninterfering landing approaches to the airport or nearby vertiports. This unique design can help off-load congested terminal-area airspace and address capacity problems at major hub airports.

Current studies have concentrated on the approach to vertiports where both noise and obstacle avoidance are important considerations. In these studies, a steep approach along a 9-degree glide slope and simulated global positioning satellite (GPS) guidance for the final approach to the vertiport have been used. A finding of these studies performed in man-in-the-loop simulations at Ames Research Center is that the workload of the pilot is relatively high during the approach. The need for further definition of the tasks and workload requirements led to the use of the human factors analysis system called MIDAS (Man-machine Integration Design and Analysis System).

A scenario was designed in MIDAS for the final approach to a vertiport along the 9-degree glide slope. The scenario included a commanded go-around close to the landing decision point in order to compare an automated discrete nacelle-movement system to control aircraft speed and climb-out with a manual nacelle-movement approach for the same tasks. The MIDAS simulation also added limited communication tasks to the scenario to simulate air traffic control and cockpit communications during the go-around. A simulated civil tilt-rotor flight deck based on the Boeing 747-400 cockpit layout was used for the simulation (first figure).

The results from the MIDAS simulation showed that the VACP workload (visual, auditory, cognitive, and psychomotor loading with 7.0 as maximum load allowable) for the pilot was high throughout the

Fig. 1. Pilot station in simulated tilt-rotor flight deck.

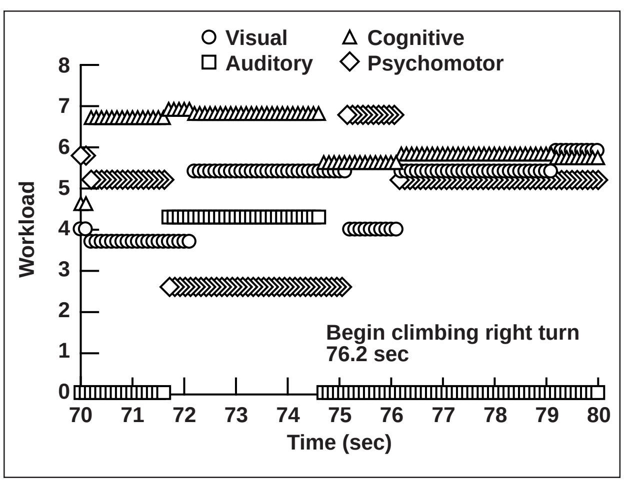

Fig. 2. Workload for manual nacelle movement during go-around.

approach and go-around. The workload was especially high for the manual nacelle movement since more tasks were involved and more time was required to complete them. The pilot had little or no spare workload capacity during the simulated operation (second figure). The automated discrete nacelle mode, on the other hand, allowed the pilot to reach nacelle position much sooner, which enabled the transition from approach to go-around to occur in a timely fashion and at a lower overall workload.

Point of Contact: A. Atencio, Jr.
(650) 604-6863
aatencio@mail.arc.nasa.gov

Control-Law Design and Optimization for Rotorcraft Handling-Qualities Criteria Using CONDUIT

Mark B. Tischler, Jason D. Colbourne, Chad R. Frost, Kenny K. Cheung, Doug K. Hiranaka

The design, integration, and flight-test development of flight-control systems for modern rotorcraft presents a challenging multidisciplinary task that factors significantly into the overall time and cost of aircraft development. Comprehensive specifications and sophisticated time- and frequency-domain evaluation techniques are applied to ensure desired performance and handling qualities and to minimize flight-test tuning of control-system parameters. The control-law design and evaluation is very laborious because of these numerous (often competing) design specifications and constraints. Further, the control-system design engineer must continually update and integrate improvements into the mathematical models and design specifications as new data become available. Clearly, sophisticated interactive computational tools are needed to efficiently integrate the many aspects of the flight-control design process. The U.S. Army Aeroflightdynamics Directorate in conjunction with Ames Research Center, the University of Maryland, the California Polytechnic State University (San Luis Obispo), and Raytheon ITSS jointly developed a state-of-the-art computational facility for aircraft flight-control design and evaluation referred to as CONDUIT (Control Designer's Unified Interface).

Two comprehensive design studies of control-system designs using CONDUIT have been completed and documented this year. They clearly show the capability of this design environment to improve handling qualities and control-system performance. The first example examined the process of designing a new control system for an existing helicopter. This design is based on a simulation study of the SH-2F helicopter with an updated design of the flight-control system (FCS). CONDUIT was used to model and modify the control system, and to select appropriate initial gains. Performance of the SH-2F was evaluated for this control system against a combination of stability, performance, and ADS-33D (rotorcraft handling-qualities specification) criteria. The CONDUIT optimized design exhibited improved handling-qualities and stability margins and it reduced actuator use compared with the baseline control system. The second design example based on the UH-60 RASCAL Blackhawk helicopter highlights some fundamental trade-offs between achieved performance and actuator activity. The first figure illustrates the trend of increased actuator energy and actuator saturation with increasing design margin. From this figure, design points that improve handling qualities and increase fatigue life can be chosen.

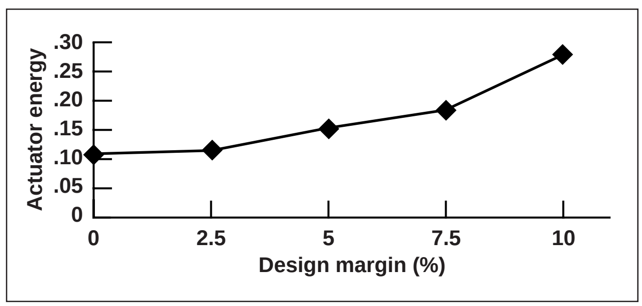

Fig. 1. Increased penalty of actuator energy as a result of increased design margin.

On February 23–27, 1998, a comprehensive 5-day training class conducted at the University of Maryland was attended by 20 flight-control-system experts representing all key segments of the U.S. aircraft/helicopter community (second figure). CONDUIT is presently in use at several universities and helicopter and fixed-wing aerospace companies in the United States through cooperative R&D agreements. Improvements in control-system performance achieved by using CONDUIT are already being validated in industry aircraft development programs.

Point of Contact: M. Tischler
(650) 604-5563
mtischler@mail.arc.nasa.gov

Fig. 2. CONDUIT National Training Course (Feb. 23–27, 1998).

Powered High-Lift Testing

Donald A. Durston, Scott D. Poll

A powered, high-lift, semi-span transport aircraft model was tested in the Ames 12-Foot Pressure Wind Tunnel during the summer and fall of 1998. Turbine-powered simulator (TPS) units mounted on the wing provided scaled fan and turbine exhaust streams; the model had deployable slats, flaps, aileron, and spoilers. The overall objective of the test was to evaluate the propulsive effects on the wing's high-lift performance at various Reynolds numbers. The model and the simulators were made to take full advantage of the tunnel's 6-atmosphere pressure capability at speeds corresponding to takeoff and landing conditions.

Various high-lift configuration studies were conducted by changing selected wing components or by deflecting the surfaces, and vortex generators were run on some configurations. A variety of flow-visualization methods were used in the test to observe features in the flow field or in the flows over the surface of the model. Fluorescent mini-tufts were used to determine areas of flow separation and general flow patterns on the wing and flaps. A quantitative wake-survey system, consisting of remotely controlled rotating arms, moved interchangeable pressure and temperature probes in a survey plane normal to the free-stream flow behind the wing. Skin-friction and boundary-layer-transition measurements were made with a fringe imaging skin-friction interferometry technique, and the use of temperature-sensitive paint for detecting transition was demonstrated for the first time in the test at high tunnel total pressures. Video model deformation measurements, taken by imaging reflective dots placed on the model, were acquired to compute the deflection of the wing and flap surfaces under the wind tunnel and propulsive loads.

The test of this powered model in the 12-foot wind tunnel has provided a vast quantity of force, pressure, and flow-visualization data from which a more detailed understanding of jet-flap interactions can be acquired. The use of the TPS units was essential for meeting the objective, and the successful integration of the operation of the units with the model demonstrated that high-quality powered data can be obtained on a complex model at high tunnel pressures.

Point of Contact: D. Durston
(650) 604-1515
ddurston@mail.arc.nasa.gov

Evaluation of Dynamic Stall Models in Rotorcraft Analyses

Khanh Q. Nguyen, Wayne Johnson

Accurate prediction of blade stall is crucial in the design of helicopters and in the sizing of the rotor structural components; it remains as one of the major challenges of the rotorcraft aeromechanics community. This research aims to evaluate the five dynamic stall models available in the rotorcraft comprehensive analysis CAMRAD II. These are the Johnson, Boeing, Leishman–Beddoes, ONERA Edlin, and ONERA BH models.

Oscillating airfoil results show that all five models can compute the lift-stall reasonably well, and the Johnson, Leishman–Beddoes, and ONERA BH models can compute the stall peaks in the pitching moment fairly accurately.

In the rotor environment, blade pressure data from the UH-60A Airloads Program are used to evaluate the accuracy of the stall models. Results indicate that all stall models predict the stall locations fairly well, but none is able to compute the correct magnitudes of the pitching-moment peaks. The figures show the comparison of the rotor-lift distribution between the flight-test data and the CAMRAD II results using the Leishman–Beddoes dynamic stall model. These figures indicate that the Leishman–Beddoes model captures only the first stall event and that the lift magnitude is underpredicted. Research findings also indicate that proper wake modeling can be crucial in the calculation of the stall events. Small changes in collective pitch and in blade-twist distribution do not significantly affect the stall calculation.

Point of Contact: K. Nguyen
(650) 604-5043
knguyen@mail.arc.nasa.gov

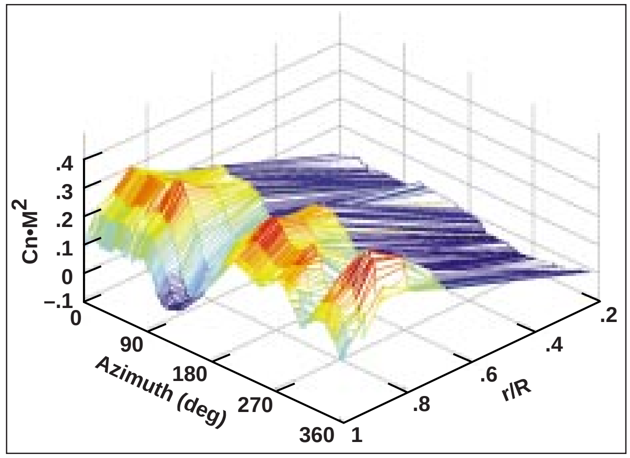

Fig. 1. UH-60A lift distribution, flight-test data (Counter 9017).

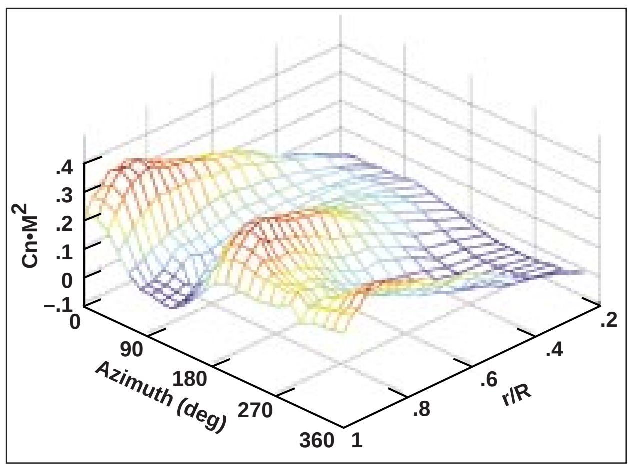

Fig. 2. UH-60A lift distribution, CAMRAD II computed with the Leishman–Beddoes dynamic stall model.

Sensitivity of Rotor Dynamic Stall Calculations to Changes in Control System Stiffness

Robert Kufeld

Accurately predicting the dynamic stall characteristics of a helicopter rotor has become one of the major goals of the rotorcraft industry. The loads generated during a dynamic stall flight condition are important, for they are used to size the helicopter control system. In addition, improved prediction capability should reduce the design and development cost of new helicopters. To accurately predict dynamic stall characteristics, accurate models of the rotor structure, control-system stiffness, linear and nonlinear aerodynamics, and rotor inflow are required.

The objective of this work was to vary the value of the control-system stiffness parameter and to evaluate the effects on predicting the dynamic stall characteristics by using a comprehensive helicopter prediction tool, CAMRAD II. Data from the UH–60A Airloads Program performed at Ames Research Center provided a baseline validation of the calculated dynamic stall characteristics. The value of the control-system stiffness parameter was varied using two different techniques. First, a single-element control-system stiffness model representing the stiffness of the pitch link was varied through a range of 300 to 1100 foot-pounds per degree (ft-lb/deg). These values are representative of the measured value of the UH–60A control-system stiffness. Second, a complex four-element control-system stiffness model using four springs representing the stiffness of the pitch link and swashplate as a system was compared with the single-element model.

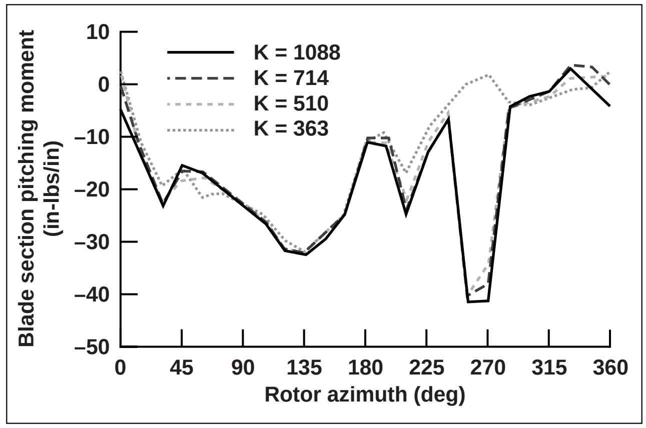

Fig. 1. Blade section pitching moment vs rotor azimuth for different values of control system stiffness.

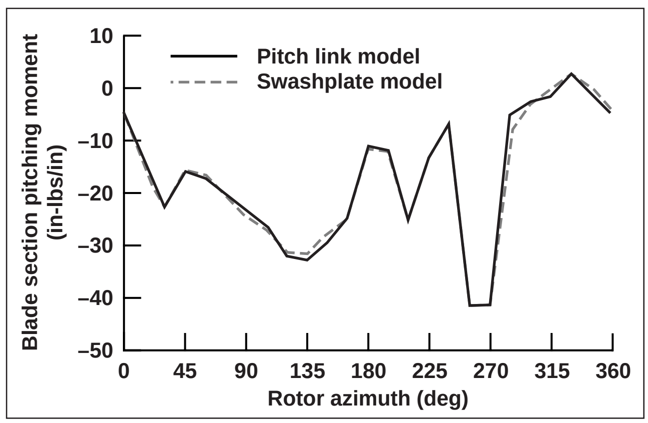

Fig. 2. Blade section pitching moment vs rotor azimuth for a single element pitch link model of the control system stiffness and for a four element swashplate model of the control system stiffness.

The results of the investigation are shown in the figures. The first figure shows the results of comparing four different values of single-element control-system stiffness when predicting blade-section pitching moment caused by the dynamic stall. It is easily seen that within the target range (around 700 ± 200 ft-lb/deg) the pitching moment is insensitive to small changes of control-system stiffness, and once outside the target area the response of the blade pitching moment makes a sudden change. In the second figure, the effects of the four-element control-system stiffness model on blade pitching moment is shown to be very minor compared with that of the single-element control-system stiffness model. These results lead to the conclusion that a highly accurate complex control-system stiffness is not required to accurately predict the aerodynamic behavior of a rotor system during dynamic stall conditions.

Point of Contact: R. Kufeld
(650) 604-5664
rkufeld@mail.arc.nasa.gov

Revolutionary Technology

ERAST Alliance Heat Exchanger Design

Andrew Hahn

Ames Research Center, in supporting the Environmental Research Aircraft and Sensor Technology (ERAST) program, developed a design and analysis tool for heat-exchanger system design. The tool was used in developing the propulsion system design for the ERAST Alliance I Proof of Concept flight vehicle. The propulsion system for this vehicle is a triply supercharged Rotax internal combustion engine. There are intercoolers after the first and second turbocompressors and an aftercooler after the third turbocompressor. In addition to these three heat exchangers, there is a fourth heat exchanger to cool an aqueous glycol solution which is used to reject heat from the engine and oil cooler. These four heat exchangers are housed together in a ram air duct and cooled with ambient air. An interim design was completed of the four heat exchangers and the nacelle that houses them. This nacelle includes an inlet lip, a diffuser, the four heat exchangers in parallel, a transition piece for flow mixing, and an exhaust nozzle. In addition, piping to connect the heat exchangers to the turbocompressors is included in the design. Considerable work was done to analyze the geometric layout of the piping to insure that there are no space conflicts and to estimate internal pressure losses. A cutaway of the heat exchanger system housed in a nacelle is shown in the first figure.

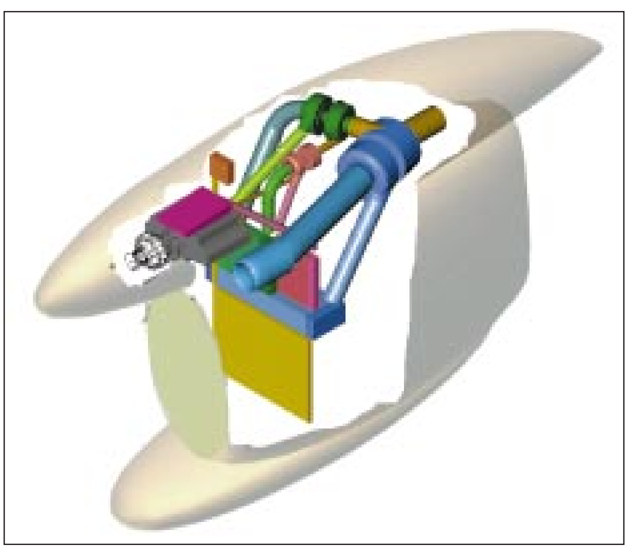

Fig. 1. Isometric view of complete propulsion pod.

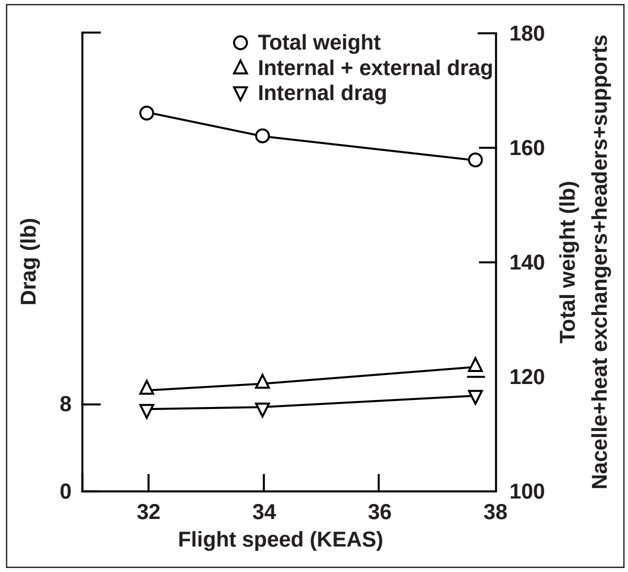

Fig. 2. Total nacelle drag and weight versus flight speed.

The computer program, entitled the Heat Exchanger Analysis Program (HEAP), developed at Ames, addresses the complete nacelle and heat-exchanger design. An inlet pressure-recovery routine predicts total pressure recovery from the free stream to the heat-exchanger face, a heat-exchanger design routine sizes the four heat exchangers, and a convergent nozzle routine sizes the exhaust nozzle. The piping between heat exchangers and turbocompressors was modeled using large-scale computer-aided design (CAD) programs, and the four heat exchangers in the duct were arranged to simplify piping requirements.

Numerous parametric studies of design and mission parameters were conducted using the HEAP program. The second figure illustrates the design trade-offs between heat-exchanger system weight and drag with flight speed when operating at an altitude of 85,000 feet.

The data show that the variation in heat-exchanger system weight with changes in flight speed is much greater than the variation in drag. However, since the performance figure-of-merit used for the Alliance I aircraft is rate of climb at the top of climb, the sensitivity to drag is more important than the sensitivity to weight. Thus, understanding the complete drag of the system, which consists of internal drag caused by pressure losses in the diffuser and across the heat exchangers and of external drag caused by skin friction and form, was the more critical design consideration for this vehicle. The HEAP tool allowed a complete systems approach to address these critical design trade-offs.

Point of Contact: A. Hahn
(650) 604-1223
ahahn@mail.arc.nasa.gov

Measurement of Model Rotor Blade Pressures in Hover Using Pressure Sensitive Paint

Benton H. Lau, Edward T. Schairer

Flow over a helicopter rotor in forward flight is extremely complex and is poorly understood. At any instant, a full spectrum of problems in three-dimensional, unsteady subsonic and transonic aerodynamics is likely to exist: (1) near-sonic flow and the propagation of an unsteady shock wave near the tip of the advancing blade; (2) unsteady flow separation at low speed and high angle of attack on the retreating blade; (3) possible passage of one blade through a vortex generated by another blade (blade–vortex interaction); and (4) large spanwise (hub-to-tip) flow gradients and flow transients on each blade.

One obstacle to understanding rotor flows has been the difficulty in measuring pressures on the blades with adequate spatial resolution. It is not possible to instrument a rotor blade with enough conventional, unsteady pressure transducers, each of which measures pressure at a single point to map complex pressure distributions. Pressure-sensitive paint (PSP) offers a solution to this problem since it provides a surface measurement. PSP requires coating the surface of a model with luminescent paint, exciting the paint with light of an appropriate wavelength, and imaging the model with one or more cameras. Pressure at each point on the model is inferred from the intensity of the paint's luminescence, which decreases as pressure increases. Typically, luminescence intensity is measured by imaging the paint with a camera. Although PSP has been widely used to measure steady pressure distributions on rigid, stationary wind tunnel models, extending the technique to helicopter rotors poses a number of significant challenges. These include improving the frequency response of pressure paints; imaging a moving blade; accounting for nonuniformity of the incident light field; and calibrating the paint without reference to data from pressure taps in the model.

As part of a program to address these challenges, PSP measurements were made on a sub-scale two-bladed rotor (ADM-1) in hover in the Ames Anechoic Chamber. Hover simplifies the general forward-flight problem because, ideally, the flow is steady and thus the frequency response of the paint is of no concern. The upper surface of one of the blades was painted with a pressure paint that luminesced at two wavelengths; the output at one wavelength was not sensitive to pressure and was used to normalize the other, pressure-sensitive signal. The blade was illuminated by a flash lamp that was suspended on a boom over the blade (first figure) and triggered by a once-per-rev signal. The boom also supported two scientific digital cameras, each fitted with a bandpass filter matching one of the output wavelengths. In order to get an adequate signal, images were integrated over many revolutions. Measurements were made at rotational speeds up to 1600 revolutions per minute (rpm), corresponding to a maximum tip speed of 628 feet per second. The relationship between paint luminescence intensity and pressure was determined by measuring the response of a paint sample in a calibration chamber after the experiment.

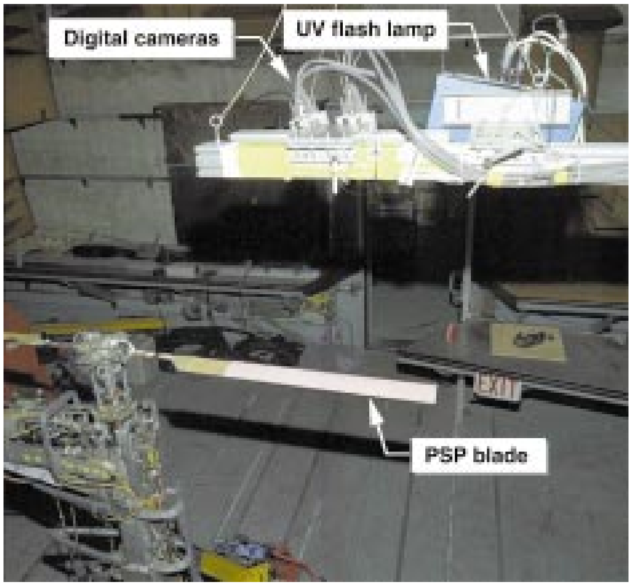

Fig. 1. Digital cameras and flash lamp mounted on a stand above the rotor to capture images of painted blade.

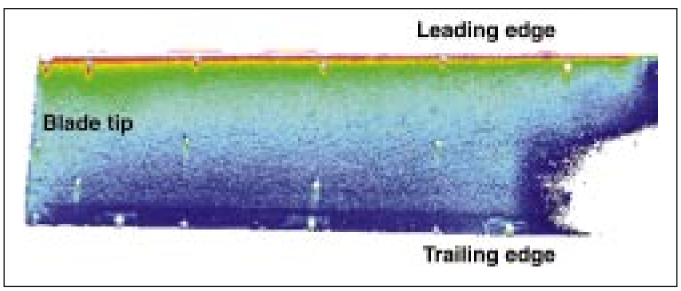

Fig. 2. Sample image of the pressure-sensitive paint with the rotor operating at 1600 rpm and 3.1 degrees of blade pitch.

The second figure shows a typical false-colored image of the blade at the maximum rpm. Red and blue indicate relatively high and low pressures, respectively. Quantitative results at this condition were unreliable because of temperature effects: the paint temperature was significantly higher than the temperature at which it was calibrated (calibration temperature could not be increased above ambient temperature). An unfortunate characteristic of all pressure paints is that they exhibit some temperature sensitivity. Pressures derived from PSP images at lower rpm's, where the paint temperature was nearly the same as the calibration temperature, were near the expected range.

Point of Contact: B. Lau/E. Schairer
(650) 604-6714/6925
blau@mail.arc.nasa.gov
eschairer@mail.arc.nasa.gov

A Web-Based Analysis System for Planetary Entry Vehicle Design

David R. Olynick

An integrated analysis environment for designing planetary entry vehicles has been developed. The figure illustrates that the system has a Web-based graphical user interface, which drives analyses on a network of servers. Members of a geographically dispersed design team, with heterogeneous hardware, can readily access analysis modules located at other sites. The design tool includes analyses for geometric definition, aerodynamics, aerothermal environment, trajectory, and thermal-protection system sizing. Disciplinary specialists can maintain each analysis locally, and ensure that input and output data conform to a prescribed description for entry vehicles. Specialists also provide documentation that describes the range of applicability for each analysis method and the validation cases that have been run.

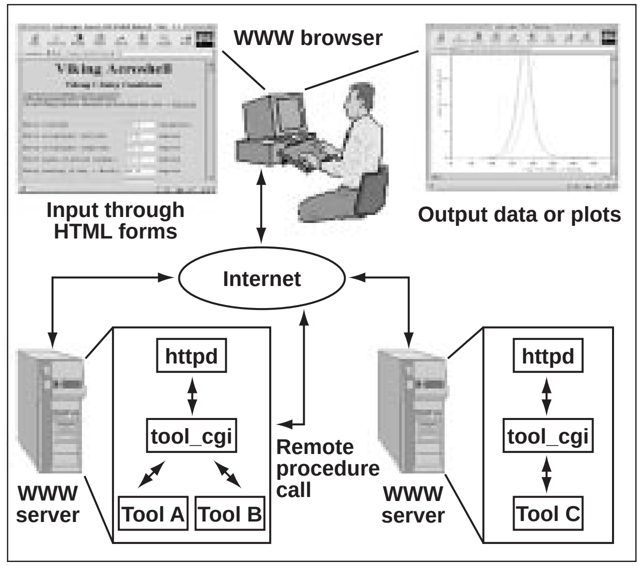

Fig. 1. Design analysis execution on the Internet.

This Web-based analysis system has already been applied in several entry body design projects. Engineers at Ames Research Center performed preliminary sizing studies for a manned Mars entry vehicle. At NASA Langley it was used for Mars Sample Return studies. Students at several universities have conducted thermal-protection sizing studies for a sample-return mission and calculated heating environments for Mars entry vehicles.

Ames is collaborating with researchers at NASA Langley, the Jet Propulsion Laboratory, and Sandia National Laboratory to continue development of this system. Libraries of disciplinary analyses are being developed, with varying levels of fidelity being offered for each discipline. Users will be able to construct personalized analysis sequences by selecting from these libraries. Interface development is continuing, with particular attention being devoted to parametric variations of selected variables. This work was performed in collaboration with Gary A. Allen, Jr., and Peter J. Gage of ELORET Thermosciences Institute.

Point of Contact: D. Olynick
(650) 604-6966
dolynick@mail.arc.nasa.gov

Virtual Laboratory

Steve Cowart

The Virtual Laboratory (VLAB) at Ames Research Center constitutes a fresh approach to conducting simulation experiments. It allows researchers at remote sites to interactively direct and participate in live simulation experiments conducted in research laboratories at Ames.

Using a virtual reality environment, remote users can monitor and react to various simulation data as if they (the users) were physically present in the Ames Vertical Motion Simulation (VMS) complex. In addition, they can view the pilot's front-window scene, head-up and head-down displays, a graphical depiction of the motion platform, strip charts, and end-of-run data displays. Also integrated into the package are two-way communication, video conferencing, and ambient sound capabilities that enable the remote user to direct the experiment and even speak directly with pilots in the cab.

VLAB embodies Ames' mission to lead the world in information technology, and it allows government and industry greater hands-on access to NASA expertise. VLAB is an extension of a national research facility that enables industry to improve and accelerate its design processes, yielding cutting-edge aeronautical products.

VLAB's most important deployment to date occurred in September of FY98 during the simulation of the space shuttle orbiter at Ames. During the semiannual shuttle simulations, VLAB was deployed to NASA's Johnson Space Center (JSC) to enable researchers to remotely monitor and interact with simulations and to capture data for analysis. This marked the first time that the full VLAB user organization used a public network, the NASA Science Internet Network. Data transmission, including video of the out-the-window display, achieved rates from Ames to JSC and back of between 50 and 150 milliseconds. For the first time, JSC researchers did not come to Ames, but relied solely on VLAB to conduct the necessary research. Their reliance on VLAB's many remote capabilities validated VLAB in theory and in practice.

The VLAB project team is currently working to enhance the fidelity of the immersive nature of VLAB; providing additional user input/output features; increasing VLAB's applicability to several simulation experiments; collaborating with technology experts, both within and outside of Ames; and increasing its diversity by applying the VLAB technology in areas beyond flight simulation at the VMS. Additionally, the team is exploring possible partnerships with educational institutions and with local aeronautics museums. For more information, visit VLAB's web site (http://www.simlabs.arc.nasa.gov/vlab).

Point of Contact: S. Cowart
(650) 604-5644
scowart@mail.arc.nasa.gov

Fig. 1. Using VLAB, researchers in remote locations monitor and interact with VMS simulations as they occur.

Compact Fiber-Optic Microphones

Y. C. Cho

Research into advanced pressure sensors using fiber-optic technology is aimed at developing miniature microphones. Fiber-optic sensors are inherently immune to electromagnetic noise, are very sensitive, are lightweight, and are highly flexible.

In FY98 NASA researchers successfully designed and assembled a prototype fiber-optic microphone, which is schematically illustrated in the figure. The sensitivity of this fiber-optic microphone is better than that of any existing fiber-optic pressure sensor by at least three orders of magnitude. The sensor has a diameter of 2 millimeters and includes a silicon nitride diaphragm that was fabricated and mounted on a miniaturized ferrule for this purpose by collaborators at the Jet Propulsion Laboratory. Preliminary tests demonstrated excellent performance: The frequency response was steady and uniform within the design frequency limit (200 to 4,200 hertz). It is at least as good as that of the B&K microphone of a similar size (0.125 inch in diameter), which is the best condenser microphone that is commercially available. The sensitivity of the fiber-optic microphone, measured in terms of signal-to-noise ratio, is almost 2 or 3 decibels better than that of the B&K microphone. The overall performance of this sensor exceeded initial expectations.

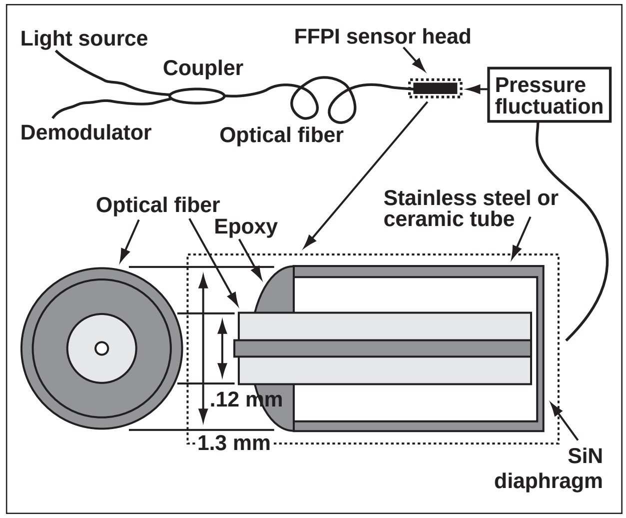

Fig. 1. Schematic of prototype fiber-optic microphone.

The compact size and light weight of this sensor give it several advantages. Because it is so small, tens or hundreds of sensors can be used together for applications such as microphone arrays. Also, their size permits these sensors to be placed nondestructively on flight surfaces, in contrast to present techniques. Yet another important potential application is in the health monitoring of space vehicles.

Point of Contact: Y. Cho
(650) 604-4139
ycho@mail.arc.nasa.gov

Distributed Computation on Information Power Grid Using Globus

Stephen Barnard, Rupak Biswas, Subhash Saini, Rob Van der Wijngaart, Maurice Yarrow

To meet NASA's ambitious Enabling Technologies Goals, a significant improvement is required in its ability to create, process, understand, store, and communicate data. Therefore, NASA is building a nationwide infrastructure called the Information Power Grid (IPG). The IPG is to provide ubiquitous and uniform access, through a convenient interface, to a wide range of computational, communication, data analysis, and storage resources, many of which are specialized and cannot be duplicated at all user sites. The goal is to demonstrate how IPG technology can solve, in a distributed fashion, large-scale computational fluid dynamics (CFD) applications that are currently intractable on single, tightly integrated parallel supercomputers.

The Globus metacomputing tool kit is used to enable the geographically distributed computation. The first figure shows how Globus was used to combine homogeneous but distributed resources (SGI Origin 2000 systems, Evelyn at Ames and Denali at Argonne) to simulate an X-38 Crew Return Vehicle (CRV). This experiment provided experience with Globus and insights into the requirements for future IPG technology. The focus was on identifying and implementing the minimum changes to a state-of-the-art parallel CFD program necessary to run efficiently as a distributed application in an IPG environment.

The CFD software used is an enhanced version of OVERFLOW, the most widely used flow solver at Ames. OVERFLOW deals with the geometrical complexity of application-solution domains by allowing sets of separately generated and updated overlapping discretization grids that periodically exchange information. As shown in the first figure, each grid is assigned to a unique processor, resulting in the distribution of the entire set of grids among available processors. Each processor computes the flow solution on the grids assigned to it. In this coarse-grained data-distribution scheme, it is only necessary to communicate some of the grid-boundary information between processors.

The second figure shows the major software and hardware components involved in the experiment. Communication among processors was implemented through MPICH-G, a “Grid-enabled” version of the Message Passing Interface (MPI) library. Globus provides core IPG services, including resource location and allocation, communication, gathering of unified resource information, authentication, remote process creation, fault detection, and remote data access.

The main technical challenge in implementing scientific applications on the IPG lies in accommodating the sizable and variable latencies as well as the reduced bandwidths incurred in distributed computations on geographically separated machines. Algorithmic modifications related to latency hiding

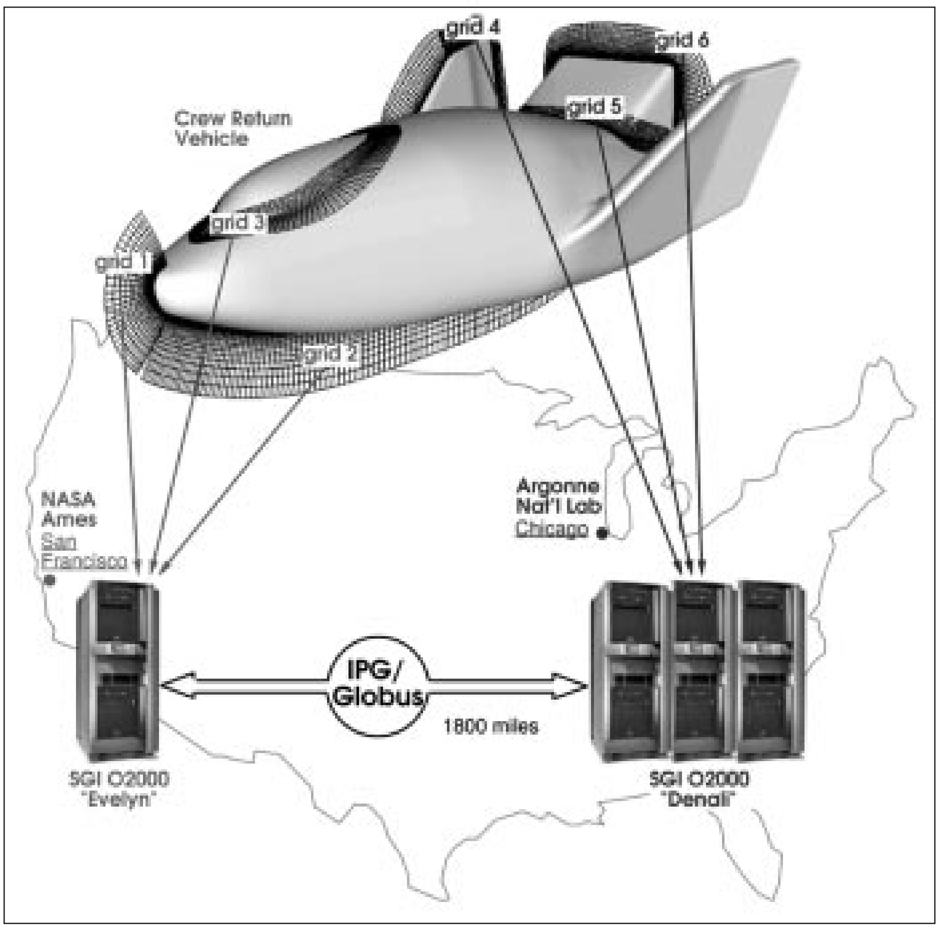

Fig. 1. Distributing a CFD application on IPG using Globus.

and load balancing were therefore necessary for an efficient implementation. Latency tolerance was obtained by lagging the boundary-value update between overlapping grids by one time step. This allowed the overlap of computation and communication for as much as one entire time step. Balancing processor workloads while minimizing interprocessor communication was realized through the application of a general-purpose graph partitioner.

Performance results indicate that real applications can be implemented on the IPG; however, a significant amount of effort is required to make such an environment generally useful and widely accessible for solving the major computational problems that are of interest to NASA.

Point of Contact: R. Biswas/S. Saini
(650) 604-4411/4343
biswas@nas.nasa.gov
saini@nas.nasa.gov

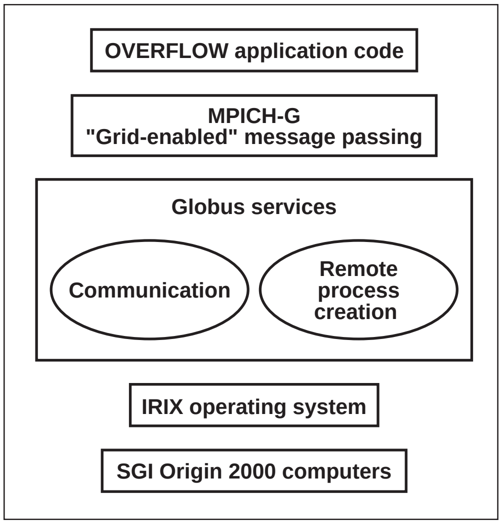

Fig. 2. Major software/hardware components involved in the experiment.

High-Performance Scalable Computing on Steger: A 256-CPU Origin System

James R. Taft

In 1997 Ames Research Center embarked on a multiyear cooperative agreement with Silicon Graphics, Inc. (SGI) to jointly pursue the development of a single Origin system with 256 CPUs (the Origin is SGI's supercomputer, the Origin 2000 System). At that time SGI had not yet announced formal product plans for even a 128-CPU system.

The impetus for the agreement came from preliminary work on Origins that involved optimizing production computational fluid dynamics (CFD) codes (see Production Parallel Computing—OVERFLOW-MLP on p. 64 in this volume). This work had shown near-perfect linear parallel scaling for the ARC3D and OVERFLOW codes to 64 CPUs. The OVERFLOW test in this series was an execution of a 35-million-point production problem—the largest ever attempted at Ames at that time.

Shortly after the 64-CPU tests, Ames entered into a research agreement with SGI, and purchased two preproduction 128-CPU systems. The two new systems quickly demonstrated near-perfect scaling for ARC3D and OVERFLOW-MLP on 128 CPUs. Further tests using the HIPPI networking interconnect between the systems showed that OVERFLOW-MLP scaling was also linear to 256 CPUs, though connections between the systems through the HIPPI interface required code modifications for the test.

In the second half of 1998, the two 128-CPU systems were combined into a single system as part of the research agreement. This required special operating-system and compiler development efforts on the part of SGI, as well as rigorous testing of hardware cache coherency mechanisms that had never been exercised before. The modifications were successful, and the system (named Steger and shown in the figure) was declared operational in October. Tests with OVERFLOW-MLP immediately showed linear scaling to 256 CPUs with unmodified code.

Fig. 1. NAS System Division's Steger System: SGI Origin 2000, 256 CPUs.

Further scaling tests with OVERFLOW-MLP have been performed on the 256-CPU system. These tests show that the 35-million-point problem will scale to 512 CPUs as well. This amounts to being nine times faster than a dedicated 16-CPU C90 system executing the same problem. At these computation rates, full convergence of problems involving high-fidelity simulations of full-scale aircraft can be accomplished in 2 hours, resulting in vastly faster times to market for aerospace products.

Point of Contact: J. Taft
(650) 604-0704
jtaft@nas.nasa.gov

Tilt-Rotor Test Data Validation Using Neural Networks

Sesi Kottapalli

In general, rotorcraft testing is complex. It is difficult at times to even heuristically know the functionality of the measured data, for they vary with the test condition. Therefore, it is difficult to quickly isolate any bad data points or, even more difficult, to interpret the quality of the measured data. Thus, validating rotorcraft wind tunnel performance test-data measurements is important to the achievement of a successful test. The present study involved two XV-15 isolated tilt-rotor test databases that were separately acquired at Ames: the hover and forward-flight 80- by 120-foot wind tunnel database, and the hover outdoor-aerodynamic-research-facility database. Hover-performance test data acquired using an outdoor facility require "wind corrections." These wind corrections are important and account for the effect of outdoor, ambient winds on the tilt-rotor hover performance. Because the wind corrections help in providing a true measure of the tilt-rotor hover performance, it is necessary to use an accurate wind-correction procedure.

For the present neural-network-based test-data validation study, the first objective was to obtain neural network representations, conduct data quality checks, and demonstrate sensitivity to test conditions. The second objective, using outdoor hover test data, was to formulate and implement a neural-network-based wind-correction procedure.

Neural networks were successfully used to represent and assess the quality of full-scale tilt-rotor hover and forward-flight performance test data. The neural networks accurately captured tilt-rotor performance at steady operating conditions, and it was shown that the wind tunnel forward-flight performance test data were generally of very high quality. The figures show the neural-network-predicted and the test blade-yoke mean flatwise and chordwise bending moments. The first figure shows that about 5% of the test flatwise bending moment database may not be usable; however, the second figure shows that the test chordwise moment data quality is very acceptable.

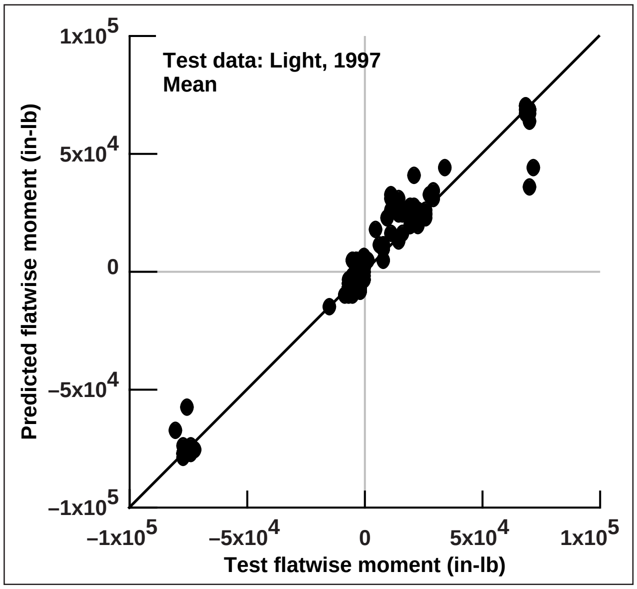

Fig. 1. Flatwise moment correlation.

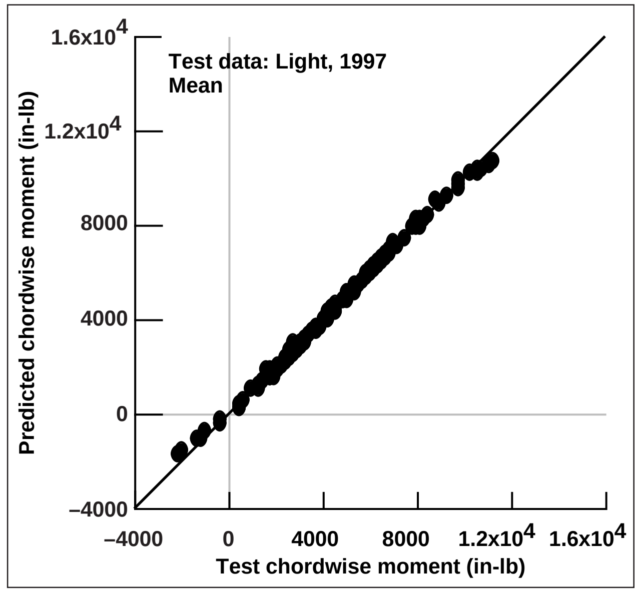

Fig. 2. Chordwise moment correlation.

For outdoor tilt-rotor hover performance test data, compared to wind corrections that were obtained using an existing wind-corrections method (the so-called "momentum-theory-method"), the present neural-network-procedure-based corrections were better (the respective root-mean-square errors were 0.02 and 0.01). The present neural-network-based wind-corrections procedure, based on a well-trained neural network, captured physical trends present in the outdoor hover test data that had been missed by the existing method.

Point of Contact: S. Kottapalli
(650) 604-3092
skottapalli@mail.arc.nasa.gov

Three-Dimensional Velocity Measurements Using Particle Image Velocimetry

Stephen Walker

Until a few years ago particle image velocimetry (PIV) was primarily used as a laboratory research tool. Through the years, however, PIV has been developed into a reliable means of obtaining instantaneous, two-dimensional velocity measurements in a plane. Advances in methodology, technology, and computers have made PIV an accurate two-dimensional planar measurement technique (with typical errors of 1%–2% of instantaneous velocity vectors), as well as a measurement technique with relatively quick setup and data turnaround. In recent years, a few researchers around the world have demonstrated the applicability of PIV to larger scales; in particular, the use of PIV in production wind tunnels has become imminent. Given the advances that have been made with the PIV method, work was performed in order to demonstrate the large-scale capabilities of PIV at Ames Research Center. In addition, a secondary focus was to develop a PIV system capable of making three-dimensional velocity measurements in a plane.

Traditional PIV is a method for determining instantaneous two-dimensional velocities in a plane; the method relies on placing tracer particles in a fluid flow. The tracer particles are larger than the particles of the fluid being studied. Large tracer particles are used in order that the positions of the tracer particles can be recorded by photographic images. The velocity of the tracer particles is determined by illuminating a plane with high-powered laser light at two consecutive instances in time. Using the light scattered from the particles, the position of individual tracer particles can then be captured on a photographic recording medium at these two instances in time. The initial and final particle positions coupled with the time between laser-light illumination results in measured fluid velocities from the photographic images.

The three-dimensional (3-D) PIV system is based on utilizing two PIV systems, each of which is two-dimensional (2-D). Each of the two PIV systems is focused on the same planar region. The Scheimpflug condition, which describes a method for focusing on a plane from an oblique viewing angle, is used for focusing. By using two PIV systems, it is possible to get two perspective views of the same fluid flow field. Each two-dimensional PIV system results in an individual estimation of the velocity field. The two camera views are combined in order to determine identical positions in each of the two views. A reconstruction is then performed using the data from the two separate velocity fields, thereby determining all three velocity components from the two 2-D velocity fields calculated from each PIV system. The initial verification and subsequent testing of the 3-D PIV system resulted in error estimates of 1.7% for the instantaneous in-plane components of velocity, and 3.4% error for the instantaneous out-of-plane components of velocity.

The first functional use of the large-scale 3-D PIV system was performed in the 7- by 10-foot wind tunnel at Ames. A half-span NACA 0015 wing with a chord of 20.4 inches was mounted in this facility, and 3-D PIV measurements were obtained at several cross-planes downstream of the model. The investigation was performed in order to study the wing-tip vortex shed from the model. The area imaged and analyzed was 25 centimeters high and 40 centimeters across. This resulted in approximately 15,000 instantaneous velocity vectors from each image pair. The PIV system used for this wing-tip vortex study is shown in the first figure; the wing, the two cameras, and the laser sheet are visible.

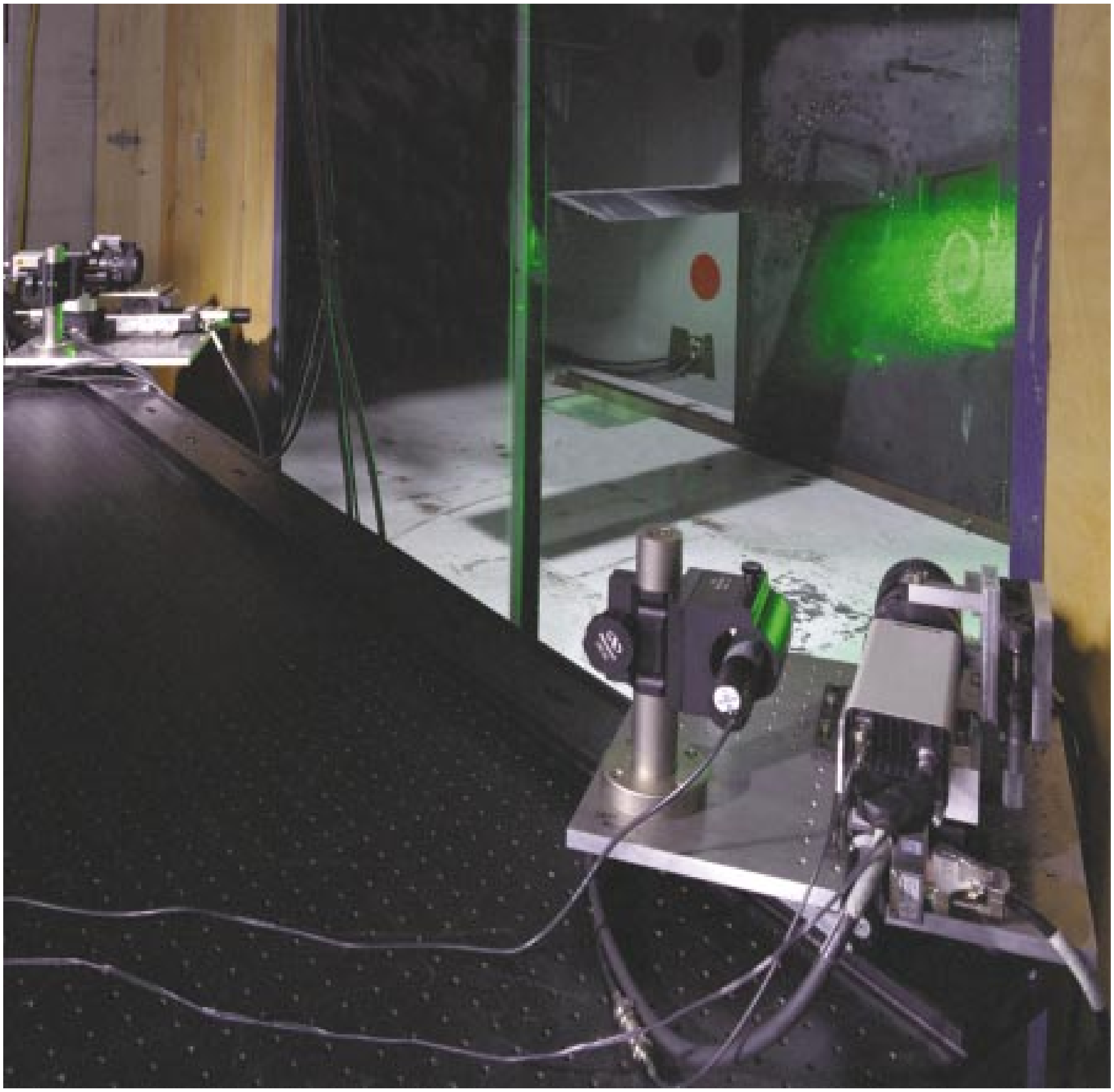

Fig. 1. Photograph of three-dimensional PIV setup used in test.

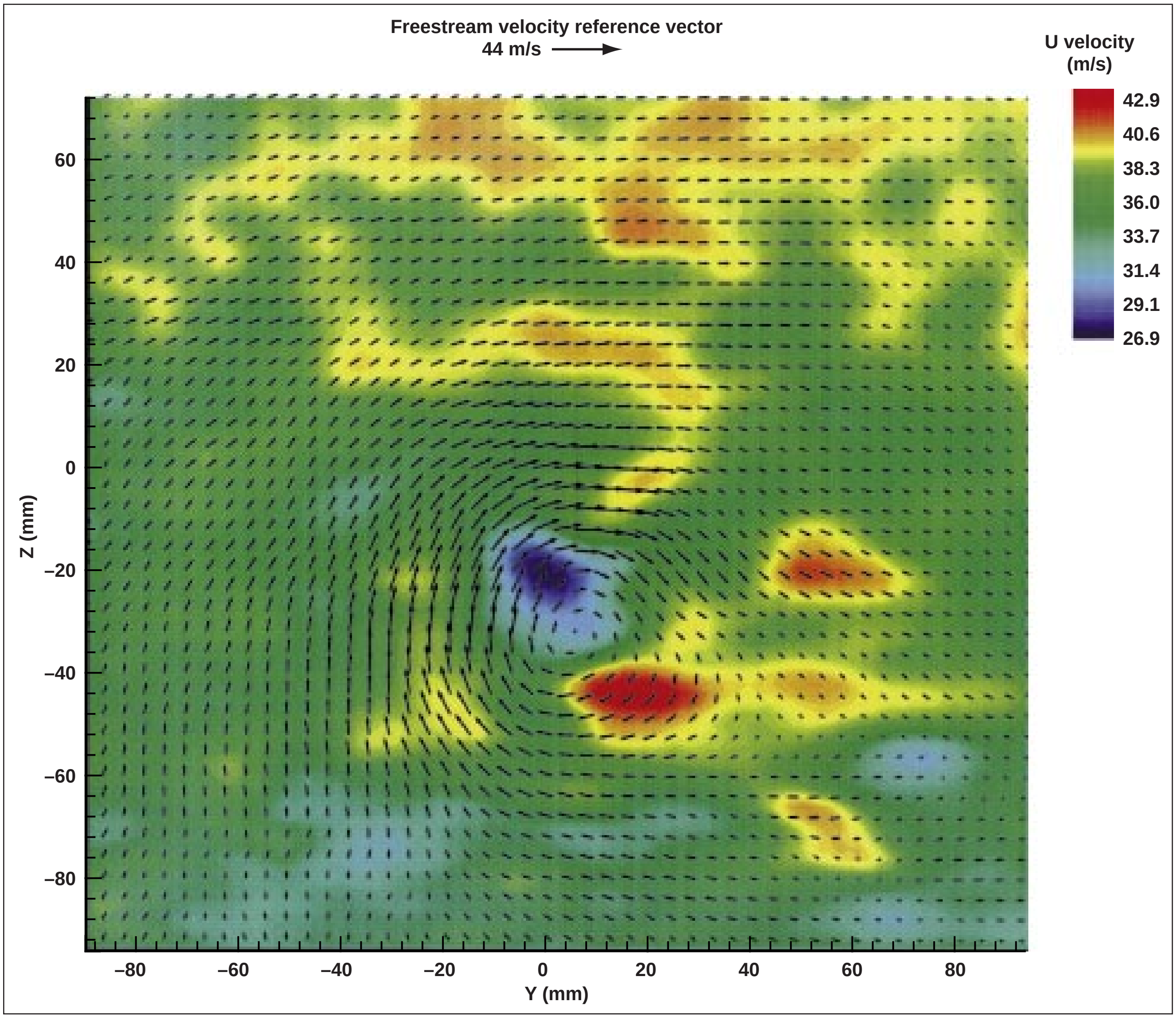

Fig. 2. Instantaneous three-dimensional velocity data.

The second figure shows instantaneous velocity data results, with the in-plane velocity shown in the black vector field; the out-of-plane component of the velocity is illustrated in the colored contour plot.

These data were taken from a position 2.04 inches downstream of the wing trailing edge.

Point of Contact: S. Walker
(650) 604-6720
swalker@mail.arc.nasa.gov

Production Parallel Computing: OVERFLOW-MLP

James R. Taft

During the past 2 years it has become clear that mainstream high-performance computing in the United States will be performed on microprocessor-based parallel systems. Historically, it was very difficult to port production computational fluid dynamics (CFD) codes to this computer architecture with much success. Many of the early designs forced developers into high-latency message-passing approaches that the hardware simply did not support well. Consequently, performance was often very poor when compared with that of the classic vector systems from Cray Research. This is no longer the case.

Two major changes in system design have allowed this to occur. The first is that cache memory associated with the new microprocessors has risen dramatically in size, such that 4- and 8-megabyte caches are typical for high-end microprocessor-based systems. Second, vendors are moving to highly parallel systems with hundreds of central processing units (CPUs) which support true shared memory throughout the system.

These two major architectural shifts have allowed researchers at Ames Research Center to develop a new approach to highly scalable parallel computing that demonstrates impressive performance potential for production CFD computing at NASA. The new approach is termed shared-memory, multilevel parallelism (MLP).

MLP was developed at Ames during an Origin 2000 evaluation effort in 1997. The effort demonstrated that MLP, used in CFD production code executing on new systems like the Origin 2000, could provide substantial performance gains over the in-house 16-CPU Cray Research C90 system (reported in the 1997 edition of this report).

During FY98, the OVERFLOW production CFD code has been used as the test bed to demonstrate the potential for continued scaling to very large CPU counts (256 total) on Origin systems. The figure shows the results to date. As can be seen the performance is perfectly linear out to 256 CPUs for a 35-million-point production problem executed at Ames. The maximum sustained performance is

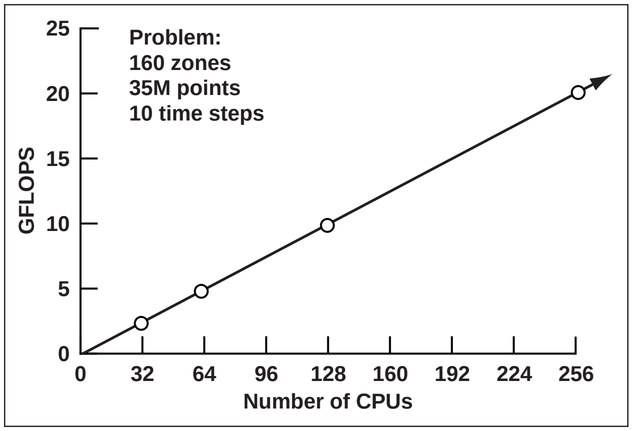

Fig. 1. 256-CPU Steger System Performance on the OVERFLOW production CFD code.

20.1 billion floating-point operations per second (GFLOPS); on the local 16-CPU C90 system it is 4.6 GFLOPS. This results in a cost/performance that is better by a factor of 23.5 than that of the vector system.

The MLP technique has been codified into a small library of five routines that is in the process of being distributed to a limited number of NASA researchers for test and evaluation. The MLP technique, as implemented in OVERFLOW-MLP at Ames, is also in the process of being integrated by NASA Langley Research Center into the standard OVERFLOW production release for Origin systems.

During the past year, MLP scaling studies using OVERFLOW demonstrate that production CFD supercomputing can achieve significant breakthroughs in performance on the new architectures for the largest problems of today. More importantly, the new techniques and systems offer the promise of solving much larger problems at a dramatically reduced cost.

Point of Contact: J. Taft
(650) 604-0704
jtaft@nas.nasa.gov

OVERGRID: Overset Grid Generation Interface

William Chan, Robert Meakin

For many years, generation of overset grids for complex configurations has required the use of a number of different independently developed grid and visualization software utilities. A new software tool called OVERGRID allows a user to perform all of the grid generation and visualization under a single environment. Applications include commercial and military aircraft, launch and return vehicles, ships, and submarines.

OVERGRID provides a unified graphical interface for users to perform grid and geometry visualization, as well as grid manipulations such as redistribution and projection (see figure). It also contains hyperbolic surface and volume grid-generation modules that are specifically suited for the overset grid approach. These features dramatically reduce the overall time required for the simulation of vehicle aerodynamics.

Since its initial availability just under a year ago, OVERGRID has been distributed to over 40 groups and organizations in industry, government laboratories, and universities. User feedback indicates that OVERGRID has reduced the time required to

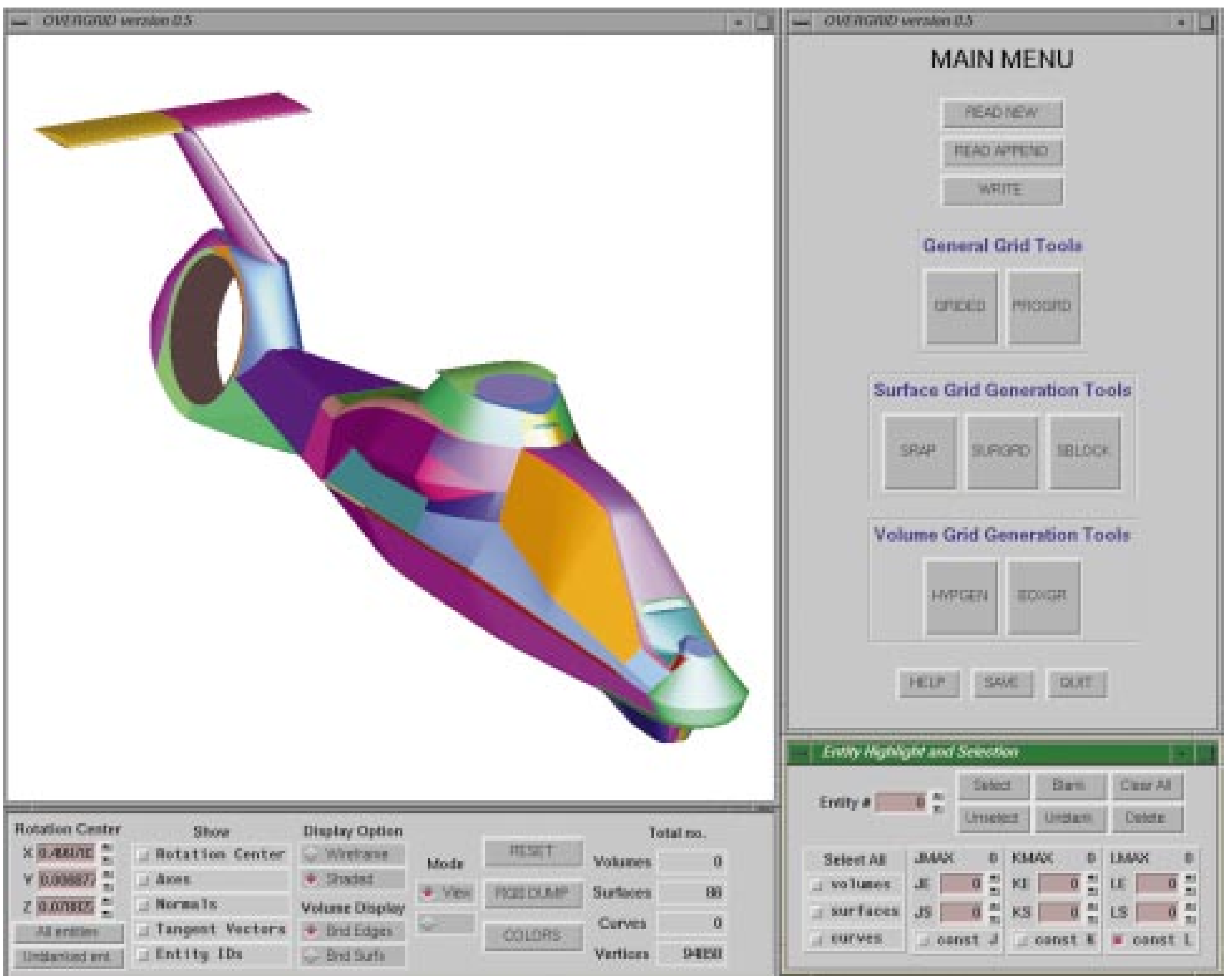

Fig. 1. An example of the OVERGRID interface for overset-grid generation.

produce high-quality grids by 75% relative to that of previously available software tools.

New features and improvements will be continually added to OVERGRID, including automatic seam curve extraction, more automatic surface grid generation, the use of Non-Uniform Rational B-Spline (NURBS) surfaces, and trimmed NURBS surfaces as input geometry definition.

Point of Contact: W. Chan/R. Meakin
(650) 604-6607/3969
wchan@nas.nasa.gov
rmeakin@mail.arc.nasa.gov

Automated Aerodynamic Simulation of Complex Vehicles

Michael Aftosmis, Marsha Berger, John Melton

As numerical simulation plays an increasing role in aerospace vehicle design, mesh generation has emerged as a major stumbling block in the simulation process. Ames researchers, with partners from the Courant Institute (New York University), have developed and deployed a novel simulation tool aimed at removing this bottleneck and at greatly automating numerical aerodynamics. Traditional approaches to computational fluid dynamics (CFD) rely upon body-fitted meshes to discretize the space

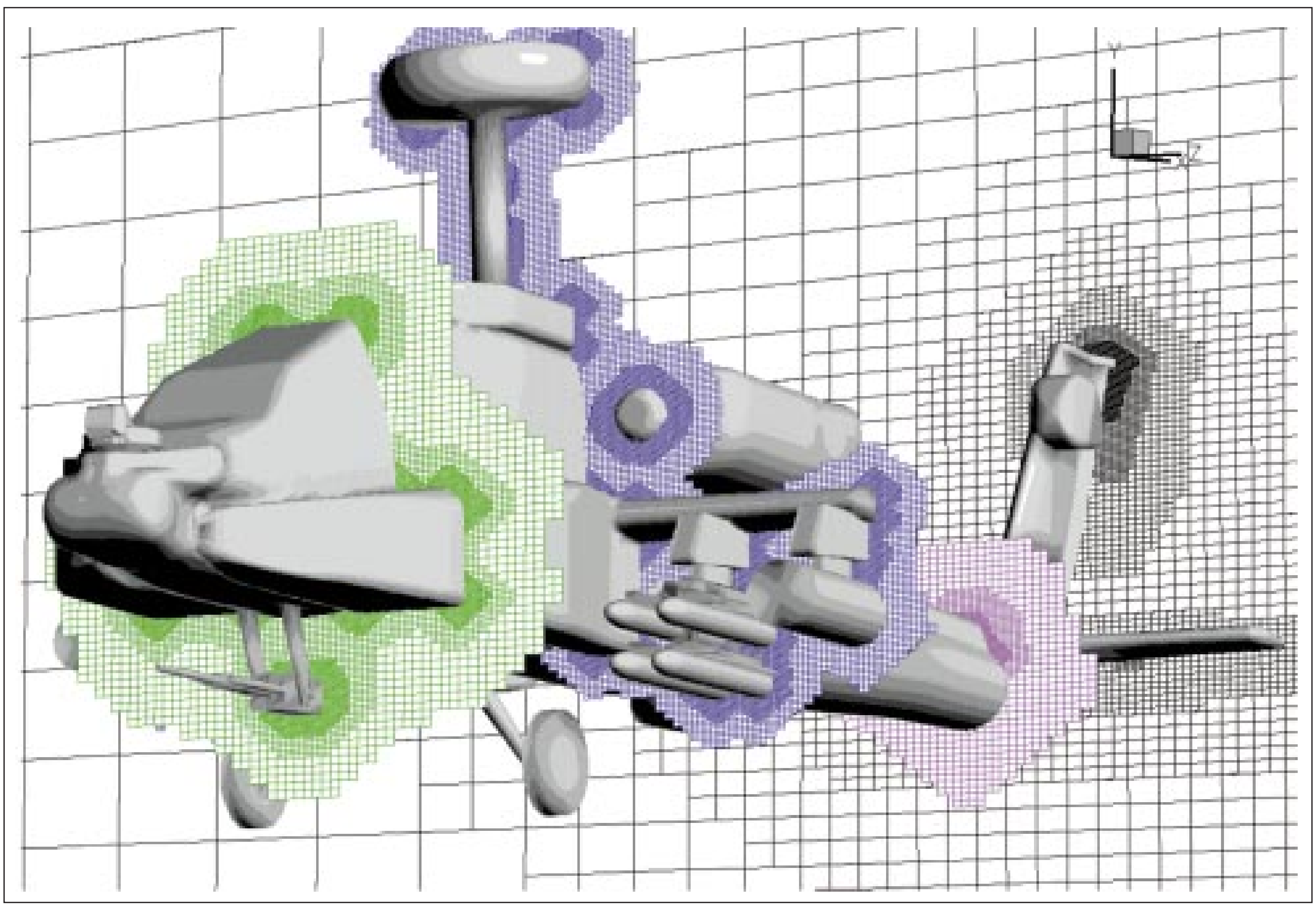

Fig. 1. Geometry and adapted Cartesian mesh for an attack helicopter configuration with 82 components and 5.8 million cells.

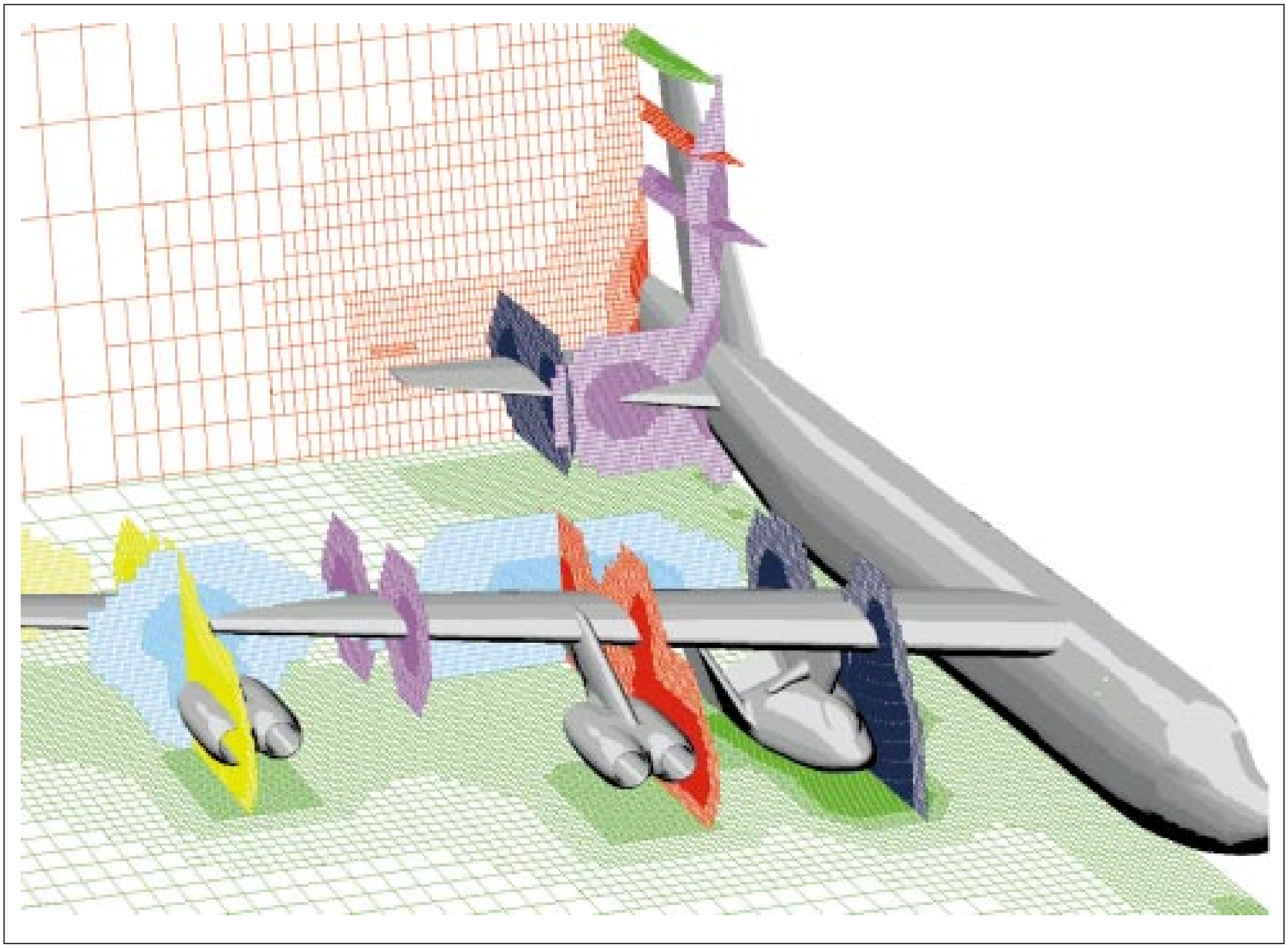

Fig. 2. Sample computational mesh with 4.5 million cells for analysis of X-38 installation under wing of B-52 aircraft.

surrounding a vehicle. Since the mesh must be fitted to the geometry, simply meshing a complicated configuration can actually consume several months of the CFD cycle. In contrast, Ames's new approach is based on the use of nonbody-fitted Cartesian cells which are free to arbitrarily intersect the surface of the vehicle being analyzed.

Using techniques from computational geometry, cells that lie internal to the geometry are removed, and those actually intersecting the surface are trimmed such that only the region of the cell that is exposed to the flow remains. Fundamentally, the approach trades the case-specific problem of generating a body-fitted mesh for the more general problem of computing and characterizing intersections between rectangular cells and the vehicle's surface.

The figures illustrate the degree of geometric complexity that can be routinely accommodated by this approach. The first figure depicts several mesh-planes surrounding an attack helicopter configuration. This configuration contains 82 separate components; the 5.8 million cell mesh was generated in only slightly over 5 minutes on a moderately powered desktop workstation. Since the process is fully automated, additional meshes may be easily generated as components in the configuration are moved, added, or removed.

The second figure depicts an example done in support of NASA's flight test of the X-38 research vehicle. This work sought to predict the near-field aerodynamic environment created by installing the X-38 under the wing of a B-52 aircraft. The figure shows several planes through the computational mesh surrounding the geometry. Although it contains over 4.5 million cells, this mesh was also created in under 5 minutes. This application emphasized the importance of developing a robust and fully automated simulation capability since it permits engineers to experiment with different installations of the X-38 on the mothership.

The mesh-generation system demonstrated in the figures has been incorporated into a simulation package known as Cart3D. This package includes tools for surface preprocessing, mesh generation, flow solution, and postprocessing, and is capable of simulating inviscid flow around arbitrarily complex vehicles. The package is in use at four NASA research centers, at several military laboratories, at Department of Energy research centers, and within U.S. industry. Current development efforts focus on intermodule automation, and an improved multilevel parallel flow solver for use on computers ranging from simple desktops to high-performance parallel platforms.

Point of Contact: M. Aftosmis
(650) 604-4499
aftosmis@nas.nasa.gov
http://george.arc.nasa.gov/~aftosmis/cart3d/

High Fidelity Aerodynamic Shape Optimization

Susan Cliff, James Reuther

Higher-order computational fluid dynamics (CFD) codes that solve the inviscid Euler equations or viscous Navier–Stokes equations have been used extensively in the past for analyzing a wide variety of configurations. This has proved very beneficial, but to make full use of these powerful methods requires that they be incorporated into the framework of an automated design process that can be used to optimize the aerodynamic contours of flight vehicles. However, automating the design process has proved to be extremely difficult, expensive, and time consuming for applications involving complex aircraft configurations. The reason is the thousands of CFD solutions that are required to gain an understanding of the aerodynamic design space and its related optimum.

Traditional aerodynamic shape-optimization methods use finite-difference methods to obtain the necessary gradients of an aerodynamic objective function, such as drag, with respect to the design variables. These methods are computationally expensive because they require a separate flow solution for each design variable used in the design in order to obtain the gradient information during each design cycle. Typically, of the order of 100 design cycles are required to optimize a complex configuration. Through the use of an adjoint system of equations derived from the application of control theory, it is possible to reduce the large computational requirement associated with the traditional approach to the equivalent of only two flow solutions per gradient computation, independent of the number of design variables. This typically results in a computational savings of one to two orders of magnitude. Furthermore, since the gradient computation is independent of the number of design variables, complex configurations can be treated using hundreds of design variables versus tens of design variables for the traditional approach.

These fundamental fluid-flow and adjoint solution methods, which are available commercially, have been combined with a large collection of software developed at Ames Research Center to yield an effective design environment applicable to a wide variety of complex aerodynamic configurations. The Ames-developed software provides for the generation and perturbation of the computational grids, the application and tracking of the design variables used in the design process, the implementation and validation of both linear and nonlinear constraints, the application of the optimization algorithms, and

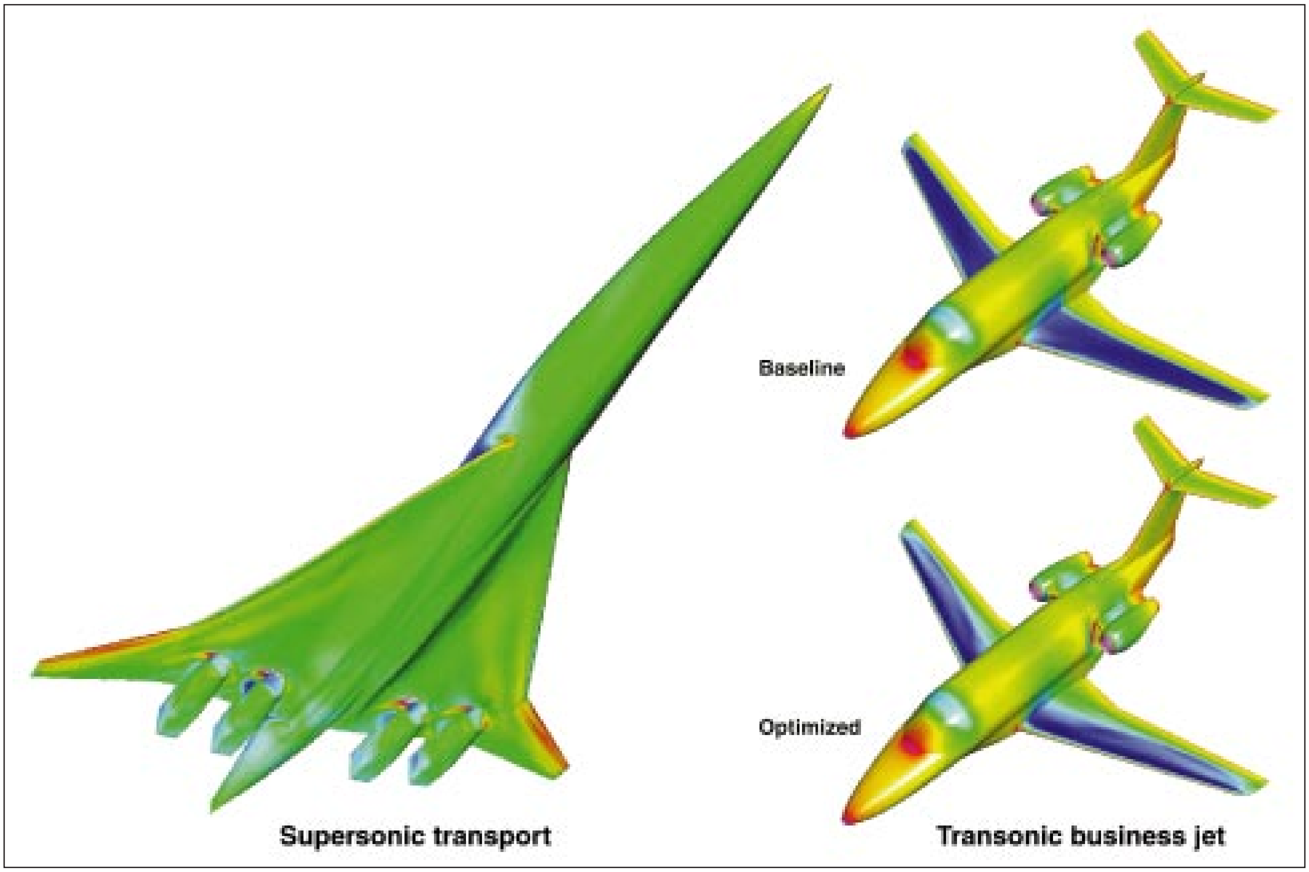

Fig. 1. Design/optimization studies.

the postprocessing and presentation of results. In addition, this aerodynamic surface design/optimization capability has been coupled with computational structural mechanics (CSM) codes to allow both the static aeroelastic deflections and the sizing of the structural elements to be included in the design process.

These techniques have been applied to a variety of configurations and have proved to be very effective. The figure illustrates the two classes of configurations that have been studied in detail: a supersonic transport and a transonic business jet. A number of supersonic transport configurations have been examined starting with simple wing-body configurations and progressing to rather complex wing-body-nacelle-diverter configurations. In each of these cases, the drag-to-lift ratio of the configuration was used as the objective function in the design optimization process. Substantial improvements in supersonic cruise performance were achieved in each case through the application of this technology. Many of the predicted performance increments were validated experimentally. The business jet application used both the drag-to-lift of the configuration and the wing pressure distribution as objective functions in the design/optimization process. In addition, these designs were multipoint problems in which the design was carried out at two or more flight conditions to achieve a more overall optimum configuration. The application of these optimization techniques significantly improved the performance of these configurations and demonstrated a significant reduction in design cycle time for wings of this class. The business jet was also the subject of the combined aero/structural optimization. The structural considerations imposed in the design problem eliminated the need for explicit thickness constraints based on independent structural considerations and permitted design trade-offs between aerodynamic and structural performance requirements.

Point of Contact: S. Cliff/J. Reuther
(650) 604-3907/1516
cliff@sus.arc.nasa.gov
reuther@ra-iris.arc.nasa.gov

Overset Structured Grids for Unsteady Aerodynamics

Robert Meakin, Andrew Wissink

The Department of Defense (DoD) is supporting the development of robust adaptive refinement methods for unsteady geometrically complex moving-body problems through the HPC (High Performance Computing) Modernization Program Initiative known as CHSSI (Common High Performance Computing Software Support Initiative). The object of the work is to exploit the computational advantages inherent in structured data in order to solve this important class of problems on parallel scalable computer platforms.

The physical domain of complex problems is decomposed into near-body and off-body regions. The near-body domain is discretized with "Chimera" overset grids that need extend only a short distance into the field. The off-body domain is discretized with overset structured Cartesian grids (uniform) of varying levels of refinement. The near-body grids resolve

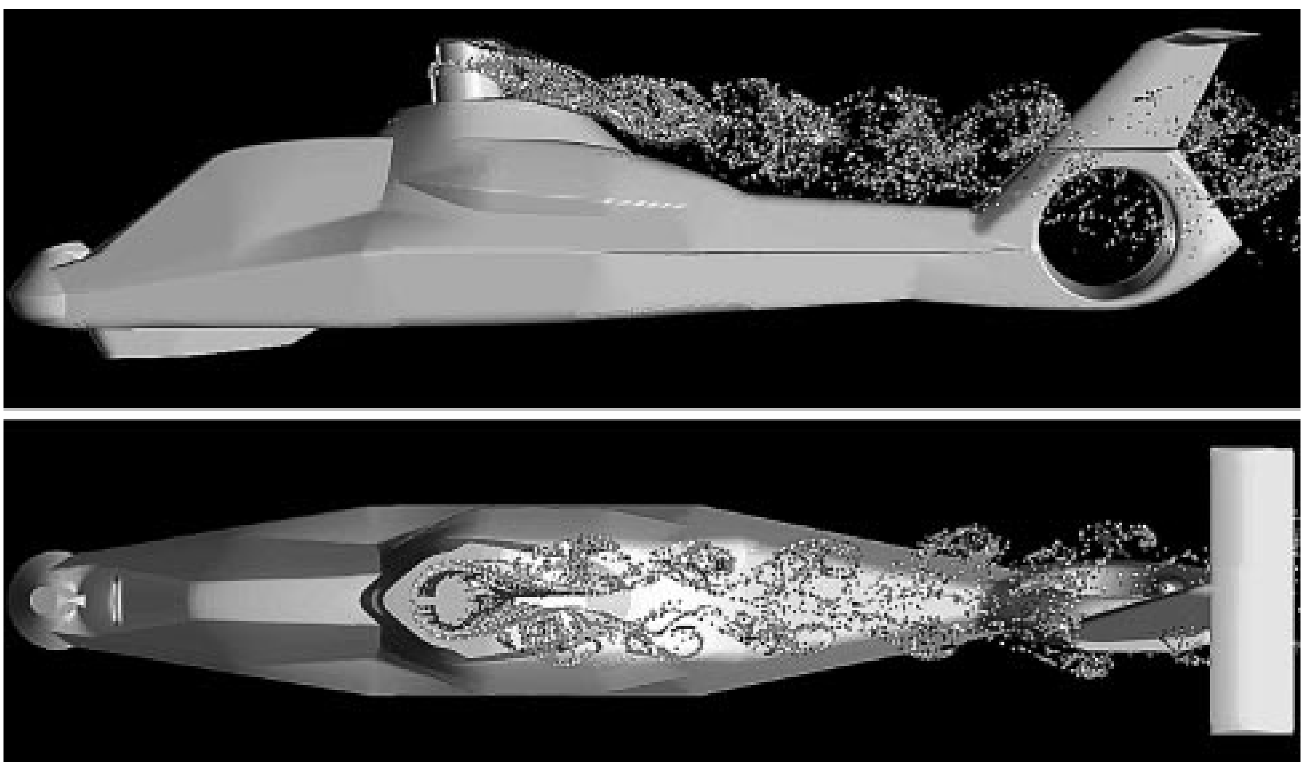

Fig. 1. Flow visualization of unsteady flow about the Comanche helicopter fuselage.

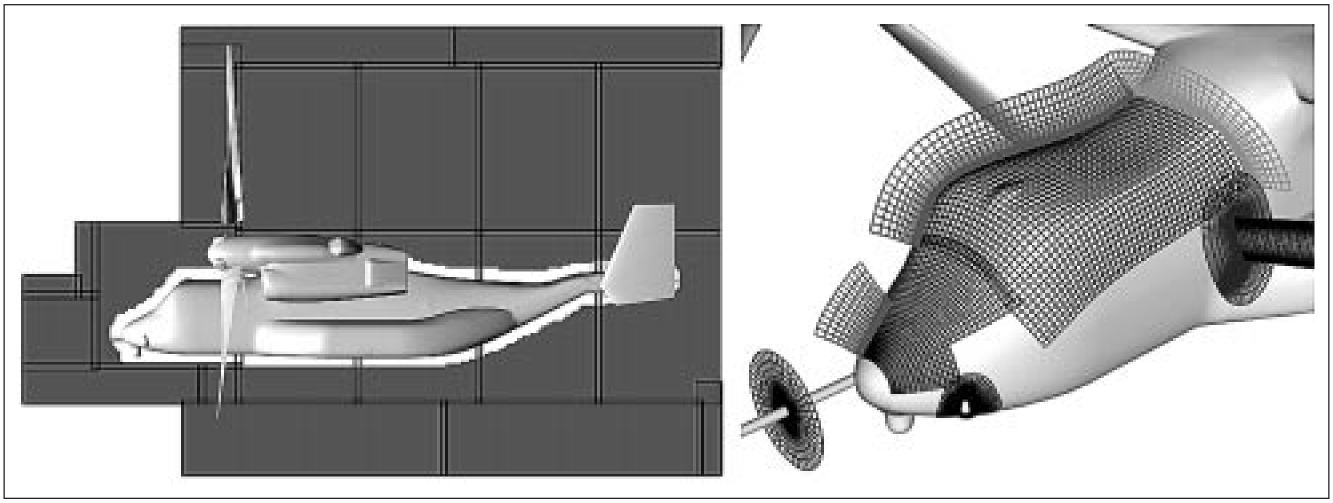

Fig. 2. Geometry and selected grid surfaces from overset grid discretization of the V-22 tilt rotor.

viscous boundary layers and other flow features expected to develop near body surfaces. Off-body grids automatically adapt to the proximity of near-body components and evolving flow features. The adaptation scheme automatically maintains solution accuracy at the resolution capacity of the near-body system of grids. The approach is computationally efficient and it has high potential for scalability. Grid components are automatically organized into groups of equal size, facilitating parallel scale-up on the number of groups requested. The method has been implemented in the OVERFLOW-D2 code.

The first figure illustrates a result from a time-accurate Navier–Stokes simulation using OVERFLOW-D2 on an IBM-SP to identify sources of unsteadiness in the Comanche helicopter aerodynamic field. The figure provides top and side views of a "snapshot" of the flow field where particles have been released from the rotor hub. The second figure shows the geometry and selected surfaces from an overset grid discretization of the V-22 tilt rotor aircraft.

Demonstrations of OVERFLOW-D2 on a large-scale application such as the Comanche and V-22 are significant because of the broad class of problems of interest to the DoD and NASA that require the accuracy available through adaptation and the computational efficiency realizable through structured data. Target problems of the method include unsteady moving-geometry applications such as aircraft store separation, helicopter rotor-body interaction, crew escape systems, flight maneuvers, and launch vehicle staging.

Point of Contact: R. Meakin
(650) 604-3969
meakin@nas.nasa.gov

CFD Methods for Rotorcraft Engineering

Francis X. Caradonna, Marvin A. Moulton

The prediction of essential rotor flows (most notably encountered in the prediction of hover performance, blade–vortex interaction noise, and vibrations) is dependent on the ability to accurately model the wake. Most computational fluid dynamics (CFD) methods are inaccurate when used for such problems because of the long-unsolved problem of numerical wake dissipation. The use of massive grids, enabled by parallel computers, will eventually solve the dissipation problem, but at a cost that precludes routine engineering applications (analysis, design, optimization). There is a need for CFD methods that can treat the repetitive, wake-related problems encountered by rotorcraft engineers. The goal of this work is to develop such methods, apply them to important engineering problems, and, where necessary, to perform validation testing.

This work involves two CFD methods: (1) a unique potential method, having a free-wake capability called "vortex embedding"; and (2) a modified Euler/Navier–Stokes method, called "vortex confinement," which incorporates additional terms that explicitly oppose vorticity dissipation. The former vortex-embedding method is in a state of advanced development/validation and is being applied to the study of the effects of rotor configuration on hover efficiency. This same approach is also being coupled to inner viscous solvers to enable the prediction of stall limits. The vorticity-confinement method is in a proof-of-concept stage of development aimed at demonstrating low-diffusion vortex transport using small grids.

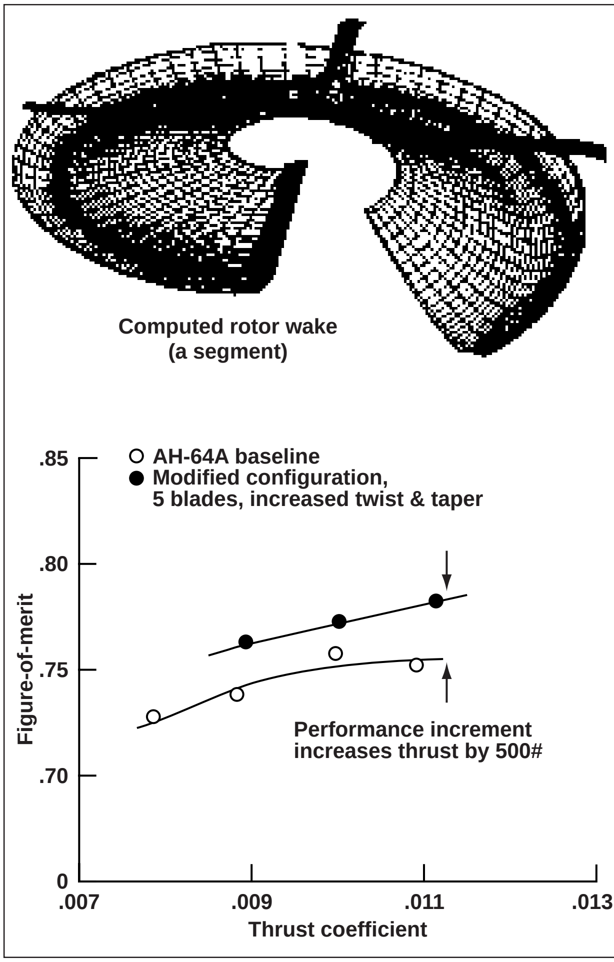

Fig. 1. Computed performance improvements resulting from rotor configuration changes. Computations are performed using the HELIX-I vortex-embedding code.

In FY98, the vortex-embedded code HELIX-I was applied to the study of alternative configurations for a modernized Apache rotor (in support of Boeing DT-2000 rotor design work). Such configuration studies require many repetitive computations and are assessing the parametric effect of rotor geometry variations (including twist, taper, and anhedral) on figure-of-merit. The first figure shows a comparison of performance for the basic AH-64A rotor and a configuration employing increased linear twist, anhedral, and blade number. This configuration, with the exception of the anhedral, is similar to a final selected configuration (scheduled for full-scale testing in 2000). In performing these Apache comparisons, configurations are characterized by performance increments relative to a standard computation, rather than as an absolute performance value. This is because of the well-known sensitivities to the wake behavior and also to the lack of reliable hover data for this rotor. This deficiency in the data is being addressed by preparations to perform a test of a model rotor.

In addition to these test preparations, major improvements have been made in the computational capability, especially with the development of the HELIX/OV code which replaces the approximate boundary-layer models with a complete viscous inner solver. First tests of this code show very good agreement with existing UH-60A hover data. Similar computations will be performed for tilt rotors and AH-64 variants.

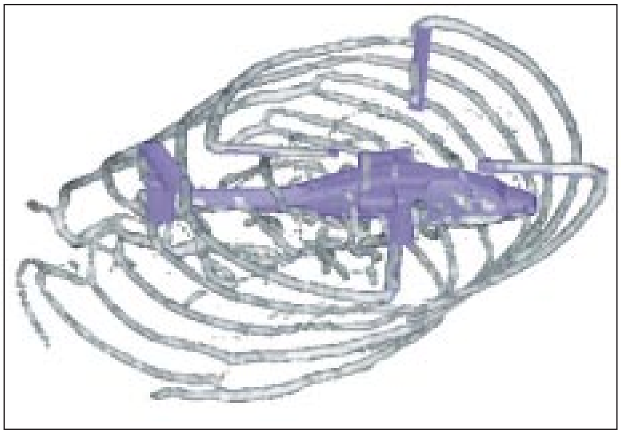

Fig. 2. Computed wake system for an AH-64A in climb. The vortices are computed using confinement and visualized as constant-vorticity surfaces.

Work on the vorticity confinement method during FY98 included the first pilot computations of an extended wake system, including fuselage interactions. This inclusion of a simplified fuselage was enabled by treating its surface as a vorticity sheet, which is then “captured” using confinement. The second figure shows this pilot computation of an AH-64A in climb. The point of this computation is that it demonstrates the ability to compute rotor/body/wake flows—not necessarily with the highest possible surface resolution, but with much smaller grids than previously thought possible (probably two orders of magnitude smaller than a conventional approach requires).

Point of Contact: F. Caradonna
(650) 604-5902
fcaradonna@mail.arc.nasa.gov

Computational Fluid Dynamics Analysis of High-Lift Aircraft

Stuart E. Rogers, Karlin Roth, Steve Nash, M. David Baker

The use of computational fluid dynamics (CFD) analysis is contributing to the analysis and understanding of the physics of complex flows over subsonic aircraft in takeoff and landing configurations. The objectives of this work are to develop an accurate and efficient Navier–Stokes analysis method for flow over an entire aircraft in a high-lift configuration and to examine the critical physics affecting high-lift system design.

The overset grid approach, the newly developed Chimera Grid Tools, and the OVERFLOW CFD flow solver, have been utilized to compute the viscous flow over several different high-lift aircraft. One such effort was the computation of the flow over a Boeing 777-200 aircraft in a landing configuration. This effort was undertaken as part of the joint NASA and industry Advanced Subsonic Technology (AST) program. The goal of the 777 computation was to demonstrate an ability to produce a CFD simulation, starting with the computer-aided design (CAD) representation, in only 50 working days, in order to meet one of the 1998 AST program milestones. A team of CFD engineers from Ames and Boeing was able to produce an initial solution for this aircraft in 256 man-hours (32 working days). The initial configuration consisted of the aircraft wing, body, vertical tail, three leading-edge slats, four trailing-edge flaps, and the engine strut and nacelle. The final configuration of the 777 aircraft included the addition of three flap-bracket fairings and details on the wing leading edge. A solution for this configuration was obtained in a total of 384 man-hours (48 working days), which is greater than a fivefold improvement over a previous effort for computing the viscous flow over a high-lift aircraft. The primary reason for the significant improvement in the CFD cycle time for such a complex geometry is the development of a script system as part of this AST activity. The script system greatly streamlines the process required to

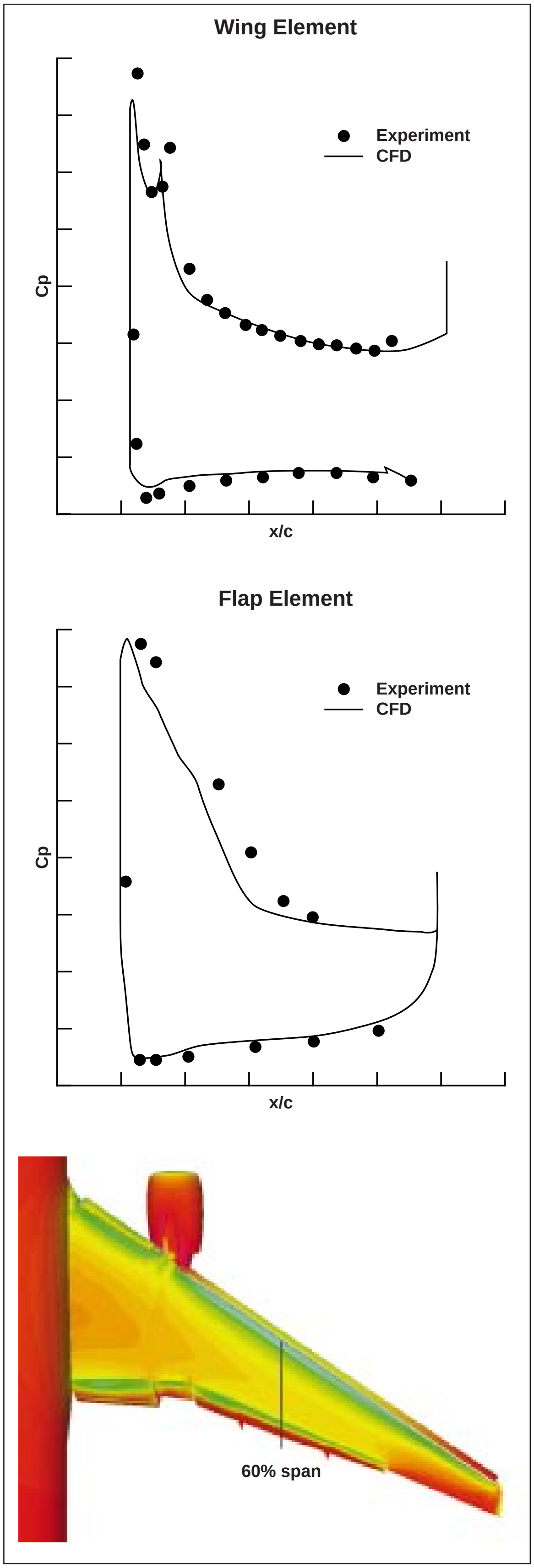

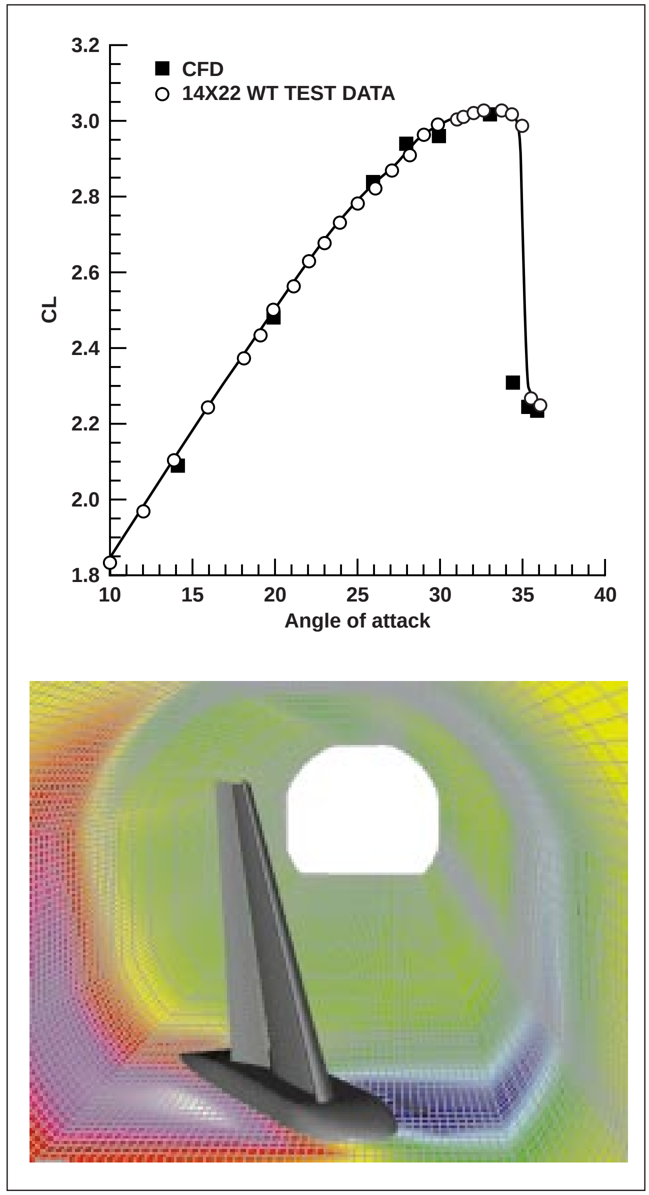

Fig. 2. Trap wing surface grids and computed lift coefficient.

Fig. 1. Surface pressure on a Boeing 777 high-lift configuration.

produce a grid system for a complex geometry, by producing most of the input required by the many software programs used to produce such a CFD analysis, and by providing significantly improved error detection and handling. This script system is now available as part of the Chimera Grid Tools software package.

The final grid system consisted of 79 zones and 22.4 million grid points. A single steady-state solution using this grid system requires approximately 200 Cray C90 CPU hours. With the use of multitasking, a solution can be obtained in as little as 3 days. The simulations are steady-state, employ the Spalart–Allmaras turbulence model, and utilize multigrid acceleration techniques. At approach conditions, the computed lift and drag coefficients were within 2% of experimentally measured values. The first figure shows the upper surface of the aircraft colored according to surface pressure. Included are pressure coefficient plots comparing the computational results with experimental measurements at the 60% span location of the wing.

A second high-lift application is shown in the second figure. This geometry is known as the trapezoidal wing, which is being tested experimentally as part of the AST program to provide CFD validation data. The wing consists of a body pod, a main element, a full-span leading-edge slat, and a full-span trailing-edge flap. Using the current overset approach, this configuration was computed for a range of angles of attack through maximum lift (CL_{max}). As shown in the figure, the agreement between the computed and experimental lift coefficient is excellent. The CFD predicted CL_{max} to within 0.5%.

Point of Contact: S. Rogers
(650) 604-4481
rogers@nas.nasa.gov

Simulations of Hot-Streak Migration

Karen Gundy-Burlet, Daniel Dorney

Experimental data have shown that combustor temperature nonuniformities can lead to the excessive heating of first-stage rotor blades in turbines. This heating of the rotor blades can lead to thermal fatigue and degrade turbine performance. The results of recent studies have shown that variations in the circumferential location of the first-stage stator airfoils can be used to control the adverse effects of the hot streaks by mixing hot-streak fluid with the cooler fluid contained in the first-stage stator wake. Less emphasis has been placed on determining the optimal radial location of the hot streaks at the inlet to the first-stage stator blade row. The focus of the present effort has been to study the effects of varying the radial and circumferential locations of hot streaks at the inlet to a high-pressure turbine, with the goal of developing passive and inexpensive techniques for controlling the adverse effects caused by the hot streaks.

A three-dimensional, unsteady, thin-layer Navier–Stokes zonal code (STAGE-3) has been developed to analyze these flows. It is based on a third-order accurate, upwind, implicit scheme. Body conforming "O" grids are used to accurately resolve the viscous effects associated with each airfoil. These are overlaid on sheared Cartesian grids which resolve the flow field between airfoils. The Cartesian grids are allowed to slip past each other, simulating the relative motion between rotor blades and stator vanes. STAGE-3 has been designed to simulate axial turbomachines with arbitrary numbers of stages; it also allows for different numbers of airfoils in each row.

The effects of combustor hot streaks on a 1-1/2-stage turbine were studied for a series of six parametric cases: hot streaks fully impinging on the first-stage stator and placed midpassage between two adjacent first-stage stators at radial locations at 20%, 40%, and 60% of span. The figure shows instantaneous surface temperatures and an isocontour of temperature for the fully impinging 20% span case. Based on the matrix of simulations the following conclusions have been drawn:

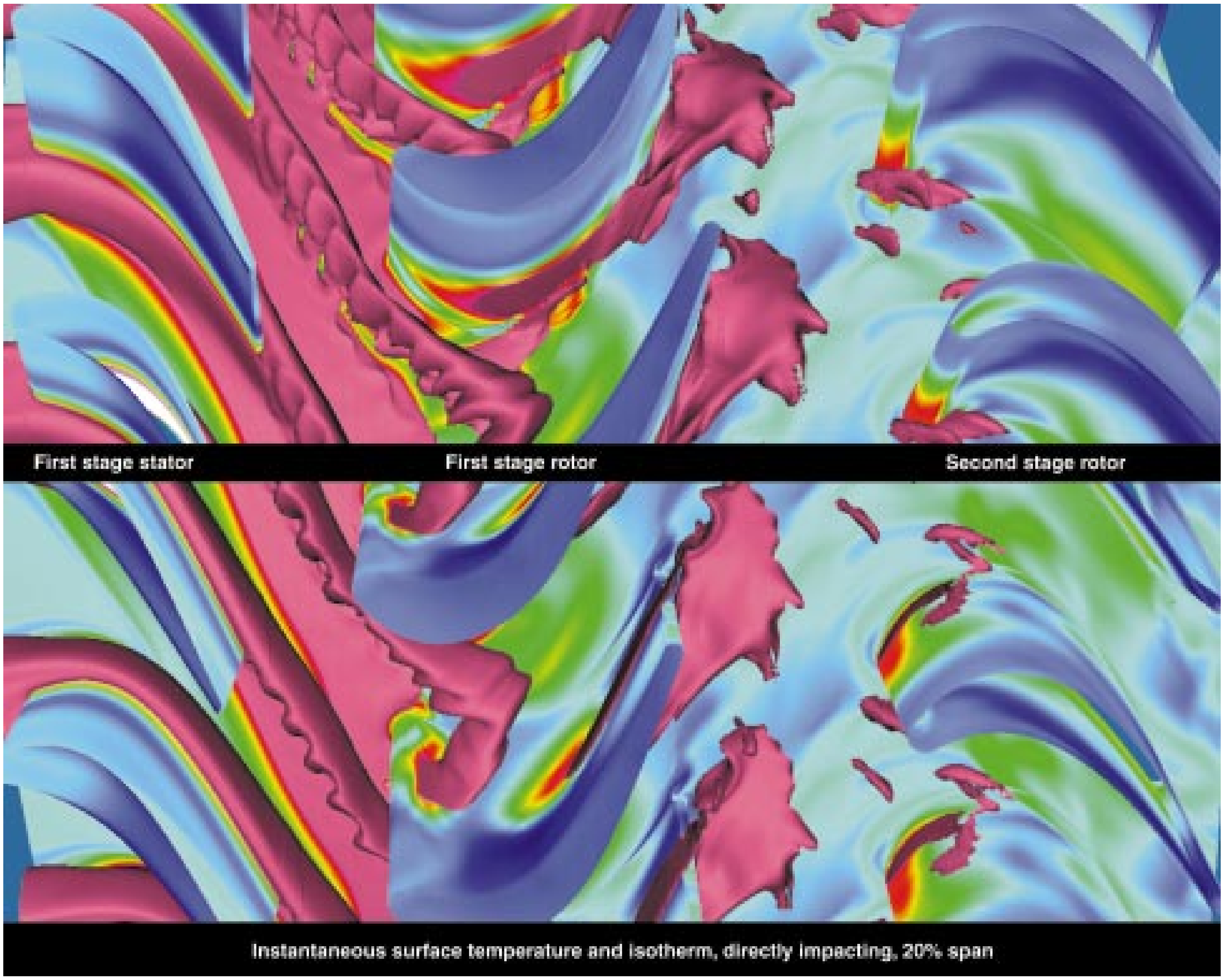

Fig. 1. Instantaneous surface temperature and hot-streak isotherm in a 1-1/2 stage turbine. Location of isotherm directly impinges on first-stage stator at 20% span.

- Direct impingement of the hot streak on the first-stage stator increases the heat load on this airfoil, but significantly reduces the heat load on the rotor and second-stage stator. This condition should be acceptable since first-stage stators are normally designed to withstand these high temperatures (through the use of film cooling, etc.).
- The increased heat load (associated with impinging the hot streak) on the first-stage stator does not vary significantly with time. This should allow the use of film-cooling schemes which minimize the amount of wasted cooling flow.
- Impingement of the hot streak on the first stator in the hub region causes migration of the hot streak from the stator pressure surface into the hub boundary layer and induces substantial, but stable in time, heating of the hub in the stator-1 passage.
- Introducing the hot streak at midspan and midpassage results in less end-wall heating, but generates severe heat loads on the pressure surface of the rotor.

- Placement of the hot streak near the tip region causes increased time-averaged temperatures in a region already prone to burning and failure.
- Impinging the hot streak on the first-stage stator desensitizes the rotor and second-stage stator heating patterns to the radial placement of the hot streak.

Based on these findings, it is suggested that a hot streak be introduced in the lower half span of a stator passage, and oriented such that it impinges directly on the first-stage stator.

Point of Contact: K. Gundy-Burlet
(650) 604-4475
gundy@nas.nasa.gov

STOVL Integrated Flight/Propulsion Controls

James A. Franklin

Ames Research Center is participating in technology development for short takeoff/vertical landing (STOVL) fighter aircraft as a member of the Joint Strike Fighter (JSF) program team. The objectives of this program are (1) to provide technical and facilities support to the JSF program office and contractors, and (2) to conduct research on controls and displays for STOVL aircraft that can be applied to the development of the JSF STOVL variant.

In conjunction with the first objective, NASA has transferred technology developed through ground-based simulation and flight research on the (vertical/short takeoff and landing) V/STOL Systems Research Aircraft (VSRA) to the JSF Integrated Flight/Propulsion Controls Integrated Project Team (IPT) for use by the program office and JSF contractors in the design of the aircraft's flight and propulsion control laws and cockpit interface. NASA has provided consultation to the program participants as a member of the IPT and has made simulation facilities available for use by the program office and contractors for the duration of the Concept Demonstrator Aircraft (CDA) development phase. The goal is to reduce technical and schedule risk for aerodynamic and propulsion system sizing and dynamic response in the design of the demonstrator aircraft. The approach is to define design factors critical to STOVL operations, determine baseline criteria from ground-based simulation, iterate with IPT members to arrive at a mutually agreed upon set of design guidelines, and assess the design as it progresses. A high-fidelity simulation of the airframe, propulsion system, control system, cockpit displays, and inceptors has been developed and used to conduct evaluations of the design on the Vertical Motion Simulator. Design guidance was provided to the JSF IPT on control-system dynamics and thrust margin. The information was used by the JSF program office and contractors to reach an agreement on the desired dynamic response for attitude control power, longitudinal acceleration and thrust control margins (the latter including the effects of jet-induced aerodynamics and hot-gas ingestion), attitude and translational rate bandwidth and phase delay, and methods for accounting for thrust loss owing to attitude control in vertical flight.

As a second objective, NASA has conducted research and has funded contracted research by the JSF contractors on integrated flight/propulsion control laws, control inceptors, and displays to define concepts, and has evaluated them in ground-based simulation at Ames. This NASA-sponsored research is intended to achieve an understanding of the integration of control modes, inceptors, and displays over all phases of STOVL operations in preparation for the Engineering and Manufacturing Development phase of the JSF program. The goal of this research is to reduce technical risk by insuring that response types match task demands, that system performance precludes aircraft/pilot coupling, and that integration of multiple control modes, inceptors, and displays receives pilot acceptance. The approach is to establish an industry/NASA team to define response types and develop control laws, with the command software based on desired response type and the inner loop control commands based on aerodynamic/propulsion system characteristics. Display and inceptor designs have been developed to provide seamless transition between operational phases in flight and on the ground. These designs are being

Fig. 1. Boeing Joint Strike Fighter.

Fig. 2. Lockheed Martin Joint Strike Fighter.

evaluated and refined on the Vertical Motion Simulator. Three simulation phases were conducted during FY98 with the two JSF contractors, Boeing and Lockheed Martin. The two aircraft configurations are shown in the accompanying figures. During these simulations, all phases of STOVL operation were conducted, including short and vertical takeoffs, accelerating and decelerating transitions, approach to slow and vertical landings, shore-based and shipboard vertical landings, and precision hover maneuvering.

Point of Contact: J. Franklin
(650) 604-6004
jfranklin@mail.arc.nasa.gov

Evaluating Taxiing Operations for the High Speed Civil Transport

Mary K. Kaiser

The conceptual design of the High Speed Civil Transport (HSCT) presents many challenges for taxiing operations. The flight-deck design excluded forward-looking windows, and the position of the pilot is far forward of the nose and main gear of the aircraft.

In October of 1998, evaluations were begun of several advanced technologies to aid pilots with taxiing operations of the HSCT. These technologies were mounted on the Surface Operations Research and Evaluation Vehicle (SOREV) sited at Moses Lake, Washington. As shown in the figure, the SOREV captures many of the critical geometric aspects of the HSCT, particularly the footprint of the landing gear and the flight-deck's position relative to the nose and main gear.

Two advanced technologies were assessed. The first permitted the forward video displays to serve as "virtual windows" by linking the scene on the monitor to the position of the pilots' head. Thus, the area of the external world visible on this display varied as the pilot's head changed position, as is the case when viewing the world through a window. The second innovation was to provide the pilot with a camera display aimed at the ground directly below the point on the aircraft that should be maintained over the taxiway centerline. This presented a display that provided the pilot with a straightforward tracking task for maintaining proper vehicle position.

The study findings indicated that there are troublesome limitations that constrain the utility of the virtual window technology. On the other hand, the guidance camera was shown to be an effective aid for taxiing operations. In fact, this guidance technology may hold promise for aiding in the taxiing of large, subsonic aircraft as well.

This research was conducted in collaboration with the other SOREV team partners: Boeing, Honeywell, and NASA Langley Research Center.

Point of Contact: M. Kaiser
(650) 604-4448
mkaiser@mail.arc.nasa.gov

Fig. 1. The Surface Operations Research and Evaluation Vehicle (SOREV) was used to evaluate several advanced technologies for aiding taxi operations of the High Speed Civil Transport (HSCT).

Computational Vortex Visualization

Roger Strawn, David Kenwright, Jasim Ahmad

Vortices that are shed from rotary and fixed-wing aircraft play an important role in determining aerodynamic forces, vibrations, and noise. Accurate modeling and subsequent identification of these vortical flow fields is particularly important for rotorcraft, in which the interactions between the rotor blades and their vortical wake systems play an important role in determining all aspects of rotorcraft performance. This project has developed a new automated method for identifying and visualizing vortices in large-scale computational fluid dynamics datasets.

The new vortex identification scheme detects vortex centers, or "skeletons," by searching for local maxima of vorticity in planes that are perpendicular to the local vorticity vector. This scheme has a straightforward physical interpretation and is easy to implement for structured-grid datasets. The two figures show sample results for computed vortices from a delta wing and from the Navy's V-22 Osprey rotor blades. Each small sphere represents the center of a vortex, and linear collections of spheres represent the trajectories of individual vortices. This scheme enables aircraft analysts and designers to rapidly identify and visualize important vortices in large three-dimensional computational datasets.

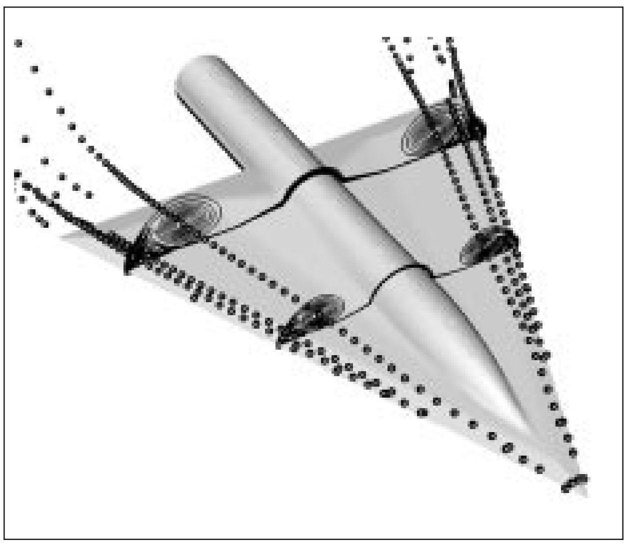

Fig. 1. Vorticity contours and automated vortex core traces for a delta wing.

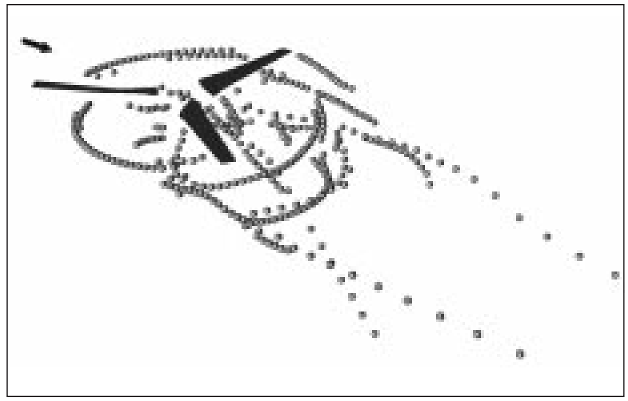

Fig. 2. Vortex core traces for the V-22 rotor blades.

Point of Contact: R. Strawn
(650) 604-4510
rstrawn@mail.arc.nasa.gov

Modeling of Plasmas in Microelectronics Processing

Deepak Bose

Space plasmas, arc jet plasmas—these are well known to many researchers at NASA. Understanding the structure of these plasmas has consumed years of research at various NASA laboratories. Computational modeling of such plasmas involves multicomponent, multitemperature flow analysis, and many NASA-developed computer codes are available for this purpose. Now Ames researchers have applied their expertise to the understanding of a different kind of plasma—one that is used in integrated circuit manufacturing. A weakly ionized plasma is used to etch fine patterns (about 1/10,000,000 meter) in a silicon wafer. The discharge gas may be chlorine or some type of fluorocarbon, depending on the material to be etched or the functionality. The objective is to obtain a highly directional (even vertical) feature of the etched profile at a rapid rate with minimum use of chemicals. If one were to use the chemicals in their liquid form—in what is known as "wet etching"—the above objectives would be compromised. An isotropic feature results from wet chemistry since chemical etch is "directionally blind." In contrast, the dry etch with the help of a plasma achieves desired directionality through the combined action of the reactive atom or radical and the vertical ion bombardment of the surface to clear off chemical reaction products.

It is of interest to the microelectronics community to understand this dry process in order to optimize it and to design the right kind of reactor. That is where computational modeling is valuable. A code has been developed that solves multicomponent, multitemperature, chemically reacting flow equations. This set includes Navier–Stokes equations (subsonic gas flow), the gas energy equation, an electron energy equation, multicomponent species conservation equations, and, finally, Maxwell's equation that determines the power coupled to the plasma from an external power source such as an inductive coil. Coupling of several such equations with disparate time scales results in a stiff problem. Time scaling of the equations for rapid solution is being explored.

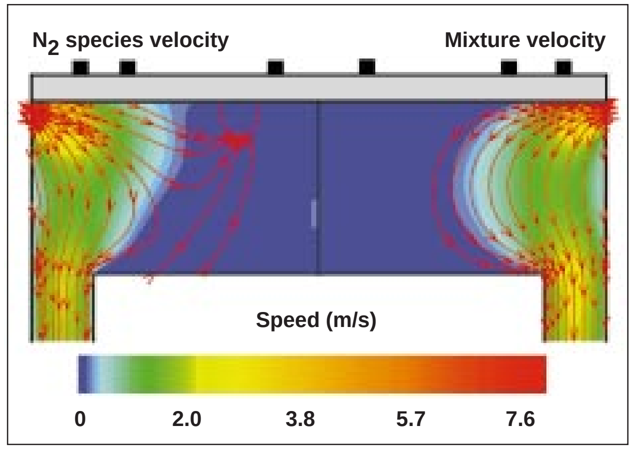

Fig. 1. Flow streamlines in an inductively coupled plasma reactor at 500 watts of absorbed power and 100 standard cubic centimeters per minute flow rate.

The code has been applied to commercial reactors manufactured in the Silicon Valley and to processes common in integrated circuit fabrication. Results have been obtained for nitrogen plasmas and chlorine plasmas to date in a reactor capable of processing 300-millimeter wafers—in preparation for the next-generation circuits. The first figure shows flow streamlines in an inductively coupled plasma reactor that uses a chlorine plasma to etch silicon.

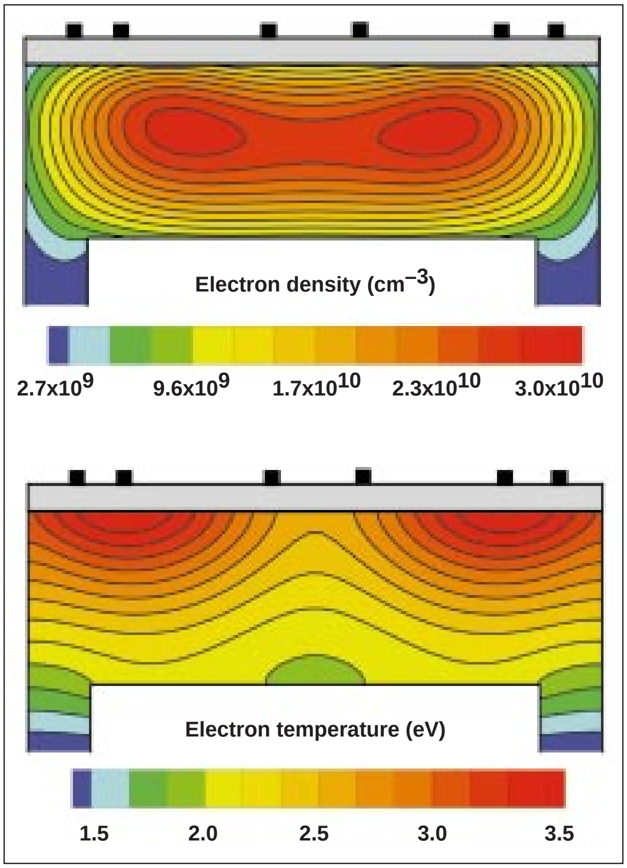

The second figure shows the electron density and temperature in the reactor. Uniformity of etch is a critical figure-of-merit. This depends on the flux of active radicals and ions—all of which are created by electron-impact reactions. Therefore it is important to understand the electron characteristics.

Point of Contact: D. Bose
(650) 604-3945
bose@dm2.arc.nasa.gov

Fig. 2. Electron density and temperature in an inductively coupled plasma reactor at 500 watts absorbed power and 100 standard cubic centimeters per minute rate.

Chlorosilane Thermal Decomposition Pathways and Rates

Stephen P. Walch, Christopher E. Dateo

As part of the new initiative to create a reliable database in microelectronic processing, calculations of gas-phase reaction rates have been carried out for use in modeling thermal chemical vapor deposition (CVD) reactors. Modeling has become an important design tool in the microelectronics industry. However, for the modeling to be useful on equipment design, the prototype code must be accompanied by a reliable database of the chemical and physical properties of the gases and surfaces involved. In many cases, direct experimental measurements of gas-phase reaction rates are unavailable or unreliable. Theoretical calculations then become an important source of data.

In conventional CVD processes, film growth occurs on a hot surface from thermally activated reactions. The initial process in the deposition is the gas-phase thermal decomposition of the starting materials. Secondary gas-phase reactions can enhance or inhibit film growth by affecting the population of molecules that can react with the surface. Surface reactions can also introduce other species that might desorb and subsequently contribute to the gas-phase chemistry. Accurate modeling and, ultimately, the control of the CVD process, will require knowing the identity of these species and their reaction rates at the temperature and pressure of the reactor chamber.

The most widely used CVD process in the microelectronics industry is silicon deposition. There has been extensive work in investigating the kinetics of silicon growth using silanes. In contrast, fewer studies have examined silicon deposition using chlorosilanes. The initial studies at Ames concern reactions involved in thermal decomposition of the chlorosilanes in the presence of hydrogen ($SiCl_xH_{4-x}$–H_2) and the secondary reactions that might play a role in the CVD process. State-of-the-art ab initio quantum mechanical methods are used to determine chemical reaction pathways and to evaluate reaction-rate coefficients.

In particular, reactant, product, and transition state (saddle point) geometries and vibrational harmonic frequencies are computed by using the complete-active-space self-consistent-field (CASSCF)/derivative electronic structure methods with the correlation-consistent polarized-valence double-zeta (cc-pVDZ) basis set. Reaction pathways are constructed by following the imaginary frequency mode of the saddle point to the reactant and product. Accurate energetics are determined by using the singles and doubles coupled-cluster method that includes a perturbational estimate of the effects of connected triple excitations (CCSD(T)) which are extrapolated to the complete basis set limit using second-order Moller–Plesset perturbation theory (MP2). Reaction-rate coefficients can then be obtained using conventional and variational transition state (TST) and unimolecular Rice–Ramsperger–Kassel–Marcus (RRKM) theories.

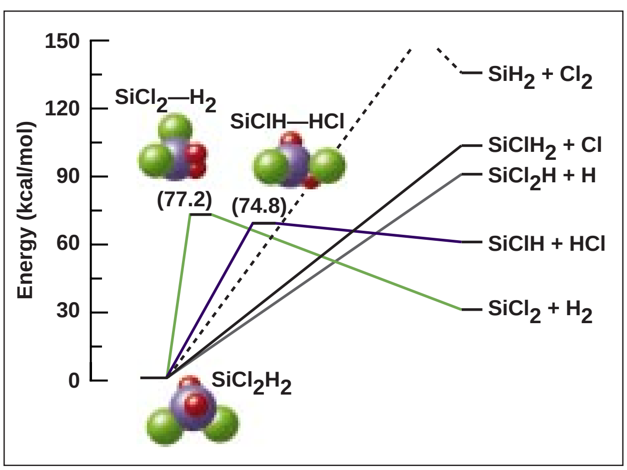

Fig. 1. Dichlorosilane decomposition pathways.

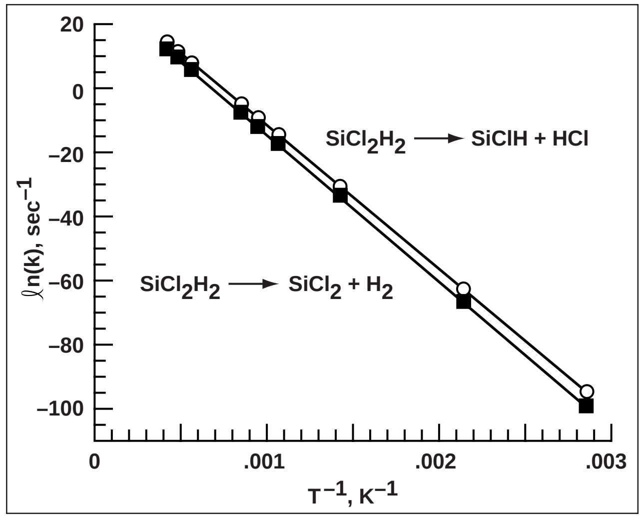

Fig. 2. High-pressure limit of unimolecular rate constants.

The two figures show representative results from the current studies at Ames. The first figure shows the reaction pathways for the thermal decomposition of dichlorosilane ($SiCl_2H_2$). Barrier heights in kilocalories per mole are given in parentheses. At reactor temperatures (600–1000 kelvin), only the two lowest reaction pathways are predicted to be important. The second figure is a plot of the logarithm of the high-pressure rate coefficient from TST versus the inverse of the temperature in degrees kelvin. These calculations predict SiClH + HCl to be the dominant product channel despite being energetically higher than the $SiCl_2$ + H_2 product channel. This is due to the lower reaction barrier to reach the SiClH + HCl product, as shown in the first figure.

The data generated from this study will be used in chemical reactor models in an effort to understand and control silicon CVD processes.

Point of Contact: S. Walch
(650) 604-6189
swalch@mail.arc.nasa.gov

Characterization of Novel Low-Dielectric Constant Materials

Richard L. Jaffe, Cattien V. Nguyen, Do Y. Yoon

As the feature dimension in integrated circuits continues to shrink, insulating materials with lower dielectric constants are needed to mitigate the resistance and capacitance (RC) delay and cross talk between metal interconnects. One class of materials that is receiving attention for this application is polysilsesquioxane, having the empirical formula $(R\text{-}SiO_{1.5})_n$ where R can be hydrogen or methyl (denoted HSSQ and MSSQ, respectively). Silsesquioxanes have dielectric constants less than 3, compared to conventional insulator materials such as silicon dioxide with dielectric constant equal to 4. However, future electronic devices will require even lower dielectric constants (less than 2) which may be achieved by introducing nanoporosity into MSSQ or HSSQ.

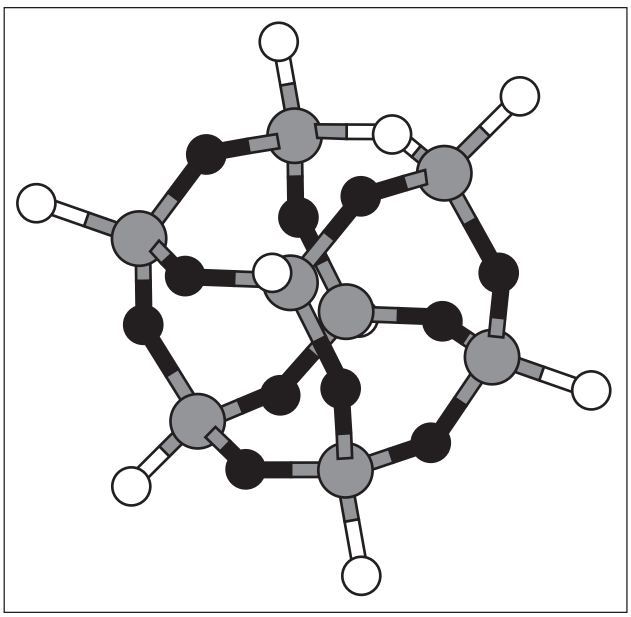

Fig. 1. The computed structure of an HSSQ cage molecule ($Si_8O_{12}H_8$). The white circles represent hydrogen atoms, the light gray circles represent silicon atoms, and the dark gray circles represent oxygen atoms. The silicon atoms are arranged 3 angstroms apart at the vertices of a cube.

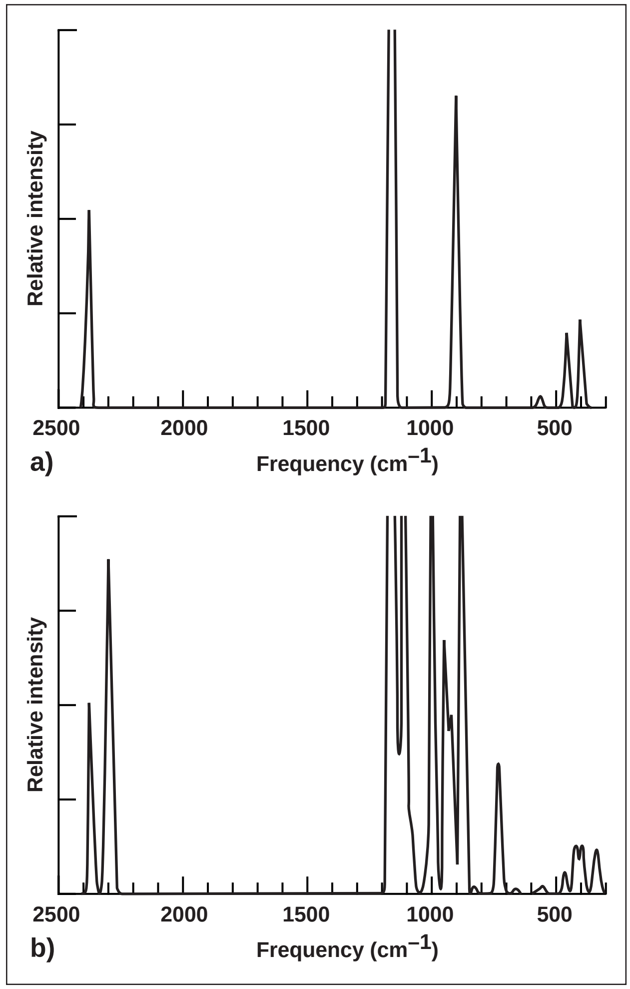

Fig. 2. Typical computed IR spectra of HSSQ molecules. The relative intensity is shown as a function of frequency in wave numbers (cm^{-1}). The ordinate is scaled to give the most intense band an intensity of 1.0. Part (a) is the spectrum of a symmetric cage molecule and part (b) is the spectrum of a nonsymmetric ladder molecule.

It is generally believed that HSSQ and MSSQ form small cages, as shown in the first figure, that are cross-linked together to form larger structures. However, they may also form open-ladder structures. It is not known whether the nature of the structures affects their dielectric properties. To better understand the silsesquioxane structure-property relationship, a quantum chemistry study was carried out for HSSQ and MSSQ cage and ladder models. This study included the determination of infrared (IR) spectra which were compared with experimental data. Of particular interest is the 1000–1200 wave-number region which contains extremely strong asymmetric Si-O stretching modes. Typical IR spectra are shown in the second figure where it can be seen that nonsymmetric structures exhibit more complex spectra. The result of this analysis indicates that (1) HSSQ starts from symmetric cage-like structures and is transformed to highly nonsymmetric structures during the annealing process because of the loss of Si-H groups, and (2) MSSQ forms nonsymmetric ladder-like structures that remain stable during annealing.

Further studies have shown that nanoporosity can be introduced into MSSQ films by co-depositing them with a sacrificial globular polymer that is decomposed during the thermal curing process. This leads to films with dielectric constants as low as 2.1. Similar attempts with the HSSQ films have not been successful. The resulting nanoporous MSSQ film should be well-suited for current semiconductor processing methods.

Point of Contact: R. Jaffe
(650) 604-6458
rjaffe@mail.arc.nasa.gov

Electron Collision Data for Plasma Modeling

Winifred M. Huo, Darian T. Stibbe

Electron collisions provide the driving mechanism behind the plasma processes employed in semiconductor manufacturing and related industries. The radicals and ions produced by the collision of electrons with the feed gas interact with the surface through a series of complex chemical reactions, leading to etching, deposition, or cleaning. In order to understand and control these processes, it is necessary to study electron-molecule collisions and the resulting products. Thus electron-collision data are part of the necessary database in device modeling. Such modeling has become a vital tool in the design of future electronic devices, while shrinking device size and the associated requirement for diminished defect-density make the traditional approach of design by trial and error obsolete.

In response to the demand for a reliable database, calculations of electron-collision data have been carried out. Using the Binary-Encounter-Bethe model, we have calculated electron-impact total ionization cross sections of molecules and radicals involved in plasma processing. The total ionization cross section determines the number density of electrons in a reactor. It also provides the total number density of ions which are responsible for some of the surface reactions. The molecules studied so far are CF_x(x = 1–4); SiF_x(x = 1–4); $SiCl_x$(x = 1–4); C_2F_6; C_3F_8; NF_x(x = 1–3); BF_x(x = 1–3); BCl_x(x = 1–3); and WF_6. The electron energy ranges from threshold to 10,000 electron volts. The figure presents the cross-section data of CF_x and SiF_x, (x = 1–3). Numerical tables of the cross-section data are available on the IPT web page (http://www.ipt.arc.nasa.gov).

Both electron-impact dissociation and dissociative ionization are mechanisms that produce the radicals responsible for many surface reactions. Dissociation into neutral products is particularly difficult to measure. Two of the most recent measurements of electron-impact dissociation cross sections of CF_4 differ by almost an order of magnitude. Theoretical studies so far have all been carried out at the equilibrium geometry of the target molecule, and nuclear dynamics have been neglected entirely. The electron-impact dissociation pathways of CF have been studied in this work and a number of competitive pathways have been found that include curve crossings and multistep processes with the low-lying $^4\Sigma^-$ state as the intermediate step. Based on the CF result, nuclear dynamics is expected to be an important factor in the cross-section calculation, and neglecting its contribution will lead to large errors in the resulting data.

Point of Contact: W. Huo
(650) 604-6161
whuo@mail.arc.nasa.gov

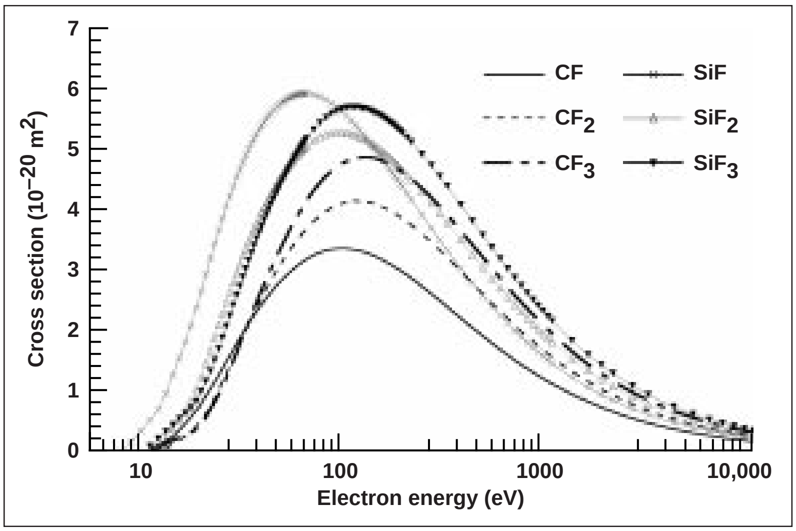

Fig. 1. Total electron-impact ionization cross section of CF_x(x = 1–3) and SiF_x(x = 1–3).

Access to Space

NASA Pegasus Hypersonics Experiment

Rex Churchward

The most recent Orbital Science Pegasus Mission to deliver a Brazilian satellite to Earth orbit and to fly a NASA hypersonics experiment was successful. The payload was placed at the desired orbit and the NASA glove assembly transmitted hypersonic flight data that will aid in the design of future high-speed vehicles. There has not been a flight to validate computer code solutions since the X-15 flew some 30 years ago. Several technological advancements in materials, construction, and electronic data collection/transmission were made in the effort to build and fly the glove. The Pegasus air-launched booster is shown in figure 1 and the wing glove in figure 2.

The Orbital Science Pegasus is an expendable, three-stage, solid rocket vehicle. The vehicle with payload was carried to 39,000 feet with a modified Lockheed L-1011 and dropped at a flight speed of Mach 0.8. Ignition of the rocket occurred at five seconds after drop. Flown as a piggyback experiment, the glove collected aerodynamic data during the firing of the first stage and up through the ignition phase of the second stage. During separation of the first and second stages, the speed of the vehicle was just beyond Mach 8. The winged first stage successfully transmitted flight data to ground support personnel and was not recovered.

The glove program was a joint effort between NASA Langley, Dryden, and Ames Research Centers.

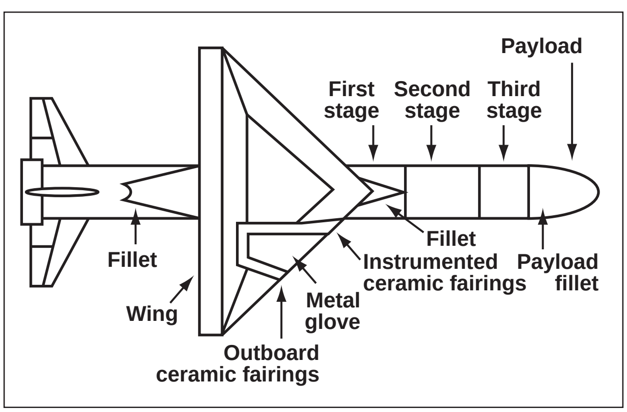

Fig. 1. Pegasus air-launched booster.

Fig. 2. View of glove.

The original concept was conceived by participants from all three centers. The final design and construction was carried out at NASA Dryden. NASA Kennedy Space Center provided launch support services for those who traveled to Cape Canaveral to participate in the launch.

Ames Research Center's major contribution to the glove assembly was the instrumented toughened uni-piece fibrous insulation (TUFI) tiles, which surround the metallic portion of the glove. Developed by Ames personnel, the methodology demonstrates the most cost-effective means of applying instrumented reusable tiles to an aerospace vehicle. This technology will be passed to NASA industry partners for use on future aerospace vehicles. Ames also provided materials engineering support during the design phase of the program and quality assurance certification of the various adhesive bonds that held the glove intact during the flight. The quality of the temperature data generated by the Ames instrumented tiles was excellent. The response of the tile-temperature hardware was sufficient to collect documentation of the rapid increase in leading-edge surface temperatures. There were approximately 24 type K thermocouples installed into the inboard set of tiles. The leading-edge tile contained the greatest number of surface thermocouples. There are now sufficient data to validate leading-edge models that have been generated from computer code and arc-jet phenomena. The flight experiment also helped validate the instrumentation methodology that will be used on the leeward side of the X-33 vehicle.

Point of Contact: R. Churchward/D. Rasky
(650) 604-3741/1098
rchurchward@mail.arc.nasa.gov
drasky@mail.arc.nasa.gov

Slender Hypersonic Aerothermodynamic Research Probe–Lifting #1

Paul Kolodziej, Daniel J. Rasky

Early hypersonic vehicle concepts were based on extrapolations of the knowledge and experience acquired in developing supersonic aircraft with slender bodies and sharp leading edges to minimize wave drag. At hypersonic velocity, however, the extreme heating of re-entry rapidly melted or ablated sharp leading edges fabricated from metals such as Inconel X and titanium. These material limitations led to the development of the blunt-body concept at Ames Research Center in the late 1950s by Harvey J. Allen, and this concept rapidly evolved into the Mercury, Gemini, and Apollo capsules. Because of the aerodynamic advantages, it is important to reexamine the feasibility of sharp-body concepts for operation as commercial, reusable launch vehicles using state-of-the-art thermal-protection-system (TPS) materials. One enabling technology for "sharp-body" reusable launch vehicles is ultra-high-temperature ceramic composite (UHTC) material currently under development at Ames. Arc-jet testing at Ames of UHTCs has demonstrated reusable performance of sharp-leading-edge components at temperatures approaching 5000°F. The first flight test of a sharp UHTC nose tip was conducted on May 21, 1997, by Ames, Sandia National Laboratory, and the U.S. Air Force. This SHARP-B1 (Slender Hypersonic Aerothermodynamic Research Probe—Ballistic #1) was the first of several planned flight demonstrations of advanced TPS technologies for sharp-body concepts. Temperature measurements of the SHARP-B1 nose tip (0.141-inch radius) during this flight test indicated that the UHTC material began to ablate, or melt, shortly after crossing the aerothermal performance constraint. The aerothermal performance constraint defines where the extreme heating of re-entry exceeds the reusable capability of the material and provides a designer with a new method for evaluating sharp-leading-edge components for reusable launch vehicles.

For demonstration purposes, assume that the SHARP-B1 nose tip has been attached in place of the existing nose cap (31.5-inch radius) on the Space Shuttle Orbiter. Instead of performing a complicated, transient thermal analysis to determine if the nose tip ablates, simply compare the Shuttle re-entry trajectory to the SHARP-B1 aerothermal performance constraints shown in figure 1. Because the Shuttle trajectory does not cross over the SHARP-B1 constraint, the nose tip will not ablate, and it may be flown again with minimum refurbishment.

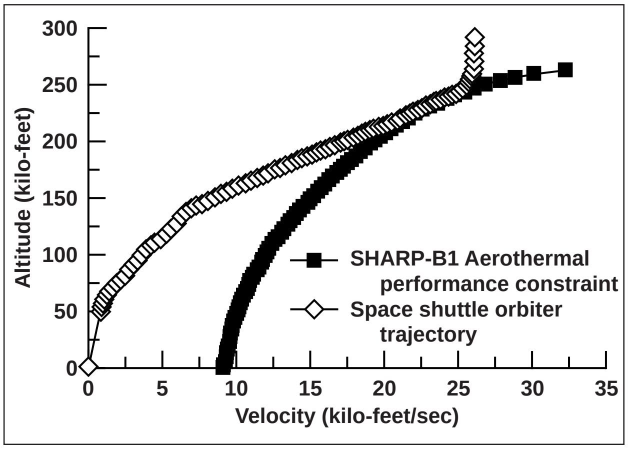

Fig. 1. Comparison of a nominal Shuttle re-entry trajectory to aerothermal performance constraints for the SHARP-B1 nose tip.

It is important to recognize that the radius of the SHARP-B1 nose tip is 200 times smaller than the existing Shuttle nose cap, and still operates without ablation along the Shuttle re-entry trajectory. This phenomenal capability opens a new frontier in the design of hypersonic vehicles. Flight demonstrations of new sharp-body concepts with UHTC leading edges and other advanced TPS components are essential to quickly advancing this new technology. SHARP-L1 (Slender Hypersonic Aerothermodynamic Research Probe—Lifting #1) is an example of a revolutionary sharp-body concept designed to maximize hypersonic aerodynamic performance represented by the lift-to-drag ratio (L/D) and volumetric efficiency (η). The historical trend shown in figure 2 was largely caused by the emphasis to reduce costs by performing "airplane-like" runway recovery instead of "Apollo" splashdown recovery. W. L. Hankey completed an optimization study in 1968 that demonstrated that significant improvements were possible if the runway landing constraint was removed. Increasing L/D is important for enabling new mission scenarios in the future when global cross range (L/D = 3.4) may become economically important. Minimizing cost is accomplished by increasing the volumetric efficiency to enclose the internal volume with less surface area, or TPS.

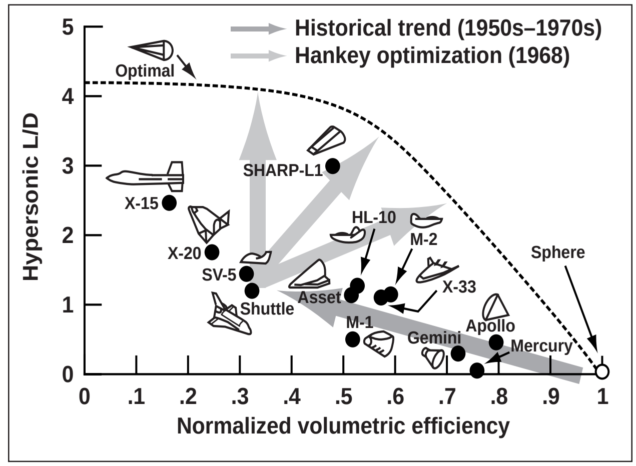

Fig. 2. Approach for maximizing hypersonic aerodynamic performance (L/D) and volumetric efficiency (η) of SHARP-L1 flight demonstration.

Point of Contact: P. Kolodziej/D. Rasky
(650) 604-0356/1987
pkolodziej@mail.arc.nasa.gov
drasky@mail.arc.nasa.gov

Mars Pathfinder Entry Heating and Temperature Data

Frank S. Milos, Y-K. Chen

The Mars Pathfinder probe contained instruments to measure heat-shield internal temperatures during the hypersonic entry into the Martian atmosphere. A separate experiment enabled reconstruction of the actual entry trajectory and the variation of atmospheric properties with altitude. With these data now available, the objectives of this work were to compute aerothermal heating and heat-shield thermal response for the actual entry conditions and atmospheric structure using the most up-to-date flow-field and material-response models, and to demonstrate if the data are consistent with believed uncertainties of the computational models.

The aerothermal heating environment was calculated using a nonequilibrium full Navier–Stokes equation solver that includes general multicomponent mass diffusion, catalytic surface boundary conditions, and an algebraic turbulence model. The surface was assumed to be fully catalytic for exothermic recombination of oxygen atoms and carbon monoxide to form carbon dioxide. This assumption is believed to be conservative, overpredicting the convective heating by 10 to 20%, but a general finite-catalycity model has not yet been developed. Flow-field solutions were obtained at 14 trajectory times between 30 and 100 seconds (sec). Both laminar and turbulent flow solutions were obtained starting at 66 sec, the earliest estimated time for turbulent flow based on Mars Viking data. Figure 1 shows the surface heating history at the locations of the stagnation-point and shoulder heat-shield temperature sensors. The fully catalytic peak heat flux and heat load at the stagnation point are 118 watts per square centimeter (W/cm^2) and 3.8 kilojoules per square centimeter (kJ/cm^2), respectively. Also shown is the stagnation-point radiative heat flux, estimated by correlation, which is much lower than the convective heating. At the shoulder, both laminar and turbulent heat flux are shown; the radiation is negligible. Depending on the onset time for turbulence, the fully catalytic peak heat flux is 53 to 69 W/cm^2, and the heat load is 1.8 to 2.2 kJ/cm^2.

Heat-shield temperatures were calculated using a charring thermal response code and material property models developed at Ames Research Center. The calculations used surface heat-transfer coefficients derived from the flow-field solutions, modified by appropriate "blowing corrections" that account for the effect of pyrolysis gas released from the heated materials. This procedure is reliable for the relatively low surface blowing rates considered here. Predictions were obtained for unscaled (100%) and scaled (85%) convective heating, where the latter is an approximation to account for the finite catalycity of the heat-shield material. Figure 2 presents the stagnation point midthickness temperature data

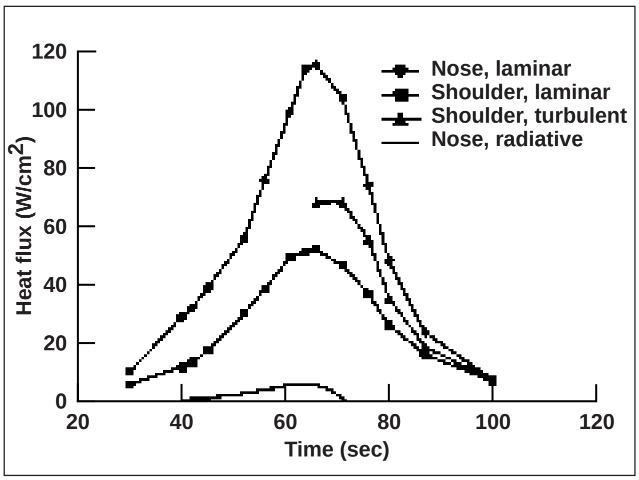

Fig. 1. Predicted surface heating at thermocouple locations.

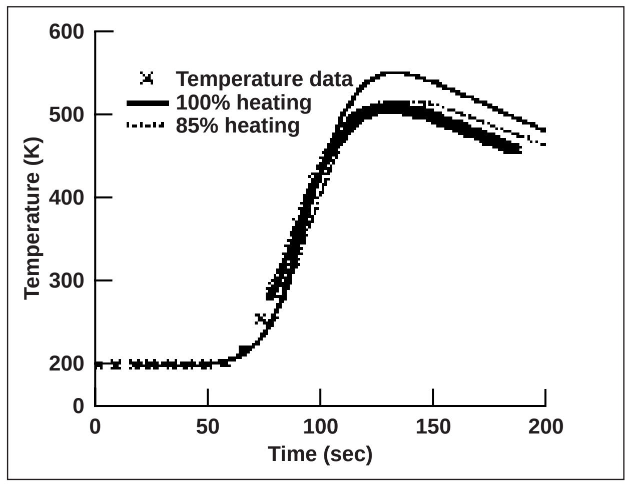

Fig. 2. Temperature data and predictions at stagnation-point midthickness thermocouple.

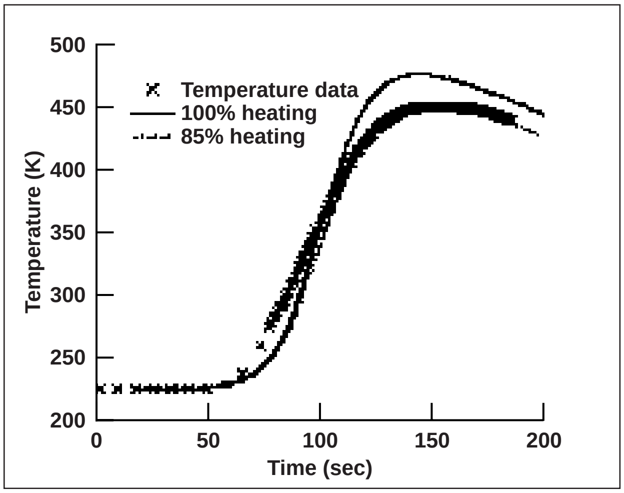

Fig. 3. Temperature data and predictions at shoulder midthickness thermocouple.

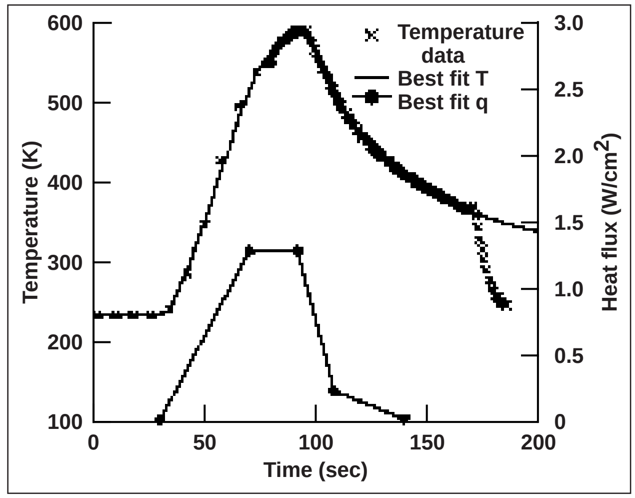

Fig. 4. Estimated heat-flux profile, temperature data, and predictions at aft near-surface thermocouple location.

(symbols) and the model predictions. The prediction using the 85% scaling provides a reasonable approximation to the data; however, there is a time lag in the initial temperature rise. For the shoulder thermocouple location, the material response was calculated using turbulent heating with transition at 66 sec and scaled (85%) turbulent heating with the same transition time. The temperature data (symbols) model predictions are illustrated in figure 3. The scaled case again provides a reasonable match to the data except for the initial temperature lag. Thus, the data are consistent with a modest (15%) reduction in heating from the values calculated for fully catalytic turbulent flow. This result is reasonable, considering the finite catalycity of the material and the perturbation of the flow-caused surface mass blowing.

Additional temperature data were obtained from a near-surface thermocouple located at the rear of the vehicle. In this case, because the emissivity and low-temperature properties of the material are well known, an approximate surface-heat-flux history is easily reconstructed. Figure 4 shows a simple "best-fit" heating profile, the calculated near-surface temperature history, and the thermocouple data. The temperature history is closely reproduced up to 170 sec, when parachute deployment abruptly changed the heating environment. Comparison of figures 1 and 4 indicates that the aft heat flux is a few percent of the forebody heating, but the aft heating profile is broader. These results are fully consistent with afterbody flow-field solutions recently performed for Pathfinder and other vehicles.

Point of Contact: F. Milos
(650) 604-5636
fmilos@mail.arc.nasa.gov

Ballistic-Range Tests at Ames Research Center

Tim Tam, Stephen Ruffin, Peter Gage, Grant Palmer

Ballistic-range tests of two concepts that may impact the design of future supersonic aircraft and launch vehicles were conducted at the Hypervelocity Free-Flight Aerodynamic Facility (HFFAF).

The first concept is an artificially blunted leading edge (ABLE). Georgia Tech Research Corporation developed this concept and is in the process of applying for a patent. Computational fluid dynamics (CFD) studies predicted that the ABLE concept, which modifies the shape of the detached bow shock by channeling some flow through slots in the body, may reduce the sonic boom by "blunting" the detached bow shock. In addition to reducing the sonic-boom levels, ABLE models have a lower drag coefficient than their blunt-body equivalent. The objective of this effort was to provide ground-test data to evaluate different ABLE configurations and to compare results with prediction methodologies.

Ames provided ballistic-range model design, fabrication, and testing of four different ABLE configurations. Ames performed detailed design of four different ABLE configurations to ensure that the corresponding models would be aerodynamically stable and survive the severe launch loads in the ballistic range. Ballistic-range models with several different multichanneled ABLE geometries have been designed, fabricated, and tested in the HFFAF to establish aerodynamic and sonic-boom characteristics at Mach 2. Nine of the 16 shadowgraph stations along the 75-foot test section were modified and instrumented with pressure-transducer ports to record sonic-boom signatures. Shadowgraph data and sonic-boom signatures were obtained for every test. Shadowgraphs were analyzed to obtain aerodynamic data (drag, lift, and pitch coefficients) for each configuration and to correlate the sonic-boom data with the model orientation at each station. Measured aerodynamic coefficient data and sonic-boom signatures were also compared with CFD predictions. Figures 1 and 2 show the comparison between CFD predictions and a shadowgraph from one of the 14 tests completed. Shock waves emanating from the nose and channel exit are clearly seen from both the computational predictions and the experimental picture. A previously unknown inaccuracy in sonic-boom prediction theory is being updated based on these tests. Lockheed Martin Skunkworks, Gulfstream, Georgia Tech, and NASA are using ballistic-range data and CFD predictions to evaluate each of the candidate ABLE configurations for potential application on their Advanced Supersonic Vehicle Technology (ASVT) program. As a result of these tests, Ames has demonstrated new capabilities by launching complex configurations with internal channels and recording sonic-boom signatures of models in free flight at multiple stations.

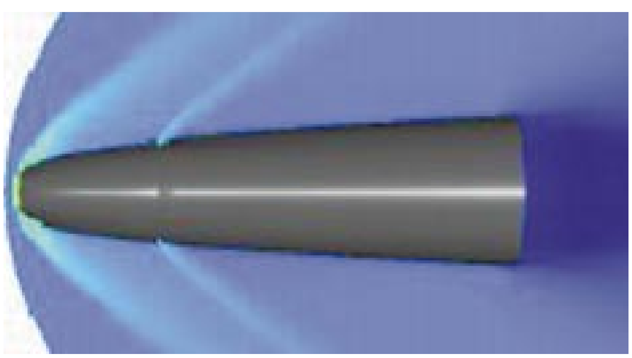

Fig. 1. ABLE CFD predictions.

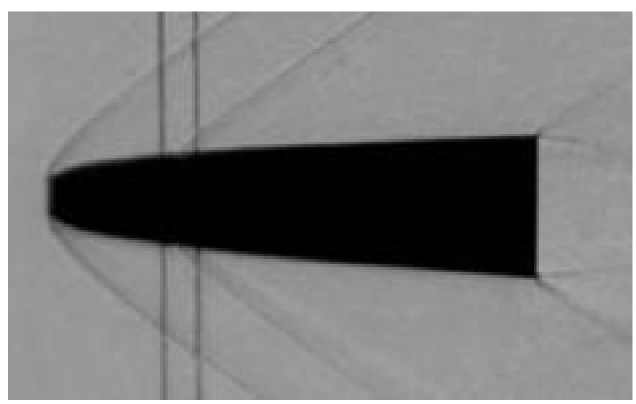

Fig. 2. ABLE experimental shadowgraph test conditions: Mach 2, pressure = 1 atmosphere, velocity = 2280 feet/second.

Another concept tested in the ballistic range was the Slender Hypervelocity Aerothermodynamic Research Probe—Lifting #1 (SHARP-L1). This configuration has the potential to reduce the cost of access to space by enabling a new class of volume-optimized, sharp-body hypersonic vehicles. The sharp-body geometry would provide significantly improved mission design flexibility and reduced life-cycle costs compared to current blunt-body designs. The objective of these tests was to characterize aerodynamics at the low supersonic (Mach 2) conditions where the vehicle is least stable.

Ames provided ballistic-range model design, fabrication, and testing of the baseline SHARP-L1 configuration. These tests provide aerodynamic data to compare with CFD codes. Preliminary results from the test indicate that the CFD aerodynamic prediction methodologies used in the design of this three-dimensional vehicle and model are accurate at these conditions.

Point of Contact: T. Tam
(650) 604-6094
ttam@mail.arc.nasa.gov

CFD Analysis of X-34 Flight Experiments Surface Heating

Grant Palmer

Computational fluid dynamics (CFD) analysis was performed on the X-34 vehicle to obtain a time history of surface heating rate and pressure on the Model Holder and very-large-panel-array (VLPA) flight experiments. These experiments hold samples of thermal-protection-system (TPS) materials whose performance will be assessed. The CFD data were used as input to a finite-element heat-conduction analysis. Computations over the nominal geometry were performed at four points on the X1004701 Mach 8.5 trajectory. Additional computations were performed at the expected peak heating point to determine the effect of front Model Holder interference on the VLPA and to determine the heating consequences if the experiments were to “fall out” during flight.

The surface and volume grids used by the three-dimensional (3-D) Navier–Stokes flow solver were generated from the initial graphics exchange standard (IGES) geometry data using the GRIDGEN grid generator. The flow solutions were computed using the General Aerodynamic Simulation Program (GASP) version 3 Navier–Stokes flow solver. GASP is an established commercial code that has been applied to a wide array of internal and external flow problems. GASP solves the full Navier–Stokes equations that model the conservation of density, momentum, and energy. A five-species, finite-rate, reacting-gas air chemistry model was used. All the flow solutions were assumed to be fully turbulent and used the Baldwin–Lomax turbulence model.

The Model Holders and VLPA are located on the bottom of the X-34 vehicle. For simplicity, the vehicle strakes were included in the CFD geometry but the wings were not. Figure 1 shows surface heating-rate contours at the 324-second trajectory point. The highest heating rate is at the nose and is 12.3 British thermal units per square foot-second (Btu/ft^2-s). The heating rate decreases as the flow expands around the nose. The bottom of the X-34 vehicle is essentially flat, so the heating rate is relatively constant for a given axial location and decreases gradually from the front part of the vehicle to the rear. There is an increase in heating rate on the forward-facing ramps of the Model Holders and VLPA caused by flow compression. A decrease in heating rate on the aft-facing ramps is caused by flow expansion. The duration of the heating pulse is short. The nominal heating rate is above 2 Btu/ft^2-s for less than 60 seconds. Nowhere on the vehicle, even on the forward-facing ramps, does the heating rate on the Model Holders and VLPA exceed 7 Btu/ft^2-s. The heating rate over the areas containing the TPS experiments is relatively constant, with a peak heating rate of approximately 5 Btu/ft^2-s.

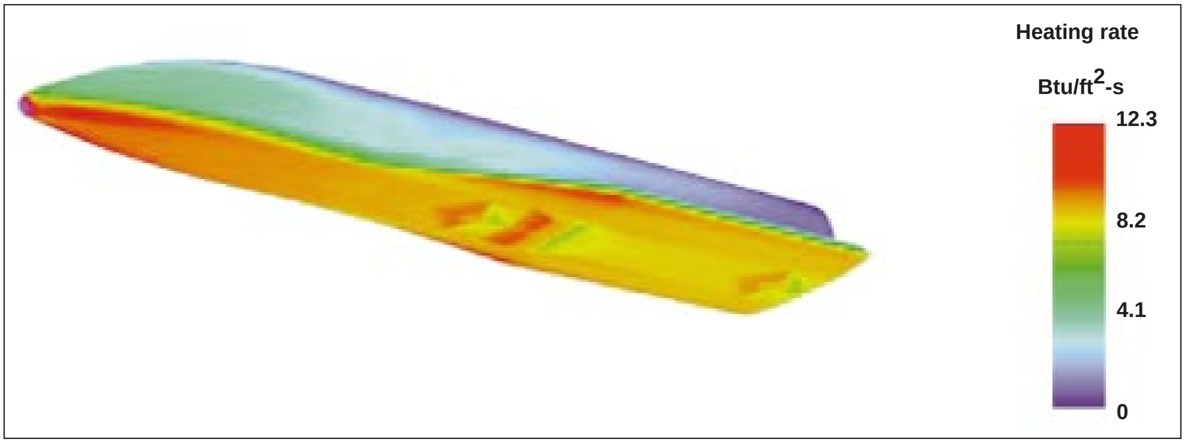

Fig. 1. Surface heating-rate contours.

Additional CFD computations showed that the location of the front Model Holder had little effect on VLPA surface heating. The final investigation determined the change in front Model Holder surface heating rate if all four TPS experiments were to "fall out." As would be expected, there is significantly increased heating on the forward-facing steps in the experiment-out configuration. The maximum heating rate with the experiments out is 12.7 Btu/ft^2-s. That value exceeds the stagnation-point heating rate on the vehicle nose at this trajectory point.

Point of Contact: G. Palmer
(650) 604-4226
gpalmer@mail.arc.nasa.gov

X-33 Aerothermal Preflight Predictions

Dinesh Prabhu, Dean Kontinos, Ethiraj Venkatapathy, Periklis Papadopoulos

Ames Research Center has provided analyses to support the design and flight testing of the Lockheed Martin Skunkworks X-33 Phase II vehicle. Hypersonic computational fluid dynamics (CFD) has been employed to predict the surface temperatures that will be experienced by the X-33 in flight. These data are used to design the X-33 thermal protection system and to support the flight test program.

The X-33 has been designed to fly at hypersonic speeds surpassing ten times the speed of sound. At speeds greater than six times the speed of sound, the shock wave emanating from a hypersonic vehicle is sufficiently strong to break apart the molecular constituents of the air through which the vehicle flies. Nitrogen and oxygen, which naturally exist as diatomic molecules, absorb the compressive energy imparted by the vehicle shock wave and dissociate into single atoms. These atomic species recombine as the air flows over the vehicle. The vehicle surface tends to promote the recombination of the chemical constituents. This tendency is termed "surface catalytic recombination." The energy that was originally absorbed to break apart the molecule is released when the atoms recombine at the surface. The released dissociation energy is absorbed by the vehicle and increases the surface temperature. It was critical to model the surface catalycity to accurately predict the surface temperatures of the vehicle.

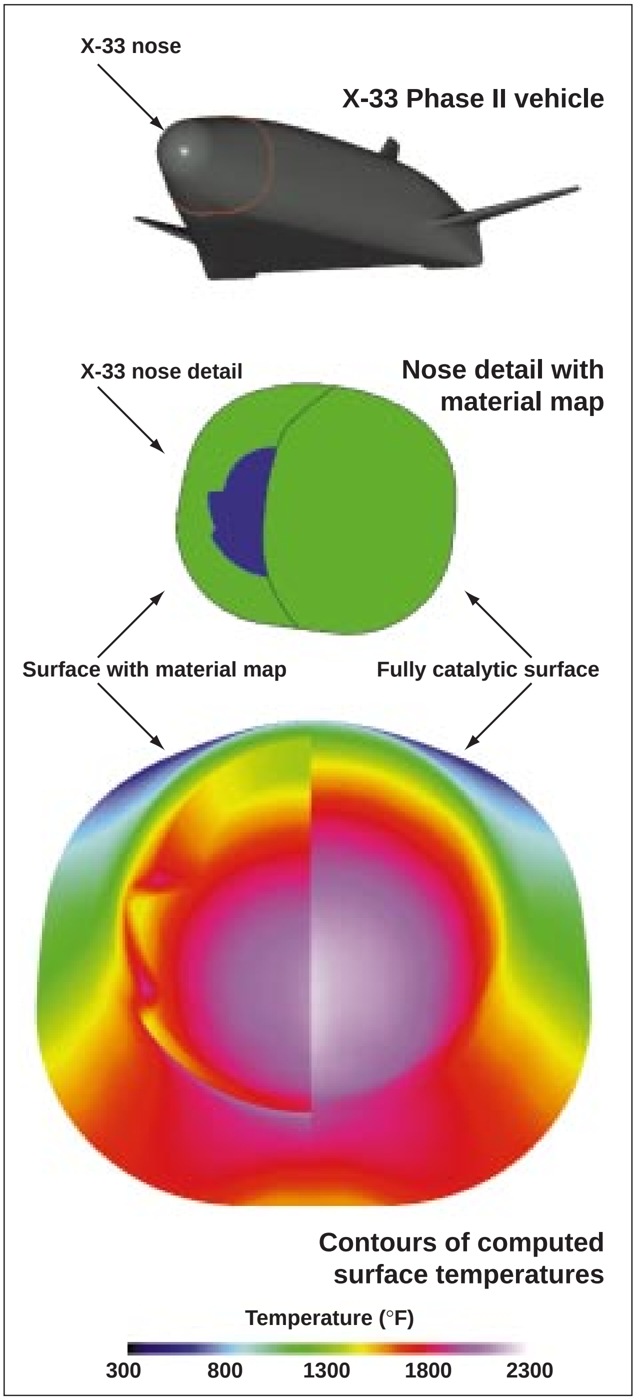

Fig. 1. X-33 surface temperature comparison: fully catalytic surface vs. catalytic material map.

During the design phase of the X-33 vehicle, the surface was assumed to be fully catalytic, that is, the rate of atom recombination at the surface is at a maximum. This assumption produces a worst-case scenario in that all the available dissociation energy is absorbed by the vehicle thermal protection system. In actual flight, however, the catalytic rate depends on the material of the surface; the rate will be less than the maximum. To predict the actual flight surface temperatures, a map of material-specific surface catalycity was incorporated into the CFD analysis to correspond to the material distribution on the X-33. The figure shows the surface temperatures on the nose of the X-33 that were computed assuming a fully catalytic surface compared to those computed using the material map. It is evident that the temperature distribution at the nose changes considerably when accounting for the differing catalytic properties of the various materials. The temperature distribution using the material map shows dramatic changes in surface temperature due to changes in the surface catalycity. This information is used to place flight instrumentation on the vehicle as well as provide vehicle performance predictions to certify the flight test trajectory.

Point of Contact: D. Prabhu
(650) 604-1145
dprabhu@mail.arc.nasa.gov

Space Science Enterprise

Overview

Scientists in NASA's Space Science Enterprise seek to answer fundamental questions about the origin and evolution of life and celestial objects (planets, planetary systems, stars, galaxies, etc.) in the Universe. Ames is recognized as a world leader in astrobiology, the study of life in the Universe and of the chemical and physical forces and adaptations that influence life's origin, evolution, and destiny. In pursuing its primary mission in astrobiology, Ames conducts basic research and technology development for the purpose of advancing our fundamental knowledge of the origin, evolution, and distribution of life within the context of cosmic processes. For example, research and technology development are currently conducted for the following purposes.

- To study the mechanisms of the origin, evolution, and distribution of life in the Universe
- To determine the abundance and distribution of the biogenic compounds that are conducive to the origin of life
- To identify locations on bodies within the solar system where conditions that are conducive to life either exist or have existed
- To explore the other bodies (planets, comets, asteroids) of the solar system
- To locate planets and planet-forming regions around other stars
- To study extrasolar matter such as interstellar gas and dust

At Octopus Spring, a thermal spring in Yellowstone National Park, a "rainbow" of microorganisms presents a striking visual image of the temperature sensitivity of the various thermophilic microorganisms living in the pool. The temperature in the spring varies from ~60°C to 87°C. (Photo courtesy of Linda L. Jahnke of the Exobiology Branch.)

Exobiology

Ames serves as NASA's lead Center in exobiology, and Ames' Exobiology Program is a key element of NASA's Astrobiology Initiative. Research in exobiology at Ames ranges from studying the mechanisms of the origin of living systems to the processes governing the evolution of life to the distribution of life on other planets. Ames' pioneering research into the dynamics of galaxies, molecular gases and clouds, planetary systems, and the solar system facilitates the study of life by providing a better understanding of the cosmic environment within which life originates and evolves.

Because molecules of exobiological significance are ubiquitous in the Universe, it is important to understand the sources and interactions of these basic building blocks of nature and to understand how living systems emerge from prebiotic molecular chaos.

Highlighted in this report are studies of the following:

- Evidence of life in the Martian meteorite ALH84001
- The ecology of modern microbial mats and stromatolites and the evolutionary ecology of microbial communities
- Prebiotic syntheses of activated amino acids
- Chemical biomarkers that represent ancient terrestrial life in the fossil record
- Simulations of a model transmembrane proton-transport system
- Organic molecules in comets and meteorites
- The synthetic pathways that produce the amino acids found in meteorites

Planetary Systems

Scientists in the Space Science Enterprise are interested in how and where in the Universe planets form, and in the geophysical, geochemical, and atmospheric processes that occur over planetary lifetimes. Further, an understanding of the dynamics that exist between planetary processes and the origin and evolution of life helps in understanding the distribution of life in the Universe.

Planetary Systems research highlighted in this report includes the following:

- Numerical simulations of the process of accretion, by which comets and asteroids are formed from micron-size dust grains in protoplanetary nebulae
- Development of instruments and techniques for detecting Earth-size planets outside of the solar system
- Studies of the effects of meteoritic impacts on the presence of highly oxidizing compounds in the martian soil

Astrophysics

As NASA's lead Center in airborne astronomy, scientists at Ames pioneered the field of astrophysics. Their study topics range from star-forming regions and processes to interstellar photochemistry to protoplanetary disks. Attaining an understanding of the cosmic processes—the evolution of the Universe itself—is a vital part of the Origins Initiative.

Ames astronomers and astrophysicists utilize a wide variety of methods. Ground-based telescopes and facilities such as the Keck and Mount Lemmon observatories, are regularly employed for observations of celestial objects and processes. Development continues on the Stratospheric Observatory for Infrared Astronomy (SOFIA), an infrared telescope that will be carried aloft aboard a Boeing 747 aircraft that is being specially modified for the task. Space-based observations are also made using such instruments and facilities as the Hubble Space Telescope (HST), the European Infrared Space Observatory (ISO), and the Japanese Infrared Telescope in Space (IRTF). Computer modeling and laboratory analogs of chemical processes are used as valuable adjuncts to these observational studies.

Astrophysics research highlighted in this report includes the following:

- Numerical modeling of the structure of solar nebulae and the structure's relation to planet formation
- Studies of the chemical composition of ices in the Kuiper disk

- Development of a far-infrared spectrometer for deployment on SOFIA
- Development of a faster and more accurate method for calculating instrument response functions in order to enhance analysis of measured spectra
- Studies of the dispersal stage in the formation of planets from protoplanetary disks
- The discovery of magnesium-rich crystals in the coma of comet Hale-Bopp

Space Technology

To support the Space Science Enterprise in conducting future space science and exploration missions, Ames scientists and engineers develop and validate relevant technologies and instruments, develop calculation-based and modeling algorithms, and refine analytical methods. The following developments are described in this report.

- An instrument capable of measuring the major elemental composition and mineralogy of small fine-grained or powdered samples
- A novel material for use in low-temperature regenerative coolers
- Focal-plane array detectors to allow reliable, background-limited infrared spectroscopy from space-based platforms
- A monitor capable of measuring the water vapor content of the atmosphere so that SOFIA's 3-meter-class telescope can be properly calibrated for detection of infrared signals
- The Marsokhod rover, an all-terrain vehicle developed as a prototype for future Mars rovers
- The organic optical material bacteriorhodopsin used for holographic optical data storage
- Computing-tools that can be used to enhance crew and payload operations in human space exploration missions

EXOBIOLOGY

The Ecology of Modern Microbial Mats and Stromatolites

Brad Bebout, Pieter T. Visscher, Jack Farmer

Work in the Microbial Ecology/Biogeochemistry Research Laboratory focuses on characterizing the biological activity of microbial mats and stromatolites. This is accomplished by using a combination of field and laboratory studies of modern microbial-mat and stromatolite communities. Microbial mats (laminated microbial ecosystems occurring in a variety of aquatic environments) and stromatolites (which can be thought of as mats in which minerals are being trapped or precipitated) are modern examples of the most ancient biological communities on Earth, examples of which are preserved in rocks as old as 3.5 billion years.

It is important to understand mineral formation in microbial mats (to make stromatolites) because it is primarily the stromatolites, and not the microbial mats, that become a part of the fossil record of life on Earth. What are the conditions under which these mat communities actually turn to stone? What happens to the organisms building the community as this happens? What are the biological consequences? In collaboration with a group of scientists led by Dr. R. Pamela Reid at the University of Miami, and funded by the National Science Foundation, studies of stromatolites have produced a model of one set of processes that lead to lithification (formation of rock) in stromatolites found in the Bahamas.

Trace-gas production and consumption in microbial mats are important to our understanding for a number of reasons. In addition to representing a potential loss of organic matter by the community, these gases diffuse into the atmosphere, where they can affect climate (as in the case of dimethyl sulfide and methane). In addition, the detection of some of these gases in the spectra of the atmospheres of extrasolar planets is considered to be a feasible search strategy for detecting life on those planets. Biological processes within these communities control the amounts and timing of the release of various trace gases. The trace gases produced and consumed by microbial mats from various environments have been quantified, and some of the factors affecting these rates of production and consumption have been identified.

Technology development in the laboratory has centered on finding better ways of measuring the rates of metabolic processes, on the concentrations of biologically important chemical species, and on the rates of production and consumption of trace gases in situ (in the natural environment). Naturally occurring microbial mats and stromatolites are subjected to conditions of water flow, temperature, and sunlight that are difficult, if not impossible, to simulate in the laboratory. Extensive fieldwork in Yellowstone National Park, the Bahamas, and Baja California, Mexico, has therefore been undertaken. Preliminary versions of a device designed to make in situ measurements of oxygen concentrations within these communities at 100-micrometer spatial resolution were tested and evaluated. New types of sensors designed to measure the light available for photosynthesis within these communities are also under development. A new device designed to measure the degree of lithification within stromatolites (as hardness) was developed and tested in the Bahamas.

Point of Contact: B. Bebout
(650) 604-3227
bbebout@mail.arc.nasa.gov

Evaluation of Evidence of Life in the Martian Meteorite ALH84001

David Blake, Sherry Cady, Kannan Krishnan, Allan Treiman

In 1996, an announcement was made that fossil evidence of bacterial life had been found in a meteorite known to have originated on Mars. One of the main lines of evidence for the putative bacterial fossils in the martian meteorite ALH84001 is the presence of submicroscopic crystals of the mineral magnetite that are similar in size and shape to biogenic magnetite crystals formed by primitive bacteria on Earth. The terrestrial organisms, called magnetotactic bacteria, use the magnetite to navigate in Earth's magnetic field. Although some bacterial species are able to mediate the deposition of minerals in the local extracellular environment, magnetite from terrestrial magnetotactic bacteria is known to be formed only within the cell membrane of the bacterium. In ALH84001, the submicroscopic magnetite is found in large aggregations associated with iron- and magnesium-rich carbonates, and the supposition is made that the magnetite survived the demise of the organisms and was passively incorporated into the surrounding carbonate. In this report, new evidence is presented concerning the ALH84001 magnetite, evidence that points to an inorganic origin.

The work done at Ames utilized a petrographic thin section of the meteorite, obtained from the curatorial collection at Johnson Space Center. Small portions of the meteorite material, which contained both carbonate and magnetite, were removed from the thin section and attached to electron microscope sample grids. The grids were placed in a sample preparation device which milled the material to a thickness less than 0.1 micrometer (one 10-millionth of a meter, or about 1/1,000 the diameter of a human hair). The thinned material was viewed in a high-resolution field-emission transmission electron microscope (FETEM) at the National Center for Electron Microscopy, Lawrence Berkeley Laboratories. In the FETEM, magnifications are achieved in which planes of atoms making up the magnetite and carbonate crystal structures can be directly viewed.

At high magnifications, the relationship of the magnetite crystal structure to that of the carbonate crystal structure is apparent. For example, the figure shows a high-resolution image of a single crystal of magnetite within the carbonate matrix. The fine lines in part (b) of the figure are planes of atoms making up the crystal structures of the carbonate and magnetite phases. One can see that certain planes of atoms or crystallographic directions within the magnetite structure are in alignment and have spacings similar to planes of atoms, or crystallographic directions of the surrounding carbonate. A significant number of magnetites were found to be related to the surrounding carbonate in this way. This preferred orientation, which is called epitaxy, is proof that the magnetite nucleated and grew on the surrounding carbonate. If the magnetite nucleated and grew at a site removed from direct contact with the carbonate (for example, within the membrane-bound body of a bacterial cell) and was later deposited in the carbonate, it would be highly improbable that such a special orientational relationship would arise.

Not all magnetite exhibits an epitaxial relationship with the surrounding carbonate within ALH84001. However, it is highly unlikely that magnetite crystals that do not exhibit epitaxy but that occur in identical spatial and temporal settings within the meteorite, were formed by an entirely different mechanism. Indeed, evidence obtained by Ames researchers suggests that the magnetite was precipitated inorganically from a carbonate-rich hydrothermal solution. The presence of nearly identical spacings between atomic planes in the carbonate and magnetite phases facilitates nucleation of the magnetite onto the carbonate from sparingly saturated hydrothermal solutions. Epitaxial growth of one phase on another avoids the activation-energy barrier associated with homogeneous nucleation, a significant hindrance to crystallization in most

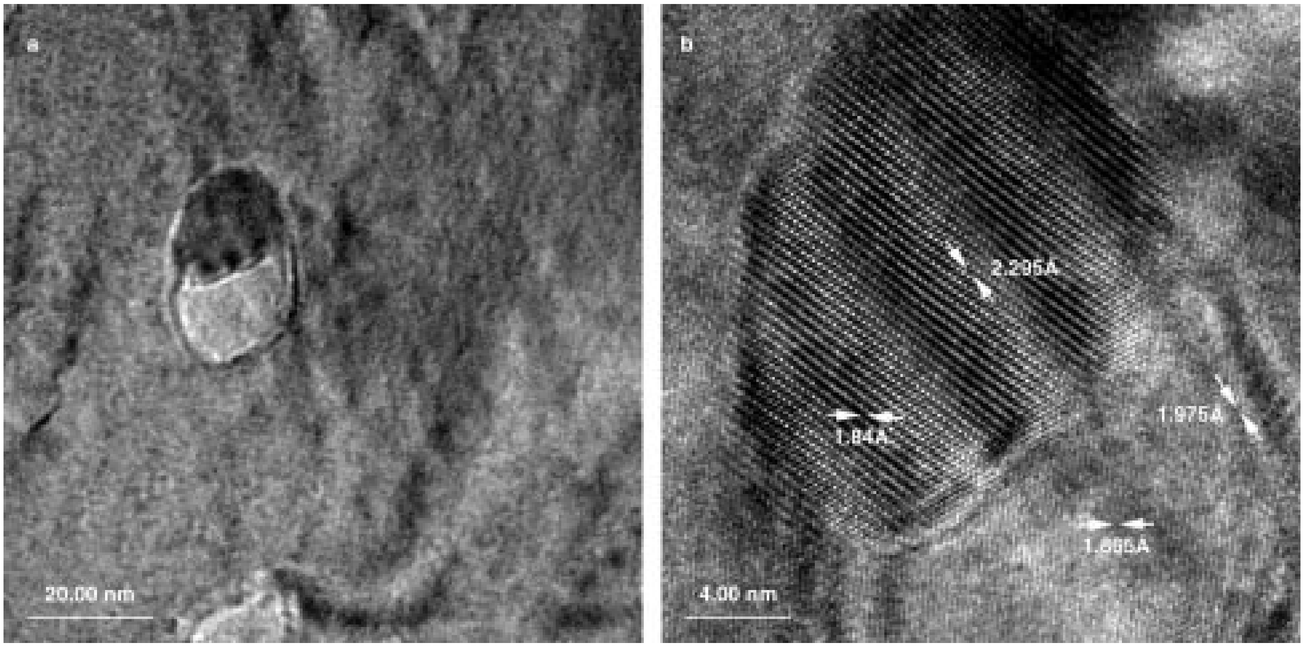

Fig. 1. High-magnification images of magnetite in epitaxial orientation to enclosing carbonate. (a) View of a single magnetite crystal enclosed within a small hole in the carbonate. (b) Lattice-resolution image of the magnetite and carbonate shown in (a). Atomic planes in the magnetite have spacings and parallel orientations that are closely similar to those in the carbonate, which is typical of an epitaxial relationship. The likelihood that this orientation occurred randomly after the magnetite was formed (for example, within a bacterial cell) cannot be entertained.

systems. During continued crystallization, a level of supersaturation must have been achieved in which magnetite could precipitate directly from solution without requiring a precursor phase.

Evidence now points to an inorganic origin for many of the features reported for the ALH84001 meteorite. However, analyses of the meteorite do suggest that carbonate-rich hydrothermal solutions existed in the near-surface environment on Mars 3.9 billion years ago, around the time that the first evidence of life is found on Earth. It remains that Mars is one of the most interesting objects in the solar system, from an astrobiological point of view, and evidence of hydrothermal systems and carbonate deposition in the early wet and warm period of Mars' history only increases interest in that planet.

Point of Contact: D. Blake
(650) 604-4816
dblake@mail.arc.nasa.gov

Polyhydroxylated Compounds in Meteorites

George Cooper, Novelle Kimmich, Katrina Brabham

Meteorites and interplanetary dust particles are the oldest objects available for laboratory study of early solar system chemical and physical processes. Most carbonaceous meteorites, a class of meteorites relatively enriched in carbon and organic compounds, are as old or older than the solar system planets, approximately 4.5 billion years. As a group they are also the most unaltered early solar system objects as illustrated by their near-solar (Sun) abundances in all but the most volatile elements. For this reason their content of organic compounds is a record of the earliest known abiotic organic synthesis. Meteorites, along with comets and interplanetary dust particles, may have delivered much organic matter to the early Earth.

The best characterized carbonaceous meteorite with respect to organic chemistry, Murchison, contains a large number of water-soluble organic compounds. These include amino acids, carboxylic acids, dicarboxylic acids, hydroxycarboxylic acids, amides, purines, pyrimidines, phosphonates, and sulfonates. Absent among the biologically important compounds reported in meteorites are sugars, which are polyhydroxylated aldehydes or ketones (polyols). Ribose and deoxyribose, five-carbon sugars, are central to the role of contemporary nucleic acids, DNA and RNA. If polyhydroxylated compounds are found in meteorites, this would demonstrate that such compounds could have been part of the initial mixture of prebiotic and biologically important compounds on the early Earth. If polyols, or any series of organic compounds are true products of abiotic chemistry, it seems likely that their synthesis would begin with smaller members of the series and gradually build, in decreasing abundance, to more complex members. This is the case with all homologous series of indigenous organic compounds seen in the Murchison meteorite, that is, amino acids, carboxylic acids, amides, etc. In the case of sugars and other polyols, one of the most generally agreed upon scenarios for natural abiotic synthesis is the "Formose" reaction, in which formaldehyde (CH_2O) in aqueous solution reacts with itself to gradually build a variety of hydroxylated compounds and sugars of increasing carbon number. Among the known products are glycoaldehyde, ethylene glycol, glyceraldehyde, dihydroxyacetone, glycerol, erythrose, ribose, and six-carbon sugars. Because there was aqueous alteration on the parent bodies of carbonaceous meteorites and because formaldehyde is a ubiquitous interstellar compound, the Formose reaction would have been possible in meteorites. Efforts at Ames have been directed toward determining the nature and abundance of polyols in carbonaceous meteorites.

The methods used for the study include isolating the meteorite polyols by ion-exchange chromatography, identification by gas-chromatography/mass-spectrometry (GC/MS), and isotopic analysis to ensure that identified compounds are extraterrestrial and not Earthly contaminants. Preliminary analysis of Murchison extracts indicates an abiotic synthesis of polyols, that is, a series of compounds of increasing carbon number (and decreasing abundance) has been observed. Some of the identified compounds are ethylene glycol, glycerol, dihydroxyacetone, and glyceric acid. There is also evidence of higher polyols. Bulk carbon ($^{13}C^{12}C$) and hydrogen (D/H) isotopic measurements also indicate that most of these compounds are indigenous to the meteorite. Determination of the isotopic composition (D/H, $^{13}C/^{12}C$, and $^{16}O/^{17}O/^{18}O$) of individual compounds, as well as further bulk measurements will help determine their synthetic origins.

Point of Contact: G. Cooper
(650) 604-5968
gcooper@mail.arc.nasa.gov

Evolutionary Ecology of Microbial Communities in Yellowstone National Park

Ken Cullings

Ecosystem function and the responses of ecosystems to both human-induced and natural change are mediated to a large extent by microbial processes. Although this fact is widely acknowledged, the role that different microbes play in this mediation is poorly understood. It is extremely difficult to identify microbes in their natural habitat, because there are few if any physical characteristics that can be used to distinguish among them. In this research, molecular-genetic tools are being developed to identify microbes in soil samples. These tools are being used to answer fundamental questions regarding ecosystem function and microbial evolution.

One set of projects is aimed at the question of to what degree co-evolution has given rise to specific interactions in a special type of plant/microbe interaction, the mycorrhizal symbiosis. Mycorrhizae are composed of plant and fungal components, and are responsible for mediating photosynthesis, carbon cycling, soil-litter breakdown, and nitrogen cycling in all terrestrial ecosystems. If patterns of specificity exist in nature, and if given plant species therefore require a certain subset of fungal species to survive, then the presence or absence of given fungal species would affect ecosystem dynamics. In addition, the question of whether human-induced disturbances to ecosystems, such as clear-cutting, and natural disturbances, such as fire, affect mycorrhizal communities differently is being addressed. Finally, because mycorrhizae enable plants to become established and to survive in extreme environments, how mycorrhizal communities in undisturbed ecosystems and thermally altered soils differ, and what adaptations these microbes have evolved in order to survive in these harsh environments, are being determined.

This research is being conducted in the forest and hot spring ecosystems of Yellowstone National Park, and is directly addressing many of these questions in the context of the 1988 park fires. Results of the co-evolution experiments indicate that specific patterns of interaction have evolved between plant and fungal partners. This indicates that exclusive patterns of carbon and nitrogen flow exist in this forest ecosystem, and suggests that mycorrhizal interactions play important roles in controlling ecosystem dynamics. Furthermore, plants that arrive in the ecosystem relatively late prefer fungal species that break down the needles of the plants that precede them. Therefore, there is evidence that fungal species facilitate the establishment of new tree species, providing rare support for a facilitation model of ecosystem dynamics. This research, which is being expanded to determine the effects of altering carbon flow to the roots and of litter manipulation on specificity patterns, is now in its initial stages.

A parallel project addresses the hypothesis that natural burning and clear-cutting will have different effects on the mycorrhizal community. The dogma is that they will not. However, there are obvious differences between fire and clear-cutting including the superheating of soils and the removal of litter, which is an important substrate for fungi and the main source of nitrogen for trees. Initial experiments indicate that there are differences between fire and clear-cutting in the short term. Experiments are now being planned to determine whether these differences extend into relatively long-time scales, and therefore whether human-induced disturbances will have long-term effects on ecosystem dynamics.

Finally, a new project has been started to determine the effects of the thermal-alteration of soils on soil microbial communities. This work has direct application to astrobiology and exobiology in that earliest organisms, and possibly organisms on Mars, first evolved in hot-springs environments. Migration into the surrounding soils would have followed shortly thereafter, and indeed these communities may have persisted long after thermal features dried and the springs disappeared. Thus these soils are suitable models in the search for life on Mars and other terrestrial planets. Initial results indicate that acid-sulfate thermal soils are inhabited by fungi that have adapted to extremely acidic conditions, but that are different from those traditionally thought to inhabit highly acidic soils. This has important implications for soil remediation strategies, and indicates that the dominant paradigm for fungal adaptation to extreme environments should be modified. This study is being expanded to include other soil microbes such as bacteria, Archea, and cyanobacteria.

Point of Contact: K. Cullings
(650) 604-2773
kcullings@mail.arc.nasa.gov

Peroxy Groups in Rocks—A Paradox

Friedemann Freund, Andrew G. Tenn

Earth—like all other solar system bodies, small and large—is chemically reduced. As a result all igneous rocks from deep within the Earth are reduced. It may therefore come as a surprise to learn that such rocks are suspected of containing peroxy, the epitome of oxidizing conditions.

An experimental verification would be quite important and might affect our thinking about rocks and about some of their key geophysical and geochemical properties, and even about some puzzling observations from the realm of biology regarding the earliest life forms on Earth.

A peroxy group consists of two oxygen anions. Normally, these oxygen anions carry two extra electrons to complete their outer shell and to achieve a stable configuration of eight. In the case of peroxy groups, both oxygens have given away one of their extra electrons, leaving seven, an unstable configuration. By pairing up and forming a short bond, the peroxy stabilizes.

To "see" peroxy groups in a mineral structure the oxygen–oxygen bond must be broken. When this happens, the peroxy group awakens from its dormant, electrically inactive state, releasing defect electrons or holes. These are charges not dissimilar to the holes in a p-type semiconductor used for building transistors. As soon as the holes appear, they crowd to the surface, leading to a positive surface charge and to an enhanced surface conductivity.

This led to a benchmark experiment. Two thin strips of gold were deposited on the surface of a single crystal of magnesium oxide to measure the surface conductivity. Part (a) of the first figure shows a view down onto the crystal on which the two thin gold electrodes were deposited and part (b) shows a cross section of the conductivity cell with the crystal between two planar electrodes for applying a cross field.

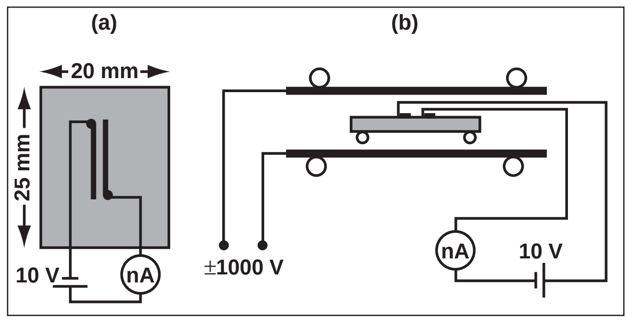

Fig. 1. (a) Gold electrodes, 1 x 15 millimeters and 3 millimeters apart, sputtered onto one side of a magnesium oxide crystal (patterned) for surface current measurements; (b) cross section of the conductivity cell with the crystal mounted between two electrodes for application of ±1250-volt-per-centimeter cross fields.

The breaking of peroxy-group bonds inside the crystal leads to an increase in the surface current because the holes come to the surface from within. A strong cross field is then applied and the field direction is alternated. The second figure shows how the surface current (bold solid line) changes with the application of ±1250-volt-per-centimeter cross fields (thin dashed line). When the cross field is positive, meaning that the upper electrode in the first figure is positively biased, the surface conductivity decreases. When the cross field is negative, the surface conductivity increases. The effect is reversible during repetitive heating and cooling cycles.

Such a response is only possible if the surface conductivity is caused by charges coming to the

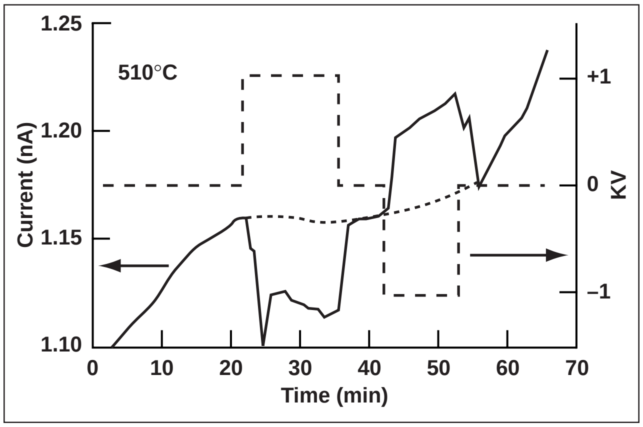

Fig. 2. Upon application of +1000-volt cross voltage the surface current decreases while at a cross voltage of –1000 volts it increases. This proves that the current is carried by positive charges, so-called holes, and that these charges exist inside the magnesium oxide crystal. The baseline drift is caused by slight temperature variations during the run.

surface from inside the crystal. The only source for such charges is the peroxy group in the structure.

Next the surface of the crystal was covered with a very thin layer of carbon and its conductivity remeasured. The conductivity was uniformly higher, indicating that it was dominated by current flowing through the thin carbon film. Application of the ±1250-volt cross fields now ceased to have any effect on the surface current, because the electrons flowing through the film were completely separate from the charges that move to and fro inside the crystal.

This experiment proves that peroxy groups exist in a crystal like this magnesium oxide which had been grown from a highly reduced melt and should therefore never contain anything as oxidized as peroxy groups. The reason peroxy groups got into the crystal has to do with the small amount of water that became incorporated when the magnesium oxide crystallized from the melt. During cooling, this dissolved water converted to a peroxy group and hydrogen. With knowledge available from other studies it is possible to boldly extrapolate to rocks. All igneous rocks on Earth and Mars have solidified from magmas, generally highly reduced and always saturated with water. The minerals in these rocks should therefore contain peroxy groups.

The presence of peroxy groups has implications for many geophysical questions related to the electrical conductivity of Earth's deeper crust and to phenomena associated with earthquakes. Another aspect relates to the earliest life forms on Earth. Rocks that contain peroxy groups, when they weather, will set free hydrogen peroxide. Any early organism living on such a rock surface will therefore experience a constant trickle of hydrogen peroxide, a potentially lethal oxidant. Assuming that early organisms lived in close contact with rocks and that they secreted acids which etched the rock surface away, these organisms would have been forced to develop a defense mechanism against this powerful oxidant. It has long puzzled observers that antioxidant enzymes appear deeply rooted on the tree of life, implying that they were "invented" early in life's evolution, long before there was free oxygen gas in Earth's atmosphere. Peroxy groups in the rocks and hydrogen peroxide at the rock–water interface may have been the driving force behind this important early evolutionary step.

Point of Contact: F. Freund
(650) 604-5183
ffreund@mail.arc.nasa.gov

2-Methylhopanoids: Biomarkers for Ancient Cyanobacterial Communities

Linda L. Jahnke, Roger E. Summons, Harold P. Klein

A variety of microbially mediated processes, which can sometimes be characterized by the identification of remnant cellular compounds (biomarker molecules) in ancient sedimentary organic matter, contributed to the cycling of carbon in ancient microbial ecosystems. One of the important goals of biomarker analysis is to link these ancient chemical fossils to modern day organisms and to understand through study of contemporary environments how many biomarkers are deposited, how they survive, and what they can tell about the evolution of ancient microbial communities. An important new tool in this work is being applied to biomarker analysis: compound-specific isotope analysis (CSIA), which allows measurement of the relative amounts of carbon-12 (^{12}C) and carbon-13 (^{13}C) in any compound that can be chromatographically separated using a gas chromatograph combustion-isotope-ratio mass spectrometer (GC-CIRMS). Biochemical processes often result in the synthesis of molecules depleted in ^{13}C relative to ^{12}C. Such carbon isotopic fractionations are described by the term $\partial^{13}C$. CSIA makes it possible to determine $\partial^{13}C$ values for individual organic compounds. This is important because as carbon is cycled through a microbial community the preference of biological systems for carbon-12 leads to synthesis of lighter biomarker molecules as the carbon flow approaches terminal processes, so that an additional degree of taxonomic attribution results in measurement of the $\partial^{13}C$.

Life began on early Earth in an environment devoid of free molecular oxygen (O_2). The rise of O_2 as a consequence of the evolution of oxygenic photosynthesis had a profound effect on the subsequent progression of Earth's biological evolution and geological history. Although oxygenic photosynthesis evolved within the cyanobacterial lineage, evidence for the timing of this event remains obscured within the molecular and rock records. One of the purposes in studying the molecular structure and carbon isotopic composition of lipid biomarkers in cyanobacteria is to link modern day cyanobacteria and their microbial-mat analog environments to an ancient organic record.

The bacteriohopanepolyols (BHPs) are a group of amphiphilic membrane biochemicals which are a particularly important group of biomarker molecules because the hydrocarbon skeletons of BHPs are extremely refractory and survive sedimentary diagenesis. The geohopanes may well be the most abundant class of natural products on Earth. BHPs are widespread among the aerobic bacteria and are therefore only of general taxonomic use. However, a supplementary methyl substituent at the 2-position of ring-A of the pentacyclic triterpane skeleton may provide some degree of biomarker specificity (see figure). Similar 2-methylhopanes have been identified in 2.5-billion-year-old organic-rich shales by a member of our group from the Australian Geographical Survey Organisation. Culture studies at Ames of a taxonomically diverse spectrum of cyanobacteria have shown that methylation at C-2 is common. It has been found that 2-methylbacteriohopanols (2-Me-BHP) are prominent membrane lipids in approximately 43% of cultured cyanobacteria and in a number of cyanobacteria-dominated environmental mat samples. Although not exclusive to this group of bacteria, the only other known sources of 2-Me-BHP occupy specialist environmental niches and do not appear capable of providing any quantitatively important contribution to sediments. The 2-Me-BHPs carry a readily measured molecular ^{13}C signature that will extend their usefulness as organism-specific biomarkers. Cyanobacteria are photoautotrophs that use the energy of sunlight to convert carbon dioxide to cellular components and, as discussed above, such biological processes can result in carbon isotope

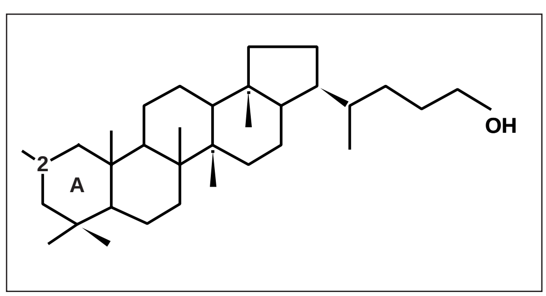

Fig. 1. 2-Methylbacteriohopanol.

fractionation. In this research it has been found that the BHPs synthesized as a result of cyanobacterial, photoautotrophic growth are depleted in ^{13}C by 28 per mil (per thousand) relative to the carbon dioxide source, with the 2-Me-BHP about 2 per mil heavier (contained 2 parts/mil additional heavier isotope) than its non-methylated analog. Similar carbon isotopic patterns have been measured for the 2-methyl and non-methyl BHPs in natural environmental samples establishing an isotopic signature for cyanobacterial BHP. Knowledge of the fractionation factors accompanying their biosynthesis also accord the potential to use 2-Me-BHP to determine the isotopic composition of inorganic carbon in modern aquatic and marine environments and their analogues in the fossil record.

Point of Contact: L. Jahnke
(650) 604-3221
ljahnke@mail.arc.nasa.gov

Organic Molecules in Comets

Bishun N. Khare, S. J. Clemett, R. N. Zare, Dale P. Cruikshank

Comets are the oldest, most primitive organic-rich bodies in the solar system, and in them is preserved the earliest record of material from the nebula in which the Sun and the planets formed. Simulations of the organic molecules in comets are undertaken in the Cosmochemistry Laboratory at Ames by depositing energy (ultraviolet light and charged particles) in mixtures of ices of various combinations of simple molecules. Colored solids of low volatility are produced by such irradiation, and analysis of the solid product reveals a complex array of polymers, C_1 through C_5 hydrocarbons, nitriles, alkanes, alkenes, and nitrogen heterocyclic compounds. The colored solid material is collectively termed “tholin.” Through special measurement techniques, the complex optical indices of this solid material are determined over a wide range of wavelengths, so that those indices can be used in mathematical models of the spectra of comets, planetary satellites, and other bodies of the solar system. Tholins made by irradiating various initial combinations of ices (and gases) appear to be uniquely capable of providing the coloration and spectral properties observed telescopically in many solar system bodies.

In a particular experiment designed to simulate the solid organic material in comets, Ice Tholin I was produced by irradiating a mixture of H_2O (water) and C_2H_6 (ethane) ices in the ratio 6:1 in the Cosmochemistry Laboratory. Analysis of the solid residue produced by the irradiation was accomplished with the newly developed technique of microprobe two-step laser mass spectrometry (mL^{2}MS) in the

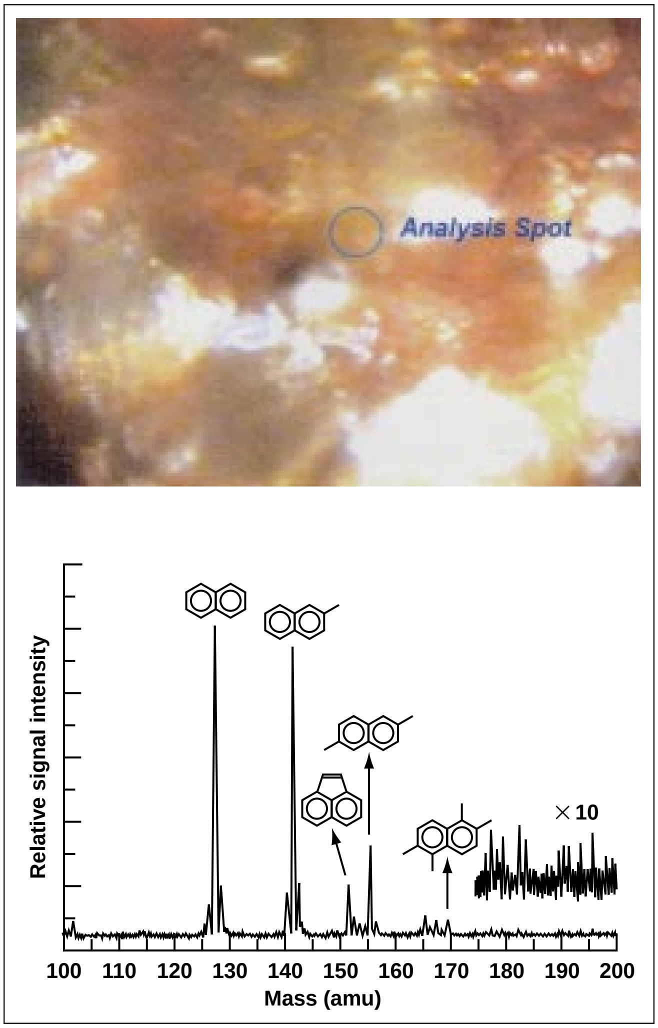

Fig. 1. Photomicrograph of a film of Ice Tholin II, showing the area in which the two-step laser technique detected polycyclic aromatic hydrocarbons.

laboratory of R. Zare (Stanford). The analysis revealed for the first time the presence of polycyclic aromatic hydrocarbons (PAHs) in tholins. A PAH-containing Ice Tholin II (see the figure) was produced from a more complex mixture of ices, one made up of H_2O, CH_3OH (methanol), CO_2 (carbon dioxide), and C_2H_6 (ethane) in the ratio 100:20:4:1. This mixture of ices simulates the composition of comets most closely.

In Ice Tholin I the PAHs are not distributed uniformly, but are found in microscopic concentrated regions where the concentration is greater than 300,000 parts per million. The PAH distribution in Ice Tholin I is characterized by simple 1-, 2-, and 3-ring PAH species with extensive side-chain alkylation (replacement of -H with $-(CH_2)_n$-H). In Ice Tholin II, the PAHs are distributed more uniformly; naphthalene and its n = 1 and n = 2 alkylated homologues dominate.

The detection of PAHs in laboratory simulations of comets opens the pathway to the interpretation of PAHs found in the comet particles that are collected in Earth's high stratosphere (interplanetary dust particles), and those collected at Comet P/Wild 2 that are to be returned to Earth by the Stardust mission early in the next century.

Point of Contact: B. Khare/D. Cruikshank
(650) 604-2465/4244
bkhare@mail.arc.nasa.gov
dale@ssa1.arc.nasa.gov

Spectroscopic Detection of Interstellar Organic Materials

Farid Salama, Thomas Halasinski, Bin Chen, Lou Allamandola, Robert Walker

Understanding the origin, properties, and distribution of the biogenic elements in the universe is central to astrobiology. At the Ames Astrochemistry Laboratory, ultraviolet (UV) irradiation of the molecular building blocks of interstellar and planetary organic materials is studied for the purpose of providing quantitative information for use in the analysis of astronomical spectra.

This laboratory work has shown that polycyclic aromatic hydrocarbons (PAHs) play an important role in the interstellar medium. PAHs are complex organic molecules with the structures shown in the figure. Their signature is present in the ultraviolet and visible spectra of starlight. PAHs, present as neutral, positively, and negatively charged species, contain a substantial amount (20%–40%) of the organic carbon in space.

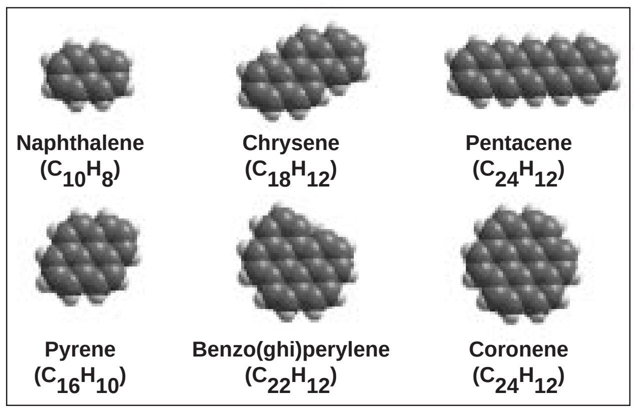

Fig. 1. The three-dimensional structures of several common polycyclic aromatic hydrocarbon molecules.

Up to now, cosmic material analogs were produced in the laboratory under conditions close to, but not exactly reproducing, those expected in the interstellar medium (cryogenic temperatures, high vacuum). The absorption and emission properties of these materials (neutral molecules, positively and negatively charged ions) are probed using the techniques of low-temperature molecular spectroscopy. Laboratory measurements of PAHs isolated in the condensed phase (matrix isolation spectroscopy, MIS) show that neutral PAHs absorb strongly in the UV. When ionized, PAHs absorb also in the visible, remarkably close to the positions of known Diffuse Interstellar Bands. Identifying the specific molecular carriers responsible for these as yet unidentified bands is crucial to the understanding of the complex organic chemistry that takes place throughout the galaxy.

There has been a great experimental challenge to measure the spectra of PAH ions in the gas phase under conditions that mimic exactly those in the interstellar medium. Within the past year, the absorption spectra of PAH cations have been measured for the first time in the gas phase using the combined techniques of supersonic free-jet expansion spectroscopy (JES) and cavity ring down absorption spectroscopy (CRDAS). This approach, achieved in collaboration with several research groups, allows the first direct comparison of laboratory results and astronomical data. Based on the initial laboratory results, it has been concluded that a distribution of neutral and ionized PAHs represents a promising class of candidates to account for the Diffuse Interstellar Bands seen in both absorption and emission spectra. The results obtained so far are a significant breakthrough in astrophysics and astrochemistry, as well as in molecular spectroscopy. For the first time, the absorption spectrum of a PAH cation has been measured under conditions that entirely mimic those of interstellar space (cold and isolated molecular ions).

Point of Contact: F. Salama
(650) 604-3394
fsalama@mail.arc.nasa.gov

Simulations of a Model Transmembrane Proton Transport System

Karl Schweighofer, Andrew Pohorille

The transport of protons across membranes is an essential process for both the bioenergetics of modern cells and for the origins of cellular life. All living systems make use of proton gradients across cell walls to convert environmental energy into a high-energy chemical compound, adenosine triphosphate (ATP), synthesized from adenosine diphosphate. In turn, ATP is used as a source of energy to drive many cellular reactions. The ubiquity of this process in biological systems suggests that even the earliest cellular systems relied on proton gradients for harvesting the environmental energy needed to support their survival and growth. In contemporary cells, proton transfer is assisted by large, complex proteins embedded in membranes. The issue addressed in this study was: How can the same process be accomplished with the aid of similar, but much simpler molecules that could have existed in the protobiological milieu?

The model system used in the study contained a bilayer membrane made of phospholipid, dimyristoylphosphatidylcholine (DMPC), which is a good model of the biological membranes that form cellular boundaries. Both sides of the bilayer were surrounded by water that simulated the environment inside and outside the cell. Embedded in the membrane was a fragment of the Influenza-A M_2 protein, and enough sodium counterions to maintain system neutrality (see figure). This protein has been shown to exhibit remarkably high rates of proton transport and is therefore an excellent model for use in the study of the formation of proton gradients across membranes. The Influenza M_2 protein is 97 amino acids in length, but a fragment 25 amino acids long, which contains a transmembrane domain of 19 amino acids flanked by 3 amino acids on each side, is sufficient to transport protons. Four identical protein fragments, each folded into a helix, aggregate to form small channels spanning the membrane. Protons are conducted through a narrow pore in the middle of the channel in response to applied voltage. This channel is large enough to contain water molecules, and is normally filled with water.

In analogy to the mechanism of proton transfer in some other channels, it has been postulated that protons are translocated along the network of water molecules filling the pore of the channel. This mechanism, however, must involve an additional and important step because the channel contains four histidine amino acid residues, one from each of the helices, which are sufficiently large to occlude the pore and interrupt the water network. The histidine residues ensure channel selectivity by blocking the transport of small ions, such as sodium or potassium. They have also been implicated in gating protons as a result of the ability of each histidine to become positively charged by accepting an additional proton. Two mechanisms of gating have been proposed. In one, all four histidines acquire an additional proton and, because of the repulsion between their positive charges, move away from one another, thus opening

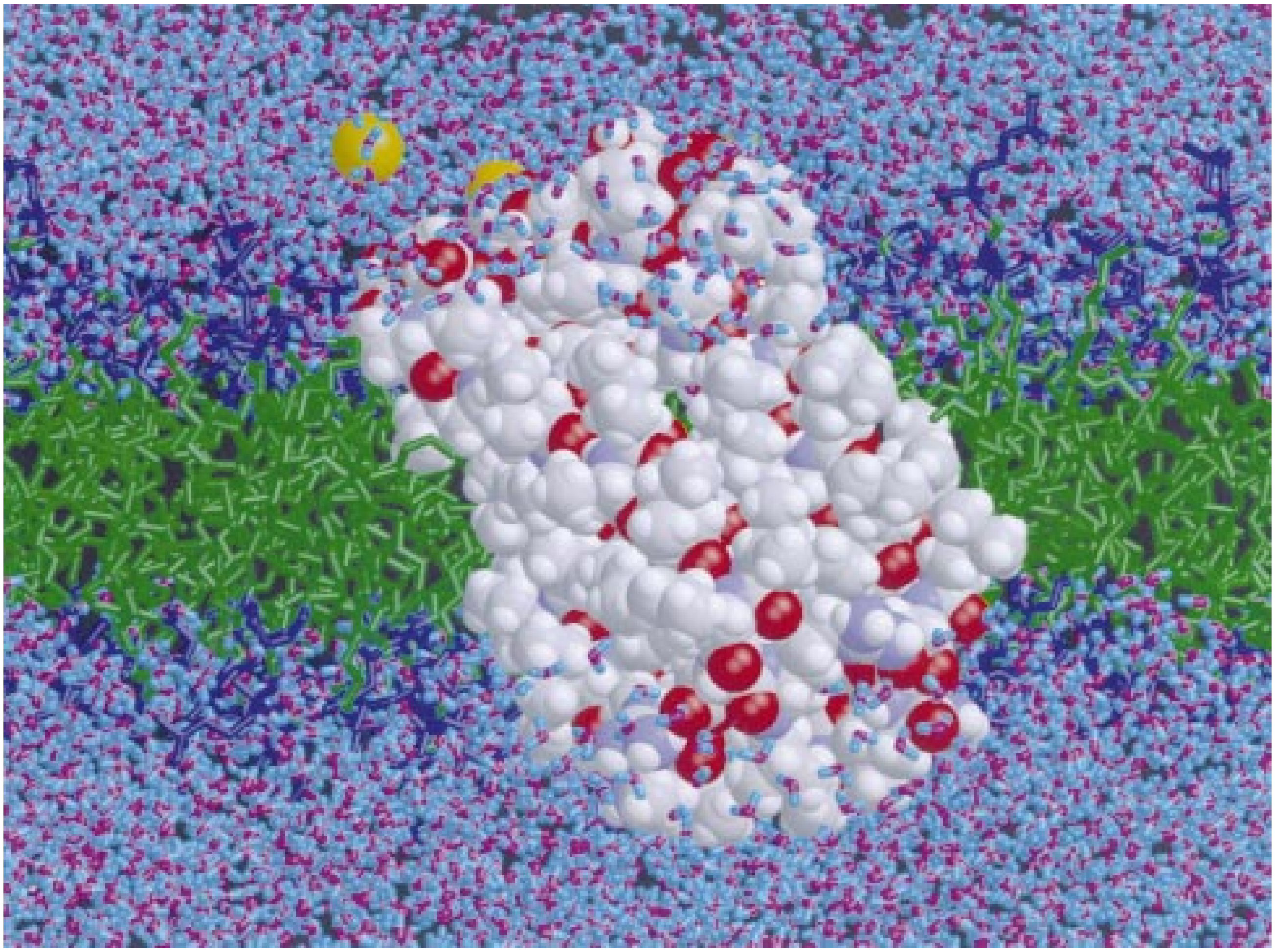

Fig. 1. The M_2 protein embedded in a DMPC membrane which is flanked by water layers. Both the water and the membrane are represented by sticks, whereas the protein is rendered as spherical or "cpk." The color legend is as follows: water hydrogen (cyan), water oxygen (magenta), membrane hydrocarbon tails (green), membrane head groups (blue), sodium ions (yellow cpk), protein (multicolored cpk). The protein is clearly tilted in the bilayer, which helps it maintain favorable interactions with the interior of the membrane. Water in the channel cannot be seen because of the opacity of the protein in this figure.

the channel. The alternative mechanism relies on the ability of protons to move between different atoms in a molecule (tautomerization). Thus, a proton is captured on one side of the gate while another proton is released from the opposite side, and the molecule returns to the initial state through tautomerization. The simulations were designed to test these two mechanisms.

Large-scale, atomic-level molecular dynamics simulations of the channel with the histidine residues in different protonation states revealed that all intermediate states of the system involved in the tautomerization mechanism are structurally stable and that the arrangement of water molecules in the channel is conducive to the proton transport. In contrast, in the four-protonated state, postulated to exist in the gate-opening mechanism, the electrostatic repulsion between the histidine residues appears to be so large that the channel loses its structural integrity, and one helix moves away from the remaining three. This result indicates that such a mechanism of proton transport is unlikely.

The simulations revealed that translocation along a network of water molecules in the channel and tautomerization of the histidine residues in the M_2 proteins is the most likely mechanism of proton transport. The results not only explain how a remarkably simple protein system can efficiently aid in the formation of proton gradients across cell walls, but also suggest how this system can be genetically re-engineered to become a directional, reversible proton pump. Such a pump could provide energy to laboratory-built models of simple cellular systems. Their successful construction would greatly advance the understanding of the beginnings of life and would find important applications in medicine and pharmacology.

Point of Contact: A. Pohorille
(650) 604-5759
pohorill@raphael.arc.nasa.gov

Molecular Imprinting of Polymeric Columns

Thomas Shen, Jay Chen, Narcinda Lerner

L-amino acids are one of the fundamental building blocks of living organisms. For this reason, their detection at trace levels is one of the major targets of many programs in which searches for the origin of life are being conducted. L-amino acids have an advantage over other biomarkers in that they contain a chiral center which is considered a biosignature for the presence of life. Amino acids of abiotic origin are racemic, with equal amounts of the L-form and the D-form. Any biological debris remaining from chemical or biological evolution or both on Mars or on other planetary bodies would be present in trace amounts as a result of decay over millions or billions of years. Highly sensitive instruments will be required to detect such debris in situ, as well as measurements on returned samples from planetary flight missions. Molecular imprinting is a simple and convenient way to prepare antibody-like materials which have been increasingly used in separation science and, more recently, in sensing technology. The principle of this technique, including surface attachment and in situ polymerization, is described in the figure. Using this technology, very small amounts of amino acids or biomolecules can be concentrated and separated for detection.

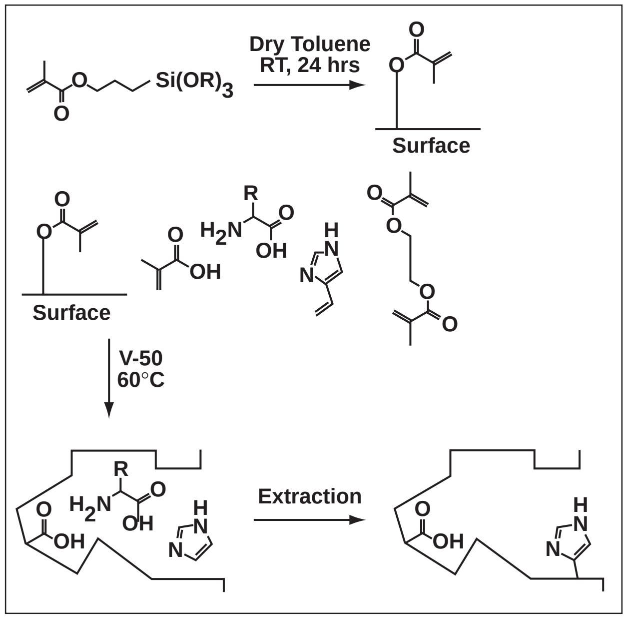

Fig. 1. The preparation of surface-linked molecular imprinting polymeric columns.

Recently, the reaction conditions for preparing molecularly imprinted polymers (MIPs) for amino acid separation were developed. The results indicated that the template effect exists by comparison of the binding effects between MIPs and the control polymers. Approximately up to 1 microgram of L-phenylaniline (L-phe) could be absorbed by 1 milligram (mg) of L-phenylaniline-imprinted polymers. Experiments on coating a capillary column with the L-phe-imprinted polymer by in situ polymerization were also studied. The inner surface of the capillary was first coated with a layer of the monomer trimethoxysilylpropyl methacrylate and then in situ polymerization was conducted inside the tube in the presence of L-phe. Observation indicates that the capillary coated with the L-phe-imprinted polymer displays a nice layer of MIP coating on the inner surface of the column (inner diameter = 0.53 millimeter). The bonded polymer layer could be observed readily without instrumentation. Further analysis based on scanning microscopy will provide information regarding the bonding structure of this coating. The good structural stability of the stationary phase produced by this procedure will allow its use in the production of capillaries that have reduced inner diameters, that is, micro-columns on glass chips. The success of coating the micro-columns with the MIPs will make possible miniaturized capillary electrochromatography with a stationary phase designed specifically for targeted molecules.

Preliminary results also indicate that a small amount of nonspecific absorption also occurred.

Point of Contact: T. Shen
(650) 604-5769
tshen@mail.arc.nasa.gov

Prebiotic Synthesis of Activated Amino Acids

Arthur L. Weber

Chemical processes occurring on primitive Earth about 4 billion years ago yielded molecules that had the ability to make copies of themselves (to replicate). These rudimentary replicating molecules eventually developed into today's life that uses both protein and DNA molecules for replication. Since the DNA of today's life is too complex to have been chemically made on the primitive Earth, the first replicating systems may have been composed solely of small proteins—called peptides. The possibility that peptides were the first replicating molecules is feasible because they are constructed from very simple building blocks—activated amino acid molecules—which could have been made by chemical processes on primitive Earth.

In order to determine how activated amino acid and peptide molecules could have been generated on, or delivered to, the primitive Earth 4 billion years ago, the catalysis of sugar synthesis and its conversion to activated amino acids was investigated in the laboratory under simulated primitive Earth conditions; the energy of carbon-carbon bond formation and cleavage for different carbon groups was calculated to evaluate the constraining role of thermodynamics in prebiotic carbon chemistry leading to the origin of life and metabolism; and samples of the Cretaceous-Tertiary boundary layer were analyzed for extraterrestrial amino acids to see if they survived the meteorite impact that delivered them to Earth.

In the past year significant progress was made in these three research areas. Amines (including amino acids) were shown to catalyze the prebiotic pathway (discovered last year) that generates activated amino acid thioesters capable of forming peptides. Specifically, amines were found to catalyze the first two reactions (aldol condensation and dehydration) of the prebiotic pathway involved in the synthesis alanine and homoserine thioesters from formaldehyde and glycolaldehyde. Catalysis of the first two steps of this pathway by alanine, a product of the pathway, demonstrates that this prebiotic pathway has the potential to function autocatalytically. This pathway is an attractive prebiotic process because it operates under mild aqueous conditions and, like modern amino acid biosynthesis, uses sugar intermediates which are converted to amino acids by energy-yielding redox reactions.

To identify the thermodynamic constraints that govern carbon chemistry involved in the origin of life, the free energy was calculated for the formation and cleavage of 100 carbon-carbon bond combinations made from 10 different aliphatic carbon groups. Overall this analysis showed that thermodynamics acts to constrain the carbon chemistry of the origin of life to reactions that proceed by redox disproportionation in which the more oxidized carbon group of a reacting pair of carbons becomes more oxidized, and the more reduced carbon group of the pair becomes more reduced. Furthermore, the analysis revealed that carbon bonds to carbonyl groups are very unstable, making them easy to cleave but hard to make; that alcohol groups are moderately unstable, making them more difficult to cleave but not hard to make; and that hydrocarbon groups are very stable, making them very difficult to cleave but not hard to make.

In preparation for the analysis of the martian meteorite ALH84001, samples of Cretaceous-Tertiary boundary sediments were analyzed for extraterrestrial amino acids. A sample of Cretaceous-Tertiary boundary sediment from Sussex, Wyoming, was shown to contain about 310 picomoles per gram of the meteoritic amino acid, α-amino-isobutyric acid. Knowledge of the amino acids in extraterrestrial materials, like meteorites, contributes to understanding the processes involved in the delivery of amino acids to primitive Earth during the origin of life.

Point of Contact: A. Weber
(650) 604-3226
aweber@mail.arc.nasa.gov

Refugia from Asteroid Impacts on Early Mars and Earth

Kevin Zahnle, Norman H. Sleep

Impacts by large comets and asteroids were relatively frequent events in the early solar system. These impacts posed a major recurrent hazard to the continuous existence of life on early Mars, as on early Earth. The chief danger was presented by globally distributed ejecta. These ejecta include large suborbital projectiles; mountains of finely subdivided dust; and in the worse case, thick transient rock-vapor atmospheres. On Earth, downwelling thermal radiation from the hot atmosphere boils the surfaces of the oceans. Water evaporates until either the energy contained in the rock-vapor atmosphere is exhausted or the oceans are boiled off. Earth's oceans thereby provide an enormous thermal buffer that limits thermal excursions triggered by very large impacts, provided that the impact is not *too* large. Life can survive in deep cool waters or in deep subsurface hideouts until the danger has passed and the rock has returned to its desirable crustal status. But when the impact is truly enormous (>10^{28} joules, or a 500-kilometer-diameter impactor "the size of Texas"), the oceans are vaporized and it takes at least 3000 years—the time required to recondense and rain out all the water of the oceans—for conditions to return to some semblance of normality. Thermal conduction carries the thermal pulse to considerable depths, while from below upwelling geothermal heat—much more than today—leaves any habitable niches wedged between the pan and the fire. Under such conditions the survival of life on Earth is threatened.

Mars is different. The lack of deep oceans means that there is no thermal buffer against relatively small impacts. Even an impact as small as the K/T event (the asteroid that is thought to have killed the dinosaurs and 95% of the other lifelines on Earth) would raise the martian surface to the melting point. This would be bad for life at the surface (for example, for photosynthesizers). But the melting would not be deep, and the effects would soon (hours to days) be forgotten as the energy of the impact quickly radiates to space. Even for larger events the effects, although briefly scalding, are mitigated on Mars. For example, the low martian escape velocity permits a fair fraction of the hottest and most energetic ejecta to escape entirely, and thus not contribute to the hazards confronting the hypothetical biota. Instead, because the gravity is lower the global ejecta on Mars are relatively massive but relatively cool. Survival of subsurface ecosystems is more likely on Mars than on Earth because (1) Mars's lower geothermal heat flow and lower gravity permit deeper colonies (it is gravity that crushes rocks and seals pores so lower gravity permits deeper circulation of fluids, etc.), and (2) the thermal pulse from a major impact is briefer. Thus there is more space between the pan and the fire.

The possibility that Mars may have provided a more survivable platform for life in the earliest solar system, coupled with the demonstrated fact that Earth at least can receive lightly shocked ejecta from Mars, brings us to consider briefly the implications of trade between the two worlds. Lightly shocked ejecta, launched by impact and possibly stocked by crews of inadvertent microbial spacefarers, could make the voyage. It does seem possible, even likely, that viable organisms have been launched by impact from Earth to Mars on favorable trajectories, so that after a relatively brief and altogether survivable trip through interplanetary space, the terrestrials might have found suitable homes. Of course the story could be reversed, which would make us all, in a sense, martians.

Point of Contact: K. Zahnle
(650) 604-0840
kzahnle@mail.arc.nasa.gov

Planetary Science

Primary Accretion in the Protoplanetary Nebula

J. N. Cuzzi, R. C. Hogan, J. M. Paque, A. R. Dobrovolskis

The primary accretion processes of comets and asteroids are not understood. Yet, these so-called primitive objects represent the parent bodies for the entire meteorite record—a vast data set that has little context for interpretation. The focus of this work is on three-dimensional direct numerical simulations of particles in turbulence, in which aerodynamically selected particles are concentrated in turbulence by a factor that can be as great as a million in the nebula. Optimally selected particles have Stokes numbers of unity, where the Stokes number is the ratio of particle stopping time to the Kolmogorov eddy turnover time, and is proportional to the particle radius and density. The code that was used handles Reynolds numbers (Re) as high as 1300, and a million particles at each of 16 different Stokes numbers simultaneously.

In FY98, the shape of the turbulent concentration (TC) function was shown to be independent of both turbulent intensity (Re) and the concentration factor (in the high concentration limit appropriate for the nebula). The predictions are well-fitted by a lognormal function. Also, a so-called "unequilibrated ordinary chondrite" ALH 85033 was disaggregated and the size distribution of the chondrules was measured directly. These results are far superior to similar data obtained by examining slices of rock in a microscope; they provide direct determination of the chondrule density, which cannot be attained in any other way. Previous research merely measured particle radius and assumed an average density for all particles. The new data change the shape of the distribution curve for concentration.

In the first figure model predictions are compared with the actual relative abundance of chondrules, as a function of the product of particle radius and density. The open circles are the predictions for all three Re values that were simulated—there is no significant Re dependence of the shape. The solid curve is the best fit of a lognormal function to the actual simulations. The filled squares are the meteorite data. The data and the predictions are normalized

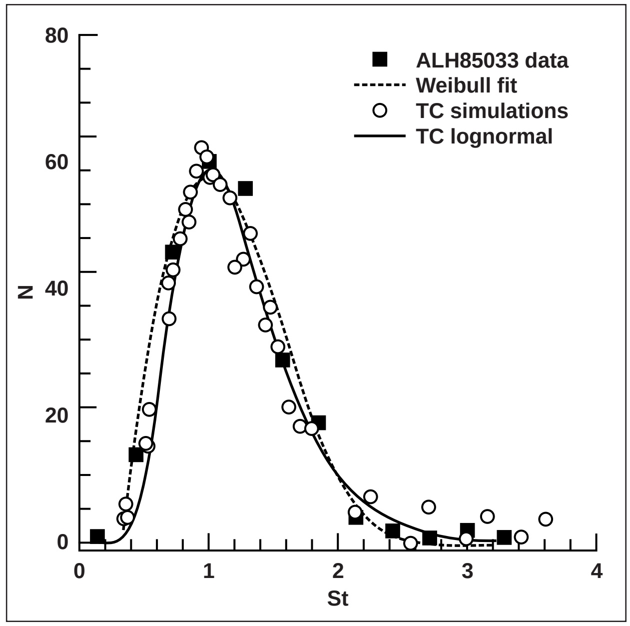

Fig. 1. Model predictions versus actual relative abundances of chondrules.

together at their peaks, and the shapes agree very well without any free parameters in the theory. The so-called Weibull function previously assumed (also shown) is based not on aerodynamic sorting but on fracture processes; it has several free parameters.

The theory was also generalized to other particle properties and nebula locations. Not all particles in the nebula are likely to be solid silicates. The earliest condensate grains probably stick into fluffy fractal puffballs and then into porous aggregates which have lower average density. These particles will incur preferential concentration in areas of the nebula where the gas density is commensurately lower, such as the formation regions of the gas giants and comets. The second figure shows the expected particle radius-density product amenable to preferential concentration as a function of turbulent intensity (the latter expressed as scaling parameter alpha). Current

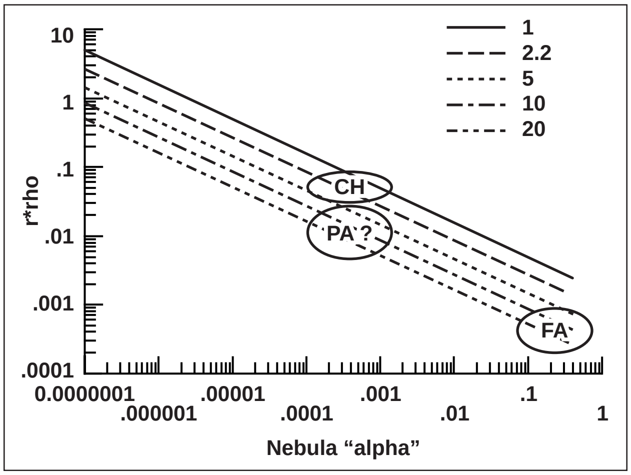

*Fig. 2. Preferred radius-density product r*rho versus alpha.*

estimates for nebula alpha are in the range of 0.0001–0.01. Thus, while solid chondrules (CH) are concentrated in the terrestrial planet region (1–2.2 AU, or astronomical units, where 1 AU is Earth's distance from the Sun), porous aggregates (PA) are concentrated at the same level of turbulence in the lower density regions at the locations of Jupiter, Saturn, and Uranus (5, 10, and 20 AU). Low gas density is also found at large heights above the nebula midplane, even at 1–2 AU. The most fluffy aggregates (FA) are concentrated at extremely low density or high turbulent intensity or both.

Point of Contact: J. Cuzzi
(650) 604-6343
cizzo@cosmic.arc.nasa.gov

A Test-Bed for Detecting Earth-Sized Planets

David Koch, William Borucki, Larry Webster

Detection of Earth-size planets beyond our solar system is one of the fundamental questions identified in NASA's Strategic Plan. Only recently have any planets beyond the solar system been detected. The masses of those found to date are all of the order of the mass of Jupiter or larger. The challenge is to find planets that are 30–600 times less massive than Jupiter, that is, 0.5–10 times the mass of Earth. The concept for a space mission to accomplish this has been developed: the *Kepler Mission*. This mission, as proposed, would perhaps discover about 500 habitable planets, if most stars like the Sun have planetary systems. The capabilities have been set high, so that even a null result would have a profound effect on our understanding of planet formation. The mission's purpose is to continuously and simultaneously monitor the brightnesses of 100,000 solar-like stars. The "light-curves" for each star would be analyzed for changes owing to transits of Earth-size planets. Three transits of a star, all with a consistent period, brightness change, and duration, provide a rigorous method of detection and confirmation. From the relative brightness change the planet's size can be calculated. From the period, the size of the orbit can be calculated and the planet's temperature estimated. The objective of the current test-bed project is to demonstrate the technological readiness of the mission.

At the heart of the proposed Kepler space mission is an array of charged-coupled-device (CCD) detectors for measuring stellar brightnesses. These devices are similar in principle to those used in today's video cameras, but are much larger and more sensitive. The critical property of the CCDs is their relative photometric precision, that is, how well they can measure the brightness of a given star relative to the average brightness of the many thousands of stars nearby.

To demonstrate this, a test-bed is being constructed that will utilize a CCD similar to that being proposed for the space mission. The test will consist of viewing a star field with a ground-based instrument. Unfortunately, distortions caused by the atmosphere prevent measuring to the relative precision required (1 part in 100,000) for the same reason that the entire mission can not be done looking through the atmosphere. The best photometric precision that has been achieved from the ground is somewhat better than 1 part in 1,000. To overcome this problem and to demonstrate that the CCDs have the inherent relative precision required, an instrument is being constructed in which a calcite beam splitter is placed in front of the CCD. This produces a pair of identical images on the CCD. The photometric capability of the CCDs will be demonstrated by comparing the ratios of the brightnesses for each star pair. The instrument that will be used to make these measurements is being constructed. Successful completion of the test should demonstrate the readiness of this technology for a space mission. For further information on the proposed *Kepler Mission*, see the worldwide web (at http://www.kepler.arc.nasa.gov).

Point of Contact: D. Koch
(650) 604-6548
dkoch@mail.arc.nasa.gov

Detecting and Modeling Extrasolar Planets

Jack J. Lissauer

The objective of this project is to study planets around stars other than the Sun both observationally and by developing theoretical models of the formation and stability of planets and planetary systems.

A team of astronomers at San Francisco State University, the Anglo-Australian Observatory, the Lick Observatory, and Ames Research Center discovered a planetary-mass companion orbiting the star Gliese 876. The newly found body has a mass multiplied by the sine of the inclination of its orbit normal to the line of sight of 1.9 times that of Jupiter, a period of 61 days (implying a semimajor axis of 0.2 astronomical units) and an eccentricity of 0.37. The planet was identified at the Keck and Lick observatories by using Doppler measurements of the radial velocity of the star. This planet is closer to the Sun than any other extrasolar planet thus far identified. More significant is the fact that Gliese 876 is an M4 star with a mass about one-third that of our Sun. This is the first planet to be discovered in orbit about an M-type star, and since most stars in our Galaxy are faint M stars like Gliese 876, its existence suggests that billions of planets probably are present within our Galaxy.

A set of plausible outer planetary systems was constructed by a team of astronomers at Southwest Research Institute, Queen's University, and Ames by using direct numerical integrations. It was found that some sort of dissipation was required for timescales longer than 10 million years during the accretionary epoch in order to construct systems like ours. The number of planets can vary from one to seven. Systems with a large number of planets never contain very massive, Jupiter-like planets, but instead are made up of Uranus-like planets. Stable planetary systems can include planets in mean motion resonances with one another. Perhaps most surprisingly, it is possible to construct stable systems in which planetary orbits can undergo large, semi-periodic changes.

Models of the growth of giant planets close to their stars were constructed by a group from Lick Observatory and Ames. If adequate solid planetesimals are available near stars, planetary cores can grow massive enough to accrete large amounts of gas from the protoplanetary disk. However, for conditions similar to those believed to have existed around the Sun, planetary growth at distances of several astronomical units from a star followed by subsequent inward migration appears to offer a more likely scenario.

Point of Contact: J. Lissauer
(650) 604-2293
jlissauer@ringside.arc.nasa.gov

Martian Oxidant Mixing by Impacts

Aaron P. Zent

It is the objective of this work to revise previously published profiles of the oxidative stratigraphy of the martian regolith to include the effects of regolith stirring by impact cratering. The fundamental objectives are to estimate the depth from which samples must be obtained in order to access martian organics, and to clarify the unknowns in the problem for use in directing future research.

One of the fundamental operational objectives of NASA's Exobiology Program is to obtain and examine organic material from the martian regolith. This objective derives from observations of the martian surface that indicate liquid water played an as-yet-unexplained role in the evolution of the martian surface early in the planet's history, the same period during which life is suspected to have made its first appearance on Earth. The chemical evolution that lead to terrestrial life might have begun to operate on Mars as well. The opportunity to compare the paths of prebiotic chemical evolution on two planets is likely to illuminate fundamental principles that govern the abiotic origin of life.

The most salient barrier to this objective is that the martian regolith is highly oxidizing, thus destroying putative martian oxidants. The specific chemical mechanisms that are responsible for the oxidizing nature of the martian surface remain unknown, but the photochemistry of atmospheric water is thought to be the ultimate source of the oxidants. This hypothesis predicts that strong oxidants are present at the base of the martian atmosphere and that they diffuse into the martian regolith, where they can react with any organics that may be at some depth. The depth to which the oxidants might diffuse is unknown, but the regolith sampled by Viking was found to be oxidized to a depth of 10 millimeters. Therefore, considerable effort is being expended to understand the adsorptive and diffusive properties of hydrogen peroxide (H_2O_2) through silicate materials, as well as their reaction and complexation pathways, so that the thickness of the oxidizing layer can be predicted. However, it may not be sufficient to understand the diffusion of a vapor phase oxidant into the martian regolith, because the martian stratigraphic column is not stable and was even less so early in its history. Aeolian and impact mechanisms act to erode and deposit material across the martian surface, effectively stirring the surface materials.

It is possible to estimate quantitatively, the mixing of a near-surface oxidized layer into the martian subsurface by impact cratering. Impact craters leave a clear signature in a planetary surface. Mixing models can be constructed based on simplified geometric and probability assumptions that will describe the movement of materials up into the oxidizing zone, and down again, in response to subsequent burial.

The effects of regolith gardening by impacts are quantitatively estimated, and combined with the effects of oxidation by atmospheric gases to produce estimates of the degree of oxidation of the martian surface with depth. We explore the effects of different crater-production populations along with variations in H_2O_2 extinction depths, and hydrothermal oxidation of ejecta. In very select circumstances involving very early onset of oxidizing conditions during heavy bombardment, 150 to 200 meters of regolith could be fully oxidized. More likely scenarios for the crater-production population, the onset of oxidizing conditions, and the oxidant extinction depth yield estimates of no more than a few meters to putative reducing material. In addition, uncertainties remain regarding the degree to which hydrothermal or other high-temperature chemistry might oxidize materials in ejecta blankets. The trade between accessing unlithified sediments or rock interiors must be considered.

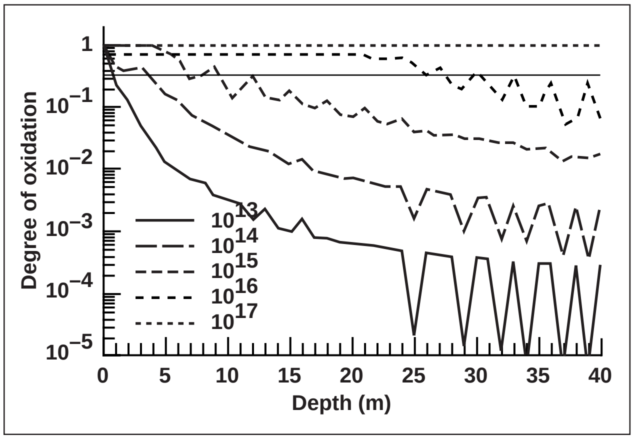

Fig. 1. Oxidation profiles: sensitivity to production populations.

The sensitivity of the regolith oxidation profile to the pre-exponential factor in the production population is shown in the figure. Each factor of 10 increase in impact frequency increases the depth from which samples must be acquired considerably. The horizontal line represents a 50% likelihood of retrieving putative organics.

Point of Contact: R. Quinn
(650) 604-6501
rquinn@mail.arc.nasa.gov

Meteorites and Solar Nebula Analogs

P. M. Cassen, K. R. Bell

The planets in our solar system formed from a gaseous disk known as the solar nebula. Analogous nebulae are now commonly being observed in external systems by facilities such as the Hubble Space Telescope (HST) and the infrared astronomical satellite (IRAS). Learning about these external systems provides insight into the processes that led to the formation of our own life-supporting planetary system. In FY98, research continued into the preplanetary evolution of the solar nebula with the study of analogs in external systems and the evidence in our own meteoritic record.

Stars typically form in dense stellar aggregates. In some clusters of young stars such as the Orion nebula, radiation from high-mass stars disperses nebular material from nearby low-mass systems (this process is discussed more fully in the Hollenbach et al. report). In many systems, however, flattened nebulae of mass sufficient to form planets in our own solar system survive for millions of years after the coalescence of the central star. Temperatures and densities at the midplanes of these protoplanetary disks determine the characteristics of planetary systems that ultimately arise as well as the elemental and isotopic compositions of the meteoritic material that survived from that era.

Until recently, purely theoretical considerations were the main source of information regarding the thermal evolution of these protoplanetary disks. P. Cassen and D. S. Woolum (California State University at Fullerton) examined astronomical data regarding the photospheric temperatures of disks around T Tauri stars (young solar mass stars), as constrained by observations at optical, infrared, and radio wavelengths. They developed theoretical models to use these observations to infer the internal thermal structure of the disks. The models account for obscuring circumstellar matter (dust high in the nebular atmosphere) and the optically thick nature of the disks themselves. They found that most disks in the planet-forming stages were quite cool (at temperatures permitting the condensation of water or ice in what would correspond to the terrestrial planet region), but that disks were likely to be very hot early in their evolution, when they are still heavily obscured by infalling material. In the latter cases, the total system luminosity provides an estimate of accretional energy. Comparisons with revealed T Tauri luminosities provide a basis for estimating the properties of embedded disks. High temperatures at early stages would explain a variety of properties characteristic of the primitive meteorites.

Evidence for nebular temperatures as deduced from meteorite properties was explored in more detail in collaborative research by K. R. Bell, P. M. Cassen, J. T. Wasson (of the Institute of Geophysics and Planetary Physics, University of California, Los Angeles), and D. S. Woolum. Patterns of elemental and isotopic abundances in meteorite components indicate that they formed in a nebula with temperatures ranging from 1400 degrees kelvin (K) (above the destruction temperature of most solids such as silicates) to 400 K (a temperature low enough to permit the incorporation of water into rocky material). This wide range suggests that meteorite components were formed over an extended time during the cooling of the solar nebula. Midplane temperatures of optically visible T Tauri disks fall at the cool end of this temperature range. Under the assumption that our solar system underwent thermal evolution typical for systems with similar stellar mass, Bell et al. argued that T Tauri systems are nearing the end of their meteorite formation phases. Further, T Tauri systems must at one point have experienced a hotter, more active phase of disk evolution. This earlier phase presumably occurred while the system was still optically obscured (embedded) and is, therefore, associated with the high-accretion-rate, protostellar phase.

Point of Contact: P. Cassen
(650) 604-5597
cassen@cosmic.arc.nasa.gov

Ices in Kuiper Disk Objects

Dale P. Cruikshank, Yvonne J. Pendleton

Beyond the planet Neptune lies a disk-shaped distribution of small, primitive bodies called the Kuiper Disk. This region is named after the prominent astronomer, Gerard P. Kuiper, who predicted its existence in 1951. Kuiper speculated that such a population must exist in order to explain the orbital characteristics of the short-period comets (periods less than 200 years) that currently come to the inner part of the solar system at the rate of about 10–20 per year. The first of these trans-Neptunian objects was found in 1992, and about 80 of them have been detected so far. Their dimensions are approximately 50 to 500 kilometers; much smaller ones surely exist, but they are too faint to be found with telescopes presently available. Because these bodies are implicated in the transport of volatiles and complex organic materials to the prebiotic Earth and other terrestrial planets, Ames researchers have conducted astronomical observations to establish their compositions.

The trans-Neptunian objects are expected to be composed of the same materials that make up the short-period comets, typically one-third ices (frozen water, carbon dioxide, carbon monoxide, and others), one-third silicate dust, and one-third complex organic solid material. Remote-sensing measurements of these bodies to establish their compositions and to search for variations among them are a challenge for presently available astronomical techniques; only the largest 15–20 bodies can be observed with infrared spectrometers on the world's largest telescopes.

A new Ames spectroscopic study with the Keck 10-meter telescope on Mauna Kea, Hawaii, is showing that the trans-Neptunian objects are diverse in their surface compositions. At least one (designated 1993 SC) shows evidence for hydrocarbon ices (possibly methane), while others show the spectroscopic signature of frozen water. In addition, the strong red color of the surfaces of several of these bodies is evidence for the presence of organic solid material that has been produced in interstellar space and further processed since incorporation into the solar system. The color and spectral properties of the red trans-Neptunian objects are closely matched by "tholins," which are complex organic materials synthesized in the laboratory by the irradiation of simple gases and ices with ultraviolet light and charged particles.

The results of the spectroscopy of ten trans-Neptunian objects, their "cousins" the Centaurs (bodies in temporary orbits that cross the paths of the major planets), and the irregular outer satellites of the major planets show that they are compositionally diverse. The planet Pluto and Neptune's satellite Triton probably represent two of the largest bodies in the Kuiper Disk population, and each of these two bodies has a complex icy surface and a tenuous atmosphere. The Ames study includes remote-sensing observations of all these objects, in search of unifying threads of evidence that may link their compositions with the comets and other bodies that have impacted Earth and the other planets, bringing volatile and organic matter from the most distant reaches of the solar system.

This research was done in collaboration with Robert H. Brown of the University of Arizona and Glenn J. Veeder of NASA's Jet Propulsion Laboratory.

Point of Contact: D. Cruikshank
(650) 604-4244
dale@ssa1.arc.nasa.gov

AIRES—A Facility Spectrometer for SOFIA

Edwin Erickson, Michael Haas, Sean Colgan

The Stratospheric Observatory for Infrared Astronomy (SOFIA) will be a Boeing 747 carrying a 2.7-meter telescope to operating altitudes up to 45,000 feet. SOFIA will enable astronomical observations with unprecedented angular resolution at infrared wavelengths obscured from the ground. It is being developed jointly by NASA and the Deutsche Forschungsanstalt für Luft- und Raumfahrt (DLR), the German aerospace center. Based at Ames Research Center, it will begin operations in 2002.

An Ames team was one of six American groups selected by peer review to build a focal plane instrument for early observations with SOFIA. The Ames instrument, AIRES, the airborne infrared echelle spectrometer, will be a general-purpose facility instrument. After development by the Ames team, it will be operated for the science community by the Universities' Space Research Association (USRA), NASA's prime contractor for SOFIA.

AIRES will operate at far-infrared wavelengths, about 30 to 400 times the wavelengths of visible light. Therefore, it will be ideal for spectral imaging of gas-phase phenomena in the interstellar medium (ISM), the vast and varied volume between the stars. Measurements of far-infrared spectral lines with AIRES will probe the pressure, density, luminosity, excitation, mass distribution, chemical composition, heating and cooling rates, and kinematics in the various gaseous components of the ISM. These lines offer invaluable and often unique diagnostics of conditions in such diverse places as star-forming regions, circumstellar shells, the galactic center, starbursts in galaxies, and the nuclei of active galaxies energized by accretion of material on massive black holes. AIRES will provide astronomers with new insights into these and other environments in the ISM. It will also be useful for studies of solar system phenomena such as planetary atmospheres

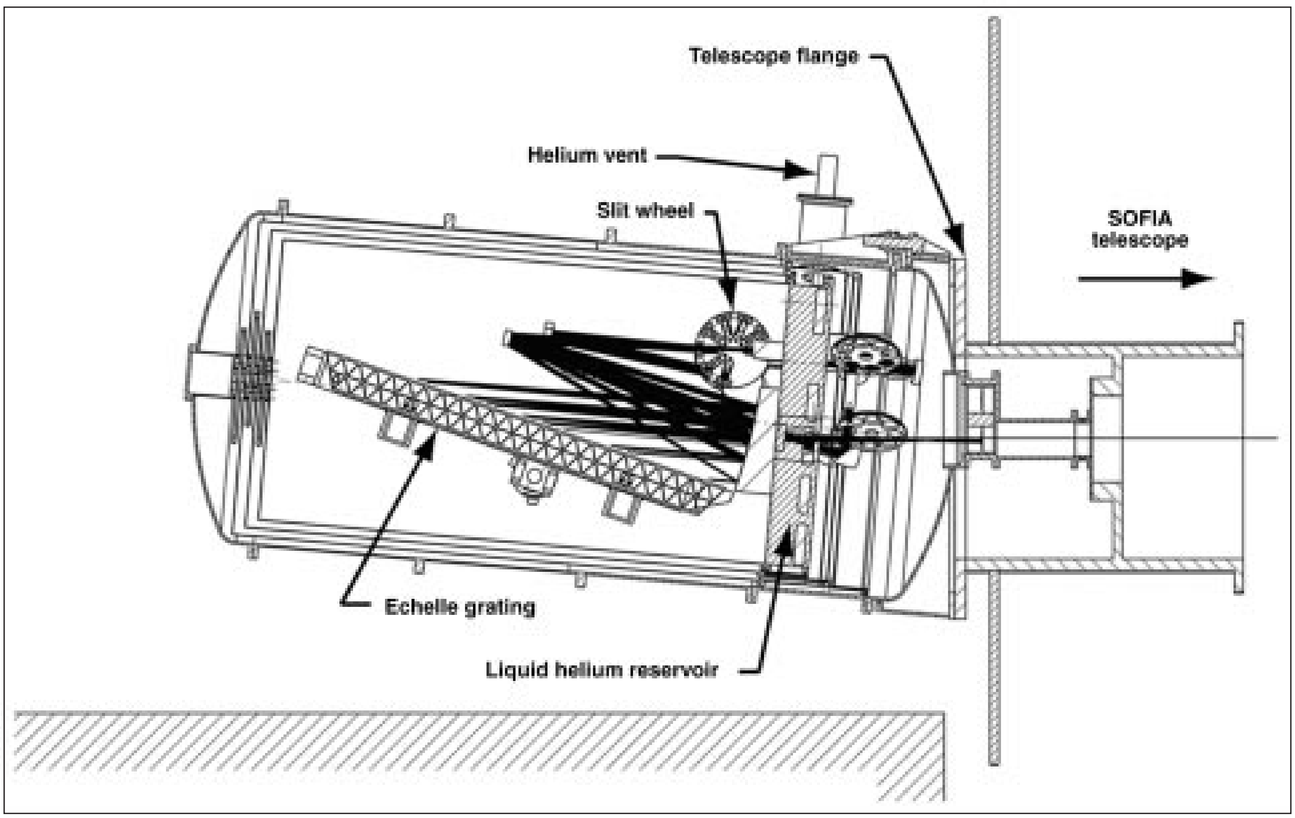

Fig. 1. The AIRES design concept; the echelle grating is about 42 inches long.

and comets, and a variety of other astronomical problems.

The AIRES design incorporates what will be the world's largest monolithic (echelle) grating (see the figure), and four different types of infrared array detectors operating at temperatures between 2 and 8 kelvin. In FY98, the team demonstrated that the cryogenic optical system can be designed to achieve the theoretically limited performance required by AIRES. Development of a comprehensive data system and associated software system, which will permit effective utilization of AIRES, is well under way.

Point of Contact: E. Erickson
(650) 604-5508
erickson@cygnus.arc.nasa.gov

Calculation of Instrument Functions

David Goorvitch

In many situations, analysis of a spectrum is contingent on knowing the response of the measuring instrument. A popular analysis method is to obtain these parameters by iteratively fitting a theoretical spectrum to the observed spectrum until they match. This method involves convolving the theoretical spectrum with the response function of the measuring instrument. The iteration process is usually nonlinear and is repeated many times to reach convergence. Since the instrument response function is convolved with the theoretical spectrum in each measurement, knowing the response function can eliminate potential errors in the derived spectroscopic information. A new Ames study has shown how instrument response functions can be calculated more rapidly and accurately.

The calculation of a response function, more commonly called the instrument function, is complicated even in a simple case. The complication arises when the instrument function is made up of several effects. For example, the mathematical instrument function for the Fourier transform spectrometer, even for the unapodized case, is composed of a rectangle representing the physical travel of the instrument and a sinc function (equal to the sin function divided by its argument) representing the collimation of the beam. Each of these functions is also well described in the frequency realm of the measured spectra. However, the composite mathematical instrument function results in an integral of a sinc function between finite limits. This integral cannot be represented as a simple analytical function, so it must be approximated.

A new Ames research effort has attacked this problem by transforming it into an orthogonal physical space where its equations can be solved analytically or by a simpler approximation. Transformation to an orthogonal space is facilitated by the convolution theorem, which states that the convolution of two functions can be obtained by multiplying their transforms and back transforming to the original space. In addition, the convolution theorem has the added advantage that calculating the Fourier transform and inverse Fourier transform is faster than computing the direct calculation of the convolution. The computing time it takes to perform a transformation using the fast Fourier transform is proportional to $N \log_2 N$, while the direct convolution time is proportional to N^2. Thus this new technique has a potential savings in computational time that is proportional to $N/\log_2 N$ for N measurements in each spectrum.

This study has shown the power of using the convolution theorem in calculating instrument functions in several examples, including an apodized Fourier transform spectrometer that is illuminated with uncollimated radiation and has misaligned mirrors. The instrument functions in these cases are far from ideal, but the new technique was successful in calculating them quickly and accurately.

Point of Contact: D. Goorvitch
(650) 604-5502
dgoorvitch@mail.arc.nasa.gov

The Center for Star Formation Studies

D. Hollenbach, K. R. Bell, P. M. Cassen

The Center for Star Formation Studies, a consortium of scientists from the Space Science Division at Ames Research Center (ARC) and the Astronomy Departments of the University of California at Berkeley and Santa Cruz, conducts a coordinated program of theoretical research on star and planet formation. The Center, under the directorship of D. Hollenbach (ARC), supports postdoctoral fellows, senior visitors, and students; meets regularly at Ames to exchange ideas and to present informal seminars on current research; hosts visits of outside scientists; and conducts a week-long workshop on selected aspects of star and planet formation each summer.

In FY98 one focus of the Ames portion of the research work involved the dispersal of the protoplanetary disks that ultimately form planets. The formation of a planetary system includes numerous sequential stages. The collapse of a giant cloud of interstellar gas and dust results in a central protostar with a protoplanetary disk of orbiting gas and dust. The gas and dust spirals onto the star, causing the star to grow in mass, a process called "viscous accretion." At the same time, the dust in the disk settles to the midplane, and coagulates into large, ice/rock planetesimals. The collisions of these planetesimals leads to larger planets. If the mass of the planet becomes greater than about 15 Earth masses, the gravity of the planet can attract the gas in the disk, and the planet rapidly adds considerable more mass in gaseous hydrogen and helium. In this way, a giant gaseous planet such as Jupiter is formed. During the same period, the wind from the central star "blows" on the disk and carries gas and dust back out into the interstellar medium. In addition, the ultraviolet radiation from the central star, or from a nearby luminous star, heats the surface of the disk to thousands of degrees, and the gas and dust are evaporated into the interstellar medium. Therefore, the gas and dust in a protoplanetary disk have four possible fates: accretion onto the star, accretion onto planets, wind-stripping, or photoevaporation. D. Hollenbach, H. Stoerzer, D. Johnstone (University of Toronto), and H. Yorke (Jet Propulsion Laboratory) studied the relative importance of these four disk dispersal mechanisms. They showed that winds are probably not significant, and that the photoevaporation and viscous-accretion mechanisms compete with planet formation in dispersing the disk in a timescale of order one to ten million years. The outer disk is especially susceptible to photoevaporation, a situation that may explain why Uranus and Neptune have so much less gas mass than Jupiter and Saturn. Many planetary systems form in clusters that include massive, luminous stars. The ultraviolet radiation from these luminous stars can evaporate their own disks, and nearby disks circling lower mass stars, in timescales of order 100,000 to 1,000,000 years, perhaps preventing or truncating planet formation.

Disks observed around low-mass young stars that are not disrupted by nearby bright stars are expected to give rise to planetary systems. Research by P. M. Cassen and D. S. Woolum (California State University at Fullerton) has led to a derivation of disk midplane conditions from observations of disks around young, low-mass systems (see the Cassen and Bell report (p. 120) for more details on this research). They find that disks in the planet-forming stage are quite cool. They, along with J. T. Wasson (of the Institute of Geophysics and Planetary Physics, University of California, Los Angeles), argue from meteoritic abundance patterns that an earlier, hotter phase of nebular evolution must have existed. This phase is identified with embedded protostars.

The theoretical models of the Center for Star Formation Studies have been used to interpret observational data from such NASA facilities as the Infrared Telescope Facility (IRTF), the infrared astronomical satellite (IRAS), the Hubble Space Telescope (HST), and the Infrared Space Observatory (ISO, a European space telescope with NASA collaboration), as well as from numerous ground-based radio and optical telescopes. In addition, they have been used to determine requirements for future missions such as the Stratospheric Observatory for Infrared Astronomy (SOFIA) and the proposed Space Infrared Telescope Facility (SIRTF).

Point of Contact: D. Hollenbach/P. Cassen
(650) 604-4164/5597
hollenbach@ism.arc.nasa.gov
cassen@cosmic.arc.nasa.gov

The Opacity of TiO

David W. Schwenke

Observational astronomy, either space based or ground based, provides the only way to gain detailed information about the stars around us. The analysis of the observed spectra is complicated; it involves the comparison of observations with the theoretical model of a given star, and since every atom and molecule has its own unique spectrum, it is essential to have an accurate database of the opacity of the atoms and molecules in the model. A very important molecule for many stars is TiO, and model calculations have been hampered by the lack of quality opacity data for TiO. The goal of the present work was to produce a significantly more complete and accurate opacity database for TiO.

The transitions of interest for TiO involve excitations of rotational, vibrational, electronic, and electron spin degrees of freedom, and there have been extensive efforts around the world to characterize the various bands via laboratory experiment. However, the analysis of the results can be very complex and some bands are very poorly characterized. Previous opacity databases for TiO have been computed using models neglecting coupling between the various degrees of freedom and using Hamiltonian parameters based on experimental analysis when available and reasonable guesses when not available.

A recent advance was the work done at Ames Research Center to compute ab initio the transition moments for the bands of interest for TiO. This calculation predicted the dependence of the transition moment on bond length, a parameter that is essential for an accurate prediction of the intensity of the lines in the spectrum. Although these data could be used with existing models to improve the TiO opacity database, new computational advances opened up the possibility of the development of a much more accurate model.

Ideally the improved model would have two characteristics: it would give line positions that agree with all existing experimental results, and all unknown parameters in the Hamiltonian would be fixed by high-quality ab initio calculations. It is easy to satisfy the latter constraint, but more difficult to satisfy the first. In order to approach experiment as closely as possible, a Hamiltonian including full rotation/vibration coupling, full spin/orbit, and full rotation/orbit was used to predict the energies. Selected parameters were optimized using least squares to match experiment as closely as possible. It was possible to achieve near experimental accuracy for all except two electronic states. These two states are highly perturbed, and more extensive ab initio calculations and experimental analysis will be required to improve on the situation.

The new model has been used in conjunction with the transition moments computed previously at Ames to produce a line list containing 112 million lines. This line list contains results for the five principal isotopes of Ti, and should be very useful for simulations up to a temperature of about 4000 kelvin. More information about the line list is available (http://ccf.arc.nasa.gov/~dschwenke).

Point of Contact: D. Schwenke
(650) 604-6634
schwenke@pegasus.arc.nasa.gov

Magnesium-Rich Pyroxene Crystals Discovered in Comet Hale–Bopp

Diane Wooden

Analysis of silicate features in comet Hale–Bopp led to the discovery of abundant Mg-rich pyroxene crystals in the coma. Hale–Bopp's pyroxene crystals are analogous to pyroxene interplanetary dust particles (IDPs), which also may be of cometary origin. The Mg-rich pyroxene crystals represent either pristine solar nebula condensates or relic interstellar grains. If the Mg-rich pyroxene crystals are relic interstellar grains, their preponderance in cometary comae implies that the outer solar nebula, where icy planetesimals formed, received significant contributions of presolar materials. Interstellar relic grains in comets are probable sources of complex organic molecules. Such complex organic materials may have been delivered by comets to early Earth during the heavy bombardment period.

The Ames High-Efficiency Infrared Faint-Object Grating spectrograph (HIFOGS) mid-infrared (IR) spectrometer acquired 7.5–13.5 micrometer (μm) spectra of comet Hale–Bopp over a large range of heliocentric distances from July 1996 through August 1997. Silicate minerals have Si–O vibration modes in this portion of the electromagnetic spectrum. Comet Hale–Bopp was observed over a large range of heliocentric distances (3.6 to 0.95 astronomical units (AU), and back out to 2.4 AU), and the silicate feature was discovered to change in shape as the comet approached the Sun and revert to its previous shape upon recession from the Sun. From analysis of the temporal evolution of these mid-IR spectra, a cooler, Mg-rich crystalline silicate grain component—crystalline pyroxene $(Mg,Fe)SiO_3$—was discovered in the comet. The pyroxene crystals are so Mg-rich that they absorb sunlight less efficiently, making them cooler than the other silicate mineral grains. These pyroxene crystals are about ten times more abundant than the other silicate grains, and have been previously spectroscopically undetected in comets. The preponderance of Mg-rich pyroxene crystals in comet Hale–Bopp agrees with the dominance of pyroxene IDPs and with the dominance of Mg-rich pyroxenes in the reanalysis of PUMA-1 flyby measurements of comet Halley.

Point of Contact: D. Wooden
(650) 604-5522
wooden@delphinus.arc.nasa.gov

Space Technology

Intelligent Mobile Technology

Rick Alena

The Intelligent Mobile Technology research project is developing intelligent applications and system architecture to support NASA human space exploration missions. These computing tools can enhance crew and payload operations by providing automated status and command functions, along with digital communications, document retrieval, and expert system capabilities. In addition, research is under way to develop intelligent, portable assistants that will incorporate advanced human-computer interface methods to allow roaming access to mobile intranet avionics and payload data systems aboard the International Space Station. Intelligent mobile systems are also being designed to assist astronauts who will return to the Moon and one day explore the surface of Mars.

FY98 saw the completed integration and deployment of the Mobile Science Workstation (see figure), a collection of computer tools that supported geological and biological surveys during an expedition to the Haughton impact crater on Devon Island in the Canadian Arctic. The tools included high-resolution digital photography, and video and audio media records shared among explorers using high-bandwidth radio networks boosted with solar-powered repeaters. The Haughton/Mars expedition combined planetary geology studies of an environment similar to early Mars, with advanced technology demonstrations to prepare the way for future planetary exploration missions. The next-generation Mobile Exploration System combines rugged servers with multiple radio networks to allow scientists

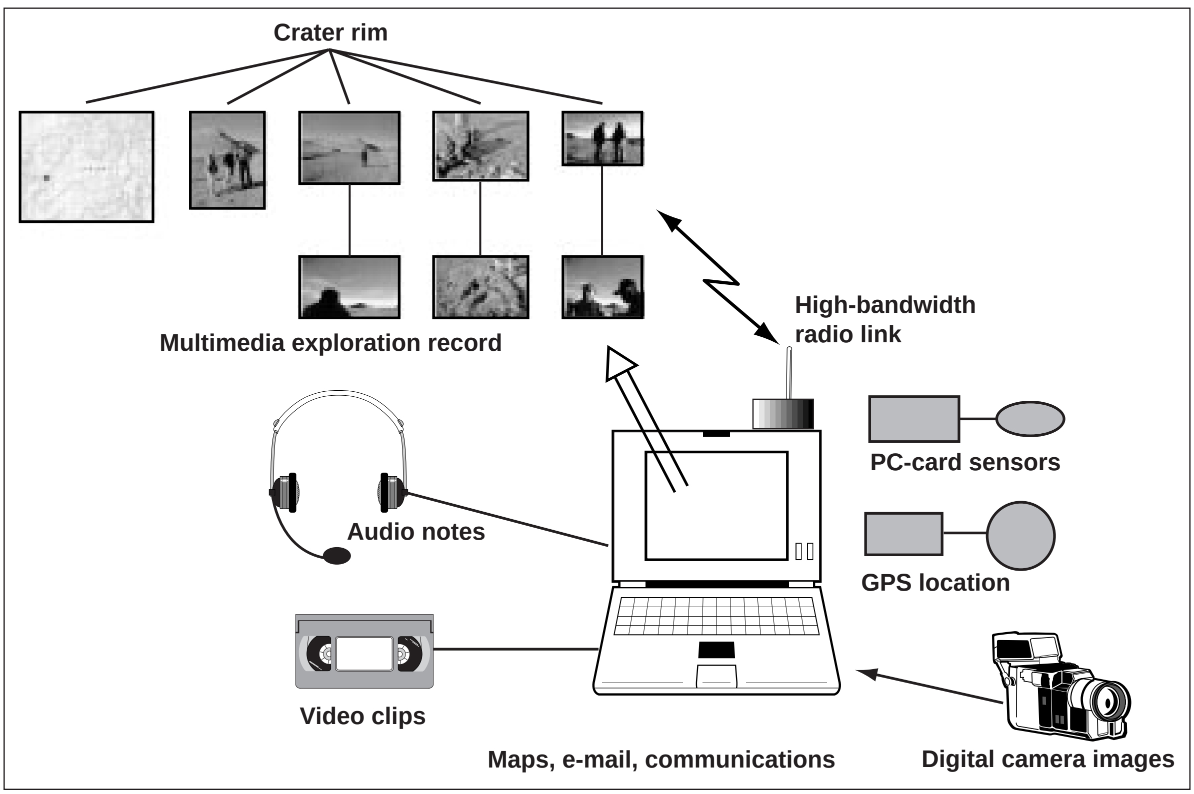

Fig. 1. Mobile Science Workstation.

around the country to view the field exploration activities as they are conducted, allowing remote participation.

The Intelligent Mobile Technology project also completed work on the avionics status display prototype by improving the network utilization and successfully converting the graphical display client program to a Java applet. Through the use of the browser applet, the data from the 1553 avionics bus becomes available to any client computer, without the need to download any software. This achievement demonstrates a key property of the mobile intranet architecture being developed for the International Space Station and other spacecraft: universal access to real-time data sources using Web-based intranet tools.

The Databus Analysis Tool (DAT) was also developed, a diagnostic tool consisting of both hardware and software running on a Space Shuttle computer that allows detailed monitoring and logging of all 1553B avionics bus messages, the nerve system of the Space Station. The DAT has network downlink capability of up to 2 gigabytes (GB) of bus messages, allowing mission engineers to conduct extensive review of avionics system functions. The DAT was flown aboard the Shuttle Endeavor (STS-88) mission in FY98, the first International Space Station assembly flight, which accomplished the on-orbit integration of the Zarya and Unity modules. The DAT was available for contingency troubleshooting of the Unity node's 1553B avionics bus during on-orbit integration activities.

The DAT is the first of a series of diagnostic aids being developed for the Space Station program. It will be reflown on subsequent assembly flights and included as a permanent diagnostic aid aboard the Space Station.

Point of Contact: R. Alena
(650) 604-0262
ralena@mail.arc.nasa.gov

Laboratory Version of CHEMIN, an X-Ray Diffraction/X-Ray Fluorescence Instrument

David Blake, Philippe Sarrazin, David Bish, David Vaniman, Stewart A. Collins

CHEMIN is a miniaturized charged coupled device (CCD)-based x-ray diffraction/x-ray fluorescence (XRD/XRF) instrument. The name CHEMIN refers to the combined CHEmical and MINeralogic analytical capability of the instrument. The instrument, for which a patent was awarded to NASA in 1996 ("X-ray diffraction apparatus," U.S. Pat. No. 5,491,738), is designed to characterize the major element composition and mineralogy of small, fine-grained, or powdered samples. Both diffraction and fluorescence data are obtained simultaneously by exposing a two-dimensional CCD imager directly to the x-rays and sorting out the photons according to their energies. CHEMIN was originally designed as a spacecraft instrument, and it has been proposed for five flight missions, including most recently the Mars 2001 opportunity. However, during the development and characterization of the flight instrument, it was found that CHEMIN was superior in many ways to the laboratory instruments from which it was derived. The CHEMIN design team has recently begun adapting the flight instrument for use in terrestrial laboratories and in remote locations on the Earth.

Several aspects of the design make the instrument ideal for certain types of laboratory analysis. CHEMIN is the first combined XRD/XRF device for which data of both types are recorded concurrently from the same microarea of the sample. Areas as small as 30 micrometers in diameter can be analyzed using conventional laboratory x-ray sources. The CCD detector is two-dimensional, allowing for detection of the entire front reflection region of the diffraction pattern, from the primary beam direction to nearly 60 degrees in 2θ space. This setup results in a nearly two-orders-of-magnitude improvement in counting rate over conventional x-ray diffractometers. In addition, because full debye rings are collected, one can record fully quantitative data from as-received or poorly prepared materials. Preferred crystal orientation and variation in crystallite size, important parameters in geology, biology, and materials science, can be assessed directly using CHEMIN.

Because the CCD detector can discriminate x-ray photons according to their energies, several diffraction patterns can be collected at once, using different x-ray source energies. This scenario allows concurrent collection of data from large d-value materials (that is, clays) at the same time as small d-value materials such as ceramics. The real-time nature of data collection will allow researchers to follow the course of reactions or phase changes using x-rays in much the same way that Fourier transform infrared spectroscopy is performed today. The CHEMIN laboratory instrument is equipped with a miniaturized (about the size of a pencil stub), low-power, micromachined, field-emission x-ray source developed by MOXTEC, Inc., as a Small Business Innovative Research (SBIR) project. An advanced CCD with improved x-ray energy resolution, developed by the Jet Propulsion Laboratory for an astrophysics mission, will be used as a detector for the instrument. X-ray diffraction data are recorded (in transmission mode), for atomic spacings from 1.66 to 15 angstroms (Å), a range that covers definitive maxima for nearly all minerals (see, for example, first and second figures).

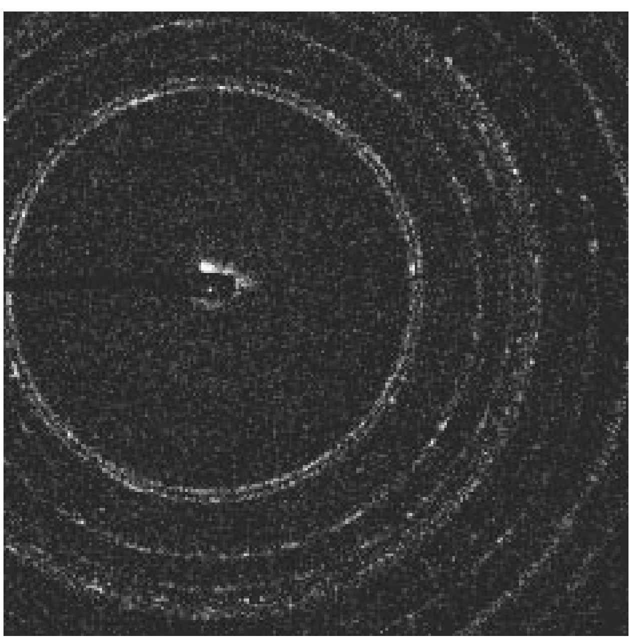

Fig. 1. Diffraction pattern for aragonite ($CaCO_3$), using an unfiltered copper x-ray source. The pattern comprises monochromatic copper Kα photons, chosen according to their energy.

X-ray fluorescence data may be obtained for elements $4 < Z < 92$ (beryllium to uranium) (third figure). Energy discrimination is used to differentiate between diffracted primary beam characteristic photons and secondary fluorescence photons. The diffraction mode line resolution of 0.02 Å is sufficient

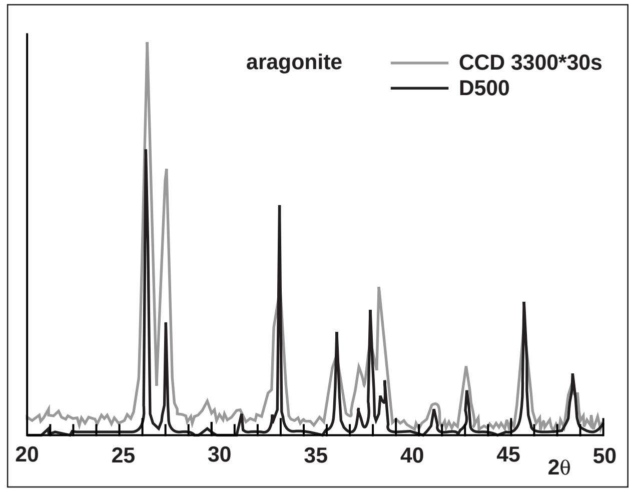

Fig. 2. Aragonite diffractogram, assembled from the data of figure 1. The inset pattern, also aragonite, was obtained using a commercial laboratory instrument. The peak width of the CHEMIN instrument is 0.2 degrees 2θ, as compared to 0.06 degrees 2θ for the commercial instrument. Despite the slightly greater peak width, CHEMIN data are fully quantifiable using Rietveld refinement.

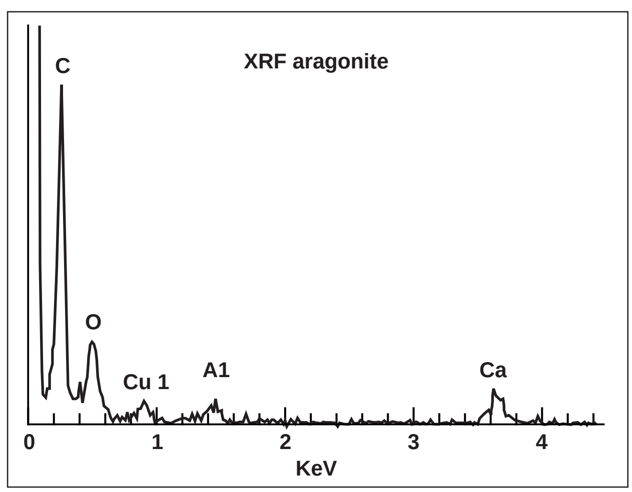

Fig. 3. Aragonite XRF spectrum. Aluminum and copper x-rays originate from components of the camera system of the prototype instrument and are not part of the sample.

to allow application of the Rietveld refinement method to the data. The proposed CHEMIN development effort will include combining diffraction and fluorescence data, using simultaneous linear equations to derive the most accurate mineral and chemical composition. A prototype version of the CHEMIN instrument, developed with NASA Planetary Instrument Definition and Development Program funding, has been operable since July 1996.

Point of Contact: D. Blake
(650) 604-4816
dblake@mail.arc.nasa.gov

Bacteriorhodopsin as a Holographic Material for High-Density Optical Data Storage

John Downie

NASA researchers are studying the organic optical material bacteriorhodopsin (BR) for use in holographic optical data storage. In this paradigm of data storage, data are stored and retrieved in parallel a page at a time, and occupy the full three-dimensional volume of a holographic medium. In principle, this scenario can lead to extremely high capacities, densities, and readout rates, and can be applied as radiation-resistant data storage for spacecraft. Holographic optical data storage has the potential for vastly increased density, capacity, and data-retrieval rates in comparison to current storage technologies such as magnetic hard disks, magneto-optic disks, CD, and DVD.

The dynamic formation of holographic gratings in bacteriorhodopsin films was successfully modeled in FY98. This type of modeling allows the optimizing of BR film and system parameters to maximize performance in a holographic system such as the intended application of holographic data storage. The simulation results for the time evolution of diffraction efficiency closely matched experimental results, providing confidence in the accuracy of the modeling.

Long-term holographic data recording in a bacteriorhodopsin film was demonstrated for the first time in FY98. Genetic engineering of the bacteriorhodopsin molecule yielded a form with an indefinite photochromic lifetime, and further chemical engineering of the film polymer matrix ensured that holographic gratings recorded in the film do not decay via molecular motion. Laboratory experiments show long-term holographic data lifetimes on the order of weeks or longer. This level achieved a necessary step toward the development of high-capacity (~100 gigabyte (GB)), high-readout rate (~1 gigabit per second (Gb/sec)), holographic data storage systems.

Preliminary experiments measuring the bit error rate of digital images holographically stored in a BR film demonstrated the potential of this material for the data storage application, and also indicated where improvement is necessary in the film fabrication process. This accomplishment was important in the process of proving the viability of BR for use in holographic data storage systems.

Point of Contact: D. Timucin
(650) 604-1262
timucin@ptolemy.arc.nasa.gov

A Novel Regenerator Material for Use in Low-Temperature Regenerative Coolers

Ben P.M. Helvensteijn, Ali Kashani, Pat Roach, Peter Kittel

NASA is interested in the development of long-life, low-temperature coolers. Such coolers are applicable to future missions, including sample return from Mars and Earth- or Sun-orbiting space telescopes. Ten-kelvin (10 K) coolers will be required for the liquefaction of hydrogen on Mars, needed for the propulsion of the return vehicle. Three-kelvin coolers are essential for cooling of the detector arrays in a space telescope focal plane.

Researchers at Ames Research Center are testing regenerator materials that are suitable for low-temperature regenerative coolers. An experimental study was carried out in order to determine the suitability of AL-272-1, a new proprietary compound developed at Ames Laboratory in Ames, Iowa, for use as the regenerator material in a pulse tube cooler. Pulse tube coolers are regenerative coolers that have no moving parts in the low-temperature region. AL-272-1 has a volumetric heat capacity higher than lead for temperatures between 17 and 83 K. Lead is often used in regenerators below 75 K, where its heat capacity exceeds that of stainless steel (SS).

In order to demonstrate the merit of the compound AL-272-1, an orifice pulse tube cooler, driven by a Gifford McMahon compressor, was designed, built, and tested (see figure). The design criterion for the cooler was to achieve temperatures at which the heat capacities of lead and AL-272-1 are significantly higher than that of stainless steel. The regenerator for the cooler consisted of a stack of 250-mesh SS screen disks. The stainless steel regenerator was extended with a section filled with lead or AL-272-1 powder. The cooler configurations used in this comparison study all employed the same pulse tube and the same heat exchangers.

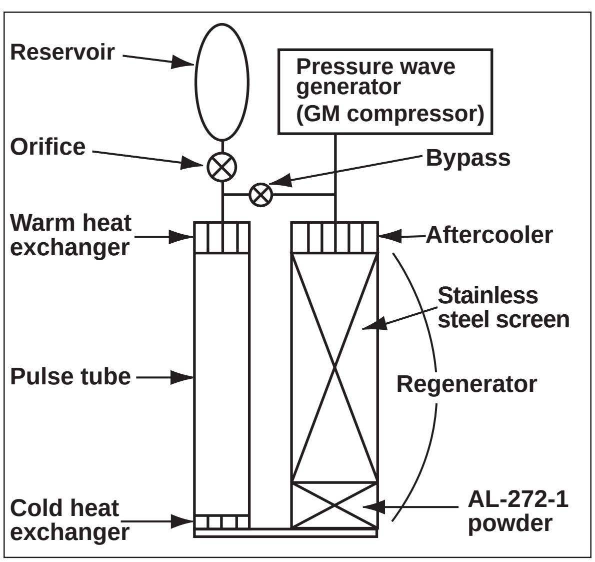

Fig. 1. Schematic of the single-stage pulse tube cooler.

In order to establish the baseline performance of the cooler, it was first tested with just the upper SS screen regenerator section. For this case, a no-load minimum temperature of 55 K was achieved. Then the lower section of the regenerator was added and filled first with the compound AL-272-1 powder. With this regenerator configuration, the cooler achieved a no-load temperature of 36 K. In the final test, the lower regenerator section was filled with lead powder (same particle size as the AL-272-1). The minimum temperature that the cooler achieved with the lead powder section added to the baseline SS screen section was 42 K. Thus, adding the second regenerator section dropped the no-load temperature in either case, but with AL-272-1 the drop was nearly 50% greater than with lead. In this study, the stacking ratios and other specifications of the single-stage cooler were not optimized, yet the experiments demonstrate notable gains in the performance of the cooler by incorporating the high-heat-capacity material AL-272-1 in the regenerator. This regenerator material can also be employed in multistage regenerative coolers that cool below 20 K to improve their performance.

Point of Contact: B. Helvensteijn
(650) 604-6534
bhelvensteijn@mail.arc.nasa.gov

Focal-Plane Sensor Array Development for Infrared Astronomy in Space

Roy R. Johnson, Mark E. McKelvey, Robert E. McMurray, Jr., Craig R. McCreight

The Infrared Detector team at Ames Research Center is evaluating the suitability of numerous detector and readout-device technologies for infrared (IR) astronomy applications. This program aims to foster development of focal plane array (FPA) detector technology that will allow reliable background-limited IR astronomy from space-based platforms such as the Space Infrared Telescope Facility (SIRTF) and the proposed Next-Generation Space Telescope (NGST). Microelectronics advances to provide low-noise, low-power device operation in the radiation environment found in Earth orbit are keys to the success of this program.

Evaluation of state-of-the-art impurity band conduction (IBC) focal-plane detector arrays produced by Raytheon Corporation is continuing for applications in the 5–30 micrometer wavelength range. These detectors rely on a thin, highly doped IR-active layer to provide elevated quantum efficiency from a small detector volume, minimizing the ionization cross-section for cosmic ray events. A high-purity blocking layer prevents excessive dark current, despite the high doping levels in the IR-active layer. IBC arrays also exhibit wider spectral response than alternative photoconductor (PC) architectures, without many of the performance anomalies associated with PC devices. IBC architectures are well suited to modern epitaxial fabrication methods, and the technology has progressed to the point where large-format hybrid FPAs sensitive to IR wavelengths as long as 28 micrometers can be reliably produced.

In FY98, the Ames IR Detector team played a critical role in the evaluation and selection of flight detectors for the SIRTF infrared array camera (IRAC). The team at Ames enabled selection of flight arrays for the IRAC instrument based on their evaluation of a matrix of prototype detectors constructed by Raytheon Corporation in Santa Barbara, California. Work concentrated on evaluating state-of-the-art, large-format (256 × 256 pixels) IBC detector arrays of varied construction. To date, several flight candidate arrays have been developed into a full-flight mount configuration specifically for the IRAC instrument (see figure). The IR Detector team has participated in testing selected parts in the flight configuration.

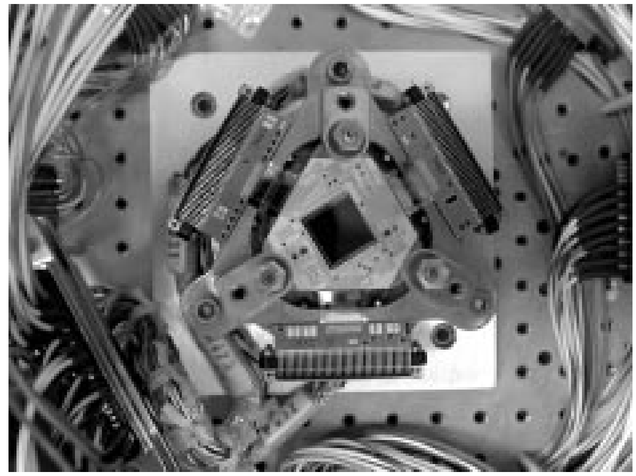

Fig. 1. A 256 × 256 infrared detector array in its flight configuration mount for the IRAC instrument.

The IR Detector team tests detector arrays and makes evaluations based on measurable parameters such as quantum efficiency, dark current, and low read noise. The prototype testing also includes exposing the detector arrays to simulated on-orbit radiation environments using a high-energy proton beam from the 76-inch Crocker Cyclotron on the campus of the University of California at Davis. Information gathered from the radiation environment testing has been fed back to manufacturers in order to advance the state of the art. Data gathered in FY98 confirm continuing advancement in radiation hardness, a step that is crucial in the on-orbit environment expected for SIRTF and NGST.

Other recent efforts involve hardware and software upgrades to the suite of test instrumentation maintained in the IR detector lab. The test instrumentation has undergone advances that allow improved data acquisition with faster information transfer and increased resolution. These progressions are part of a continuous effort to proficiently test the next generation of large-format IR detector arrays to the order of 1024 x 1024 pixels.

Point of Contact: R. Johnson/R. McMurray, Jr.
(650) 604-1131/3179
rrjohnson@mail.arc.nasa.gov
rmcmurray@mail.arc.nasa.gov

The SOFIA Water-Vapor Monitor

Thomas L. Roellig, Robert Cooper, Anna Glukhaya, Michael Rennick

The Stratospheric Observatory for Infrared Astronomy (SOFIA), a 3-meter-class telescope mounted in a Boeing 747 aircraft, is being developed by a consortium consisting of the University Space Research Association, Raytheon E-Systems, and United Airlines. This new facility will be a replacement for the retired Kuiper Airborne Observatory that used to fly out of Moffett Field. As part of this development, NASA Ames Research Center is providing an instrument that will measure the integrated amount of water vapor seen along the telescope line of sight. Since the presence of water vapor strongly affects the astronomical infrared signals detected, such a water-vapor monitor is critical for proper calibration of the observed emission. The design of the water-vapor monitor is now complete and is described as follows.

The SOFIA water-vapor monitor measures the water-vapor content of the atmosphere integrated along the line of sight at a 40-degree elevation angle by making radiometric measurements of the center and wings of the 183.3-gigahertz (GHz) rotational line of water. A picture of this water-vapor line as it would appear from SOFIA, together with the measurement bands of the SOFIA water-vapor monitor, is shown in the figure. The SOFIA water-vapor monitor must provide a knowledge of the amount of precipitable water vapor to 2 micrometers (μm) or better, 3σ, measured at least once a minute, along the telescope line of sight. In addition, a knowledge of the water vapor to the zenith is needed to equivalent accuracy. Water-vapor levels along other telescope lines of sight or to the zenith will then be determined by calculation from the 40-degree measurements. This scenario imposes more restrictive accuracy requirements on the water-vapor-monitor sensitivity, namely 1.33-μm precipitable, 3σ, measured at least once a minute. The monitor hardware consists of three physically distinct subsystems:

1. The radiometer head assembly, which contains an antenna that views the sky, a calibrated reference target, a radio-frequency (RF) switch, a mixer, a local oscillator, and an intermediate-frequency (IF) amplifier. All these components are mounted together and are attached to the inner surface of the aircraft fuselage, so that the antenna can observe the sky through a microwave-transparent window.
2. The IF converter box assembly, which consists of IF filters, IF power splitters, RF amplifiers, RF power meters, analog amplifiers, analog-to-digital (A/D) converters, and a RS-422 serial interface driver. These electronics are mounted in a cabinet just under the radiometer head and are connected to both the radiometer head and the water-vapor-monitor computer.
3. A host computer that converts the radiometer measurements to measured micrometers of precipitable water and communicates with the rest of the SOFIA mission and communications control system. These electronics are located in a rack elsewhere in the aircraft and are connected to the drive electronics through a RS-422 serial line.

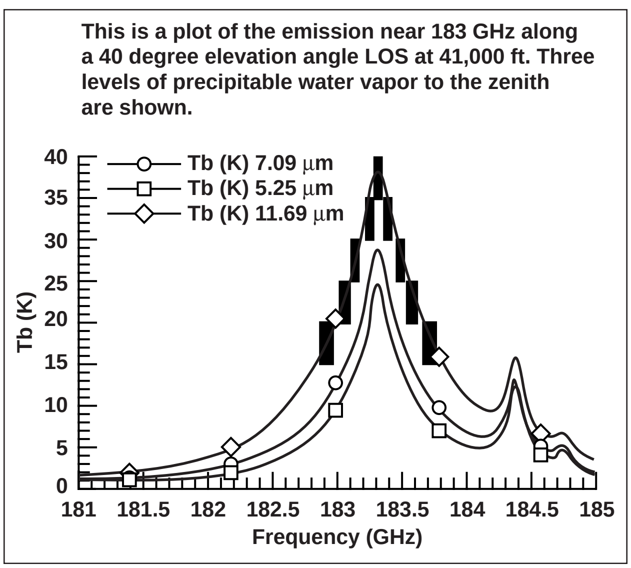

Fig. 1.The 183.2-GHz water line at 41,000 feet, with three levels of water vapor. The 184.4 line of ozone can also be seen. The shaded areas delineate the frequency coverage of the five double side-band water-vapor-monitor intermediate frequency bands.

Point of Contact: T. Roellig
(650) 604-6426
troellig@mail.arc.nasa.gov

Human Exploration and Development of Space Enterprise

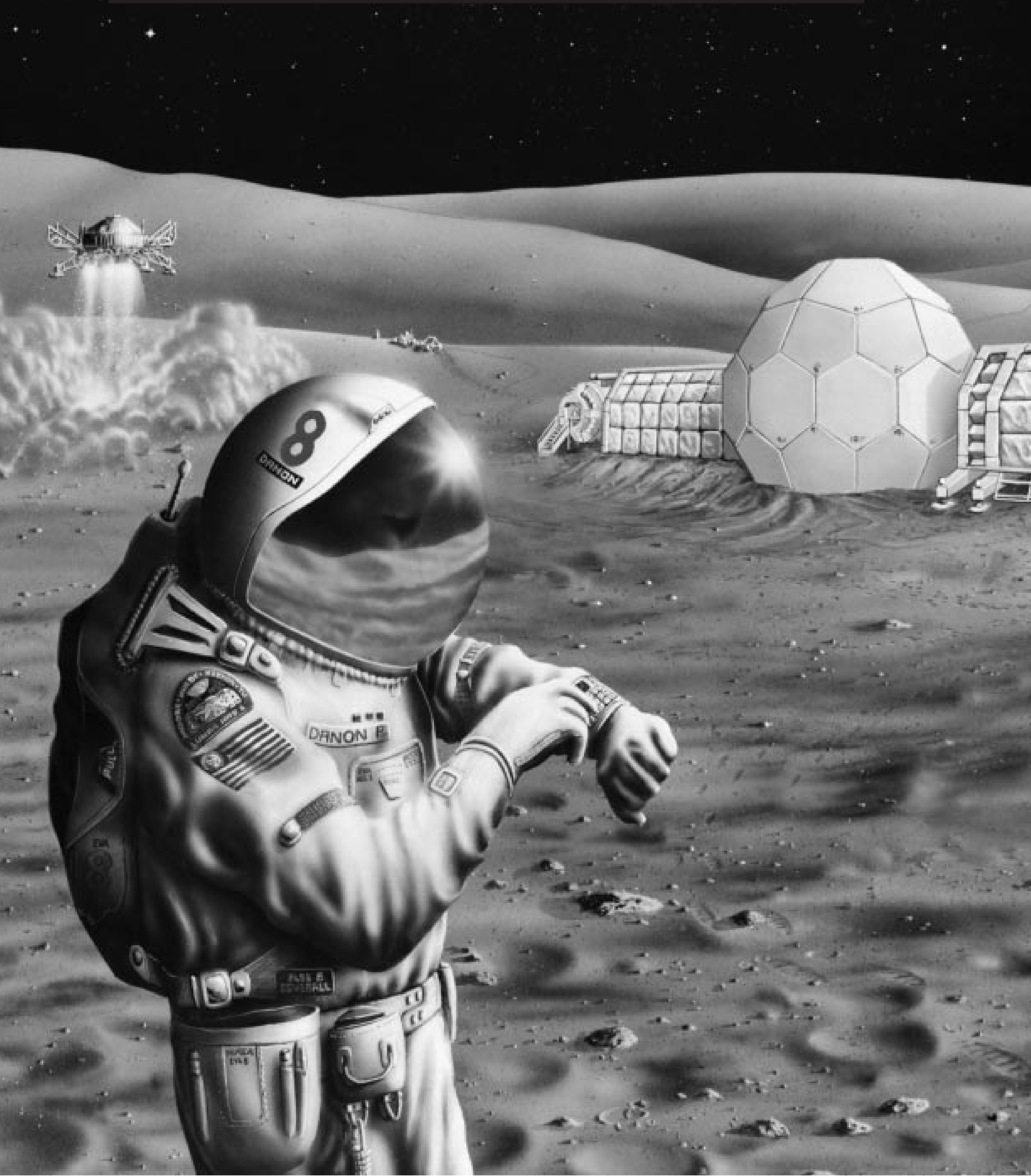

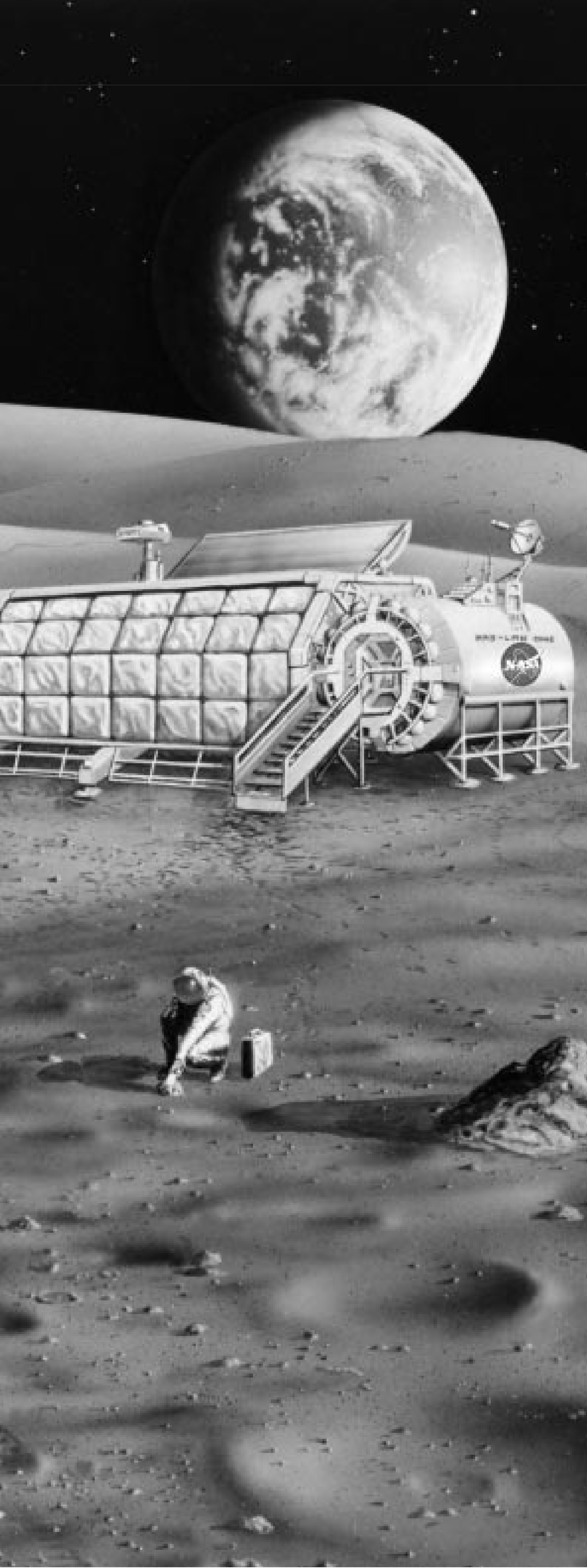

Overview

NASA's Human Exploration and Development of Space (HEDS) Enterprise provokes a new awareness of how humankind benefits from the exploration of space. It does so by contributing new scientific knowledge through the study of the effects of gravity and the space environment on critical and often phenomenal biological, chemical, and physical processes. The HEDS Enterprise plays a vital role in obtaining answers to key fundamental biological questions that provide additional pieces to the puzzle of how life evolved on Earth, and how adaptable we may be to environmental conditions elsewhere. HEDS examines the role of gravity and cosmic radiation on various systems (organic and inorganic) in space, on other planets, and on Earth. These findings build upon knowledge obtained from four decades of human space exploration. It is the ultimate goal of the HEDS Enterprise to utilize this vast base of knowledge to help establish a permanent human presence in space, and to improve life on Earth. HEDS also plays an important role working with the other enterprises to pursue answers to other fundamental questions, including the most intriguing and controversial: Does life exist on other planets?

In FY98, Ames Research Center continued its accomplishments in scientific and technological research directly in line with the following HEDS goals:

- To prepare to conduct human missions of exploration to planetary and other bodies in the solar system
- To use the environment of space to expand scientific knowledge
- To provide safe and affordable human access to space, establish a human presence in space, and share the human experience of being in space
- To enable the commercial development of space, and to share HEDS knowledge, technologies, and assets that promise to enhance the quality of life on Earth.

The articles presented in this section are loosely divided into four key areas, reflecting each of the HEDS objectives and based upon the primary objective the work was designed to address. The four areas are: astronaut health, fundamental science, progress in improving space travel, and technology transfer. These categories span the various directorates and divisions within Ames, and often, more than one objective is addressed with each endeavor. For instance, a question is asked about preventing bone loss in space that leads researchers to the development of a noninvasive measurement device that can be used in the health industry to replace more invasive systems. Similarly, a study exploring a basic biological phenomenon such as muscle fatigue is conducted that generates findings that can help to ensure astronaut health and productivity in space. Finally, the need for advanced technology to capture data from remote subjects stimulates the joint development of devices that can be used in space, modified, and then applied to various Earth applications. Nearly all of the work reported herein satisfies more than a single HEDS objective, either serendipitously, through the unpredictable nature of scientific research, or intentionally, by design.

Two classic examples of research are described that aim to improve astronaut health but also result in the development of new and advanced bone density measurement techniques for use here on Earth. Advances in image registration and computer tomography allow scientists to noninvasively monitor very small changes in density within a particular section of bone. Because previous space research has indicated that bone loss differs regionally within a bone, this new methodology is particularly valuable in assessing the effectiveness of countermeasures designed to maintain bone mass in targeted areas.

Muscle fatigue is a concern to all of us who are painfully aware of the burden gravity imposes when we exert ourselves. Its source, or sources, are of interest to researchers, physicians, employers, and civilians worldwide. Research aimed at understanding the fundamentals of muscle physiology directly benefits Earth-bound inhabitants who must battle the relentless pull of gravity, and astronauts who must face widely changing gravitational conditions. Ames researchers examined the effect reduced blood flow had on muscle force in the forearm, and found that a surprisingly small reduction in oxygenation to the muscle caused significant muscle fatigue. This fundamental finding has important implications regarding the need for adequate recovery time to the performance of any task, whether on Earth or in space. In this instance, research into a fundamental mechanism contributes to astronaut health and well being.

Ames continues to work toward the improvement of space travel, particularly in the area of data collection. This is achieved through the development of advanced technologies to capture, display, and evaluate data and optimize quality. One example is a device known as “PI-in-a-Box,” which flew on both Neurolab, STS-90, and the “John Glenn Flight,” as STS-95 is commonly referred to. This hardware was developed to assist astronauts in performing specialized science protocols in space with the same level of sophistication as the principal investigator on Earth. On STS-95, PI-in-a-Box provided the astronauts, who were involved in a melatonin sleep experiment, with instant readout of the 16 physiological signals obtained from various electrodes to measure sleep quality. PI-in-a-Box ensured optimum data quality by displaying the signal quality, and offering detailed instructions for adjusting the hardware to improve the signal without having to contact the ground.

Technology transfer was an important and productive area of work for Ames again this year. For example, pill-shaped biotelemeters are being developed for capturing vital physiological data aboard the International Space Station. The biotelemeters are initially planned for use in animals within the Station’s Gravitational Biology Facility, but can be modified and applied to astronauts to monitor their health and measure key parameters over long durations as well. The development of this and other advanced technologies is part of an expanding collaboration between Ames and external partners. The synergism between Ames and its collaborators results in shortened development times for critical spaceflight technologies, and better capabilities for both ground-based health care providers and the military, to monitor the health status of those under their responsibility.

Pursuant to the HEDs mission of opening the space frontier and expanding the human presence beyond Earth, Ames employs an ongoing integrated approach—one that results in an interactive relationship between space- and ground-based research and development efforts. The result is an enabling of humans to stretch beyond our Earth limits, to add to our existing foundation of knowledge, and to develop new technologies that can be utilized for Earth-based health, environmental, and industrial applications, ultimately benefiting all humankind.

Astronaut Health

Recent Advances in Image Registration

C. H. Yan, R. T. Whalen, G. S. Beaupré, S. Napel

Development of a noninvasive experimental model to study bone adaptation in humans to cumulative daily mechanical loading is the overall research objective. An important requirement is the ability to monitor accurately and precisely small changes in bone density within small contiguous volumes of interest within a bone. Computer tomography is currently the only practical modality capable of directly imaging bone volumetrically; however, monitoring the same site requires very accurate alignment or registration of two images of the same object taken at different times. Misregistration can introduce errors which increase as the size of the volume of interest decreases. State-of-the-art, semi-automated, three-dimensional (3-D), surface-based registration techniques have been developed that do not require the use of an external frame or fiducial markers.

Accurate surface-based registration is important because the same internal volume of interest can be located regardless of changes in internal bone density. The accuracy of the new noninvasive registration technique is comparable to that which can be obtained only by using standard invasive approaches (for example, skeletal pins and frames). The high accuracy of the new registration algorithm required the development of a new gold standard for quantifying registration accuracy. For an object the size of the calcaneus, this new gold standard has a maximum error of 0.024 millimeters (obtained from a scan with an in-plane pixel spacing of 0.24 millimeters) and an average error of 0.017 millimeters. This gold standard was used to assess the accuracy of the 3-D surface registration algorithm. In an in vitro study, cadaver calcanei (heel bones) were scanned in multiple orientations in both air and water with a General Electric (GE) clinical computed tomography scanner. The surface-based registration algorithm had a maximum error of 0.36 millimeters and an average error of 0.18 millimeters; that is, on average a point anywhere within the bone is within 180 micrometers of its "true" location. The average error when scanning with a water bolus that increased image noise was 0.20 millimeters. By way of comparison, the width of a line drawn with a medium ballpoint pen is approximately 0.4 millimeters.

Another way of putting the registration accuracy into perspective is to consider that the mean error is on the order of the width of a trabecula or spicule of bone. This level of accuracy is clearly illustrated by examining registration results of the technology applied to a subject who had sprained his foot in a soccer game. As shown in the first figure, the foot was scanned with a GE computed tomography scanner in a special fixture a few days after injury, and then four weeks later. The calcaneus in both images was segmented out, the surface detected in each image, and the registration transformation (3-D translation and rotation components) computed with the surface-based registration method. Using this transformation, the entire image at four weeks was then transformed into the time zero reference frame.

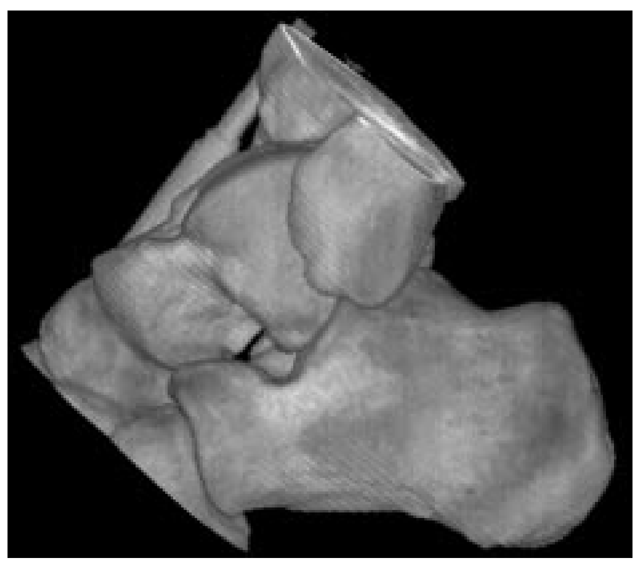

Fig. 1. Computed tomography image of the hindfoot and ankle region with soft tissue removed by image thresholding. Note that the image contains the entire 3-D volume of the heel bone (calcaneus). (Courtesy of G. Beaupré, Palo Alto Veterans Administration Medical Center.)

The second figure shows an arbitrary thin slice taken through the calcaneus of both computed tomography images following registration. Note differences in the amount of soft-tissue swelling, position of calibration vials, and the talus in each image. Now examine carefully the similarities in the two calcaneal sections, the larger of the two bones in the image. Clearly, the exactness in the registration is evident, with the same trabecular and anatomical features appearing in both images. Highly accurate and precise registration of computed tomography images is an essential component for noninvasive monitoring of changes in local volumetric bone density. Using this newly developed registration technology may enable more accurate monitoring of individuals in shorter periods of time.

Point of Contact: R. Whalen
(650) 604-3280
rwhalen@mail.arc.nasa.gov

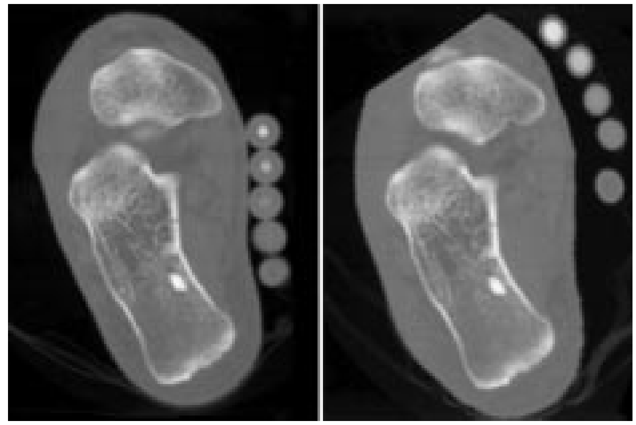

Fig. 2. Single slice through an arbitrary section of the calcaneus and foot in the two registered images (time of ankle sprain and approximately four weeks later). Note the similarities in calcaneus trabecular architecture in the two images, indicating near-exact 3-D registration of the calcaneus. (Courtesy of G. Beaupré, Palo Alto Veterans Administration Medical Center.)

Beam Hardening Correction for Quantitative Computed Tomography

C. H. Yan, R. T. Whalen, G. S. Beaupré, S. Napel

The overall research objective is to develop a noninvasive experimental model to study bone adaptation in humans to cumulative daily mechanical loading. The ability to monitor accurately and precisely small changes in bone density within small contiguous volumes of interest within a bone is an important component. Computer tomography is used to image bone volumetrically. Because the x-ray attenuation properties of a material are a function of the x-ray energy, a change in the energy spectrum of the beam as it passes through the body will result in the same density of material (for example, bone density), located in different regions, having different attenuation values. The apparent differences in density are the result of beam hardening, the shift in the x-ray energy spectrum of the imaging beam as it passes through attenuating materials such as a fixture, soft-tissue, bone, and marrow. This problem is nonlinear and uncorrectable by linear calibration. Beam hardening correction refers to new single- and dual-energy beam hardening correction algorithms that have been developed that improve both accuracy and precision of bone density measurements using computed tomography.

This new quantitative computed tomography technology is unique because it neither uses nor requires calibration vials or solid phantoms of any kind; therefore, in principle the approach is scanner-independent, although the quality of the scanner and image are still important. The algorithm does require a knowledge of the x-ray beam spectrum that created the image. (A method for obtaining the effective beam spectrum has also been developed.) The single-energy beam hardening correction algorithm relies on the assumption that each voxel within the scan field contains one, or at most, two known constituents or materials: soft tissue, bone, marrow, bone + marrow, or bone + soft tissue. While there may be locations such as the vertebra where there is a three-component mixture of bone, red (haematopoietic) marrow, and yellow (adipose) marrow, this is not the case with the calcaneus in adults. Because each voxel within the calcaneus contains a maximum of two constituents (bone + yellow marrow), it is

Table 1. Beam hardening correction results using the GE standard water correction, a GE proprietary algorithm for head scans (IBO), and the new algorithm (BHC). Scanner setting 120 kVp (120 kilovolt peak). (Courtesy of C. H. Yan, Ph.D. Dissertation, Stanford University, October 1998.)

K_2HPO_4 (mg/ml)	100	200	415	800	
GE Standard	103 ± 5	205 ± 7	403 ± 7	741 ± 16	120 kVp
GE IBO	97 ± 4	225 ± 2	423 ± 2	765 ± 6	
BHC	100 ± 3	203 ± 3	414 ± 2	803 ± 1	

possible to correct for beam hardening using a single-energy (rather than a dual-energy) algorithm.

To test the effectiveness of the beam hardening correction algorithm, the phantom shown in the figure was scanned. This phantom consists of an acrylic cylinder (10 centimeters outer diameter; 0.6 centimeters wall thickness) filled with distilled water. Inside this outer cylinder is a coaxial inner cylinder (3.6 centimeters inner diameter; 0.3 centimeters wall thickness) machined from bovine femoral bone. The bovine cylinder can be filled with various homogeneous solution concentrations of potassium phosphate (K_2HPO_4) to simulate different levels of bone density. Also contained within the large acrylic cylinder are five smaller acrylic tubes, each containing a different concentration of potassium phosphate. The five small acrylic tubes containing potassium phosphate solutions are used only for comparison with traditional quantitative computed tomography techniques that require calibration vials.

The table contains the results of a comparison of the new Beam Hardening Correction (BHC) algorithm to two commercial beam hardening correction algorithms: the General Electric (GE) standard beam hardening correction for water-like tissues, and the GE Iterative Bone Option (IBO) available when performing head scans. The column headings are the true concentrations in the inner bovine bone cylinder. The values in each table row are the voxel concentration means and standard deviations determined within the bovine cylinder using each of the three correction algorithms (voxel size: 0.3 millimeter x 0.3 millimeter x 1.0 millimeter).

Not only are the BHC values more accurate than either of the proprietary GE scanner corrections, the BHC standard deviations are generally smaller as well. The low standard deviations indicate that the precision of the beam hardening correction is significantly improved, enabling more precise estimates of the mean density within small volumes of interest. The scanning procedure was repeated with a crescent-shaped slab of teflon (a highly attenuating material) on top of the outer acrylic cylinder to mimic the presence of another bone in the image. Even with this severe challenge, the accuracy of the technique was not significantly affected.

This new imaging technology will be applied to address many long-standing scientific questions of practical interest to NASA. For example, is the rate of bone loss within a bone dependent on location in the bone? Is bone loss completely reversible with reloading? What level of countermeasure is required to maintain bone mass? Only an accurate and precise noninvasive, high-resolution imaging technology can address these questions unequivocally.

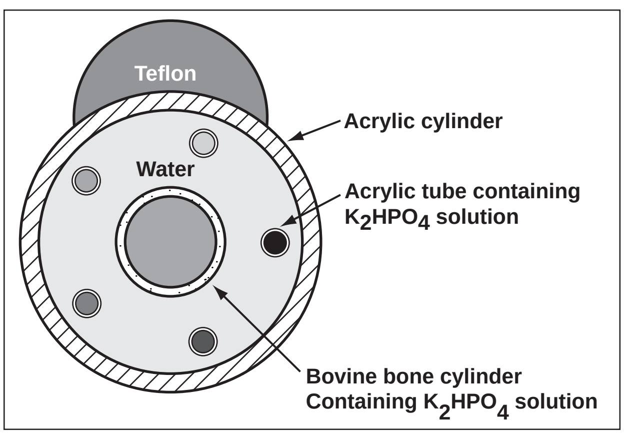

Fig. 1. Custom phantom used to test the new beam hardening correction technology. (Courtesy of C. H. Yan, Ph.D. Dissertation, Stanford University, October 1998.)

Point of Contact: R. Whalen
(650) 604-3280
rwhalen@mail.arc.nasa.gov

Cosmonaut Physiological and Performance Data: Six Months on MIR

Patricia S. Cowings, William B. Toscano, Bruce Taylor, Charles DeRoshia

This report discusses the preliminary results of a Russian experiment: "Monitoring and Correction of Autonomic and Vestibular State during Long Duration Spaceflight," for which U.S. investigators provided technical support. The broad objectives of the research were: (1) to study individual characteristics of human adaptation to long-duration spaceflight; (2) to evaluate the effect of their correction using autonomic conditioning; and, (3) to archive these data for the NASA Life Sciences Data Archive. The changes in autonomic state during adaptation to microgravity can have profound effects on the operational efficiency of crewmembers, and may result in debilitating biomedical symptoms. Autogenic-Feedback-Training Exercise (AFTE) is a physiological conditioning method that has been used to train people to voluntarily control several of their own physiological responses.

Four cosmonauts (men, ages 43–47) participated in this study. Preflight training was performed at the Cosmonaut Training Center in Star City, Russia, prior to MIR missions 23 and 25. Preflight, baseline data were collected during tilt-table tests and twelve, 30-minute AFTE training sessions. Inflight, eight data collection days were to be evenly distributed throughout the six-month missions. These days included 8-hour ambulatory monitoring of autonomic responses and computer-based performance tests. Additionally, mood, sleep, and symptom diagnostic scales were to be performed three times per day. Flight data were returned to the investigators postflight.

Because of inflight emergencies, no data were obtained from the MIR 23 mission (Subjects 2 and 3). Subjects 1 and 4 were crewmembers of MIR 25, and data were collected during this mission. On the basis of preflight training results, it was predicted

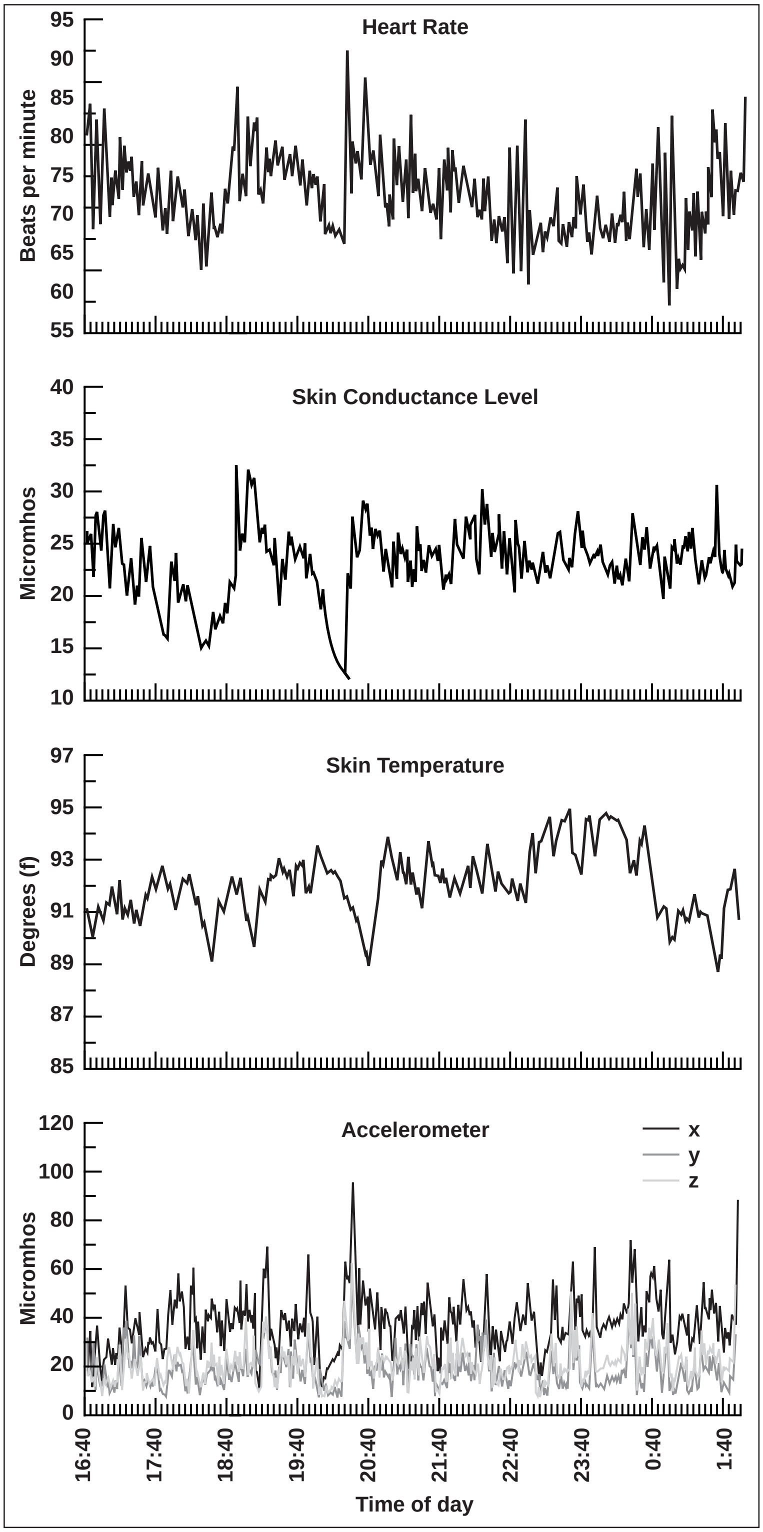

Fig. 1. Physiological responses of Subject 1, expressed as one-minute means, during mission day 137.

that Subject 1 was most likely to derive benefit from AFTE.

The first figure shows the physiological data of Subject 1 collected during mission day 137. Heart-rate data, skin conductance and temperature data, and information provided by a triaxial accelerometer on the head are shown as 1-minute averages across an 8-hour period. The three AFTE sessions, each 15 minutes long, were performed early in the shift (4:40 p.m.), mid-shift (10:40 p.m.), and at the end (12:40 a.m.) of this crewmember's shift. During each session, alternating increases and decreases in heart rate were observed for this subject. Initial analyses showed that the degree of physiological control of Subject 1 on all mission days in which data were collected was similar to that demonstrated during preflight training. Also, this crewmember did not experience any symptoms associated with postflight orthostatic intolerance. This finding suggests that AFTE may be a useful countermeasure for preventing maladaptive responses following long-duration spaceflight.

The second figure summarizes performance test data obtained during training, prelaunch, during the mission, and postflight. Both crewmembers showed a decrement in reaction time and an improvement in spatial transformation during the flight. There was a slight decrement on the manual dexterity task for Subject 4, whereas Subject 1 showed no change.

Preliminary results suggest that the use of converging indicators, physiological monitoring, performance, and symptom and mood assessment scales are an effective means of evaluating individual differences in the capacity to adapt to long-duration spaceflight and subsequent readaptation to Earth. Also, crewmembers can control autonomic responses under conditions of microgravity, and the degree of preflight learning proficiency is related to the extent that crewmembers obtain benefit from training.

Point of Contact: P. Cowings
(650) 604-5724
pcowings@mail.arc.nasa.gov

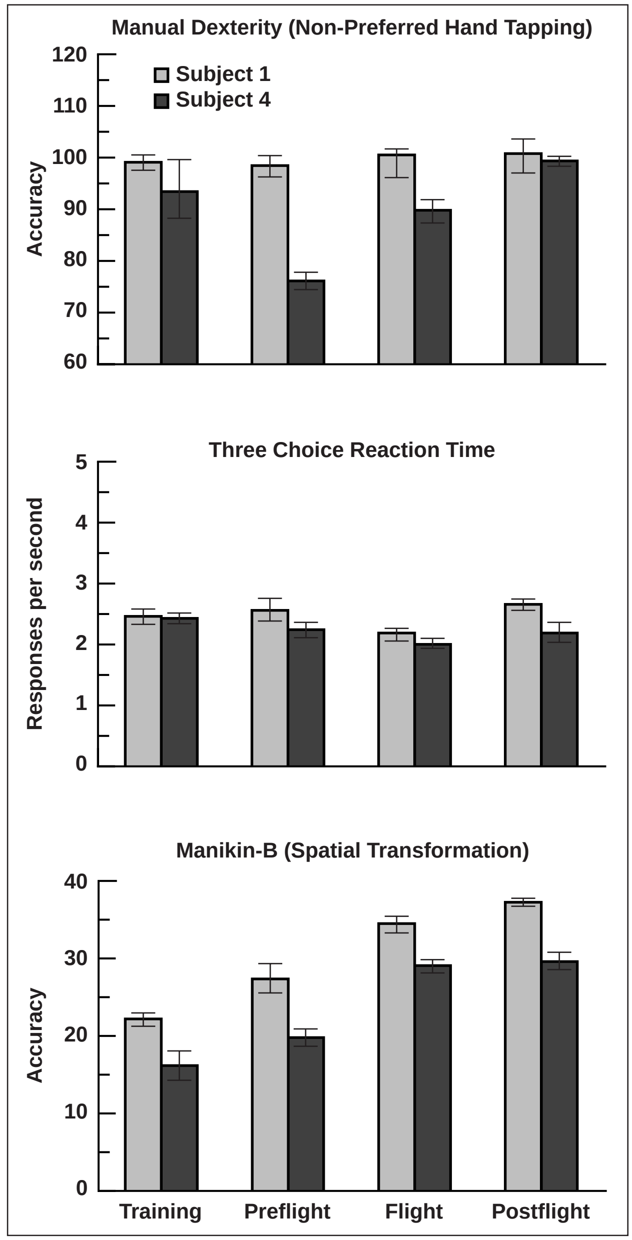

Fig. 2. Mean performance of Subject 1 versus Subject 4 on three tasks before, during, and after six months in space.

Adapting to Simulated Mars Gravity

Robert B. Welch

Because of Mars' reduced gravity (0.38 gravity), walking on the planet's surface will take the form of a *lope*, and upon their arrival, astronauts are likely to make significant errors when attempting to ambulate to a specific location. Although a couple of days' activity should eliminate these problems as astronauts adapt to the new gravitational conditions, this transition period is fraught with potential danger. For example, if an emergency took place soon after the spacecraft landed that required the astronauts to evacuate the area quickly, serious mistakes (for example, running off a cliff) might occur.

One way of eliminating this potentially dangerous adaptation period is to adapt astronauts to Mars gravity before they reach the planet. The specific aims of the present investigation are to (1) create a laboratory simulation of the bodily and visual effects of ambulating in the Martian gravitational field; and, (2) demonstrate that humans are able to adapt to this simulation while simultaneously maintaining their ability to ambulate normally in one-gravity conditions.

The Ames Gravity Simulator (AGS), a device for recreating the visual and bodily consequences of walking in 0.38 gravity (g), has been constructed and modified. To simulate the bodily sensations, subjects are enclosed from the waist down in a lower body positive pressure (LBPP) device as they walk on a treadmill. This device unloads the body as would be the case on Mars, forcing subjects to engage in a "Martian lope," and thus experience many of the same bodily sensations. The visual effects of 0.38 g are provided by a virtual environment in the form of a hypothetical Mars valley.

When locomoting in any environment, the visual world moves toward the observer in a manner precisely calibrated with his/her actions. Because ambulation on Mars requires less effort to move a given distance than in the 1 g of Earth, the resulting visual feedback will be different from that experienced on Earth. Alternatively, ambulating on Mars will take more effort to move a given distance than in the zero gravity of the Mars-bound spacecraft. The dynamic visual scene in the AGS is generated by a computer and back-projected onto a screen covering most of the subject's visual field. The scene appears to move toward subjects at a rate contingent on their treadmill walking speed. Coupling the loping treadmill walking with this visual feedback should lead to visual-motor adaptation of subjects' gait and walking accuracy. The figure depicts the AGS in action.

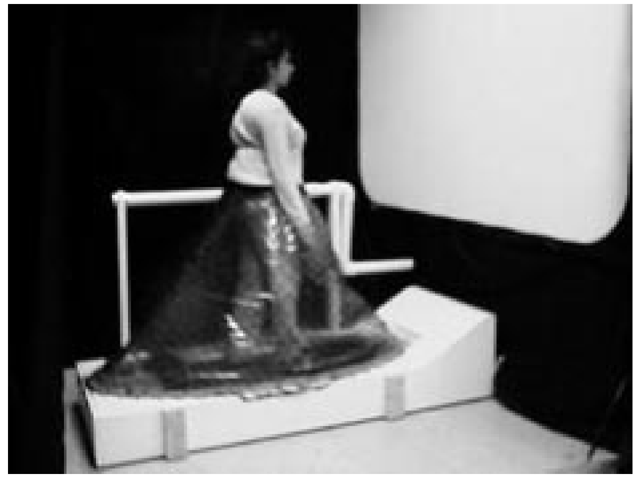

Fig. 1. The AGS: Subject walks on a treadmill with the lower half encased in an LBPP device while viewing a hypothetical Mars canyon on the screen in front of her.

This investigation represents a work in progress. During FY98, the investigators perfected the simulator and the control system for maintaining approximately constant treadmill speed irrespective of walking speed. Plans for the current year are to adapt subjects to the simulation by means of daily 1-hour exposures, and create "dual adaptation" to the simulator and normal gravity. It is assumed that the regimen of daily 1-hour adaptation sessions, separated by much longer periods of ambulation in the 1-g environment between testing sessions, will produce dual adaptation to the two gravitational conditions, as indicated by more rapid adaptation (and readaptation) than was the case the first time subjects entered (and exited) the simulation. Demonstration of this "compartmentalization" of adaptation is crucial for the future use of the simulator for the preadaptation of astronauts to Martian gravity, since it is necessary for them to be simultaneously adapted to the zero-gravity conditions of their Mars-bound spacecraft and to Mars gravity so that their adaptation to the latter will be immediately available to them upon landing.

The ultimate practical goal of this investigation is to develop a preflight adaptation trainer that could be carried aboard a Mars-bound spacecraft, preparing astronauts for their initial encounter with the reduced gravity of the planet. In addition, such a regimen would provide astronauts with an important form of exercise to help counteract the decline in muscular, cardiovascular, and bone mineralization that otherwise results from long-term exposure to hypogravity.

Point of Contact: R. Welch
(650) 604-5749
rwelch@mail.arc.nasa.gov

Human Exercise—Acceleration Countermeasure for Spaceflight

John E. Greenleaf, Jennifer L. Chou, Shawn R. Simonson

A significant problem encountered by many deconditioned astronauts is their inability to move quickly from their reentry couches immediately and for some time after landing in the Space Shuttle. The mechanisms of this deconditioned-induced gravitational reentry syndrome (GRS) are not entirely clear, but involve alterations (adaptation) in the neuro-endocrine-immune control system that are manifest by "adverse" responses of the cardiovascular, vestibular, and muscular systems to induce orthostatic intolerance (that is, a tendency to faint when one assumes the standing posture). Most space travelers experience some symptoms of the GRS: sweating, pallor, nausea, dizziness, and muscular weakness.

A resurrected countermeasure for the GRS is intermittent use of +Gz (head-to-foot) whole-body acceleration training during deconditioning. This countermeasure was first proposed and tested by W. J. White (Douglas Aircraft Co.), and L. F. Dietlein (Johnson Space Center) during a 10-day bed-rest deconditioning period with a short-arm (1.9-meter radius) centrifuge in 1965–1966. They concluded that a centrifuge exposure of 45 min/day during bed rest would essentially prevent the orthostatic intolerance that occurs after prolonged deconditioning. In the intervening years, lower-body negative pressure training was used by astronauts in flight to ameliorate the postflight GRS without significant positive effect.

Thus, a human-powered centrifuge (HPC) was fabricated at Ames Research Center in 1992–1993 (Fig. 1). Two pilot studies were conducted to test the efficiency of moving the centrifuge with leg power, and to compare physiological cardiorespiratory responses (oxygen uptake, pulmonary ventilation, respiratory exchange ratio, and heart rate) between acceleration alone, exercise alone, and exercise plus acceleration simultaneously. While acceleration alone activates most body systems significantly, it was found that physiological responses to moderate leg cycle ergometer exercise overwhelmed those from acceleration alone (that is, it looks as if only exercise was being performed). Studies are in progress at Ames to determine if deconditioning-induced orthostatic intolerance can be ameliorated with application of exercise plus acceleration simultaneously, or if acceleration alone must be used.

Ames is cooperating with the Space Medicine group at Johnson Space Center (Sam Pool) in the

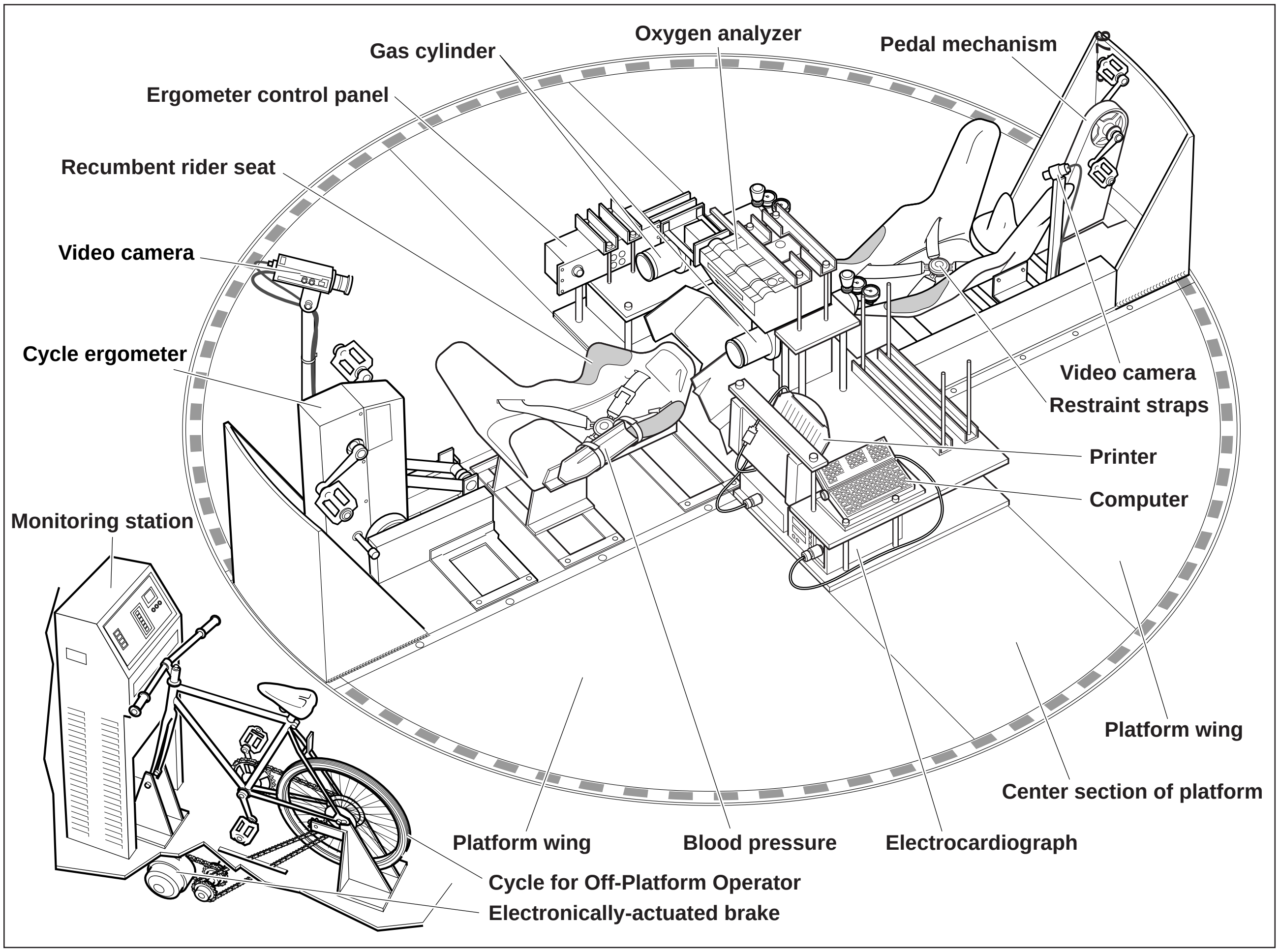

Fig. 1. The Ames human-powered centrifuge. The on-platform pedal mechanism or the off-platform operator can rotate the centrifuge. The on-platform cycle ergometer provides exercise without rotating the centrifuge.

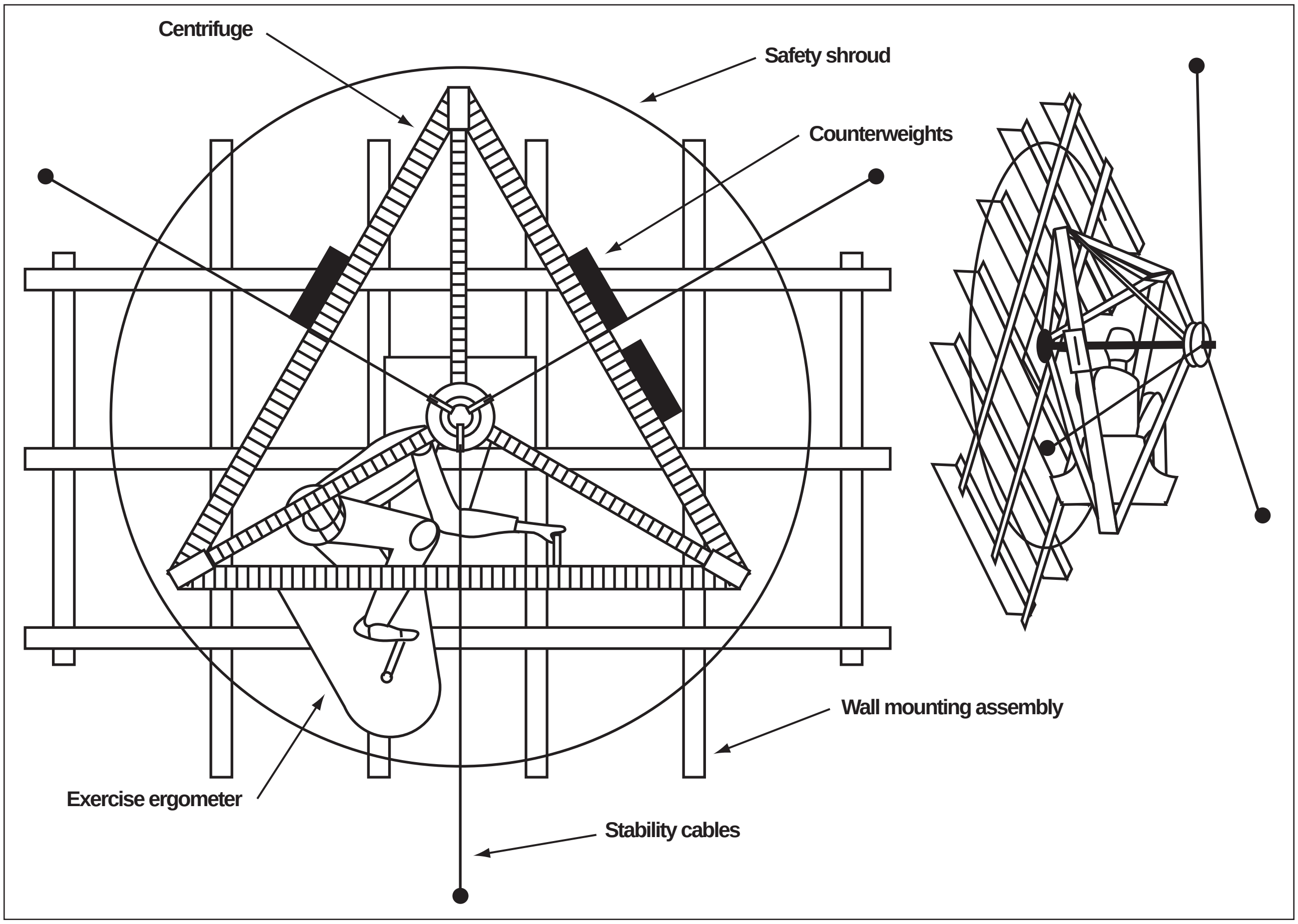

Fig. 2. The Johnson Space Center human-exercise centrifuge. The astronaut's exercise load is independent of the electrically powered centrifuge rotation.

development of a human-exercise (nonhuman-powered) centrifuge for use by astronauts on the Space Station (Fig. 2). The exercise load can be adjusted independently of the rate of acceleration of the centrifuge, which is powered electrically. This functional independence permits use of optimal exercise loads to maintain metabolic work capacity, and optimal gravitational loads to ameliorate orthostatic intolerance and the gravitational reentry syndrome.

Point of Contact: J. Greenleaf
(650) 604-6604
jgreenleaf@mail.arc.nasa.gov

FUNDAMENTAL SCIENCE

Work-Related Muscle Fatigue May Be Caused by Diminished Oxygen Delivery to the Muscle

Gita Murthy, David Rempel, Alan R. Hargens

Muscle fatigue, defined as a reduction in force despite uniform effort or stimulation, is a common musculoskeletal disorder in the workplace and may be a harbinger of more disabling cumulative trauma disorders. Such disorders are expected to increase as repetitive tasks become more common during long-duration missions. Although the cause of fatigue is multifactorial, reduced blood flow and muscle oxygenation may be the primary factors causing muscle fatigue during prolonged low-intensity muscle exertion. The goal of this study was to research the role of decreased muscle oxygenation on forearm muscle force production.

While uniform and continuous electrical stimulation elicited muscle force, noninvasive near-infrared spectroscopy (NIRS) was used to study oxygen levels in the forearm muscle when oxygen delivery to the muscle was diminished using a blood pressure cuff. Forearm muscle oxygen and force production were measured continuously during the following conditions: 5 minutes of baseline control (zero millimeters mercury (mmHg) cuff pressure), followed by upper-arm compression with the blood pressure cuff at 20, 40, and 60 mmHg, and diastolic and systolic blood pressure levels applied in random order. A recovery period (2–7 minutes) followed each level of compression and lasted until muscle force reached baseline values. Throughout the experiment protocol, subjects remained seated and did not perform any active muscle exercise. Only their forearm extensor muscle twitched involuntarily once per second for about an hour. A previous pilot study indicated that just twitching for an hour causes no reduction in muscle force production. The forearm extensor muscle was studied because it is a common site for work-related muscle fatigue and pain.

Results shown in the figure indicate that mean forearm muscle oxygen decreased from resting baseline (100%) to 99 ± 1.2% (SE), 96 ± 1.9%, 93 ± 2.8%, 90 ± 2.5%, and 86 ± 2.7% at 20, 40, and 60 mmHg, diastolic, and systolic cuff pressures, respectively. Similarly, mean muscle force decreased from resting baseline (100% oxygen) to 99 ± 0.7% (SE), 96 ± 2.7%, 93 ± 3.1%, 88 ± 3.2%, and 86 ± 2.6% at 20, 40, 60 mmHg, diastolic and systolic cuff pressures, respectively. Muscle oxygen and force at and above 60 mmHg were significantly lower ($p < 0.05$) than baseline value. Reduced muscle force was strongly associated with reduced muscle oxygenation ($r^2 = 0.99$).

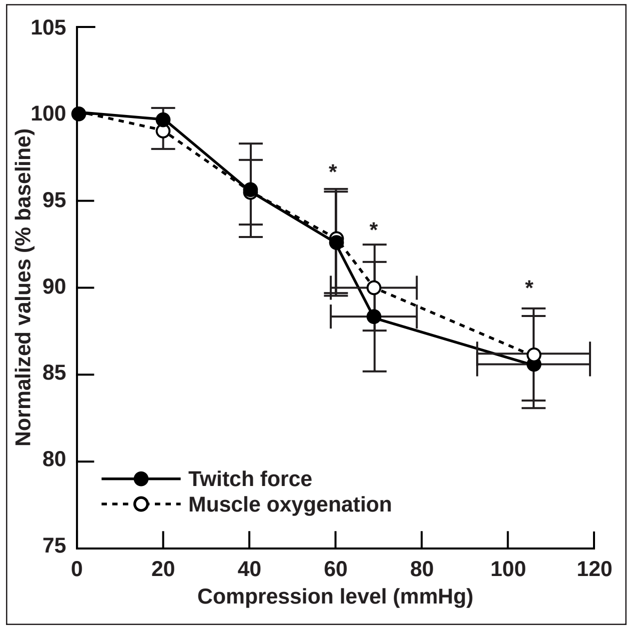

Fig. 1. Muscle oxygenation and twitch force decreases as a function of compression levels. Compression was applied to reduce oxygen delivery to the forearm extensor muscle. Bars are SE. An asterisk (*) denotes significantly lower than 100% baseline value.

These findings indicate that just a 7% reduction in muscle oxygen delivery to the forearm extensor muscle reduces force significantly, thus supporting the hypothesis that reduced oxygen can cause muscle fatigue, an issue that is highly debated. This study has important applications in the work environment because an adequate recovery period during any task performed either on Earth or in space may be required to maintain adequate blood flow and oxygenation to prevent localized muscle fatigue and maximize work productivity.

Point of Contact: A. Hargens/G. Murthy
(650) 604-5747
ahargens@mail.arc.nasa.gov
gita@uclink4.berkeley.edu

Calcaneus Bone Marrow Density and X-Ray Attenuation Properties

C. Les, T. Cleek, C. H. Yan, R. T. Whalen, G. S. Beaupré

Computed tomography is used to monitor changes in internal volumetric bone density. Bone marrow can be a significant source of error in measuring bone density with "single-energy" computed tomography if the elemental composition of marrow and the x-ray attenuation properties vary significantly among people and with age. The composition of bone marrow is known to change from red (haematopoietic, blood-cell producing) marrow to yellow (adipose) marrow as people age, with the earliest transition occurring in peripheral bones. Because of differences in x-ray attenuation properties of red and yellow marrow, a shift in marrow composition from red to yellow will appear in the computed tomography image as an apparent decrease in bone density, even though no bone mass is lost. In this study, the x-ray attenuation characteristics, density, and elemental composition of calcaneus (heel) bone marrow have been analyzed as part of an ongoing effort to enhance the accuracy and precision of quantitative computed tomography.

Thirty-four fresh-frozen cadaver calcanei were obtained from tissue banks from donors ranging in age from 17 to 65 years. Marrow was extracted by centrifugation from a 10-millimeter-thick frontal plane section, and samples were warmed to 34–36 degrees Centigrade and scanned at 80 kilovolt peak (kVp) (peak photon energy of the x-ray imaging spectrum) and 120 kVp with a General Electric (GE CT/i) clinical computed tomography scanner. Marrow material density was measured in the laboratory, and bone marrow chemical analysis (carbon, hydrogen, nitrogen, oxygen, iron percentage by weight) was performed by Desert Analytics, Inc. Density and x-ray attenuation properties for the samples are shown in the table. Coefficients of variation for computed tomography (CT) number and density were 0.5–0.7% with no age dependency. For reference, water has a density of 1 gram per cubic centimeter and an effective CT number of 1000 for both 80 and 120 kVp. The five listed chemical elements accounted for more than 99% by weight of each sample. Marrow elemental chemical analysis and density measurements indicate that calcaneal marrow is consistent with yellow marrow, not red marrow.

Table 1. Summary of calcaneus bone marrow X-ray attenuation and material density properties. (Courtesy of C. Les, National Research Council Associate, Life Sciences Gravitational Branch.)

Parameter	Mean	SD	CV (%)	Range
–(g/cm^3)	0.922	0.007	0.7	0.911–0.940
CT (80)	782.5	5.6	0.7	766.7–795.6
CT (120)	852.3	4.3	0.5	836.7–859.7

These studies also confirm that calcaneal bone marrow material properties, composition, and x-ray attenuation are virtually constant throughout adulthood. Thus, by knowing the attenuation properties of both constituent materials within the calcaneus (bone tissue and yellow marrow), single-energy quantitative computed tomography can be used to obtain the highest accuracy and precision when monitoring bone density within the calcaneus.

Point of Contact: T. Cleek/R. Whalen
(650) 604-0519/3280
tcleek@mail.arc.nasa.gov
rwhalen@mail.arc.nasa.gov

Objective Measurement of Daily Human Activity

S. M. Bowley, G. A. Breit, R. T. Whalen

The overall research objective is to develop a noninvasive experimental model to study bone adaptation in humans to cumulative daily mechanical loading. The bone selected to study is the heel bone, or calcaneus, which is loaded by internal joint, tendon (muscle), and ligament forces in equilibrium with the ground reaction force. The ground reaction force is the force the Earth exerts on the sole of the foot to support the body during upright activities such as walking and running. The NASA Ground Reaction Force (GRF) Activity Monitor records these foot-ground support forces over the course of a day. This device was used to investigate the range in baseline (nonexercising) daily activity level among a group of men [mean ± SD] (n = 12; age 40.4 ± 11.5 years) and women (n = 12; age 42.6 ± 13.3 years).

The GRF activity monitor consists of a force-sensing capacitance insole and associated data logging system, as shown in figure 1. During a walking or running step, the forces on the foot range from zero when the foot is off the ground to a peak value that occurs during the stance phase of the gait cycle. The device records the minimum and maximum values of the vertical component of the ground reaction force (GRFz) during each gait cycle. Walking cycle peak force levels typically range from 1.0 to 1.5 body weights; running cycle peak values are usually greater than 2.0 body weights, depending in

Fig. 1. NASA GRF Activity Monitor.

both cases on gait speed. Descending stairs, stepping off a curb, and other incidental events generate peak cyclic force values typically between 1.5 and 2.0 body weights.

In this study approved by the Ames Research Center Human Research Institutional Review Board, peak cyclic vertical ground reaction forces (GRFz) normalized to subject body weight (BW) were recorded for three consecutive weekdays. Average daily 24-hour histograms of the number of loading cycles sorted according to peak cyclic GRFz magnitudes (loading histories) were obtained by splitting data files into 24-hour periods and averaging. Histograms of daily GRFz loading were very distinct among subjects, representing a wide range of intensity and duration of normal nonexercising daily activity. For example, histograms from the two subjects with the fewest and most daily cycles are shown in part (a) of figure 2. From the daily histograms, the mean number of daily cycles for men was 4526 ± 1187, and for women 4744 ± 1383; the mean number of daily cycles ≥0.8 BW (gait-related) for men was 3649 ± 1139, and for women 3909 ± 1259; mean daily cycle magnitude, including all cycles ≥0.8 BW for men was 1.11 ± 0.07 BW, and for women 1.13 ± 0.09 BW; and number of daily cycles ≥2.0 BW for men was 7.3 ± 12.5, and women 5.4 ± 9.5. A trend toward reduced high-load activity (≥2.0 BW) with age was noted.

In a separate 24-hour session, the daily activity pattern of an 84-year-old female who worked part time in a retail store sorting gift cards was monitored. Her loading histogram is shown in part (b) of figure 2. A difference in the age-related frequency of daily high load is clearly evident in a comparison of the three histograms in figures 2(a) and 2(b). The 84-year-old woman had only one cycle reaching a peak value of 1.3 BW, indicative of a daily lifestyle consisting of infrequent slow walking.

Bone density in the calcaneus and lower limbs is regulated in large part by forces generated by daily gait-related activities. Loss of muscle and bone mass in space is caused by the loss or reduction, in the case of ineffective countermeasure exercise, of these support forces. In a similar way, it has been hypothesized that the gradual loss of the frequency and magnitude of high load activity with age is a contributing factor to bone loss with age. The results of this study demonstrate that "normal" human daily activity encompasses a wide range in mechanical loading of the calcaneus. In a study currently under way, daily loading histories in young and elderly sedentary women (no high load activity) and runners (high load activity) are being monitored and compared to bone density scans of the calcaneus bone in an effort to establish the functional relationship between daily mechanical loading and bone density.

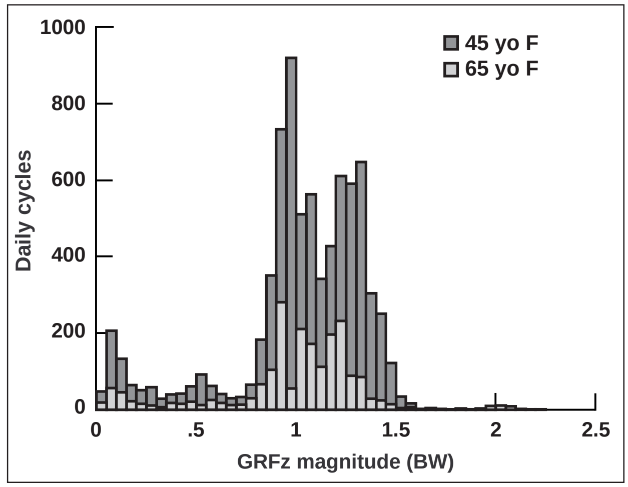

Fig. 2(a). The two subjects from the pool of 24 subjects who accumulated the minimum and maximum number of daily loading cycles.

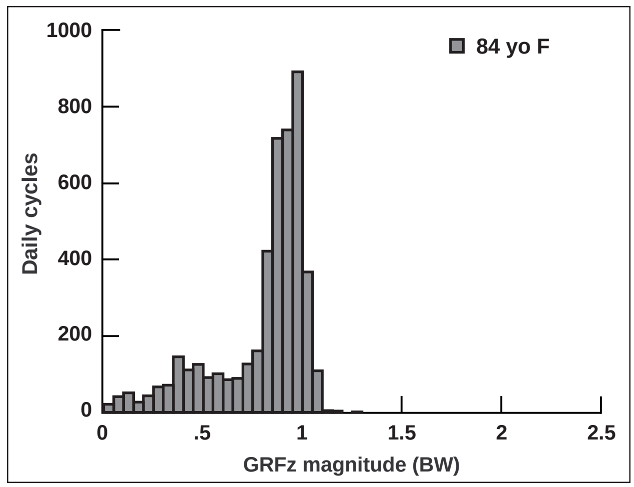

Fig. 2(b). The 24-hour loading history of an 84-year-old woman (not from the 24 subject data set). Part of her daily activity consisted of working in a retail store.

Point of Contact: S. Bowley/R. Whalen
(650) 604-3440/3280
sbowley@mail.arc.nasa.gov
rwhalen@mail.arc.nasa.gov

Computer Simulation of Bone Adaptation in the Calcaneus

V. L. Giddings, R. T. Whalen, G. S. Beaupré, D. R. Carter

Understanding the role of cumulative daily mechanical loading in the regulation of bone density and bone structure is the overall research objective. A mathematical model of bone adaptation has been derived that expresses bone density as an explicit function of cumulative daily loading, or more precisely, as a function of cumulative peak cyclic tissue effective stresses. The heel bone, or calcaneus, is loaded by joint, ligament, and tendon forces in equilibrium with external daily ground reaction forces (GRFs), and is proposed as a useful experimental model bone site to test this and other theories. In this study, the mathematical model of bone adaptation was used to predict bone density distribution in the midsagittal plane of the calcaneus, the principal plane of daily loading.

A sagittal plane, contact-coupled, finite-element model of calcaneal loading during the ground-contact phase of walking and running was constructed, as illustrated in figure 1. The kinematics of the skeletal structures of the foot and ground reaction forces during walking and running were obtained using high-speed (1000 frames per second) cineradiography and simultaneous force plate recording. These data were collected at the Henry Ford Hospital gait laboratory with the help of Dr. Scott Tashman, director of the gait facility.

The analysis of the biomechanical model of calcaneal loading showed that the highest internal stresses in the calcaneus occur during the mid- to late-stance phase; very little stress was generated in the calcaneus at heel strike. Furthermore, walking and running differed significantly only in the magnitude of the internal stresses, not in the distribution of the stress or strain field. That is, internal peak calcaneal stresses are approximately scaled by the magnitude of the ground reaction at mid- to late-stance phase. This result suggests that monitoring the vertical component of the ground reaction force with the NASA GRF activity monitor provides a good measure of the cumulative peak loading imposed on the calcaneus during walking and running.

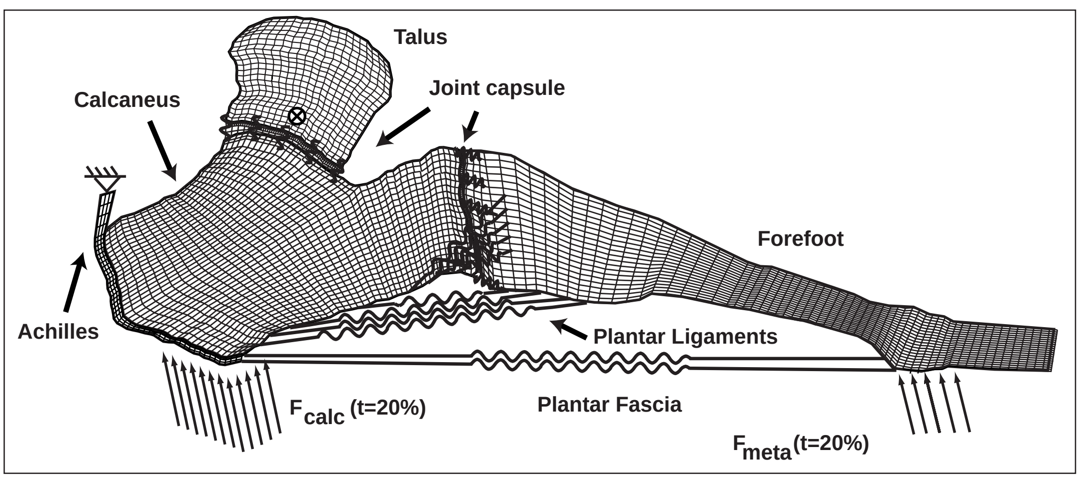

Fig. 1. Contact-coupled, finite-element model of the calcaneus shown during midstance phase of gait. Position of the bones of the foot relative to each other and the ground reaction force are known and were obtained by high-speed cineradiography with simultaneous force plate recording. All tendon, ligament and soft tissue forces, and joint pressures were computed by the model at 10% increments of stance phase. (Courtesy of V. L. Giddings, Ph.D. Dissertation, Stanford University, June 1998.)

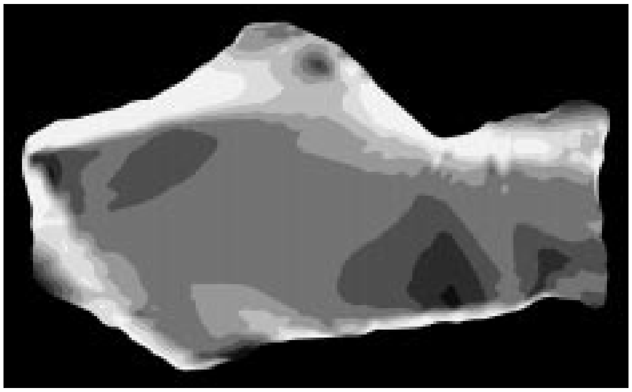

Fig. 2(a). Two-dimensional, calcaneal mid-sagittal-plane bone adaptation simulation. (Figure 2 courtesy of V. L. Giddings, Ph.D. Dissertation, Stanford University, June 1998.)

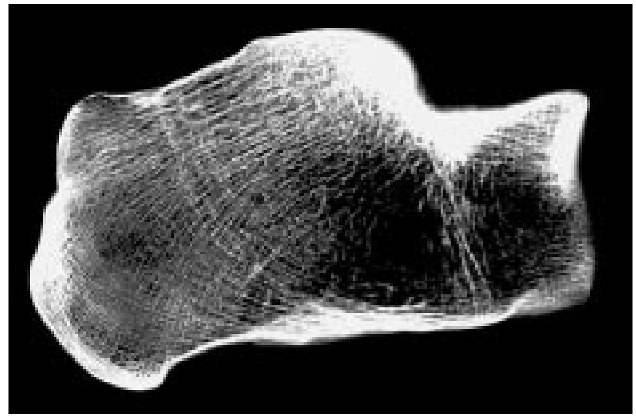

Fig. 2(b). Radiograph of a 3.5-millimeter mid-sagittal-plane section of a calcaneus with marrow removed.

Peak computed contact forces imposed on the calcaneus were used as boundary conditions to examine functional adaptation of bone tissue under conditions of normal daily activity, exercise, and disuse using the computer simulation model of bone adaptation. Figures 2(a) and 2(b) compare a remodeling simulation to a 3.5-millimeter-thick sagittal-plane radiograph of a cadaver calcaneus. In general, the predicted distribution of bone density, shown in figure 2(a), is quite similar to the radiograph, shown in figure 2(b). Note that the model predicts the Ward's triangle of very low bone density in the lower anterior region, a cortical shell, and a region of lower density in the central posterior region. Interestingly, the simulations showed significant bone distribution and density differences between "normal" daily activity level and a calcaneus subjected to higher-load running exercise (not shown). The "exercised" calcaneus had higher bone density on the periphery, effectively stiffening the shell. In future studies, it will be interesting to compare with model predictions the bone mass and density distribution of runners and non-runners obtained from computed tomography scans.

The combination of computational bone remodeling, high-resolution volumetric imaging using novel quantitative computed tomography technology, knowledge of three-dimensional morphology, and methods that monitor daily loading are critical to understanding at the organ level the regulation of bone tissue by cumulative mechanical loading.

Point of Contact: R. Whalen
(650) 604-3280
rwhalen@mail.arc.nasa.gov

Effects of a Low-Calorie Diet on Bone Formation

S. Arnaud, M. Navidi, E. Holton

The growth of bone is sensitive not only to local factors that impose biomechanical stress and load bone, but also to systemic factors that affect body weight. The general level of nutrition is a key element that affects both whole body and bone growth. Experimental animals of any age reduce food consumption during the first few days of exposure to a spaceflight model that unloads the hind limbs by suspending the tail from an overhead apparatus. To minimize the differences in final body weights in experimental and control groups, controls are fed the same restricted amount of food as the experimental animals. This scenario is called pair feeding, a technique that is effective in equalizing the body weights of animals in experiments where weight differences are primarily due to the amount of food eaten. Differences in body weights in the rat spaceflight model simulation experiments have another, unidentified cause. As shown in figure 1, after the first two weeks the pair-feeding technique does equalize growth *rates* in the groups, but final body weights are invariably lower in the experimental than in the control groups.

In order to resolve these discrepant body weights in the control and experimental groups, a "weight-matched" control was produced by reducing the amount of food in their diets. The diet fed to the weight-matched control group was formulated to contain the same relative proportions of carbohydrate, protein, and fat as in the diet fed to the other groups. Since about 20 percent less food was given to the weight-matched groups, the diet was enriched with minerals and vitamins. Essentially, the feed to the weight-matched control group was restricted in calories.

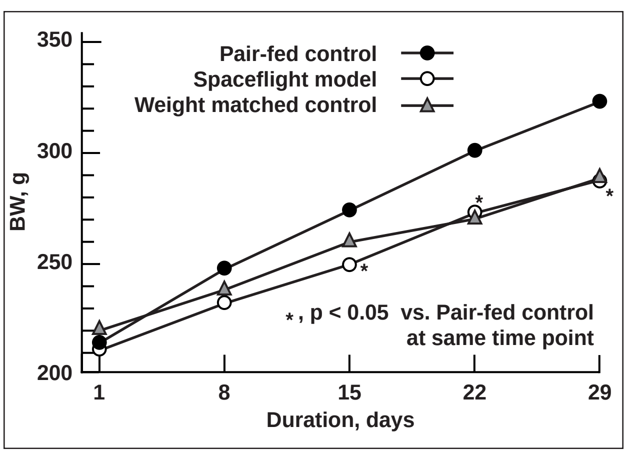

Fig. 1. Changes in the body weights (BW) of juvenile rats in three groups, pair-fed controls (•), rats exposed to the spaceflight model fed ad lib (o), and weight-matched controls (v) during a four week study.

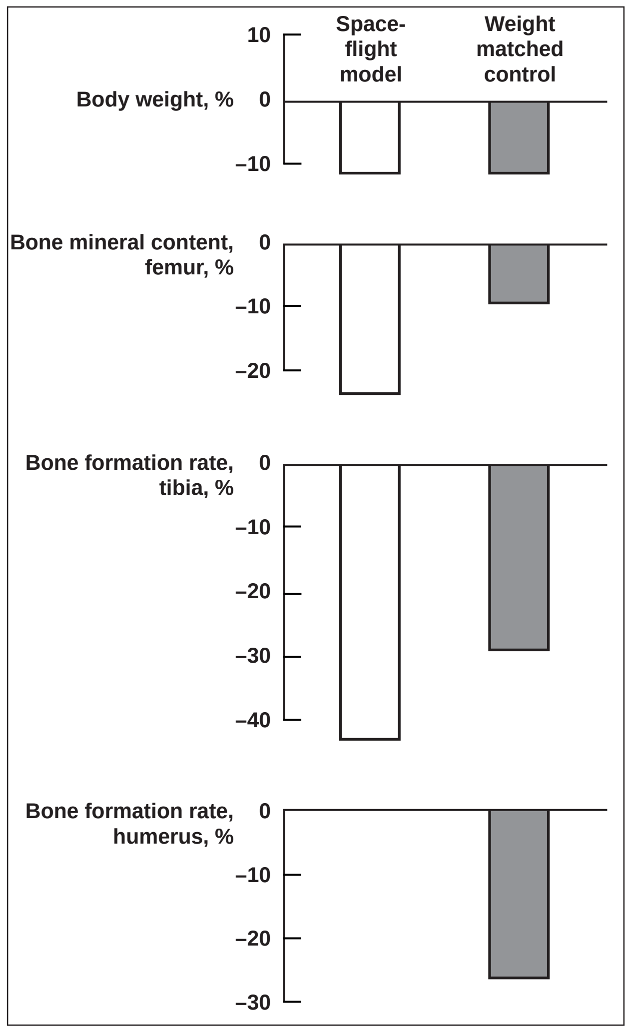

Fig. 2. Pair-fed, weight-bearing control rat data are used as the reference data for these average percent differences in body weight, mineral content, and bone histology.

The effects of reduced-caloric intakes on bone formation and mineral content were estimated in long bones from both the forelimbs and hindlimbs. After 28 days, the mineral content of the femurs in the unloaded bone was 23% less than heavier controls, and 17% less than weight-matched controls. Forelimb bones from all three groups showed identical mineral content. The results at the tissue level based on bone histomorphometry showed bone formation rates to be 43% less in the unloaded tibia than in controls, and 28% less than in the weight-matched rat tibias. Importantly, there was no difference in the histology of the humeri from controls and unloaded hindlimbs, but the weight-matched rats showed the same degree of depressed formation in forelimbs as hindlimbs (–28%).

The regional gravitational effects on bone are clearly separated from reduced caloric restriction by the hindlimb tail suspension model. After a month, femoral mineral content was three times lower than controls in unloaded bones than the decrease observed in the weight-matched controls. At the tissue level, tibial formation rates were depressed to a level one-third greater than in the weight-matched controls. These observations revealed the greater sensitivity of long bones to the change in biomechanical stress than to caloric restriction. The impact of reduced nutrition in a weightless environment was not resolved by these studies, but these data suggest that the effects of unloading plus reduced caloric intake are additive. These results also revealed the importance of weight-matched controls in evaluating gravitational models with nutritional side effects and illustrated the impact of undernutrition on bone mass.

Point of Contact: S. Arnaud
(650) 604-6561
sarnaud@mail.arc.nasa.gov

Ultrasonic Measurement of Intracranial Pressure Waveforms

Masayuki Matsuyama, Toshiaki Ueno, Brandon Macias, Robert A. Pedowitz, Sonya Waters, William T. Yost, John H. Cantrell, Alan R. Hargens

Intracranial pressure (ICP) dynamics are important for understanding adjustments to altered gravity. ICP may increase during microgravity because of a fluid shift to the head. As widely observed in clinical settings, elevated ICP causes headache, nausea, and projectile vomiting, which are similar to symptoms of space adaptation syndrome. At levels over 20 millimeters of mercury (mmHg), ICP may compromise cerebral circulation. However, there are no experimental results to support the hypothesis that ICP is actually altered during microgravity exposure, primarily because of the invasiveness of currently available techniques.

Ames has developed and refined an ultrasonic device that measures changes of intracranial distance noninvasively using a Pulse Phase Lock Loop (PPLL) technique that was initially patented by Yost and Cantrell at NASA Langley Research Center. It was previously demonstrated that the skull moves on the order of micrometers in association with ICP pulsation because of variations in arterial pressure. This ultrasonic device records ICP waveforms noninvasively from skull movements, enabling an evaluation of ICP dynamics by analyzing pulsatile components of these ICP waveforms. Amplitudes of pulsatile components of ICP yield information on intracranial compliance, representing the change in volume of any intracranial component (brain, blood, or cerebrospinal fluid) with ICP change. Clinically, intracranial compliance is important to monitor because it represents the volume-buffering capacity of the intracranial tissues and fluids. In addition, because the intracranial volume-pressure curve is generally exponential, an inverse relationship exists between intracranial compliance and pressure. Thus, mean ICP levels can be estimated from pulsatile components of ICP waveforms, as depicted in figure 1.

The investigators have reported that pulsatile changes of intracranial distances are associated with a cardiac cycle. In the present project, new data were obtained from patients in whom PPLL measurements were compared to direct invasive measurements of ICP at the University of California at San Diego

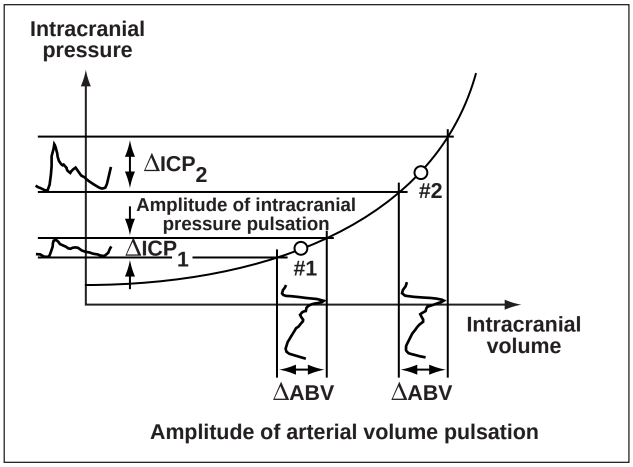

Fig. 1. Absolute ICP can be estimated from the increase of PPLL pulsatile amplitude as ICP increases in the patient. This intracranial pressure-volume curve demonstrates the variation of elastance (ΔP/ΔV slope) with intracranial volume. When intracranial volume increases from #1 to #2, the amplitude of ICP pulsation (monitored by PPLL pulsation amplitude) should increase up to an ICP level equal to diastolic blood pressure. The abscissa represents the volume of all intracranial components (brain tissue, blood, and cerebrospinal fluid).

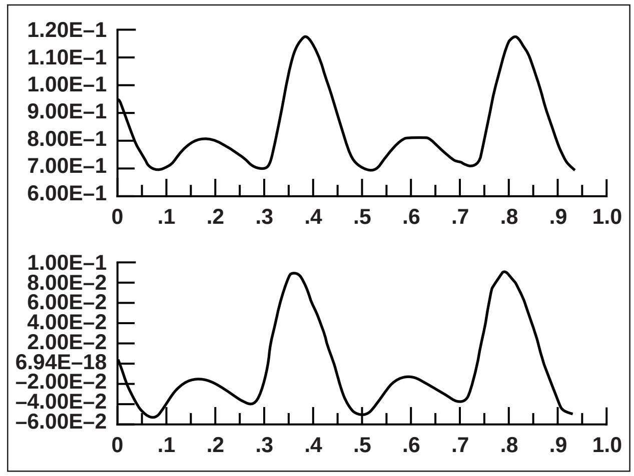

Fig. 2. Comparison of pulsatile amplitude and frequency of direct ICP waveforms (above) and noninvasive PPLL distance waveforms (below).

Trauma Center. Figure 2 illustrates the good correlation between directly measured ICP waveforms and waveforms from the ultrasonic device. When ICP was elevated, the amplitude of distance waves from the ultrasonic device also increased. These results indicate that changes in ICP on the order of mmHg may be detectable by this noninvasive technique.

Point of Contact: A. Hargens
(650) 604-5746
ahargens@mail.arc.nasa.gov

Evolutionary Adaptation of Intracranial Pressure to Gravity

Masayuki Matsuyama, Christopher Yang, Shi-Tong T. Hsieh, Harvey B. Lillywhite, Toshiaki Ueno, Alan R. Hargens

Exposure to microgravity causes a headward fluid shift that probably elevates arterial and venous pressures within the head. These factors may also elevate intracranial pressure (ICP) and cause headache, nausea, and vomiting, and reduce performance of astronauts in orbit. Various species of animals may respond differently to gravitational stress, depending upon their prior evolutionary exposure to gravity. Therefore, it is important to investigate gravitational effects on ICP from a fundamental biological standpoint.

Snakes have provided sensitive animal models for investigating circulatory regulation during gravitational stress because of their long columns of blood. Because they have evolved in very different gravity environments, aquatic and arboreal species of snakes may respond differently to gravitational stress. The purpose of this study is to test the hypothesis that snakes from aquatic habitats have limited ability to counteract gravitational stress in terms of their ICP as compared to arboreal snakes. If aquatic snakes are less able to counteract gravity, their ICP changes should be greater and more rapid than those in arboreal snakes.

In these studies, yellow rat snakes (*Elaphe obsoleta*) represented a semi-arboreal species, and diamondback water snakes (*Nerodia rhombifera*), a semi-aquatic species. Transducer-tipped catheters were inserted into the intracranial space of seven semi-arboreal species and seven aquatic species. After the surgery, the snakes were confined within individually fitted clear acrylic tubes, and underwent a whole-body head-up and head-down tilting procedure, from 0 degrees (horizontal) to the following angles: 30, 0, –30, 0, 45, 0, –45, 0, 60, 0, –60, 0, 90, 0, and –90 degrees. During this procedure, ICP was continuously recorded.

In semi-aquatic snakes, ICP increased significantly ($p < 0.001$) from –11.0 millimeters mercury (mmHg) (90 degrees head-up tilt) to 17.4 mmHg (–90 degrees head-down tilt) for the most extreme gravitational stress. For the same tilt procedure in semi-arboreal snakes, ICP increased significantly ($p < 0.001$) from –9.3 mmHg to 14.8 mmHg, as shown in figure 1. However, the average heart-to-head distance of the semi-aquatic snakes (12.4 centimeters) was shorter than that for the semi-arboreal snakes (18.3 centimeters). The ICP change per unit heart-to-head distance in semi-aquatic snakes was greater than for semi-arboreal snakes. Moreover, in semi-aquatic snakes, ICP increased more rapidly than in semi-arboreal snakes, as shown in figure 2. In conclusion, these results indicate that in terms of buffering their ICP, semi-aquatic snakes have a more limited ability to counteract gravitational stress than semi-arboreal snakes.

Point of Contact: A. Hargens
(650) 604-5746
ahargens@mail.arc.nasa.gov

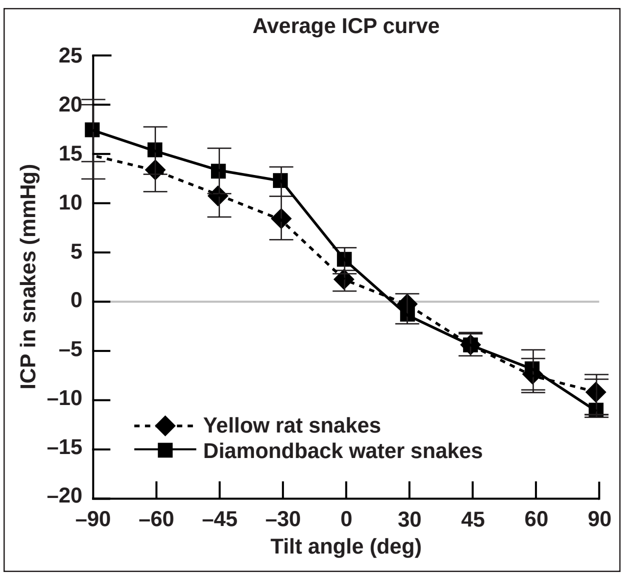

Fig. 1. In semi-aquatic species (diamondback water snake), ICP increased to 17.4 mmHg during head-down tilt, whereas in semi-arboreal species (yellow rat snake), ICP rose to 14.8 mmHg.

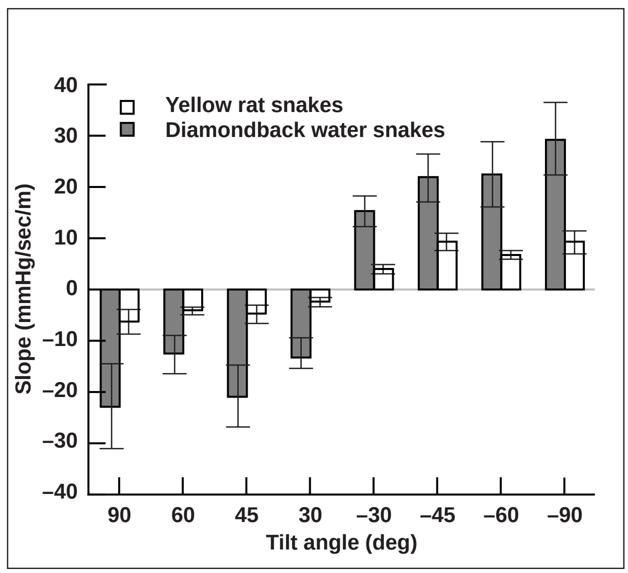

Fig. 2. Rate of ICP change in relation to tilt angle for semi-arboreal and semi-aquatic snakes. Slope of ICP is expressed as pressure change (millimeters mercury) per second of altered tilt angle per meter of heart-to-head distance.

Neurolab Biotelemetry System

James P. Connolly, Julie E. Schonfeld

The Neurolab Biotelemetry System (NBS) was developed at Ames Research Center (ARC) to support a flight experiment investigating central nervous system control of rhythm and homeostasis during spaceflight. The NBS flight hardware flew on Neurolab, April 17–May 2, 1998, as an integral part of the Spacelab payload. NBS monitored body temperature, heart rate, and activity for 12 animals implanted with small radio-frequency transmitters. Custom software was designed for sampling, processing, and storing flight data for a period of up to 21 days.

Fig. 1. Neurolab biotelemetry chassis.

The NBS was developed using a combination of commercial and ARC-developed hardware and custom software. The commercial hardware included implantable telemetry transmitters, receivers, and flash memory. Ames provided system design and integration, packaging, signal conditioner design, receiving antenna development, custom software development, environmental testing, and hardware safety verification for the NBS. The receiving antennas were custom designed to fit within Neurolab's individual metal habitats and to reliably detect near-field, radio-frequency signals from the implanted transmitters.

During Neurolab, the NBS demonstrated its ability to detect and record wireless physiological measurements under nonideal conditions without interfering with other Shuttle systems or experiments. In all, two flight biotelemetry systems, an engineering development unit, and four ground systems were developed by ARC to support the Neurolab Spacelab Mission.

Point of Contact: J. Connolly
(650) 604-6483
jconnolly@mail.arc.nasa.gov

Ensemble Neural Coding in Zero Gravity

Michael T. Eodice

The Neurolab Mission, which flew as the final Spacelab payload from April 17 to May 3, 1998, included an experiment dedicated to the study of "Ensemble Coding of Place and Direction in Zero-G." The development of flight hardware for this experiment was the joint responsibility of the Division of Neural Systems, Memory and Aging (NSMA) at the University of Arizona and NASA's Ames Research Center (ARC). The ARC team provided leadership for experiment management and premission operations, manufacturing, systems integration, and flight qualification of the experiment hardware, some of which is shown in figure 1.

Fig. 1. Laptop computer used to create a map of electrical activity within a rat's hippocampus.

The flight experiment, conceived by Dr. Bruce McNaughton of NSMA, explored how the central cortical and subcortical representation of spatial relationships is affected by microgravity. Specifically, ensemble neural activity in the parietal cortex, hippocampus, lateral dorsal thalamus, and superior colliculus was recorded in animals performing behavioral tasks using specialized behavioral apparatus. These apparatuses, namely the "Escher Staircase" and the "Magic Carpet," were developed and flight qualified by ARC engineers and technicians. The Escher Staircase consisted of three L-shaped composite tracks, covered with closed cell foam and interconnected to form a closed circuit for an animal to navigate in space. The Magic Carpet, a cross-shaped track capable of rotation in two axes, allowed astronauts to test an animal's ability to maintain accurate position information in the absence of gravity. Prototype designs of these specialized apparatuses were tested on two series of KC-135 reduced-gravity flight tests (80 parabolic arcs per test series) before finalizing the flight designs.

Experimental data were collected using a sophisticated NSMA biomedical implant that ARC reduced in size and manufactured to spaceflight standards. ARC also provided flight hardware packaging, environmental testing, and system safety verification for the experiment's signal detection, processing, and recording subsystems. These critical tasks significantly improved the reliability and robustness of the flight hardware. Two complete flight systems flew on Neurolab and allowed the first state-of-the-art neuronal measurements to be made in space.

Point of Contact: M. Eodice
(650) 604-0411
meodice@mail.arc.nasa.gov

Principal Investigator (PI)-in-a-Box Supports Sleep Experiment on STS-90 and STS-95

Dennis M. Heher

A key goal of NASA's space science program is the collection of high-quality scientific data. This goal is not always easy to achieve, because astronauts usually must perform experiments in fields outside their own areas of expertise. If an anomalous event occurs, it may not be possible to contact the principal investigator on Earth and resolve the issue, and malfunction procedures may not adequately address the issue. Conversely, if something unexpected yet scientifically significant happens, astronauts might not be prepared to modify the experiment protocol in flight. A tool is necessary to aid the astronauts to capture high-quality scientific data.

The original principal investigator (PI)-in-a-Box system aboard the space transport system (STS)-58 proved that a portable computer system and its knowledge-based software could enhance the scientific output of a life sciences space experiment. PI-in-a-Box is designed to enable a nonspecialist user to perform a sophisticated scientific experiment with the same ease that the PI of the experiment would, by encoding the experiment-specific knowledge of the PI in a knowledge-based system.

In FY98, PI-in-a-Box flew on two Shuttle missions, STS-90 in April and STS-95 in October, which included Payload Specialist John Glenn (shown training for the sleep experiment with fellow astronaut Scott Parazynski in figure 1). STS-95 was a continuation of the STS-90 (Neurolab) shuttle flight dedicated to research into neurological adaptation to space. PI-in-a-Box successfully provided signal display and signal quality analysis to the crew as part of a sleep investigation entitled "Clinical Trial of Melatonin as a Hypnotic" (Principal Investigator Charles Czeisler, Harvard Medical School and Brigham and Women's Hospital).

Fig. 1. John Glenn shown training for the sleep experiment with fellow astronaut Scott Parazynski.

The purpose of the investigation was to determine whether the use of melatonin improved astronauts' quality of sleep during spaceflight. The astronauts' sleep was characterized via recordings that assessed several sleep parameters: brain waves, eye movements, muscle tension, respiration, and other physiological signals. Applying the electrode sensors was a tedious and time-consuming task, done without any feedback from the investigators on the ground. PI-in-a-Box provided the astronauts with real-time signal display, automatic signal quality checking, and suggestions to improve the signal quality if necessary.

PI-in-a-Box used a combination of standard programming environments to accommodate the investigators' pre-existing constraints, as well as advanced reasoning back-ends to provide expert analysis and advice on the data. For the sleep experiment, researchers designed a graphical user interface in C++ to access the knowledge base encoded in CLIPS (C Language Integrated Production System). The flight computer was an IBM ThinkPad 755C.

Two astronauts per night for eight nights during the Neurolab mission attached electrodes to capture physiological signals while they slept. The PI-in-a-Box system displayed 16 of the physiological signals, providing the astronauts with a visual feedback of the signal quality, as shown in figure 2.

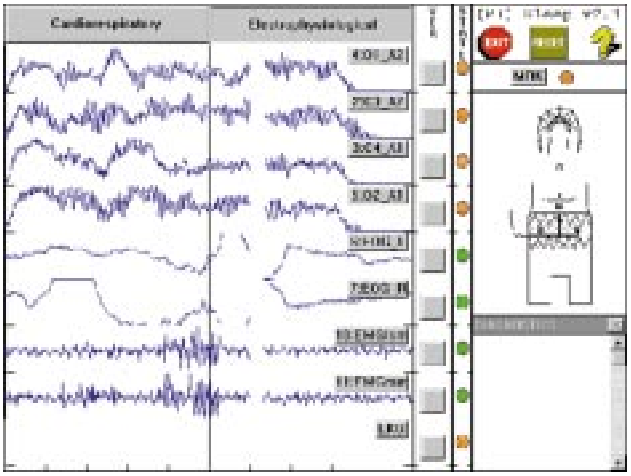

Fig. 2. System display screen showing 16 of the physiological signals, providing the astronauts with a visual feedback of the signal quality.

While the signals were being displayed, the system automatically analyzed the signals and provided real-time feedback to the astronauts regarding the quality of the data. PI-in-a-Box looked at 4-second snippets of data for each of the signals and used various statistical analyses to determine the quality of each signal. The analysis that the system was able to provide is based on numerous knowledge engineering sessions with the principal investigators and their teams. When the signal quality was less than acceptable, the system provided detailed suggestions to adjust experiment hardware to guarantee sufficient data quality to reach scientific objectives. Potential applications include supporting other spaceflight experiments on board the Shuttle and the International Space Station.

Point of Contact: D. Heher
(650) 604-1084
dheher@mail.arc.nasa.gov

Measuring Digital Video Quality

Andrew B. Watson

Digital video will form the infrastructure for much of visual communications in the coming decades. In NASA missions, visual communications will include human-to-human communications among the crew and between the crew and the ground, among ground personnel, and among a distributed network of scientists, engineers, and the public. It will also provide a means for monitoring aerospace systems and operations, as well as for storing and delivering operational knowledge such as instruction manuals and medical databases.

In all these applications, there is a need to ensure that visual quality of the communications is optimal for the given bandwidth and appropriate for the given task. There are currently no accepted means for automatically measuring or quantifying the visual quality of digital video. To remedy this situation, Ames has developed a software algorithm capable of measuring the visual quality of processed digital video. The algorithm, called DVQ (Digital Video Quality), is based upon a model of the human visual system. The algorithm has been submitted to an international competition to select an international standard for video quality measurement.

To validate the DVQ algorithm, its predictions were compared to subjective quality estimates collected from human observers for short (9 second) video sequences that had been processed using several video compression methods. The observers rated the degree of impairment of each sequence and compared it to an original, unprocessed sequence. The figure shows the correspondence between the DVQ predictions and the subjective impairment. The different colors indicate different source sequences, with the names given in the same color.

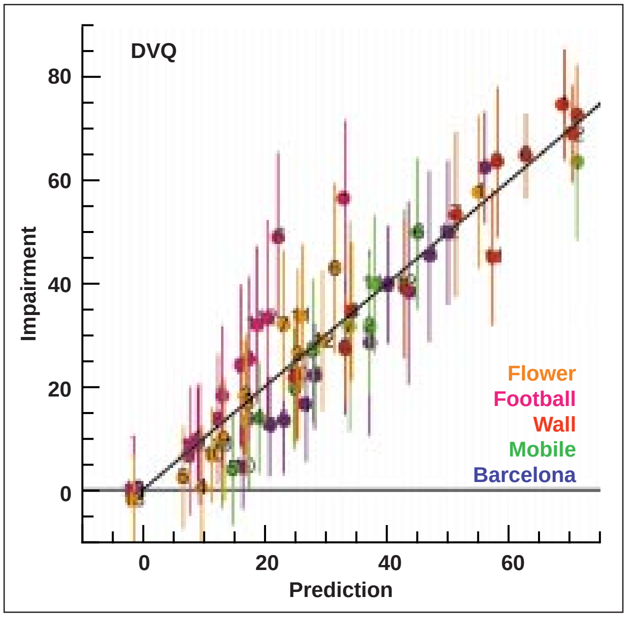

Fig. 1. Comparison of DVQ video quality predictions and human subjective quality ratings.

Each point is the mean (±1 SD) for 25 observers rating the same source and compression technique. There were a total of five sources (flower, football, wall, mobile, and barcelona), and thirteen coding methods. The number on each point indicates the coding method.

The figure shows that the DVQ method provides a good prediction of human quality judgements.

Point of Contact: A. Watson
(650) 604-5419
abwatson@mail.arc.nasa.gov

Empirical Evaluation of the Effectiveness of Independent Verification and Validation

John R. Callahan, Reshma Khatsuriya, Randy Hefner

The objective of this research is to quantify the impact of specific independent verification and validation (IV&V) activities in a software development project in terms of the time needed to find and fix problems. Previous studies examined error repair rates during development but assumed independence of errors. This research confirmed common intuition that the average time to solve a problem is significantly influenced not only by the criticality and severity of the problem, but also by the phase in the life cycle at which the issues were identified. The studies also demonstrated that IV&V finds these problems earlier, that experienced analysts find more problems, and that the skills of an analyst must be directly related to the specific project characteristics within each issue.

The IV&V facility carried out a study of issue reports collected over a certain period for two mission-critical NASA projects, the Earth Observing System Data and Information System (EOSDIS) and the Space Shuttle Day of Launch I-Load Update (DOLILU) system. The issue reports for these software projects were available in the central repositories maintained by the issue-tracking systems used for these NASA projects. The objectives of this study were:

- To determine significant factors that impact the overall progress of the project
- To build an analytical model to carry out continuous analysis on the available issue-reports data that could predict project status
- To examine the effectiveness of the real-time IV&V reporting process
- To comment on the effectiveness of the IV&V process adopted by two major NASA projects, which will help to determine the cost-effectiveness of future projects.

The function of the DOLILU system is to update the flight trajectory to account for the actual winds on the day of launch. A total of 574 DITRs (DOLILU Issue Tracking Reports) were uncovered by IV&V analysts. Time elapsed from originated date to closed date (TIME) was recorded as number of months. An analysis of issue reports from a later revision to the DOLILU phase I system, DOLILU phase II, was also performed.

Simple linear regression on 574 observations revealed that severity of the issue, life-cycle phase when the issue was identified, and expertise level of the IV&V analyst were significant in determining the time that it took to resolve the issue (TIME). Data also indicated that most of the severe problems took more time to fix than the less severe ones. Problems detected in later stages of the life cycle took less time to fix, a predictive indicator for the effectiveness of IV&V activity. Problems detected by the more expert analysts usually took longer to fix, verifying that detection of architectural and synchronization flaws requires more expertise and specialized tools.

Many large-scale software projects make use of issue-tracking tools in order to manage problems that emerge during development. An issue report may document a problem, which is a fault, error, bug, or a request for an additional feature. A formal issue report often documents the cause of the problem, its impact, and suggested fixes. Web-based issue management tools provide an online repository that is accessible to the programmers, IV&V analysts, and project managers for recording and monitoring change activities in the software development effort. Issue tracking and management systems also serve as convenient means for data and metrics collection. Continuous analysis of an issue repository can help identify and predict problems early in the development life cycle, and can even help in estimating the approximate date of the next release of the software. In this research, the IV&V facility found that it is possible to predict the average time it will take to close an open issue since it is significantly influenced by criticality, severity of the issue, phase in the life cycle when it was uncovered, and similar project-dependent characteristics. This analysis process, when applied to an ongoing project, can help management determine the health of the project and enables more accurate estimates of both the time and effort needed for completion.

Point of Contact: S. Yassini/J. Callahan
(304) 367-8367/8235
siamak.yassini@ivv.nasa.gov

Advanced Life-Support Research and Technology Development

Mark Kliss

The research and development of advanced life-support technologies at Ames Research Center (ARC) will help enable long-duration missions and the human exploration and development of space. The major objectives of advanced life support research are to: (1) reduce life support system life-cycle costs, (2) improve operational performance, (3) promote self-sufficiency, and (4) minimize expenditure of resources during long-duration human missions. The main focus of the research at Ames in FY98 was on waste processing and resource recovery, modeling and analysis, and In Situ Resource Utilization (ISRU).

Waste-processing systems that eliminate noxious wastes are a necessary component of any fully regenerative life-support system that incorporates food production. Waste processing can be accomplished by either biological/chemical or physical/chemical systems. The optimum method of processing is dependent on the ability of food production systems and humans to reutilize the reclaimed materials. A thorough understanding of the impurities in the reclaimed materials and the effect of these impurities on plants and humans is required in the development of waste-processing systems. In FY98, the research effort focused on integrating a prototype incinerator, developed by ARC in FY97, with a catalytic test stand in order to evaluate newly developed catalyst systems. Of primary interest was the use of an advanced catalyst to remove nitrogen dioxide and nitric oxide from the incinerator flue gas by reducing them with carbon monoxide to form nitrogen and oxygen. This approach is extremely promising because it requires no additional chemicals, such as ammonia, for the reduction process. Using carbon monoxide at concentrations of several thousand parts per million, it was demonstrated that nitrogen oxides can be reduced in incinerator flue gas from concentrations of 50 parts per million to less than 1 part per million.

For the modeling and analysis research effort at Ames, data from existing literature, universities, and other NASA Centers was utilized to develop individual crop models for the candidate crops that might be incorporated into the 'BIO-Plex' human-rated advanced life-support test chamber at Johnson Space Center. The models accounted for carbon dioxide uptake, oxygen production, edible and inedible biomass production, water vapor production, and water uptake from the nutrient solution as functions of the carbon dioxide concentration, light level, and crop growth area. The models were then used to evaluate system management and operations issues and to conduct system trade studies. It was shown in a comparison of separate (multiple) and single air loop configurations that, as long as food production rates are greater than 50% of crew requirements, the existing air revitalization system can be eliminated and a single loop air revitalization system linking the crew chambers, food production chambers, and waste-processing systems can adequately control the carbon dioxide level by varying the solid waste-processing rate.

Scientific analyses of soil and rock samples on Mars will require the use of carrier gases such as nitrogen and argon for moving analytes and purging instrumentation. The FY98 ISRU research efforts at Ames relating to the "mining of Mars atmosphere" culminated in the development of demonstration hardware capable of separating and purifying a nitrogen/argon carrier gas mixture from the Martian atmosphere and compressing the mixture to a usable pressure. Both the separation and compression processes were performed via adsorption. In addition to being low mass, low volume, and virtually solid state, the process consumes virtually no electrical power since the energy to perform work is taken entirely from the Mars diurnal temperature cycle. The figure shows a concept drawing of such a device.

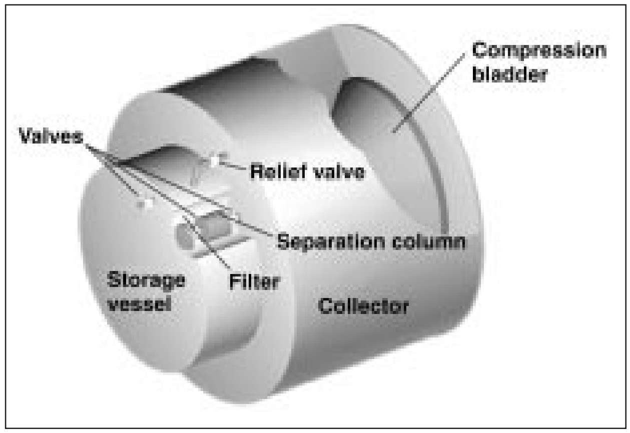

Fig. 1. A concept drawing of In Situ Resource Utilization (ISRU) hardware, which can extract and compress carrier gases from the Martian atmosphere.

It weighs less that 100 grams, occupies a volume approximately equal to a 12-ounce soda can, and produces enough carrier gas for several analyses a week for an indefinite period of time. This technology is applicable to all lander and rover missions to Mars and has other possible uses within NASA, by providing compressed carbon dioxide for generating buffer gases for life support, as well as in the private sector, by producing purified compressed gases in remote locations or in applications having stringent restrictions on power, noise, or vibration.

Point of Contact: M. Kliss
(650) 604-6246
mkliss@mail.arc.nasa.gov

Technology Transfer

Telemedicine Demonstration: Remote Monitoring and Training of Autonomic Responses

Patricia S. Cowings, William B. Toscano, Bruce Taylor

A NASA training system, originally developed to help astronauts adapt to space travel, is now providing an alternative opportunity to help people control their physiological responses to a variety of environmental conditions. This report documents a recent feasibility test that used telemedicine technology to enable remote monitoring and training of human physiological responses. In this test, video, audio, and data telecommunications were provided by a wide-area network connection over a distance of 2000 miles.

Developed at Ames Research Center, the Autogenic Feedback Training Exercise (AFTE) system enables individuals to recognize and learn to compensate for unusual environments. A U.S. Army and Coast Guard study showed that pilots, for example, can train to reduce the risk of human error accidents by recognizing adverse physiological reactions associated with emergency flying conditions. AFTE was designed to facilitate adaptation to space; improve comfort, safety, and performance during a mission; and facilitate readaptation to Earth. The AFTE system consists of three parts: an AFTE, an Autogenic Feedback System-2 (AFS-2), and an Autogenic Clinical/Laboratory System (ACLS).

In the prototype test, researchers at Ames Research Center (ARC) worked remotely with a patient at NASA Lewis Research Center (LeRC) in Cleveland, Ohio. Images and data were transmitted from the patient at LeRC to the trainers at ARC over the NASA Research and Education Network (NREN). Figure 1 is a diagram of the system configurations at both the local and remote locations. In this demonstration, the patient and trainer each had an additional monitor that provided video and audio telecommunication. The ACLS collected and displayed the remote subject's physiological data in real time; the PictureTel' computer system provided the video and audio between the patient and trainer; and Timbuktu' software transmitted the physiological information. Although the NREN ATM backbone operates at OC-3 (155 megabits per second (mbps)),

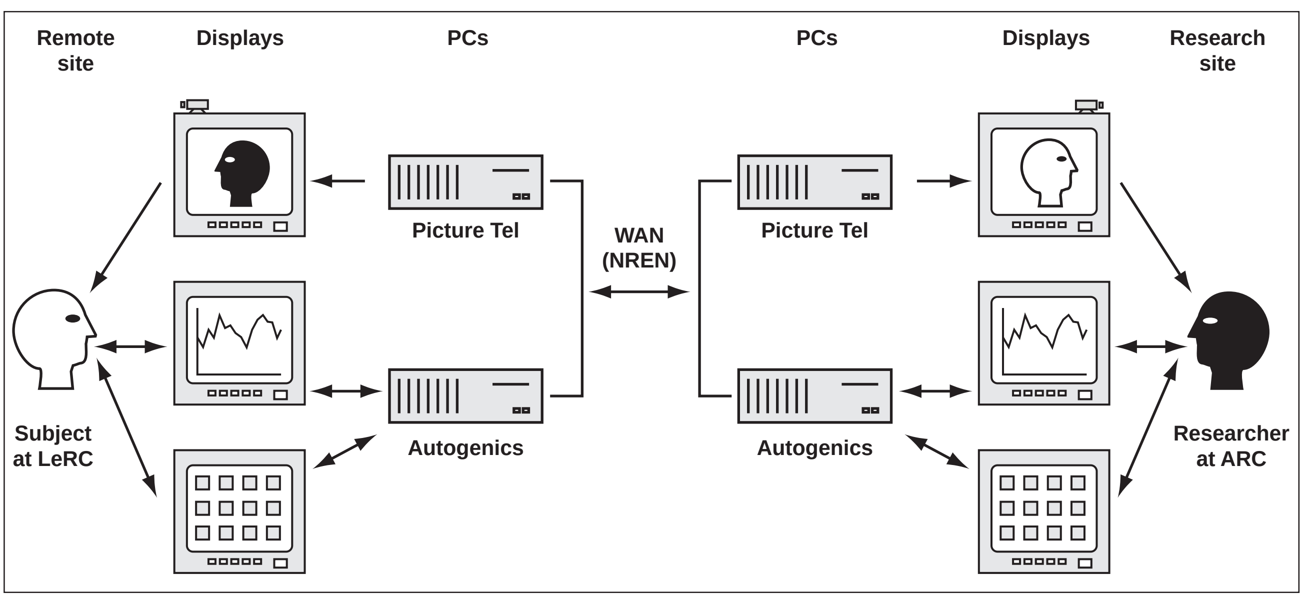

Fig. 1. System configuration at the local and remote sites during demonstration test of AFTE.

T1 (1.544 mbps) seems to be adequate for both ACLS and the PictureTel system. Dedicated Ethernet (10 mbps) network segment connections were used at both NASA centers to ensure accurate test measurements without other contending network traffic.

The primary network challenge in the AFTE application is Quality of Service (QoS). QoS constraints include the guarantee of adequate bandwidth (~1.5 mbps) and stringent delay and synchronization requirements for voice and images. Also, since confidentiality of data between researcher and subject (physician and patient) must be maintained, some form of security (for example, a firewall) will always be needed to protect the data on the Internet.

During the five-hour test, all components of the system—network elements, ACLS, and PictureTel systems—worked without problems. The average network round-trip time between ARC and LeRC, as measured by Ping Software, was less than 65 milliseconds over NREN. To determine the relationship between video quality and transmission rates, the experiment was conducted at both 174 and 384 kilobits per second (kbps) for the PictureTel portion. QoS aspects were not an issue for this demonstration because available bandwidth was greater than required, and the network was dedicated to the application. In the real world, with applications contending for limited network resources, QoS guarantees will be important to the success of the application. This demonstration shows the feasibility of providing this training to anyone having access to the Internet. More information on the test results can be found at the NREN Web site (http://www.nren.nasa.gov/auto.html).

Point of Contact: P. Cowings
(650) 604-5724
pcowings@mail.arc.nasa.gov

NASA Technology Evaluates Performance of Soldiers in Tactical Vehicles

Patricia S. Cowings, William B. Toscano, Charles DeRoshia

The purpose of this project is to use NASA technology to assist the U.S. Army in the assessment of motion sickness and performance within the command and control vehicle (C2V). The C2V is a tactical vehicle that contains four workstations where military personnel are expected to perform command decisions during combat conditions on the move. The present study also demonstrates this technology for evaluating environmental impact on individuals serving as either passengers or crew on land, sea, air, and space vehicles. The specific objectives were: (1) to determine the incidence of motion sickness in the C2V; and, (2) to determine the impact of these conditions on performance, physiology, and mood.

The subjects were 24 active duty military personnel (16 men and 8 women), aged 18–34 years. Tests of cognitive and motor skills, symptom diagnostic scales, and mood/sleep scales were administered on the computers at each soldier's workstation on the vehicles. Physiological responses were recorded using an ambulatory monitoring system developed at Ames Research Center to measure environmental impact on crewmembers during spaceflight.

Each soldier participated in two days of training in the classroom prior to operational field tests in the C2V. Training consisted of eight trials on each of the performance tasks, the diagnostic, and mood/sleep scales. There were three vehicle configurations: *oblique*—four seats were positioned at a 20-degree diagonal to the direction of travel; *perpendicular*—four seats were positioned 90 degrees from the direction of travel; and *forward*—four seats were arranged in two rows, with all seats facing the direction of travel.

Each subject participated in 12 four-hour field tests on alternate days. All subjects rode in each seat (4) of each vehicle (3) over the duration of the study. The assignment of subjects to vehicles and seats was counterbalanced. During each field test, soldiers

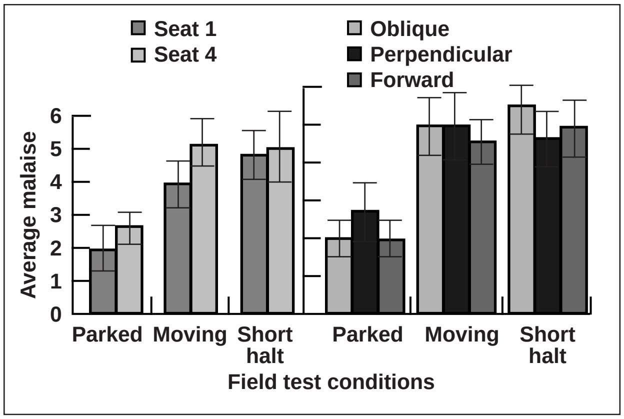

Fig. 1. Motion-sickness malaise of soldiers during C2V field operations.

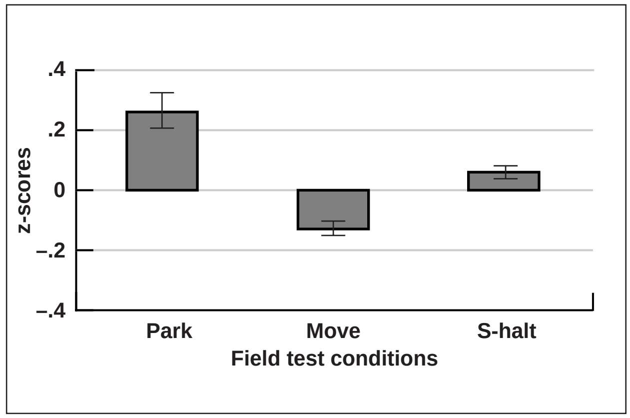

Fig. 2. Composite performance of soldiers during C2V field operations.

performed six trials of performance, mood, and symptom tasks, which were administered during parked, moving, and short-halt conditions. Because of the limited number of ambulatory monitoring systems, physiological data were collected only on subjects seated in seats 1 and 3 of each vehicle. At the end of all field tests, each subject participated in one additional post-test performance battery conducted in the classroom.

Of all 24 soldiers, 62% reported motion-sickness symptoms ranging from mild to severe malaise. Figure 1 shows that there were no significant differences in malaise between vehicles and seats. There was, however, a significant increase in malaise levels when the vehicles proceeded from parked to move ($p < 0.001$), and from parked to short halt ($p < 0.001$). There was no significant difference between moving and short halt. Composite performance (mean of seven subtests) results are summarized in figure 2. Performance showed a significant decrement when conditions changed from parked to move ($p < 0.001$) and from parked to short halt. A trend for performance recovery from move to short halt ($p < 0.05$) was observed for four of the seven performance tests.

The methodology of converging indicators based on physiology, performance, symptom, and mood measurements was successful for evaluating the impact of C2V field tests on the operational efficiency of soldiers. There was no effect of vehicle configuration or seat position on motion-sickness susceptibility. However, when field conditions changed from parked to move, there was both a significant increase in symptoms and a corresponding decrease in performance, with some recovery occurring during short halt. Physiological data may further elucidate individual differences in motion-sickness tolerance and performance. Training in control of physiology may mitigate these problems.

Point of Contact: P. Cowings
(650) 604-5724
pcowings@mail.arc.nasa.gov

Pill-Shaped Implantable Biotelemeters

John W. Hines, Robert Ricks, Carsten Mundt, Mike Skidmore

Ames Research Center (ARC) is developing pill-shaped biotelemeters for measuring physiological parameters during life sciences experiments aboard the International Space Station (ISS) Gravitational Biology Facility. Eventually, this family of devices could be used to monitor animal health parameters and the performance of self-contained biological systems. The technology can also be readily adapted to monitor the health of astronauts in the Human Research Facility. There are numerous potential applications for non-NASA users as well.

The first pill transmitter, shown in figure 1, was developed in association with the University of California at San Francisco (UCSF) Fetal Treatment Center (FTC), and is capable of measuring intrauterine pressure and temperature for up to 10 months. FTC surgeons, under the direction of Michael Harrison, pioneered the use of in utero surgical intervention to correct life-threatening fetal defects. The FTC team recently switched from a hysterotomy surgical approach to a less intrusive endoscopic technique in an effort to reduce postsurgical complications. This change means commercially available, larger telemetry devices could no longer be used to monitor postsurgical status. The Pressure/Temperature Pill (9 millimeters diameter x 35 millimeters long) is designed to pass through a 10-millimeter endoscopic tube into the womb, as depicted in figure 2, where the transmitter monitors body temperature and pressure over the course of gestation. Monitoring these parameters will help UCSF physicians to detect preterm labor, a serious problem after fetal surgery. The small size of the pill transmitter was achieved through innovative design, and by utilizing a novel "flip-chip" assembly process. In a "flip-chip" assembly, single unpackaged dies are bonded directly to a printed circuit board.

ARC has also developed a unique two-channel biotelemetry receiver/demodulator and data acquisition software, to display and record the measured physiological parameters. The radio-frequency (RF) portion of the receiver consists of a commercially

Fig. 1. Implantable pressure/temperature "pill."

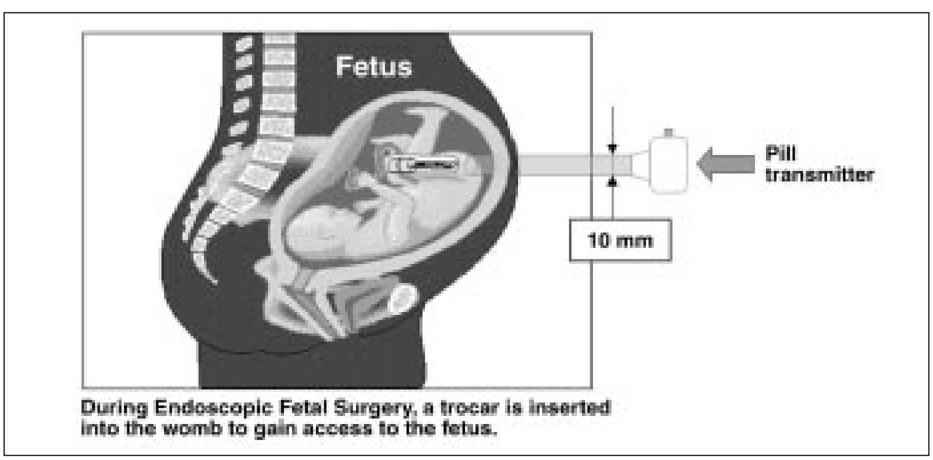

Fig. 2. Biotelemetry insertion.

available Konigsberg Instruments module that has been modified to demodulate the low-frequency pulse interval modulated signals of the pill transmitter.

NASA is interested in this technology for long-duration monitoring of research subjects in spaceflight. Astronauts and the life sciences experiments they oversee are like a fetus, in a remote and inaccessible environment. Their health and performance must be monitored as unobtrusively as possible so as not to interfere with ISS operations or with onboard experimental results. The pill-sized biotelemetry system has direct application to plant and animal experiments where the device can be inserted or implanted to obtain optimum information in situ. The same biotelemetry electronics, configured in a Band-Aid® arrangement with lightweight, flat polymer batteries, could be used for noninvasive monitoring of astronaut health.

The pressure/temperature pill transmitter is the first of a family of implantable and/or ingestible pill transmitters that will measure a variety of physiological parameters. Future measurements will include pH, ions of interest (for example, Ca++, Na, K), heart rate, ECG, EEG, EMG, blood gases (O_2, CO_2), and glucose. In fact, testing has begun on a prototype pH pill transmitter, similar in design to the pressure/temperature device.

Future commercial applications of these new pill transmitters go far beyond fetal surgery. Pill transmitters small enough to be swallowed are currently in development. Patients with digestive disorders could swallow a pill transmitter that monitors intestinal acidity and pressure, and gives data about contractions of intestinal smooth muscle, allowing doctors to better diagnose gastrointestinal diseases. There is also great potential in sports medicine. Pill transmitters can monitor the performance of athletes as they train. In addition, the military has expressed interest in similar devices to monitor the health and performance of soldiers in hostile environments.

Point of Contact: M. Skidmore
(650) 604-6069
mskidmore@mail.arc.nasa.gov
http://s2k.arc.nasa.gov/

Biological ION Analysis in the Cell Culture Module (BIONA-C)

John W. Hines, Christopher Somps, Charlie Friedericks, Robert Ricks

Ames Research Center (ARC) has developed an online monitoring system to perform accurate, real-time measurements of pH, carbon dioxide (CO_2), and temperature in a cell culture device. The system is currently scheduled to fly onboard space transport system (STS)-93 in the Walter Reed Army Institute of Research (WRAIR) Cell Culture Module (CCM), and will occupy one of the four “rail” positions within the CCM. A fully configured “rail” is shown in figure 1. The CCM is designed for experiments located in the Space Shuttle mid-deck locker. The purpose of the flight is to conduct a technology demonstration of the ability to accurately measure the biological activity of a cell culture while actively controlling nutrient additions and other environmental parameters to ensure optimum in-flight performance.

The BIONA-C system consists of a custom-designed fluid path sensor manifold board, data acquisition and storage module, and programmable control electronics to operate the pumps and valves of the fluidics system, as shown in figure 2. The sensor manifold board houses the ARC-developed ion-selective sensors (pH, CO_2), temperature sensor, and onboard signal conditioning electronics. In order to better examine the in-flight performance of the sensors and electronics that comprise the BIONA-C hardware, four unique fluid paths were integrated into the available space. This configuration makes it possible to test the sensors in an online configuration (sensors continuously in the cell-nutrient fluid loop), and in an offline configuration (sensors intermittently exposed to cell-nutrient loop with intervening exposure to a calibration solution). The system, when integrated into a “rail” in the CCM, is designed to be highly autonomous. The user is able to configure the data sampling and collection, data storage, and the in-flight sequencing and operation of the fluid path

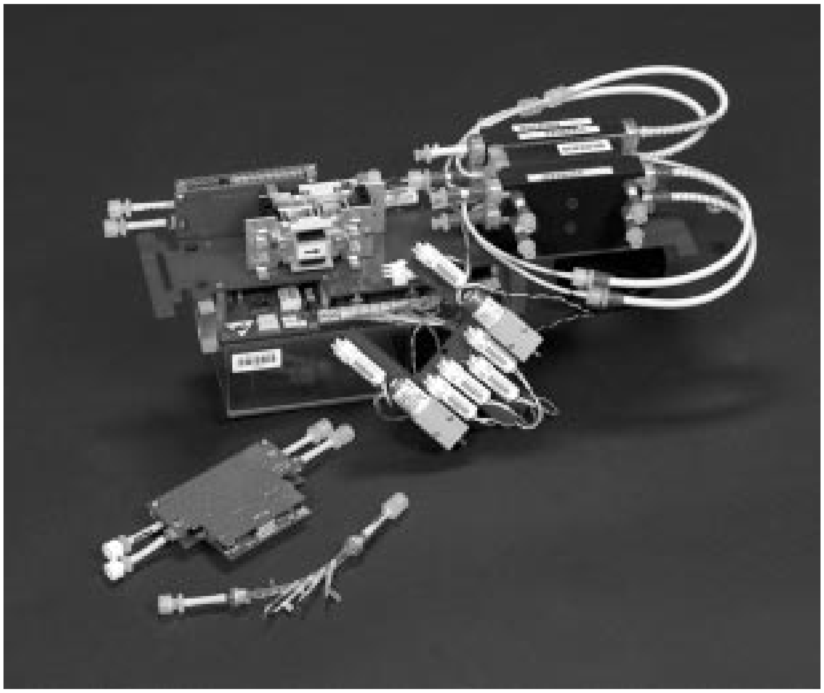

Fig. 1. BIONA-C assembly.

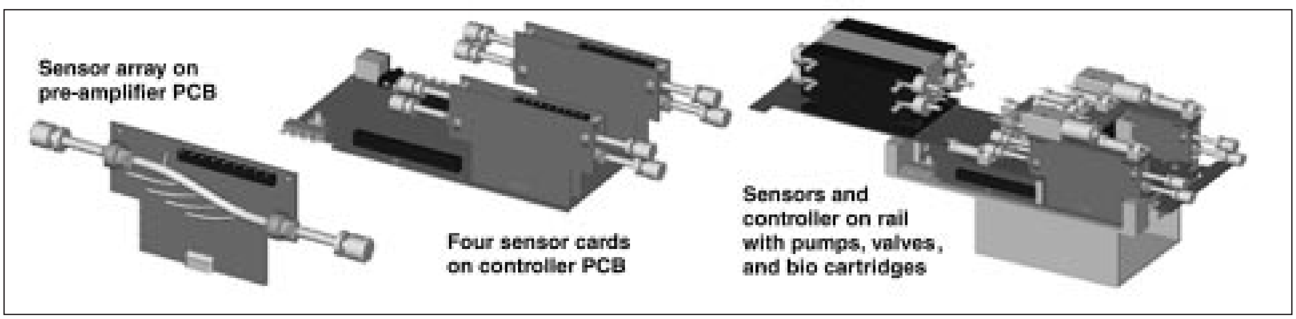

Fig. 2. BIONA-C components.

components (pumps, valves, etc.). Thus the BIONA-C requires only power and ambient environmental conditioning from the CCM host unit.

The BIONA-C is a further development of earlier ARC work on the BIONA 1, a modular array of blood calcium and temperature sensors that was developed in association with researchers at the Cedars-Sinai Medical Center in Los Angeles, in an effort to monitor the function of an experimental Bioartificial Liver.

Point of Contact: M. Skidmore
(650) 604-6069
mskidmore@mail.arc.nasa.gov
k.arc.nasa.gov/ http://s2k.arc.nasa.gov/

Physiologic Signal Conditioner-2

John W. Hines, Charlie Friedericks, Robert Ricks

The Ames Research Center (ARC) Physiological Signal Conditioner, Version 2 (PSC-2) is the proposed next-generation replacement for the existing PSC in use by the International Space Station (ISS) Human Research Facility. This new unit is designed as an easily reconfigured, modular, lightweight, programmable, low-power instrument for monitoring a variety of physiological signals. The new design concept, as shown in figure 1, includes a universal programmable core module, parameter-specific input modules, data interface output modules, and a field replaceable/rechargeable battery pack.

Features and advantages of the modular design for the PSC-2 include:

- Core module—Features mounting points for easily replaceable input modules, output modules, and battery packs. The core module houses instrumentation-grade amplifiers with programmable gain, offset, and filtering to ensure optimum signal quality. Data can be digitized in the input module or in the core module, and both analog and digital data can be presented to the output module for further processing, transmission, or storage. A memory buffer will minimize data loss during reconfiguration operations.
- Parameter-specific input modules—Mimicking the open-architecture approach used in personal computers, input modules are developed to support unique measurement parameters, and they can be inserted interchangeably into any of the PSC-2 input slots. Measurements now envisioned include: biopotential (electrocardiogram, electromyogram, electroencephalogram), biophysical (force, strain, respiration, pressure, flow), biochemical (ions, blood gasses, hormones), and environmental (temperature, pressure, radiation).
- Data output modules—Customized output modules enable data transmission to external devices via hardwire connection, radio-frequency (RF) link, infrared, or other communication modalities. They also could contain recording devices to store data locally for later transfer. The output module will also provide local control and display when these capabilities are required.

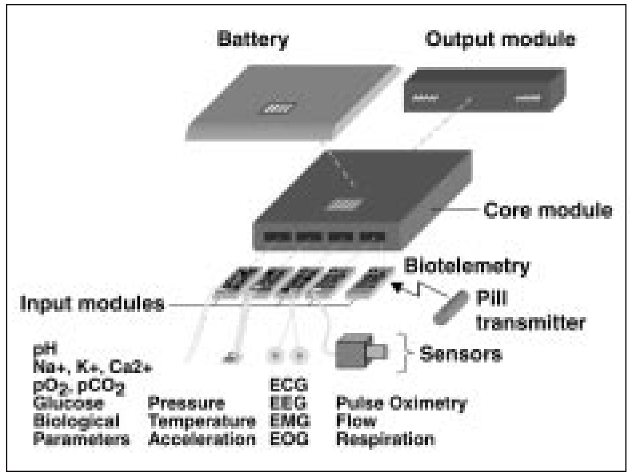

Fig. 1. PSC-2 modular components.

- Replaceable/rechargeable battery pack—Battery packs of different sizes and power densities will meet a variety of experimental and operational needs.

The need for the PSC is based upon the requirement of the Human Research Facility to monitor vital signs and other physiological parameters of ISS crewmembers, and to conduct research into the causes and effects of physiologic changes that occur during spaceflight. This same technology also has direct application in monitoring the health and performance of emergency first responders and military personnel who may be in remote or inaccessible situations. Also, ARC is working with a medical communication company to explore the use of this technology in home health care where traditional monitoring in a medical facility is either not feasible or is unavailable.

Point of Contact: M. Skidmore
(650) 604-6069
mskidmore@mail.arc.nasa.gov
http://s2k.arc.nasa.gov/

Earth Science Enterprise

Overview

The mission of NASA's Office of Earth Science (OES) is to study the total Earth environment—the atmosphere, ice, oceans, land, biota, and their interactions—in an effort to better understand the near-term changes in the global environment, whether the result of naturally occurring processes or induced by human activities, and to lay the foundation for long-term environmental and climatic monitoring and prediction. Numerous research and technology efforts were accomplished during FY98, the results of which address the following goals of the OES Enterprise:

- To expand scientific knowledge of Earth's environmental system
- To enable the productive use of OES science and technology
- To disseminate information about the Earth system

Ames Research Center supports the OES Enterprise by conducting research and by developing technology, with the objective of expanding the knowledge of Earth's atmosphere and ecosystems. OES work related to this objective also supports one of the goals of the Agency's astrobiology research and technology efforts, for which Ames is the lead Center. A complementary objective is to apply the knowledge gained to practical, everyday problems and to transfer the technology and knowledge to users outside NASA.

Key components of the Earth Science Division's research programs include the study of the physical and chemical processes of biogeochemical cycling; ecosystem dynamics of terrestrial and aquatic ecosystems; the chemical and transport processes that determine atmospheric composition, dynamics, and climate; and the physical processes that determine the behaviors of Earth's atmosphere and of those of the other solar system bodies.

Earth scientists at Ames engage in research related to all four of the NASA strategic enterprises:

RC-30 metric camera photo of Tongass National Forest, Alaska.

- The Earth Science Enterprise—*Terrestrial ecology and atmospheric assessments, airborne instrument development, application, and astrobiology*

- The Aero-Space Technology Enterprise—*Environmental assessments of aircraft operation, remotely piloted aircraft (RPA) sensor development, and science demonstration*

- The Human Exploration and Development of Space Enterprise—*Application of technology to issues of human health*

- The Space Science Enterprise—*Study of planetary atmospheres*

Throughout FY98, scientists and technical personnel continued to design, develop, and conduct remote-sensing and in situ experimental measurements. In addition, they performed computer simulations of atmospheric and ecosystems processes using both airborne and satellite sensor data in efforts to understand exchanges between the biosphere and the atmosphere. The scientists conceive and develop advanced instrumentation that is necessary to meet the measurement requirements of all supported enterprises, with emphasis on both airborne and selected spacecraft sensors. Project managers and project scientists provide science mission management and science leadership for major NASA science programs and for other agency science programs. Staff scientists conceive and develop applications programs, utilizing both proven and developing technology. Additionally, they transfer developed scientific knowledge and technology to commercial, academic, and governmental entities, both nationally and internationally.

The research is particularly concerned with atmospheric and ecosystem science and with biosphere/atmosphere interaction. Research foci include environmental concerns related to stratospheric ozone depletion, perturbations in the chemical composition of the atmosphere, and climatic changes resulting from clouds, aerosols, and greenhouse gases. Numerous state-of-the-art instruments are flown, and significant data are collected for stratospheric and tropospheric research.

The Airborne Sensor Facility (ASF) provides remote-sensing support for Office of Earth Science investigations, and for calibration and validation studies for the Earth Observing System (EOS). The facility is tasked with maintaining and operating a suite of OES facility sensors that are made available to the science community at large through the NASA flight request process. The systems are flown on various NASA, U.S. Department of Energy, and other aircraft, as required.

The ASF has component laboratories for data processing, flight operations, sensor calibration, systems development, and data telemetry. Current activities are centered on the moderate-resolution imaging spectrometer (MODIS) and the Advanced Spaceborne Thermal Emission and Reflection Radiometer (ASTER) airborne simulators (the MODIS Airborne Simulator, MAS, and the MODIS ASTER instrument, MASTER). These simulators are being used to characterize calibration sites and to develop algorithms for the new EOS AM-1 satellite systems. These data are processed into a calibrated Level-1B product at the ASF, and delivered to the instrument science teams via the EOS Distributed Active Archive Centers (DAACs).

OES's FY98 activities and accomplishments are summarized in the presentations that follow.

THERMO-PHYSICS FACILITIES

The Airborne Sensor Facility

Jeff Myers, Bruce Coffland, Ted Hildum, Mike Fitzgerald, Rose Dominguez, Dan Wolf

The Airborne Sensor Facility (ASF), based at Ames Research Center, provides remote-sensing support for NASA through the Office of Earth Science (OES) investigations, as well as support for calibration and validation studies for the future Earth Observing System (EOS). It is tasked with operating a suite of facility sensors that are made available to the NASA research community through the flight request process. The sensors, made available to other government agencies on a cost-reimbursable basis, are flown on a variety of NASA, U.S. Department of Energy (DOE), and other aircraft.

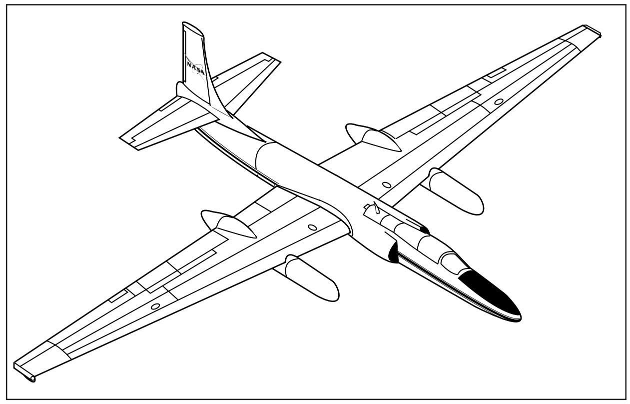

Fig. 1. Line drawing of ER-2 aircraft.

The ASF consists of five laboratories, which cover a range of functions, from initial data collection and processing, through delivery of a final calibrated product.

The Sensor-Operations Laboratory maintains and operates the facility sensors for the OES, supporting data-collection missions worldwide on a variety of aircraft platforms.

In FY98, missions totaling 487 flight hours on ER-2 (fig. 1), B200, and Cessna Citation aircraft were flown for various OES investigations, at sites ranging from Alaska to Puerto Rico. The primary focus in FY98 revolved around preparations for the upcoming EOS AM-1 satellite launch, using the moderate resolution imaging spectrometer (MODIS) Airborne Simulator (MAS). This preparation included characterization of calibration sites for the MODIS and Advanced Spaceborne Thermal Emission and Reflection Radiometer (ASTER) orbital instruments, and acquisition of scenes for EOS algorithm validation. The MAS and multispectral atmospheric mapping system (MAMS) instruments participated in three major field campaigns (First International Satellite Cloud Climatology Project Regional Experiment (FIRE), Texas Florida Underpass (TEFLUN), and Convective and Atmospheric Moisture Experiment (CAMEX-3) for severe storms studies, MODIS algorithm development, and Tropical Rainfall Measuring Mission (TRMM) satellite validation. During CAMEX, unique imagery was collected with the MAMS while documenting the evolution of four successive hurricanes as they approached the East Coast of the United States. Other missions included under-flights of the new National Oceanic and Atmospheric Administration (NOAA)-15 satellite, day/night thermal studies with MAS, and 123 hours of aerial photography in support of the Jet Propulsion Laboratory (JPL) Advanced Visible and Infrared Imaging Spectrometer (AVIRIS) project. The Tongass National Forest in Alaska was mapped with reimbursable flights for the U.S. Forest Service (fig. 2), as was Camp Pendleton in California for the U.S. Marine Corps.

The Data-Processing Laboratory reduces and calibrates the digital imagery data, distributes aerial photo products, and provides mission documentation. It also maintains a complete historical archive of the ASF data, keyed to a geographic database, which is also mirrored at several NASA Distributed Active Archive Centers (DAACs).

Fig. 2. RC-30 metric camera photo of Tongass National Forest, Alaska.

In FY98, a new data-processing system that generates Level-1B (calibrated and geolocated) MAS data in hierarchical data format (HDF) became operational. These data are now sent to the NASA Goddard and Langley DAACs for public distribution. This new system also produces browse imagery for each mission, which is then posted on the ASF Web page and hyperlinked to the NASA DAAC ordering system. Data from the new MODIS ASTER (MASTER) instrument was also integrated into this system in FY98, and is available at the Earth Resource Observation System (EROS) Data Center DAAC.

The Systems-Development Laboratory is tasked with providing new airborne sensor hardware and data systems to support OES investigations. It will either integrate and repackage commercial subsystems, or perform in-house fabrication as necessary. The lab specializes in low-noise infrared (IR) imaging and custom data-handling systems. The staff includes electrical, optomechanical, and software engineers.

The highlight in FY98 was the completion of the new MASTER airborne simulator instrument. Combining components from several outside vendors with in-house custom hardware and software, this instrument successfully completed a series of test flights. It will see extensive use by the U.S. ASTER science team in FY99, flying on both the DOE B-200 (fig. 3) and NASA ER-2 aircraft. In other work, development continued on an automated Geo-Correction System (GCS), funded by a NASA research announcement (NRA), in conjunction with the DOE. This development involves integrating a platform gyro and Differential Global Positioning System (DGPS) into a scanner data system, to enable precision pixel location within an image. Other projects include a high-resolution digital color camera, and a multipurpose 16-bit digitizer for use on 12-channel Daedalus-type scanners.

The Calibration Laboratory provides spectral and radiometric characterization for various remote-sensing devices. It maintains a set of integrating spheres and laboratory standards traceable to the National Institute for Standards and Technology

Fig. 3. Photo of Beechcraft King Air B-200 aircraft.

(NIST), as well as both conventional monochromators and a Fourier-transform interferometer. Other assets include a large environmental chamber that is used to monitor instrument performance at low temperatures. This facility operates under the guidance of the EOS calibration scientist at the Goddard Space Flight Center (GSFC).

As part of a plan to become a secondary standards facility for the EOS community, the ASF calibration laboratory began to participate in critical reviews and round-robin intercomparisons in FY98, with the primary laboratories at GSFC, the University of Arizona, and NIST. After some suggested modifications, this plan should be completed in FY99. Part of this effort includes an automated data-collection and data-processing system. A field calibration capability was also introduced, to collect ground-truth reflectance data for the validation of airborne sensors.

The Data-Telemetry Laboratory operates both the Tracking and Data Relay Satellite System (TDRSS) satellite-based data-relay system (STARLink) and a line-of-site aircraft downlink for the transmission of real-time digital imagery.

The STARLink system was declared fully operational during the CAMEX-3 experiment in FY98, after it broadcast data from three ER-2 instruments simultaneously back to the Payload Operation Center at Ames. Operating flawlessly for 11 consecutive missions, images and science data were relayed from the aircraft, flying over the Atlantic Ocean, to scientists around the country via the Internet. Engineers were also able to relay commands back up to their instruments, in several cases recovering from in-flight failures. Among the many scenes captured was the dramatic landfall of Hurricane Bonnie in North Carolina, which was presented in real time on the STARLink Web page.

For further information, including sensor specifications, sample imagery, and online flight documentation, refer to the ASF Web page (http://asapdata.arc.nasa.gov).

Point of Contact: J. Myers
(650) 604-3598
jmyers@mail.arc.nasa.gov

A Modeling Approach to Global Land-Surface Monitoring with Low-Resolution Satellite Imagery

Christine A. Hlavka, Jennifer L. Dungan

The effects of changing land use/land cover on global climate due to emissions of greenhouse gases and energy exchange rates are being addressed by Federal programs such as NASA's Earth Science Enterprise and by international efforts such as the International Geosphere-Biosphere Program. The quantification of these effects depends on accurate estimates of the global extent of critical land-cover types such as fire scars (recently burned vegetation) in tropical savannas and ponds in Arctic tundra.

To address the requirement for accurate areal estimates, methods for producing regional-to-global maps with satellite imagery are being developed. The only practical way to produce maps over large regions of the globe is with data of coarse spatial resolution, such as advanced very-high-resolution radiometer weather satellite imagery at 1.1-kilometer resolution or European Remote Sensing satellite radar imagery at 240-meter resolution. The accuracy of areal estimates based on coarse-resolution imagery is in doubt, especially for highly fragmented cover types such as fire scars and ponds.

Land satellite (LANDSAT) multispectral scanner (MSS) maps of recent fires in the Brazilian tropical savanna and synthetic aperture radar of open water in Alaskan and Siberian tundra were used to assess the accuracy of areal estimates at various spatial resolutions, to assess the effects of resolution on the distribution of observed scar and pond sizes, and to test methods for improving estimates based on models of size distribution.

Simulated moderate resolution imaging spectroradiometer (MODIS) maps of recent fires were created from the LANDSAT MSS maps. Areal estimates based on the simulated MODIS differed from LANDSAT MSS estimates by as much as 50%. The MODIS estimates were close to LANDSAT MSS estimates if there was a small bias in processing toward commission, that is, if pixels with somewhat less than half of the target cover type were labeled as fire scar or pond.

Fire-scar and pond sizes and also simulated data were assessed with graphic and quantitative techniques. The observed distributions were apparently lognormal on imagery of moderate (~100 meter) spatial resolution, but the underlying distribution was probably Pareto (that is, a power distribution). Software for adjusting estimates based on lognormal and Pareto distribution models was developed.

An initial test of the model-based software for improving estimates indicated sensitivity to parameter selection; thus, further testing and development is needed before the method can be applied.

Gerry P. Livingston of the University of Vermont collaborated in this research.

Point of Contact: C. Hlavka
(650) 604-3328
chlavka@mail.arc.nasa.gov

Astrobiology—The Future of Life Module: Rapid Rates of Change

Hector D'Antoni

The modern vegetation of South America offers an array of progressively drier ecosystems as one moves south. Annual temperature drops from 27 to 8 degrees Celsius (°C), and annual precipitation drops from 6,000 to 200 millimeters as one goes from the rain forest around the Amazon River to the Patagonian steppe. The goal of this research is to build an "end-of-life" scenario with the stipulation that the progressively drier ecosystems of South America be viewed as analogs or metaphors of the stages of a dying biosphere. In contrast to the array of modern ecosystems that evolved to the present form since the last glacial period, global phenomena exist that alter such a slow process by introducing rapid changes. The El Niño Southern Oscillation (ENSO) phenomenon affects four regions of South America:

1. Venezuela, Guyana, and Brazil (north of the Amazon River) suffer pronounced droughts.
2. Southern Colombia, Ecuador, and coastal Peru suffer largely increased rainfall and higher temperatures.
3. High temperatures occur in eastern Brazil.
4. Southern Brazil, Uruguay, eastern Paraguay, and eastern Argentina experience increased precipitation.

These primary effects have multiple secondary consequences for ecosystems (floods and fires) and profoundly affect the human population. Both floods and fires are recorded in stratigraphy that can be used to trace previous ENSO events. This record, in turn, allows the investigation of the process of ecosystem recovery (or reconstruction, if damage crossed the ecosystem resilience threshold). The stratigraphical record shows evidence of plant succession and also of the emergence of new ecosystem properties and new taxa. Thus, South America has been selected for (a) case studies of biogeography and history of ecosystems aimed at building a metaphor of a drying biosphere; and (b) the effects of rapid environmental change on the emergent properties of the ecosystem that are recovering from rapid rates of change. The first tools to be used in this study are pollen analysis and radiocarbon dating of the period between the last glacial maximum and the present time and remote-sensing analysis of vegetation. Other research tools (biochemical analyses of sediment samples, geostatistics, hydrology, fluvial and marine biology, and modeling among others) will be used as this work progresses.

In FY98, advanced very-high-resolution radiometer remote-sensing data for South America were acquired. These data were analyzed to extract vegetation indices of the four South American regions subjected to direct El Niño effects.

Point of Contact: H. D'Antoni
(650) 604-5149
hdantoni@mail.arc.nasa.gov

Detecting the Terrestrial Carbon Sink

Christopher Potter, Steven Klooster, Vanessa Brooks

Global ecosystem modeling at Ames Research Center validates earlier NASA-funded research showing that the spring growing season became longer during the 1980s. Recent simulation results from the Ames Carnegie-Ames-Stanford Approach (CASA) model of the biosphere further indicate that, over this period, land plants in the Northern Hemisphere absorbed more carbon dioxide than previously believed—about one-third of the amount that results from the burning of fossil fuels in the United States and Canada. These findings are relevant within the context of the 1997 Kyoto Protocol, whereby industrial countries pledged to cut emissions of greenhouse gases below 1990 levels by early in the next decade to mitigate global warming.

Computer-simulation analysis with the CASA model combines a time series of satellite vegetation images collected from 1983 to 1988. Solar irradiance data from the Geostationary Operational Environmental Satellite (GOES) and visible and near-infrared data from National Oceanic and Atmospheric Administration (NOAA) weather satellites 7, 9, and 11 were used in the carbon modeling research. Together with surface-climate observations, the ratio of visible to near-infrared wavelengths provides valuable information about how much carbon dioxide is absorbed by land plants.

The CASA model processes satellite data to show increasing carbon-dioxide accumulation in vegetation in extensive areas of Canada, Europe, and Russia. Model results indicate which forest and tundra areas on Earth act as temporary "sinks" for atmospheric carbon dioxide in response to warmer-than-average spring temperatures and lower summer drought stress (fig. 1).

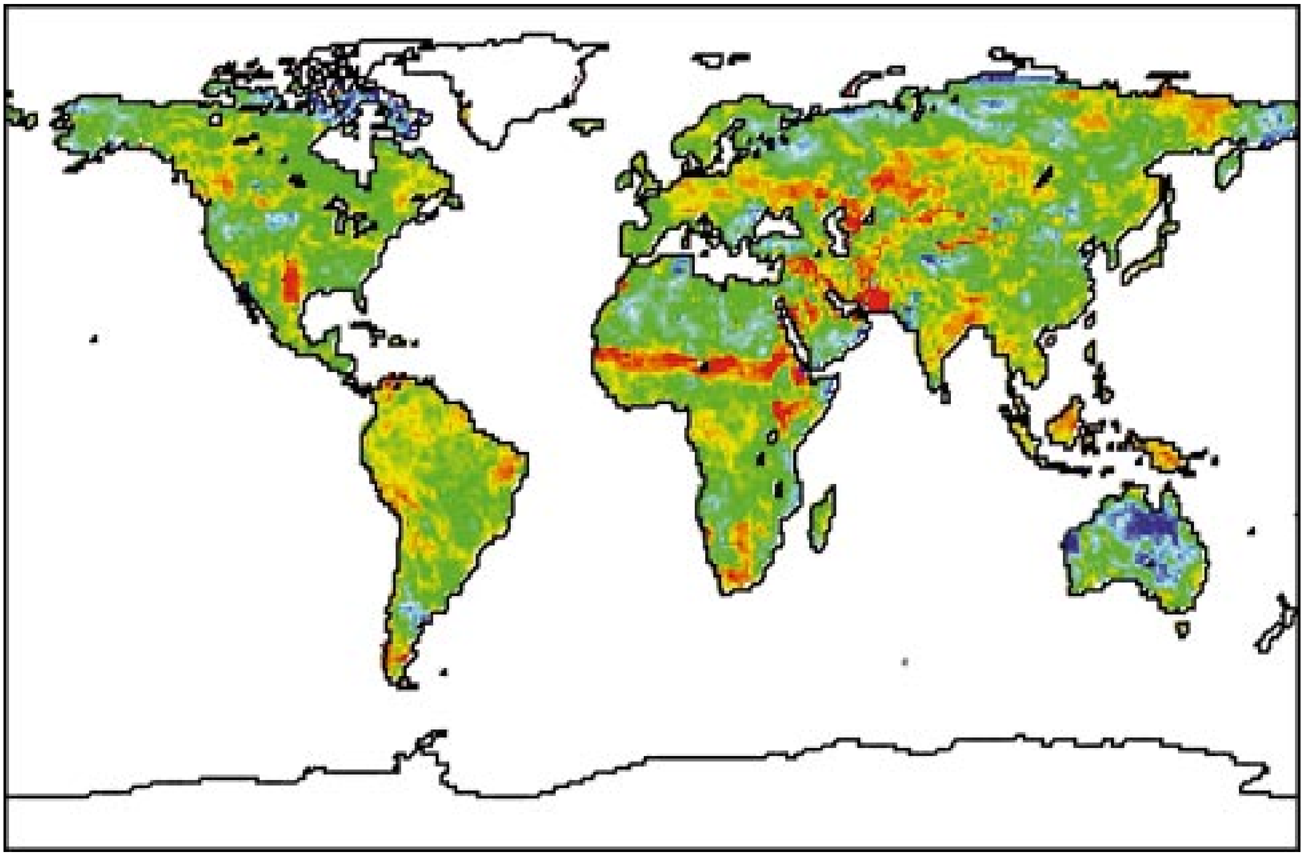

Fig. 1. This global map shows predicted changes in the terrestrial sink for atmospheric carbon dioxide during the 1980s using satellite data and climate records. Yellow and red in the Northern Hemisphere zones indicate potential areas of carbon-sink flux in response to warmer-than-average spring-time temperatures and lower summer drought stress. Accumulation rates for carbon appear to have doubled in some areas. Red in areas of the African continent and eastern Brazil show a recovery of land cover from the 1983 El Niño event and the severe drought of 1984. Land areas in white indicate no detectable changes in carbon accumulation rates.

In the tropical zones, CASA results reveal that the ecosystems of Africa and eastern Brazil have recovered strongly from the stressful effects of the 1983 El Niño and the severe 1984 drought. Satellite observations show little evidence that desertification has become permanent or irreversible in the sub-Saharan zones of Africa.

Point of Contact: C. Potter
(650) 604-6164
cpotter@mail.arc.nasa.gov

DNA Damage Repair in Nature?

Lynn J. Rothschild

DNA, the repository of genetic information, is subject to damage. The consequences of DNA damage range from small changes in base sequence, to cancer and death. Such damage, however, may be repaired by the cell. Several mechanisms of DNA damage repair have been characterized in the laboratory. Surprisingly, little is known about the mechanisms, timing, or extent of DNA damage repair in nature. Without this knowledge, it is not possible to know the role of DNA damage in exobiology, astrobiology, ecology, or, for that matter, medicine. A serendipitous discovery was made while studying microbial ecosystems in the field that may constitute the first measurement in nature of a kind of DNA damage repair called excision repair. The objective of this study is to determine if it is possible to measure DNA damage repair in nature and, secondarily, to develop a standard technique to measure excision repair in the field. The ultimate goal of this work is to develop a reliable method to measure excision repair in nature in order to apply it to questions of the role of ultraviolet (UV) radiation in astrobiology, exobiology, ecology, and physiology.

In FY98, equipment was purchased to measure UV radiation in the field, and to improve efficiency of DNA analyses in the lab. Two sets of measurements were made of phosphate uptake in Yellowstone National Park on *Cyanidium caldarium*. These measurements confirmed that increases in apparent DNA synthesis as measured by incorporation of ^{33}P-phosphate into DNA cannot be attributed strictly to increases in uptake of radioactive phosphate.

The growth rate of yeast was measured under ambient conditions in three radiation regimes using ultraviolet-blocking plastics. The three regimes were full solar UV, solar UV minus UV-B, and solar radiation minus both UV-B and UV-A. As in the case of photosynthetic organisms, UV has a measurable negative effect on growth rate in yeast.

In September 1998, specimens of *Cyanidium caldarium* were collected in the field every 1.5 hours for 24 hours. The samples were analyzed for total DNA per cell using flow-cytometry and possession of thymine dimers, a common form of DNA damage. The flow cytometry results showed two distinct populations of cells with chlorophyll in the pond, which were tentatively identified as *Cyanidium caldarium* and *Chlorella* sp. The dimer-analysis results suggested that a negligible number of thymine dimers occurred throughout the day; either they were repaired extremely quickly or the damage to the DNA occurred in some other form.

Point of Contact: L. Rothschild
(650) 604-6525
lrothschild@mail.arc.nasa.gov

Ecosystem Model Optimization and Parallel Processing

J. W. Skiles, Catherine H. Schulbach

This report documents a multidisciplinary research project involving Earth Science and Information Technology. The study area is the Great Plains (GP) of the United States, with grasslands made up of shortgrass prairie, mixed-grass prairie, and tallgrass (true) prairie. This area, which covers approximately 2.55×10^6 square kilometers (fig. 1), contributes major portions of the cereal grains consumed in the United States and in the world; provides forage from cultivation and range vegetation for livestock; provides watersheds for numerous river systems; and offers a variety of recreational activities. For these reasons and because the grassland types of the GP form a contiguous geographical area, the GP was chosen as the study area.

The study team employed a grassland simulation model that operates on a daily time step. The goal is to use this model to answer questions about the carbon and nitrogen budgets and vegetation dynamics of the GP. Parameter values are derived from published sources and from remote-sensing data.

Others have conducted similar examinations, but they used either monthly time steps, very large areas to represent each site, or both. The site size in this study is one advanced very-high-resolution radiometer pixel, or 1.1 square kilometer.

It is calculated that if the model is used to simulate five plant functional groups (warm-season grasses, cold-season forbs, etc.) at 60,000 sites on the GP for 100 years using a daily time step, it would take a Silicon Graphics, Inc. “Indy” 5000 workstation more than 766 hours, or over 31 days, to complete the exercise. Thus, the need to employ parallel processing to accomplish these simulations is apparent.

Two students from the California Polytechnic Institute, Allen Victor and Oliver Martin, worked on

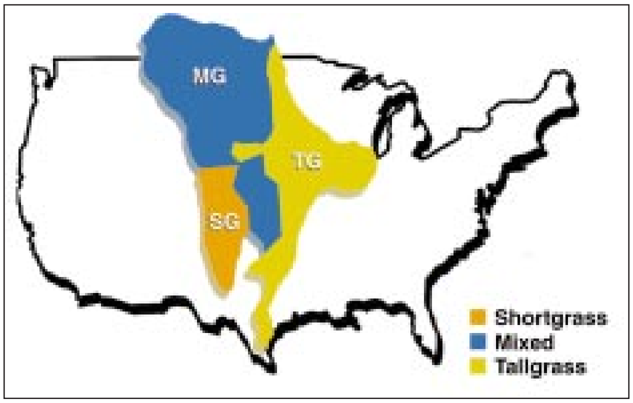

Fig. 1. Distribution of grasslands in the North American Great Plains.

this project. Hired under the Education Associates Program, the students worked on modifying the input/output interface and on developing computer code that controls simulation processing in a parallel-computing environment.

The model, called PlainMOD, employs parallel-processing techniques. The original code has been modified to run in parallel using the message passing interface (MPI) standard for communication. This tool enables the code to be run on a variety of computer systems that support MPI. The model is being run on Origin 2000 systems at the Ames Numerical Aerodynamic Simulation facility. Currently, a 128-central-processing-unit Origin 2000 is available, but a larger system may be available in FY99. PlainMOD will be able to scale to over 128 processors, to enable 100-year simulations of the GP to be performed in several hours, as opposed to a month or more. This scenario will be accomplished by dividing the area to be simulated into individual sites, with input data tailored to each site. Currently, the input data of a site consists of climate, plant, and hydrology data provided in the form of files. This input data may be specific to a site or shared among many sites. Because it is difficult to obtain data for each subdivision of the GP, interpolation methods for determining data values between sites are being investigated. Because complete climate data are not available at this fine granularity, initial simulations use nearest-neighbor and other methods to determine climate data for intermediate locations. Plant and hydrology input data are being handled in a similar manner. PlainMOD is not restricted to a particular area or site size. Areas smaller than the GP can be handled at whatever granularity is required.

Although this research focuses on Earth Science and the use of remote-sensing technology, because of the size of the simulations and the need for high-performance computing technology, this effort has ties with the high-performance community as well. In performing simulations with PlainMOD, information on scalability is being collected. For example, timing information for the simulations collected as the runs are performed on different numbers of processors is being compiled for later analysis. PlainMOD is also forming the basis for performance-optimization and load-balancing studies—improving performance and balancing work between processors as the number of processors varies.

Point of Contact: J. Skiles
(650) 604-3614
jskiles@mail.arc.nasa.gov

Effects of Increased Solar UV-B Radiation on Terrestrial Plants

Hector L. D'Antoni, J. W. Skiles

Alfalfa plants (*Medicago sativa* L.) have been grown under three levels of exposure to solar ultraviolet-B (UV-B) radiation. During the growing season of FY98, the experiment was carried out for the fourth consecutive year under a shed with three chambers. The first chamber provides a non-UV-B environment, the second chamber blocks about 15 percent of UV-B radiation, and the third chamber provides ambient conditions. This time, a modification was introduced by replacing mature plants with seeds grown in the shed under the three UV regimes. Results are presently being analyzed.

Significant progress was attained in analyzing the UV-B fluxes in the region for FY95, FY96, and FY97 (fig. 1). Results of the experiment in those years were

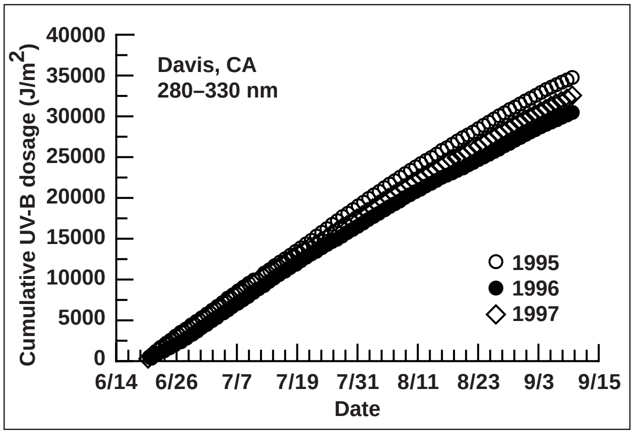

Fig. 1. Cumulative ultraviolet fluxes for FY95, FY96, and FY97 during the growing season. Curves are from an instrument maintained by the U.S. Department of Agriculture at the University of California, Davis.

different: in FY95, there were significant differences between the treatments; in FY96, the differences were minimal in the expected trends but statistically insignificant; in FY97, the largest differences were documented. The UV-B fluxes for those years are consistent with the effects on plants: the UV-B flux in FY95 was high, in FY96 it was lowest, and in FY97 it was the highest. These results suggest that alfalfa plants may be good indicators of UV-B fluxes in the field. The cumulative UV-B dosages in joules per square meter (J m^{-2}) from June 14 to September 14 were 32,500 J m^{-2} in FY95, 30,000 in FY96, and 35,000 in FY97.

The measurements of chlorophyll concentration in milligrams (mg) per liter (l) of elutent (fig. 2) were coincidental with these results. In FY95, concentration of chlorophyll under no UV-B environment decreased by 1 mg in five weeks, while it decreased by 5 mg in the same period under 15-percent UV-B reduction. In FY96, concentration of chlorophyll grew in both treatments by over 10 mg in five weeks. In FY97, chlorophyll concentration grew from 17.5 mg/l in week one to 19 mg/l in week six, under UV-B exclusion. Under 15-percent UV-B reduction, concentration decreased from 16.5 mg/l in week one to 16 mg in week six. Under ambient conditions, the concentration of chlorophyll decreased from 14.5 mg in week one to 13.5 in week six.

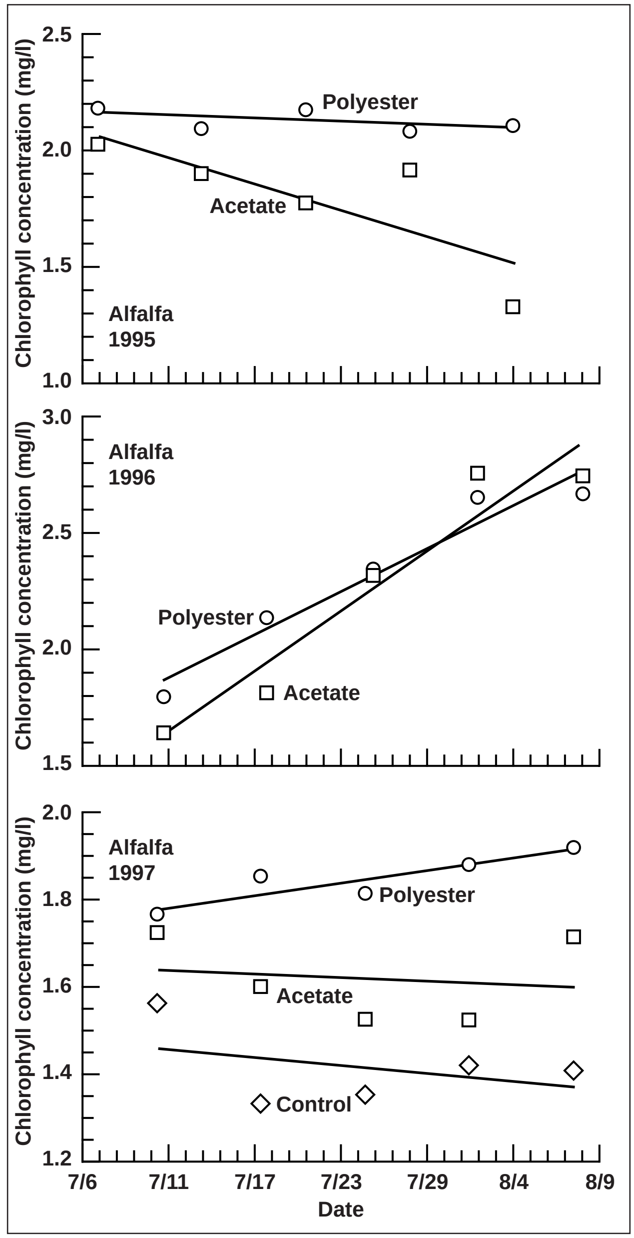

Fig. 2. Chlorophyll concentrations of leaves of alfalfa grown under polyester and acetate in FY95, FY96, and FY97. Note that although the slopes of the curves for FY96 are different from the curves for FY95 and FY97, there is no distinction between treatments in that year.

Preliminary analyses of flavonoid pigments from leaves of the FY97 experiment by high-performance liquid chromatography (HPLC) analysis suggest that plants use UV-B-absorbing pigments to prevent damage to leaf organs and molecules (fig. 3). Although no quantitative comparison should be made with the graphs, it is likely that most changes occur in the retention times of the pigments rutin (~7.8 minutes); myricetin (9–9.2 minutes); a peak in the 9.4–9.7-minute range; quercetrin (9.9–10.1 minutes); and a peak in the 10.6-minute range; other relevant peaks occur through the end of the run set at 25 minutes. These regions are being closely scrutinized so that future quantitative comparisons can be made using samples from the control (ambient) and the treatments, 15-percent UV reduction (acetate), and UV-B blocking (polyester).

These results suggest that a cumulative value of 32,500 J m^{-2} in the UV portion of the spectrum is sufficient to produce effects in terms of chlorophyll concentration, and that the larger the cumulative UV-B dosage, the larger the differences to be observed among treatments. They also suggest that above 32,500 J m^{-2}, there is a significant destruction of chlorophyll and probably other important biomolecules. Large differences in concentration and types of flavonoids appear to occur among the three

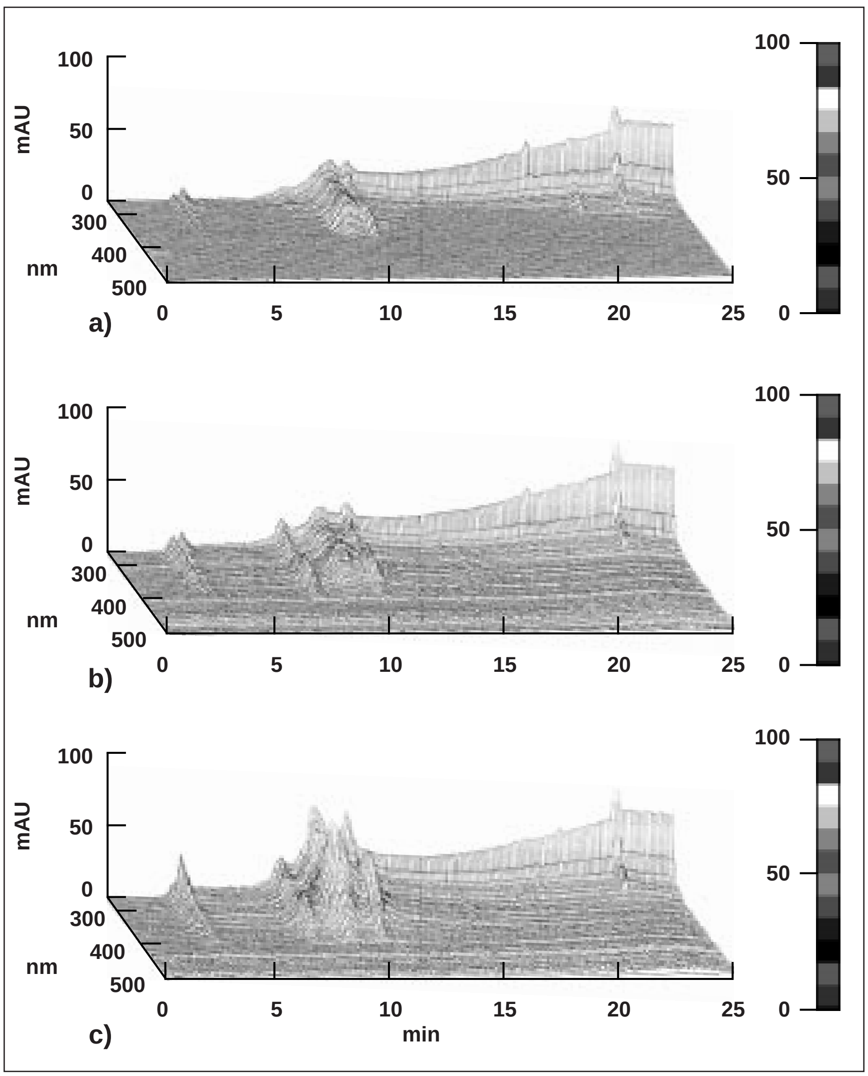

Fig. 3. Results of high performance liquid chromatography done on alfalfa leaf samples from 1997. Obvious differences can be seen in pigment concentrations between the UV shielded sample (polyester) (A), the 15% UV reduction treatment (acetate) (B), and the ambient control (C).

treatments, suggesting that 32,500 and 35,000 J m^{-2} of UV-B exceed alfalfa's tolerance to solar UV-B and that plants shield themselves under a layer of flavonoid pigments. Differences in growth, phenology, and lengths of life have also been observed among the treatments and are attributed, at least in part, to differential destruction of growth hormones.

This research was conducted in collaboration with Jeffery C. Seitz of California State University, Hayward.

Point of Contact: H. D'Antoni
(650) 604-5149
hdantoni@mail.arc.nasa.gov

Interferometric Imagery from a Solar-Powered Remotely Piloted Aircraft

Stephen E. Dunagan, Philip D. Hammer, Robert E. Slye, Donald V. Sullivan

A compact, high-spectral-resolution imaging interferometer designed specifically for the Aerovironment Pathfinder solar-powered remotely piloted aircraft (RPA) has been fabricated, tested, integrated, and deployed on a science mission to acquire remotely sensed reflectance spectra from several sites of environmental interest on the island of Kauai, Hawaii. One important purpose of this exercise was to evaluate the feasibility of developing a hyperspectral instrument within the engineering constraints associated with RPA aircraft. The Pathfinder is an ultralight, solar-powered, flying-wing design, with a wingspan of 30.5 meters and a ceiling of 21,640 meters. Payload weight and power are constrained to 12 kilograms and 150 watts, and the aircraft does not provide a controlled thermal and pressure environment for the instrument.

The digital array scanned interferometer (DASI) instrument is capable of acquiring remotely sensed imagery with very high spectral resolution. DASI produces interferograms that can be Fourier transformed to yield spectra. In contrast to hyperspectral imaging instruments (such as diffraction grating or prismatic instruments), DASI is remarkable for its very compact optical design and robust mechanical configuration. The primary sensor is a digital charged coupled device (CCD) camera with 242 (spatial) and 752 (spectral) pixels, a full-well depth of 80,000 electrons, and a peak quantum efficiency of 0.7. Array output is digitized at 10 bits and transferred to the data system via high-speed RS-422 serial link at software-selectable frame rates of 5, 9, 12, 20, and 60 hertz. DASI functions as a "pushbroom" scanner, relying on aircraft motion to scan out the second spatial dimension of the data hypercube.

The single-board computer for data acquisition and experimental control utilizes an Intel Pentium 166-megahertz (MHz) processor, onboard hard-disk and video controllers, and 256 megabytes of system random access memory for direct memory storage of hypercube data at streaming rates up to 7 megabytes (20 frames) per second. A 9.3-gigabyte fast, wide, small computer standard interface hard disk provides mass storage for up to 1.3 hours of interferometer data per flight. Global Positioning System (GPS) and magnetic compass data are encoded into the interferometric data stream for data postprocessing and georectification. The flight instrument is configured as a UNIX-like workstation with remote log-in and control capability via telemetry link through the Pathfinder ground station, and may be operated remotely from any local node with Internet access. A second dedicated microcomputer monitors the temperature, pressure, and voltage data of critical systems.

The single-board computer parallel port provides complementary metal oxide semiconductor (CMOS) latched logic outputs that are used to control several instrument components, including the input-aperture slit width, view, or interferometric video downlink selection, and the pointing stabilization system. This system comprises a fiber-optic (rate) gyro, electronic integrating circuits, and a servo-controlled galvanometer movement with steering mirror to compensate for pitching motion of the flying-wing aircraft. The system operates autonomously when activated and can be reset to zero out electronic drift. The instrument is packaged in a pressurized canister for deployment at altitudes up to 21 kilometers. The container must maintain pressure for convective

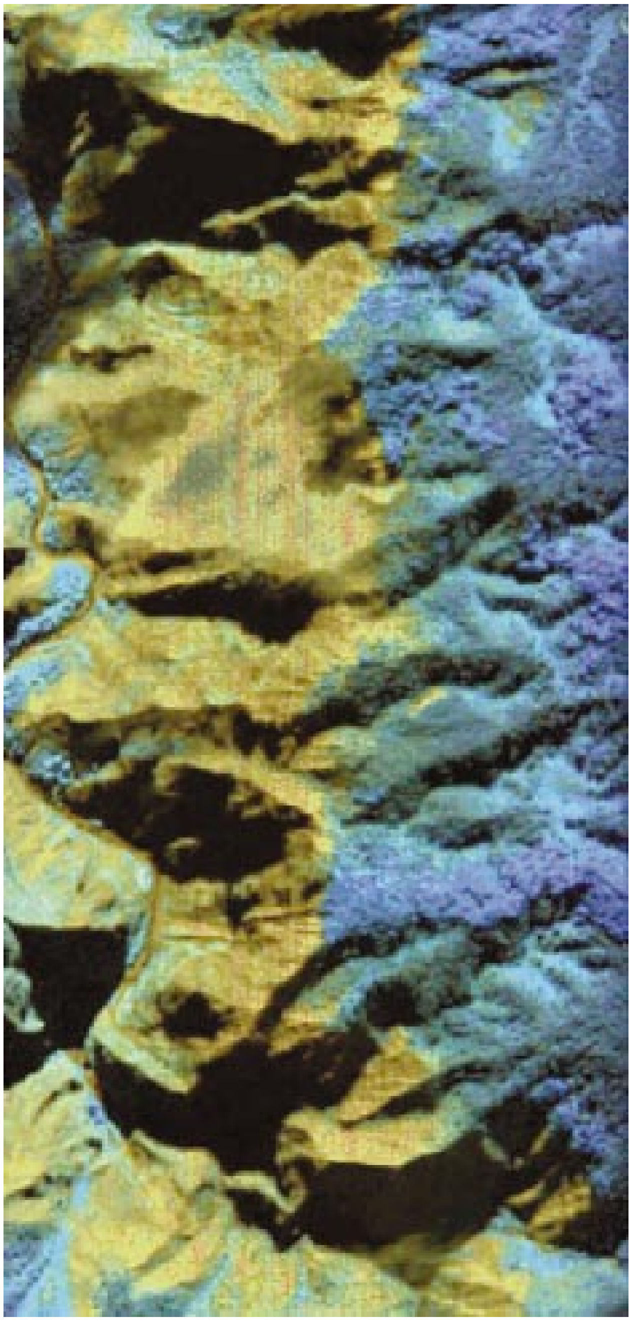

Fig. 1. False color image of the Waimea Canyon, Kauai.

cooling and disk-drive operation, over skin-temperature excursions to –70 degrees Celsius (°C) and flights of 16-hours duration. Thermal control is achieved with automatic thermoelectric heating and convective cooling circuits. Solid-state temperature sensors monitor the array detector, central processing unit, hard disk, pitch stabilization system servo board, and recirculating air temperature; canister internal pressure and fan voltage are also monitored. The instrument was deployed on the Pathfinder in October 1997 for a certification flight. Sample data were acquired over the Pacific Missile Range Facility and Na Pali coast regions of Kauai. All instrument systems and functions performed as designed. Remote "telescience" operation of the instrument from Ames Research Center was demonstrated, including real-time quick-look image transmission. Data-analysis activities in FY98 provided some interesting hyperspectral imagery, including the accompanying sample obtained over the Waimea Canyon (see fig. 1). Detailed retrieved reflection

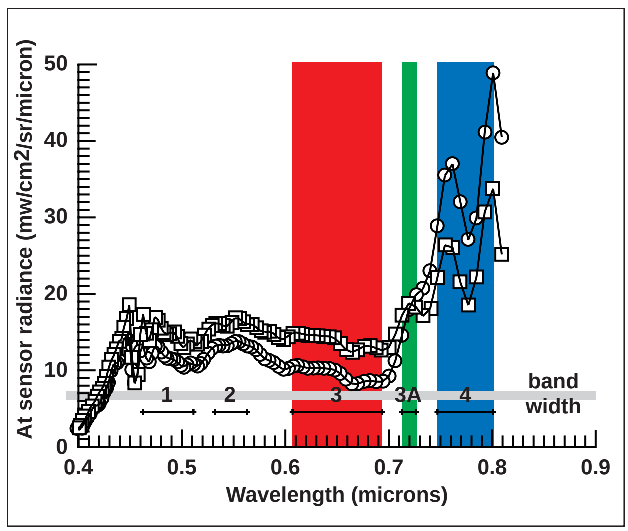

Fig. 2. Terrestrial spectra and composite bands.

spectra are presented for two image regions. DASI spectra may be sampled so as to simulate other sensors. In figure 2, bands 1, 2, 3, and 4 correspond approximately to corresponding land satellite (LANDSAT) Thematic Mapper bands. The researcher also has great flexibility in defining color bands on the basis of details in the spectra. For example, spectra from the canyon side wall display a small local peak in the region of the chlorophyll red edge spectra at 0.725 micron. This peak has been emphasized with a unique color band (3a). Red, green, and blue are mapped to bands 3, 3a, and 4 to provide a false color image that may be useful in discriminating canyon wall vegetation (mixed with red soil) having the 0.725-micron reflectance peak (green) from tree crown vegetation having stronger infrared (IR) reflectance (blue).

This study was conducted in collaboration with William H. Smith of Washington University, St. Louis, Missouri.

Point of Contact: S. Dunagan
(650) 604-4560
sdunagan@mail.arc.nasa.gov

Joint NASA/EPA Region 7 Remote-Sensing Demonstration

Jennifer L. Dungan

In addition to data from future sensors, Earth Observing System data include historical remotely sensed images. The land satellite (LANDSAT) Pathfinder products, especially the North American Landscape Characterization (NALC) database, have provided a valuable resource for land cover monitoring over a time period relevant for Environmental Protection Agency (EPA) purposes. NALC data include three LANDSAT multispectral scanner (MSS) scenes for each path and row; one from the early 1970s, one from the mid- to late-1980s, and one from the early 1990s. They are usually referred to as NALC triplicates. Chosen to minimize cloud cover, the scenes in this study were processed to a consistent map projection, reducing the preprocessing burden normally faced by individual users. An example of land-use change that can be observed in the triplicates from Kearny County, Kansas (see fig. 1), shows the agricultural intensification that has occurred in some parts of the Midwest.

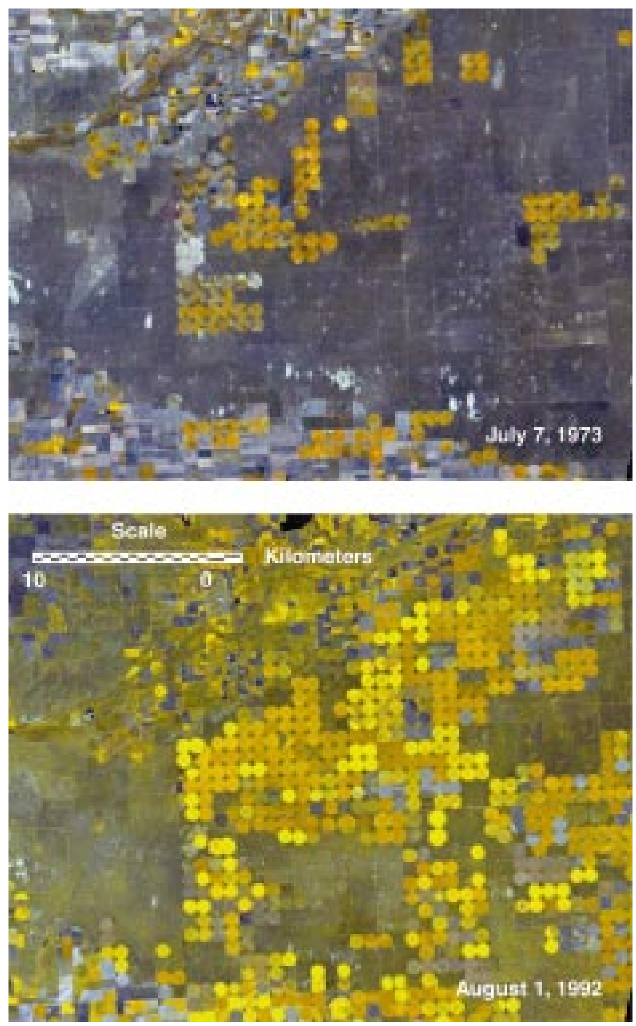

Fig. 1. NALC images from two dates showing a region on the Arkansas River. The circles (many more in 1992 than in 1973) apparent in the images are center-pivot irrigated fields.

Impediments to the use of the NALC archive include difficulties in browsing a large archive (estimated to be 9 gigabytes for Region 7 (Kansas, Missouri, Nebraska, and Iowa)), practical zooming of these large images, and weak tools for spatial exploratory data analysis. The goal of this project is to provide retrospective LANDSAT image data from Region 7 in a form useful to EPA personnel that would overcome these barriers.

All 68 NALC triplicates for the four states in Region 7 were received early in FY98. The data are being formatted and compressed to be compatible with the image processing and geographic information software used by the EPA. Data are written to CDs to make fast access possible, comparable to data access rates from hard disk drives.

A draft of the database was demonstrated within an exploratory spatial analysis tool at Region 7 Headquarters. Geographic areas were identified for use under three EPA priorities: the Resource Conservation and Recovery Act, the Superfund, and the Water, Wetlands, and Pesticides Program. The valuable feedback that was gained on the demonstration will be incorporated in the next version of the database, which will be written on 14 CDs and contain scenes for all of Region 7.

Marla C. Downing of the Environmental Protection Agency, Kansas City, Kansas, collaborated in this study.

Point of Contact: J. Dungan
(650) 604-3618
jdungan@gaia.arc.nasa.gov

Modeling Leaf and Canopy Reflectance

Lee Johnson, Christine A. Hlavka

A canopy model (CANMOD) was linked with a leaf-level model (LEAFMOD) to predict vegetation canopy reflectance as a function of leaf chemistry, leaf morphology, and canopy architecture. The resultant model, called LCM2, solves the radiative transfer equation for the case of a slab of optically uniform leaf material to estimate leaf hemispherical reflectance and transmittance. The canopy model then simulates radiation transfer for a mixture of leaves, assuming a bi-Lambertian leaf-scattering phase function. LCM2 allows a mixture of up to five different types of leaves, and four separate leaf angle distributions, and also accounts for soil reflectance.

Model predictions have a root-mean-square error of generally less than 5 percent when compared with empirical observations of maple-tree (*Acer* sp.) canopies of different leaf area index and fertilization levels, and generally less than 10% versus observations of Douglas-fir (*Pseudotsuga menziesii*) canopies. A user interface was developed to facilitate the use of LCM2 throughout the wider research community.

Collaborators in this research include Barry Ganapol of the University of Arizona and Barbara Bond of Oregon State University.

Point of Contact: L. Johnson
(650) 604-3331
ljohnson@mail.arc.nasa.gov

System Development for Natural Hazard Impact Reduction

James A. Brass, Vincent Ambrosia, Robert Higgins, Theodore Hildum, Robert Slye, Jeffrey Myers

The Natural Hazards Research and Application Program within NASA's Office of Earth Science is an ongoing effort in assisting society in reducing losses of life, property, resources, and social and economic disruptions due to natural disasters. The program has as its goal the development of technology to characterize, monitor, and understand natural disasters using remote sensing and information technology.

A limiting factor in the use of remote sensing for disaster management is the timely delivery of data. Historically, images of fires, floods, earthquakes, and volcanoes have been collected by aircraft and satellite, but the images have taken hours to days to reach disaster management personnel. Ames Research Center, in partnership with the U.S. Geological Service (USGS), Department of Energy (DOE), and the U.S. Forest Service (USFS), has been working on a prototype system for the acquisition and dissemination of geocorrected airborne scanner data. The product derived from this system will be a near-real-time, geocorrected image overlaid on a digital topographic map. This overlay product has been identified by the fire management community as a necessity for determining fire location, size, and spread. The system concept was demonstrated to the firefighting management and firefighting community in Project Wildfire.

In FY98, wildfire imagery was collected with the Airborne Infrared Disaster Assessment System (AIRDAS), sent to the ground, uplinked to a communication satellite, and finally downlinked to a ground station where it was merged with map data. The fire community was very impressed with the prototype system. Additional testing of the system is planned for FY99.

The second phase of the NASA Ames Natural Hazards Program is demonstrating capabilities and supporting the characterization of fires and deforestation in Brazil. As part of the U.S./Brazil Global Change and Environmental Assessment Program (USFS, Brazil, NASA), the AIRDAS was used in Brazil to characterize the fires resulting from El Niño effects in the north. Dry conditions resulted in numerous large fires in the northern Amazon River basin. The AIRDAS was installed on a Brazilian Air Force Learjet and flown over active fires as well as fire scars to determine the extent of damage caused by the El Niño fires. For two months, the imaging system collected visible, infrared, and thermal data. These data were downloaded to a ground station, analyzed, and printed for field use in a matter of hours.

An additional benefit of the mission was the ability of the system to penetrate smoke, thereby mapping deforestation in the Amazon River basin (fig. 1). Many deforestation areas were checked for compliance with cutting permits and environmental regulations.

These two activities, system development for near-real-time images and the environmental assessment in Brazil, will result in an effective system for hazard management/mitigation and environmental regulation. The benefit of involving the user community directly, setting requirements, and testing

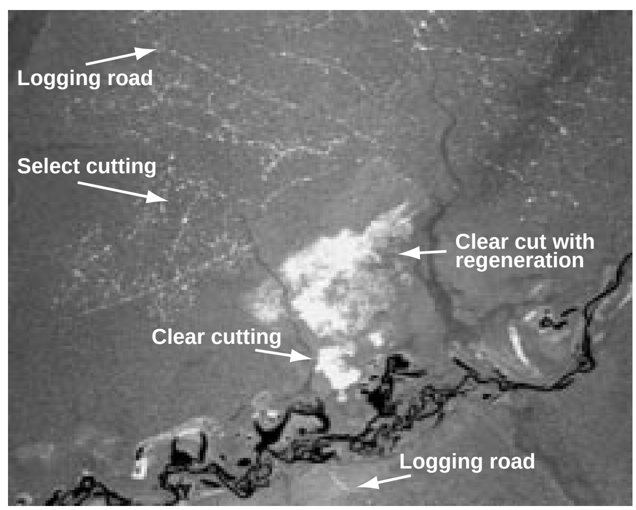

Fig. 1. AIRDAS channel 2 (1.75 millimeter) image of land clearing (white areas), select cutting (thin white lines with web-like appearance), and regeneration in Mato Grasso, Brazil.

prototype systems has resulted in a more effective and economical system to support all those affected by natural hazards.

Collaborators in this research include Philip Riggan and Robert Lockwood of the USFS; Joan Antonío Pereira of IBAMA, Brazil; Eric Stoner of the U.S. Aid for International Development, Brazil; Gene Sasso of Bechtel/DOE; Thomas Bobbe of the USFS; and Len Gaydos of the USGS.

Point of Contact: J. Brass
(650) 604-5232
jbrass@mail.arc.nasa.gov

Terrestrial Remote Sensing Using Image Interferometry—DASI

Philip D. Hammer, Stephen E. Dunagan, David L. Peterson, Lee F. Johnson, Robert Slye

Scientific observations that provide simultaneous spatial (images) and spectral (wavelength dependence) information are a powerful means for studying Earth's environment. Remote sensing of the Earth's radiative fields at visible and infrared wavelengths is an important way of exploring the structure and processes of the surface and atmosphere. Understanding complex and variable environmental phenomena such as light interaction within plant canopies or through clouds in the atmosphere requires spatial, spectral, and temporal observations that are both extensive and detailed. Thus, there is considerable motivation for designing simple, versatile, and cost-effective imaging spectrometers for Earth remote-sensing applications.

Ames Research Center, in collaboration with William H. Smith of Washington University, St. Louis, Missouri, and MEDECO, has been developing and applying a new instrument, a digital array scanned interferometer (DASI), for ground and airborne-based spectral imaging. The DASI achieves spectral discrimination using two-beam interference rather than dispersion. Recent advances in imaging-device technology have made it possible to use this new approach for a variety of scientific studies. DASI instruments have advantages over grating or prism-based instruments, particularly with regard to compactness, device simplicity, and performance. DASIs have many of the positive characteristics associated with Fourier-transform spectrometers (which have been used for several decades for making nonimaging spectral observations) with the additional capability of spatial imaging. The compactness, simplicity of design and operation, and low cost of DASIs make them particularly suitable candidates for airborne platform-based remote-sensing instruments.

Several sensor development efforts were under way in FY98. A data reduction and analysis software package for DASI hyperspectral data is under development by Skywatch, Inc., with support from a phase-2 Small Business Innovative Research (SBIR) award. This package will incorporate many of the DASI analysis routines and procedures that have been created at Ames over the last few years, including a recently patented NASA noise-reduction algorithm. This undertaking is a prime example of technology transfer from NASA to a commercial concern. Additionally, Skywatch, Inc. has begun a new phase-2 SBIR project to develop a computer/hardware interface to enhance the capabilities of DASI-type sensors. Being designed with state-of-the art technology, this interface includes some real-time instrumental correction and data-processing features.

Point of Contact: P. Hammer
(650) 604-3383
phammer@mail.arc.nasa.gov

Wetlands Discrimination Using Sun Glint

Vern C. Vanderbilt, Guillaume L. Perry, Joel A. Stearn

The areal extent of Boreal wetlands, source areas for methane (an important greenhouse gas), is poorly known—estimates differ by as much as sevenfold. This situation contributes uncertainty to present-day energy and carbon budgets and to projections of future climates. Application of optical remote-sensing technology to successfully discriminate methane source areas across large regions has proven elusive. Classifications often lead to confusion both between different wetland types, and between wetlands and non-wetlands. For classifying wetlands, a new remote-sensing technique was investigated that is based upon the properties of the glitter—the strong, unique, often visually blinding, angular signature reflection that is characteristic of surface water, and uncharacteristic of other cover types.

From analysis of data collected by the Polarization and Directionality of Earth's Reflectance (POLDER) sensor, a sensor flown aboard NASA's C-130 aircraft during the Boreal Ecosystem-Atmosphere Study (BOREAS) Experiment, three types of methane source areas displaying different emissions rates were determined: vegetation emergent above inundated soils, open water, and noninundated cover types. (Unlike the traditional "pushbroom" remote-sensing imagers, POLDER, a French sensor, operates like an aerial mapping camera, providing digital, rectangular, photographic-format images covering a field of view sufficiently large to include the sun glitter from water.)

Three hypotheses were tested. First, the visually blinding glitter of sunlight off water surfaces provides a strong, unique, angular signature reflection characteristic of inundated areas and uncharacteristic of other, noninundated cover types. The results suggest that this hypothesis is valid for nonfrozen wetlands in areas lacking canopies with a planophyll (all leaves horizontal) leaf angle distribution. It was also found that in the specular direction (the direction in which one observes the "glitter" or "sparkle" of sunlight reflected by a smooth surface) water—the key to estimation of methane exchange in northern, high-latitude, circumpolar regions—reflects sunlight significantly better than other cover types. The second hypothesis—inundated wetlands and open water areas display different, wind-dependent glitter signatures as a function of view angle—appears valid for the moderate wind speeds typical of conditions on the ground during collection of the POLDER data. Results suggest that the second hypothesis will fail as wind speed approaches zero or, conversely, as wind speed increases beyond the range for which the vegetation shelters the water surface. The validity of the third hypothesis—analysis of remotely sensed data, collected in and near the specular direction, will allow accurate discrimination of inundated wetlands (areas with high methane (CH_4) exchange rates), open water (low CH_4 exchange rates), and noninundated (non-CH_4-producing) cover types—is supported by the results representing classification of data collected in one day. More complete testing of the hypothesis must await additional classification results.

It is concluded that glitter and its observation with a wide-field-of-view imaging sensor such as POLDER is potentially a powerful new approach for discriminating northern, high-latitude, open water areas, inundated vegetation, and non-wetlands. Although this approach demonstrated the utility of using the sun glint for wetlands detection, refinement of the concept to better account for the spectral, spatial, and polarization information in the remotely sensed data must await further research. The need for a mixture analysis to more properly estimate wetland areal extent is particularly important and will be addressed in further research.

Collaborators in this research include Gerald P. Livingston and Leslie A. Morrissey of the University of Vermont; Susan L. Ustin, Martha C. Diaz Barrios, Sarah E. Zedler, and Jon L. Syder of the University of California, Davis; François-Marie Bréon and Sophie Bouffies at the Laboratoire de Modelisation du Climat et de l'Environnement International, Gif sur Yevette, France; Marc M. Leroy of CESBIO, Toulouse, France; Jean-Yves Balois and Maurice Herman of the Laboratoire d'Optique Atmosphérique Université de Science et Technologie de Lille, France; and Stanley R. Shewchuk of the Atmospheric Sciences Section of the Saskatchewan Research Council, Saskatoon, Saskatchewan, Canada.

Point of Contact: V. Vanderbilt
(650) 604-4254
vvanderbilt@mail.arc.nasa.gov

Airborne Tracking Sunphotometry

Philip B. Russell, John M. Livingston, Beat Schmid, James Eilers, Richard Kolyer, Duane Allen, Andrew Chien, Dawn McIntosh, Jill Bauman

Sunphotometry is the measurement of the transmission of the solar beam through the atmosphere. Such measurements, made in several narrow bands of ultraviolet, visible, and infrared radiation, provide valuable information on the properties of aerosols and important trace gases (such as water vapor and ozone). Atmospheric aerosols (suspensions of particles comprising hazes, smokes, and thin clouds in the troposphere and stratosphere) play important roles in influencing regional and global climates, in determining the chemical composition of the atmosphere, and in modifying transport processes. In all these roles, aerosols interact with trace gases through processes such as evaporation and condensation, photochemical reactions, and mutual interactions with the radiation field. Using a single technique, sunphotometry, to study both aerosols and trace gases is often an advantage in understanding their properties and these interactions.

The objective of the Ames airborne sunphotometry team is to provide unique measurements of aerosols, water vapor, and ozone that address current scientific issues by taking advantage of the three-dimensional mobility of aircraft and other platforms.

Recent advances in understanding climate change, photochemistry, and atmospheric transport and transformation processes have emphasized the need for better knowledge of atmospheric aerosols and their interactions with trace gases. As a result, national and international bodies have called for increased efforts to measure aerosol and trace-gas properties and effects, as a means of improving predictions of future climate, including greenhouse warming, ozone depletion, and radiation exposure of humans and other organisms.

A fundamental measure of any aerosol or trace gas is how much it attenuates radiation of various wavelengths. This attenuation is often described in terms of the quantity optical depth. The dependence of optical depth on wavelength is the optical-depth spectrum. The Ames airborne sunphotometers determine the optical-depth spectrum of aerosols and thin clouds, as well as the amounts of water vapor and ozone in the overlying atmospheric column. They do this by pointing detectors at the sun (tracking it) and measuring the (relative) intensity of the solar beam in several spectral channels. The tracking head of each instrument mounts external to the aircraft cabin so as to increase data-taking opportunities relative to in-cabin sunphotometers, and also to avoid data contamination by cabin-window effects.

In FY98, efforts of the Ames airborne sunphotometry team focused on analysis and publication of data from recent field campaigns, as well as on improvements of instrumentation for future campaigns. The recent campaigns include the Tropospheric Aerosol Radiative Forcing Observational Experiment (TARFOX, July 1996), the Second Aerosol Characterization Experiment (ACE-2, June–July 1997), and the Atmospheric Radiation Measurement Intensive Observation Campaigns (ARM IOCs, October 1997). In TARFOX, the 6- and 14-channel Ames Airborne Tracking Sunphotometers (AATS-6 and AATS-14) flew on two aircraft (C-131 and a modified Cessna) to measure aerosols and water vapor in the U.S. pollution haze over the Atlantic Ocean. The sunphotometer measurements, coordinated with measurements by four satellites, two other aircraft, and other sensors on the sunphotometer aircraft and surface sites, led to many important findings about the properties and effects of the U.S. East Coast haze plume. In ACE-2, AATS-14 flew on the Pelican (modified Cessna), while AATS-6 operated on a research ship to measure European pollution aerosols, African dusts, water vapor, and ozone. Those measurements, which were also coordinated with others from satellites, land sites, and the ship, were analyzed extensively in 1998. They are now being combined with the TARFOX results to derive regional assessments of the effects of North Atlantic aerosols on climate. The ARM IOC measurements of water vapor and aerosols made by AATS-6 on the ground in coordination with many other water-vapor and aerosol measurements have been used extensively to evaluate and improve water-vapor and aerosol retrieval algorithms by several sensors.

In FY98, the AATS-14 data set from ACE-2 was also used in preliminary studies of several techniques for separating aerosol and ozone contributions to solar-beam attenuation. The goal of these studies is to provide insights into aerosol/ozone separation for the Stratospheric Aerosol and Gas Experiment (SAGE) II and III spaceborne sensors, particularly when their measurements extend downward from the stratosphere into the troposphere. Related studies by team members combined SAGE II measurements with those by the Cryogenic Limb Array Etalon Spectrometer to develop maps and histories of stratospheric aerosol properties before and after the Pinatubo volcanic injection to the stratosphere.

Collaborators in this research include the NASA Goddard and Langley Space Centers; the National Oceanic and Atmospheric Administration (NOAA); the Lawrence Berkeley National Laboratory; the University of Washington; the California Institute of Technology; University of California, Los Angeles; the U.S. Naval Postgraduate School; the University of Miami; San Jose State University; Stockholm University; Dalhousie University, Canada; UK Meteorological Research Flight; the Max Planck Institute of Chemistry, Germany; the University of Science and Technology of Lille, France; and the TNO Physics and Electronics Laboratory, Netherlands.

Point of Contact: P. Russell
(650) 604-5404
prussell@mail.arc.nasa.gov

Determining Properties of Polar Stratospheric and Tropospheric Ice Clouds Using Advanced Very-High-Resolution Radiometer Thermal Infrared Data

Kathy L. Pagan, R. Stephen Hipskind

This work explores the detection of stratospheric and tropospheric ice clouds over the polar regions using nadir radiances measured at 10.8- and 12.0-micrometer (μm) wavelengths by the advanced very-high-resolution radiometer (AVHRR). Primary interests in cirrus clouds include the role they play in radiative forcing of the climate system, and more recently, their role in the chemical balance of the atmosphere. Polar stratospheric clouds (PSCs) have been implicated as key factors in the loss of ozone under cold polar conditions.

AVHRR instruments onboard a series of National Oceanic and Atmospheric Administration (NOAA) polar-orbiting satellites have provided excellent temporal and areal coverage of the polar regions since 1979. Poleward of 60 degrees, each point on the Earth's surface is visible in two or more consecutive passes twice a day for each of the two or three polar-orbiting satellites. These images can be combined to provide daily coverage for each entire polar region at a horizontal spatial resolution of 1.1 kilometers (km) at nadir. Recent efforts at Ames using AVHRR infrared emission measurements have explored the identification of optically thick and optically thin PSCs using radiative temperatures from a single channel, or the difference between radiative temperatures from channel 4 (10.8-μm wavelength) and channel 5 (12.0-μm wavelength). This difference, known as brightness temperature difference, was originally proposed by others for inferring properties such as effective radii of cirrus clouds.

In this project, one entire PSC season (1992) of Antarctic AVHRR imagery has been processed, as well as selected dates from other Arctic and Antarctic PSC seasons in order to identify the ice clouds in the imagery. Methods have been developed and are now being tested to calculate the optical depth and mean effective radius of these ice clouds in order to classify and map these clouds as PSC or tropospheric cirrus.

Collaborators in this research include Mark E. Hervig of the University of Wyoming and Patricia G. Foschi of San Francisco State University.

Point of Contact: K. Pagan
(650) 604-0713
pagan@cloud1.arc.nasa.gov

ER-2 and DC-8 Meteorological Measurement Systems

T. Paul Bui, Stuart W. Bowen, K. Roland Chan, Cecilia Chang, Jonathan Dean-Day, Leonard Pfister, Antonio A. Trias

The Meteorological Measurement System (MMS) provides high-resolution meteorological parameters (pressure, temperature, turbulence index, and the three-dimensional wind vector). The MMS consists of three major systems: (1) an air-motion sensing system to measure the air velocity with respect to the aircraft, (2) an aircraft-motion sensing system to measure the aircraft velocity with respect to the Earth, and (3) a data-acquisition system to sample, process, and record the measured quantities. Because much of the instrumentation is attached to the aircraft at judiciously chosen locations, the MMS is a platform-specific instrument that cannot be transported from one aircraft to another.

The MMS is a unique instrument designed to investigate atmospheric mesoscale (gravity and mountain lee waves) and microscale (turbulence) phenomena. An accurate characterization of the turbulence phenomenon is important for the understanding of dynamic processes in the atmosphere, such as the behavior of buoyant plumes within cirrus clouds, diffusions of chemical species within wake vortices generated by jet aircraft, and microphysical processes in breaking gravity waves. Accurate temperature and pressure data are needed to evaluate chemical reaction rates as well as to determine accurate mixing ratios. Accurate wind field data establish a detailed relationship with the various constituents, and the measured wind also verifies numerical models used to evaluate air-mass origin. Because the MMS provides quality information on atmospheric-state variables, MMS data have been extensively used by many investigators to process and interpret in situ experiments aboard the same aircraft.

Over the past decade, the ER-2 MMS has successfully participated in major NASA field missions: the Stratosphere Troposphere Exchange Project (STEP) in 1987; the Airborne Antarctic Stratospheric Experiment (AAOE) in 1987; the Airborne Arctic Stratospheric Expedition (AASE) I in 1989; AASE II in 1991–1992; the Stratospheric Photochemistry Aerosols and Dynamics Experiment (SPADE) in 1992–1993; the Airborne Southern Hemisphere Ozone Experiment/Measurements for Assessing the Effects of Stratospheric Aircraft (ASHOE/MAESA) in 1994; the Stratospheric Tracers of Atmospheric Transport (STRAT) study in 1995–1996; and Photochemistry of Ozone Loss in the Arctic in Summer (POLARIS) in 1997.

The DC-8 MMS has successfully participated in the Subsonic Aircraft: Contrail and Cloud Effects Special Study (SUCCESS) in 1996; the Subsonic Assessment (SASS) Ozone and Nitrogen Oxides Experiment (SONEX) in 1997; and the Convective and Atmospheric Moisture Experiment (CAMEX-3) in 1998. CAMEX is a series of field research investigations to study the atmospheric water-vapor and precipitation processes. CAMEX-3 is the third campaign in the series, focusing on hurricane tracking and intensification. The DC-8 MMS configuration during CAMEX-3 successfully incorporated a Differential Global Positioning System (DGPS) LandStar receiver from Racal Survey Limited. The LandStar DGPS receives differential data from the Inmarsat satellite network, thus providing global coverage.

All field data have been distributed for collaboration and interpretation. Detailed analyses and precise calibration are in progress to improve data products and instrument performance.

Point of Contact: P. Bui
(650) 604-5534
pbui@mail.arc.nasa.gov

Measurements of Stratospheric Tracers for the Study of Atmospheric Effects of Aviation

Max Loewenstein, Hansjürg Jost

The Argus instrument for stratospheric measurement of methane (CH_4) and nitrous oxide (N_2O) as dynamical tracers has been part of an ongoing study of stratospheric dynamics. The balloon element of the Stratospheric Tracers of Atmospheric Transport program, called Observations from the Middle Stratosphere (OMS), was initiated in FY96. During FY97, the Argus team participated in two tropical studies, with balloon launches from Juazeiro do Norte, Brazil, at 7 degrees South (°S). In FY97 and FY98, additional measurements using the OMS balloon payload were carried out from Ft. Sumner, New Mexico, at 33 degrees North (°N).

Tropical stratospheric studies have concentrated on a region popularly called the tropical pipe. This region of the atmosphere is "pumped" by midlatitude stratospheric wave action, with the net effect of an upward circulation in the tropics (the pipe) and downward motion in the polar regions. This single-cell, stratospheric circulation is distinguished from the more complex multicellular circulation in the troposphere, which is driven by heating near the ground in the tropics.

The importance of the tropical pipe studies is to quantify the amount of midlatitude air that is "pumped" up into the stratospheric ozone production region near 30-kilometer altitude. Entrainment of midlatitude air into the tropics has implications for ozone-layer effects produced by supersonic aircraft that may eventually fly in the midlatitude stratosphere.

The main results from the Argus studies in FY97 and FY98 are: (1) observation of distinctly different vertical stratospheric profile structures of tracers in the tropics and midlatitudes; and (2) observation of laminated filaments of midlatitude tracers entrained into the tropics on some occasions. These observations contribute to the effort to quantify mass motions vectored from the midlatitude stratosphere into the upwelling "tropical pipe."

Point of Contact: M. Loewenstein
(650) 604-5504
mloewenstein@mail.arc.nasa.gov

Open-Path Tunable Infrared Monitor of the Atmosphere Instrument for Tropospheric Nitrogen Studies

James R. Podolske

The oxides of nitrogen play important roles in the chemistry of the Earth's troposphere and stratosphere, affecting both the production and loss of ozone, as well as influencing the partitioning of the halogen and hydrogen oxide compounds found there. To date, the ability to validate theoretical models of these regions of the atmosphere has been hampered by large experimental uncertainties both in the abundances of the odd-nitrogen reservoir species and in the partitioning of reactive nitrogen between nitric oxide (NO) and nitrogen dioxide (NO_2). Among the nitrogen reservoir species, nitric acid (HNO_3) is expected to be one of the predominant compounds. Similarly, NO_2 is a major chemically active species of this family. Current instrumentation has been shown to be inadequate for measuring HNO_3 and NO_2 with the speed and accuracy required to advance understanding in this area.

The Open-Path Tunable Infrared Monitor of the Atmosphere (OPTIMA) instrument measures gas-phase HNO_3 and NO_2 in the free stream of the NASA DC-8 aircraft. The instrument uses an infrared laser spectrometer coupled to an actively aligned, multiple-pass Herriott sampling cavity whose open absorption path between the fuselage and the inner engine pylon achieves a free-stream absorption path length of 384 meters. To further enhance the detection sensitivity of this tunable infrared diode laser system, high-frequency wavelength modulation spectroscopy is employed. Detection sensitivity for HNO_3 is currently in the 25–50 parts per trillion by volume (pptv) range, and NO_2 at about the 5 pptv range. An intercomparison campaign with several HNO_3 instruments, including OPTIMA, is being planned by the NASA Global Tropospheric Experiment program for FY00.

In FY98, OPTIMA participated in the NASA Subsonic Assessment Ozone and Nitrogen Oxide Experiment mission, sampling air in and around the North Atlantic flight corridor to look for signatures of aircraft emissions that perturb the natural chemistry of the upper troposphere and lower stratosphere. Data analysis has produced water-vapor mixing ratios to compare with near-infrared hygrometer measurements. Several important advances in second-harmonic lineshape theory have been developed in order to model the spectral data.

David Littlejohn of the Bay Area Environmental Research Institute (BAERI) collaborated in this research.

Point of Contact: J. Podolske
(650) 604-4853
jpodolske@mail.arc.nasa.gov

Quantifying Industrial and Aircraft Plumes and the Southern Global Plume

Robert B. Chatfield, Zitian Gao, Robert Esswein

The Atmospheric Modeling Group makes detailed comparisons of theory and observations in an effort to test and improve understanding of the composition of the lower atmosphere. The purpose is to explore the interaction and coevolution of biota, human responses, and the natural environment in the next decades and over the millennia. Fundamental understandings of Earth's biogeochemistry are now frequently clouded by the large influence of anthropogenic emissions, causing changes in the atmospheric composition, stresses on natural tissues, and well-known problems such as global greenhouse–gas warming and smog activity. The group has made highly detailed studies of immense intercontinental plumes that affect the chemistry of the global atmosphere, especially the region below the ozone layer whose chemical composition defines the conditions for healthy humans and the biosphere. For some decades, there has been curiosity about the pollution from cities and industrial burning and its possible effect in increasing smog ozone, not only in continental regions, but also in plumes that spread downwind. Recently, there has been new concern about another kind of pollution plume. Projections for a greatly expanded aircraft fleet imply that there will be plumes of nitrogen oxides from jet exhaust in the Northern Hemisphere downwind of major air traffic routes.

A large aircraft observational project, the Subsonic Assessment Ozone and Nitrogen Oxides Experiment, was mounted over the North Atlantic in October and November, 1997. The group provided detailed pollution forecasts to the aircraft scientists in the field. These forecasts and retrospective simulations aided in flight planning and analysis of what had been seen shortly after measurements were made. Tracer simulations were made for the spread of nitrogen oxides (NO_x) across the North Atlantic. Separate tracers were used to follow NO_x from industry and cities, from the newly suspect aircraft, and also from lightning. If most of the NO_x in the upper troposphere turns out to be from lightning, then the NO_x is not a pollutant at all, and its emission from aircraft is not a major concern. In addition, carbon monoxide (CO) was simulated, because the prevalence of the compound, a notorious and occasionally deadly urban pollutant, is widely taken as a quantitative indicator of industrial-urban influence on a parcel of air. It is not, as these simulations showed. Furthermore, simulations and observations made during the experiment revealed the need for more precise ideas on predicting the location of lightning and its emissions of NO_x.

In FY98, the Atmospheric Modeling Group continued its highly detailed studies of global lower-atmospheric chemistry to describe the spread of smog-like pollution around the world. So dramatic an impact does this plume have on tropospheric composition that the group has named it the Southern Global Plume of biomass burning. Studies have documented the exact African sources of pollutant compounds such as carbon monoxide and ozone that NASA's DC-8 aircraft discovered in the middle and upper troposphere over Tahiti and even more remote regions of the Pacific Ocean. Previous ideas held that this region was a permanently pristine region. However, work recently published by the group has illustrated the role of thunderstorm clouds in producing large plumes of pollution over the continents of Africa and South America. Additionally, that work made important quantitative checks on the simulation of cloud venting. Long, coherent strands of pollution were discovered to pulse along the subtropical jet region. Regions of the South Pacific once thought to be months removed from pollution effects were sporadically affected within 5 to 7 days. Individual storms over Africa were pinpointed as major pollution sources for several cases, but the large-scale buildup over the burning continents also contributed. This work continued the group's efforts in explaining important carbon monoxide features observed from the NASA Measurement of Air Pollution from Space (MAPS) satellite and on board the NASA DC-8.

The group has used two major simulation models to demonstrate these conclusions. The Pennsylvania State University/National Center for Atmospheric Research (NCAR) MM5 mesoscale model is run to forecast or to resimulate the weather of a period of months in full, three-dimensional detail, and reconstruct the prevalence of cloud and other mixing processes. In the next step, the reconstructed history of the meteorology of a region and period are combined, using the same grid, with chemical tracer information on sources, transformation rates, and removal from the atmosphere. This complex, multifaceted model is called the Global Regional Atmospheric Chemistry Event Simulator, or GRACES. Gigabytes of information are analyzed and compared to a large variety of observations for the period under study. Sometimes the chemical information becomes too great; then, more incisive simulations can be made to detail the chemistry of a single parcel. The NASA DC-8 aircraft and satellite observations for the period provide scientifically intensive and spatially extensive views of the actual chemistry of the period. When used to guide aircraft sampling, forecast pollutant-distribution maps were sent by fax and via the Internet to the field deployment airports. In retrospective analysis, other remotely sensed data may be used to assess the burning sources or the consequences. The modeling activity plays a central role in harmonizing and improving the sometimes contradictory views of Earth processes that the observations present. It is an achievement to harmonize all the observational work with detailed theory, but the simulation is even more useful when it helps pinpoint errors in observation or theory.

Collaborators in this research include Ian Folkins of Dalhousie University, Halifax, Nova Scotia, and Glenn Sachse and Victoria Conners of the NASA Langley Research Center.

Point of Contact: R. Chatfield
(650) 604-5490
chatfield@clio.arc.nasa.gov

Tropospheric Aerosol Radiative Forcing Observation Experiment

Philip B. Russell, John M. Livingston, Robert W. Bergstrom, Andrew Chien, Dawn McIntosh

Aerosols (particles suspended in the atmosphere) can affect the climate by changing the way solar energy is scattered and absorbed by the Earth-atmosphere system. Lack of knowledge about global aerosol properties and effects is now a major source of uncertainty in predicting the future climate. As a result, the International Global Atmospheric Chemistry Program (IGAC) has established a Focus on Atmospheric Aerosols (FAA) and endorsed a series of aerosol field campaigns. The Tropospheric Aerosol Radiative Forcing Observation Experiment (TARFOX) is the second in the IGAC/FAA series. The objective of TARFOX is to reduce uncertainties about aerosol effects on climate by studying aerosol properties and effects in the U.S. Eastern Seaboard, where one of the world's major plumes of industrial haze moves from the continent over the Atlantic Ocean. In FY98, the major efforts of TARFOX focused on (1) analyzing and archiving data acquired in the July 1996 Intensive Field Campaign (IFC), and (2) reporting results at scientific conferences and in refereed journals.

Ames Research Center contributed to TARFOX by supplying the project coordinator, project manager, an ER-2 aircraft, and two airborne sunphotometers. The TARFOX IFC measured aerosol effects on solar radiation fields and simultaneously measured the properties of the aerosols causing those effects. Coordinated measurements were made from four satellites, four aircraft, land sites, and ships. Conditions examined ranged from relatively clean to moderately polluted. Aerosol gradients were sampled to help separate aerosol effects from other radiative effects. This sampling also strengthened tests of closure (that is, consistency) among different measurement and calculation techniques.

In FY98, most of the TARFOX data were moved from individual archives to the NASA Langley Distributed Active Archive Center, where they are available for public access. TARFOX results include:

- Demonstration of the unexpected importance of carbonaceous material in the aerosols of the United States mid-Atlantic haze plume and of the increase of the carbonaceous fraction with increasing height.
- Demonstration that values of the aerosol humidification factor (ratio of light scattering at 80% relative humidity (RH) to that at 30% RH) in the haze plume are greater than values previously used in aerosol climate-effect calculations.
- Agreement between (1) the total dry aerosol mass and (2) the sum of independently derived masses of carbonaceous material (organic and inorganic) and sulfate.
- Agreement (to within ~30% on average) between aerosol-layer optical depths measured by the airborne sunphotometer and computed from airborne nephelometer, absorption photometer, and measured humidification factors.
- Chemical apportionment of the aerosol optical depth, showing the dominant importance of water condensed on aerosols, with carbonaceous material second, and sulfate a close third.
- The first airborne measurements of the changes in downwelling and upwelling shortwave radiative fluxes caused by the United States Atlantic haze plume, along with simultaneous measurements of the haze broadband visible optical depth; dividing the measured flux change by the corresponding haze optical depth change yields the flux sensitivity, a quantity useful in determining aerosol radiative forcing of climate.
- Agreement between shortwave radiative flux changes measured from aircraft and computed from measured aerosol properties, provided the calculations use midvisible single-scattering albedos ≈ 0.89 to 0.93; these values of single-scattering albedo (the ratio of aerosol scattering to extinction) are in accord with independent measurements of the TARFOX aerosol particles.
- Agreement between aerosol optical-thickness magnitudes and wavelength dependencies obtained by the moderate resolution imaging spectrometer (MODIS) Airborne Simulator (MAS) on the ER-2 and by an Ames airborne sunphotometer and surface sunphotometers.

- Remarkable year-to-year consistency in the characteristics of the aerosol in the TARFOX region during episodes of heavy haze; at high-aerosol loading, the aerosol phase function at backscattering angles varied by less than 7 to 10% over a 5-year period, including 1996, the TARFOX year.
- First validation of a dual-view algorithm that retrieves two-wavelength aerosol optical depth over land and ocean from radiances measured by the along-track scanning radiometer-2 on the European Environmental Remote Sensing satellite.
- Numerous comparisons between aerosol optical depths derived from satellite scattered-radiance measurements and determined by transmission measurements (from aircraft, ships, and land); most comparisons agree to better than 10%, but a few disagree by more than 30%.

These results are now being used to assess and reduce uncertainties in estimates of aerosol climate effects, as well as to guide future field programs. TARFOX comparisons have helped to validate and improve algorithms used to derive aerosol properties and radiative effects from satellite measurements. The resulting validated algorithms are now enabling extensions of the TARFOX results to other times and locations that have aerosol properties similar to those of the TARFOX IFC. More information is available on the TARFOX World Wide Web site (http://geo.arc.nasa.gov/sgg/tarfox/index.html).

Collaborators in this research are affiliated with NASA Goddard Space Flight Center and Langley Research Center; the National Oceanic and Atmospheric Administration (NOAA); the Lawrence Berkeley National Laboratory; the University of Washington; University of California, Los Angeles; the U.S. Naval Postgraduate School; the University of Miami; UK Meteorological Research Flight; the University of Science and Technology of Lille, France; and the TNO Physics and Electronics Laboratory, Netherlands.

Point of Contact: P. Russell
(650) 604-5404
prussell@mail.arc.nasa.gov

Tracer Field Measurements in STRAT and POLARIS

Max Loewenstein, James R. Podolske

The Airborne Tunable Laser Absorption Spectrometer (ATLAS) instrument has been deployed on the ER-2 high-altitude aircraft during the past several years as part of two important stratospheric studies.

The Stratospheric Tracers of Atmospheric Transport (STRAT) project has been active during the period 1994–1997, studying the interaction of the tropical and midlatitude regions of the stratosphere. There is both fundamental and practical motivation for these studies. The tropical stratosphere has been little studied experimentally, yet it is known to be the region where tropospheric source gases, such as the fluorocarbons, enter the stratosphere and potentially influence the stratospheric ozone layer. Practically, the environmental impact of high-flying aircraft depends significantly on transport of aircraft plumes from midlatitude flight corridors into the tropical uplift region and thence into the ozone-production region at 30 kilometers over the tropics. ATLAS has contributed accurate nitrous oxide (N_2O) tracer field measurements to the STRAT measurement suite, and an improved understanding of the tropical upwelling region of the stratosphere is beginning to emerge from the intensive STRAT studies.

During FY97, a large-scale campaign called Photochemistry of Ozone Loss in the Arctic in Summer (POLARIS) was deployed to Fairbanks, Alaska, to study the chemistry of stratospheric ozone at high latitudes in summer. This campaign filled in data on ozone behavior that had not been previously studied in detail using a range of in situ chemical sensors. Again in this campaign, the ATLAS instrument provided accurate N_2O tracer field data, core constituents for the analysis of active chemical radical species, providing the POLARIS team with a reference coordinate against which to interpret measurements of active chemical species such as the chlorine oxides, hydrogen oxides, and nitrogen oxides (NO_x) radical families, all of which enter actively into ozone chemistry.

As a practical example of the application of the ATLAS N_2O data, it is now possible to cite the discovery of a canonical regression relation between NO_y (active nitrogen species, including the active radicals NO_x) and the inert N_2O. This regression is useful as a predictive tool to interpret unusual heterogeneous chemistry that tends to remove NO_y in particles in the Arctic winter. The removal of NO_y is a precursor of ozone destruction by chlorine radicals in the stratosphere.

Point of Contact: M. Loewenstein
(650) 604-5504
mloewenstein@mail.arc.nasa.gov

Transport and Meteorological Analysis

Leonhard Pfister, Marion Legg

This study has provided real-time meteorological satellite data as well as the meteorological satellite data archive for the Subsonic Assessment (SASS) Ozone and Nitrogen Oxides Experiment (SONEX) in FY97. In addition, this study has used a technique that forecasts air masses that have been convectively influenced using trajectory analysis combined with meteorological satellite data. This technique has been used to understand where the observed strong enhancements in nitrogen oxides (NO_x) due to lightning have originated, how much time has elapsed since the convection, and how high the clouds were. Results show that NO_x enhancements are qualitatively consistent with the elapsed time since the occurrence of the convection. Little dependence on cloud height was noted. In fact, other work has shown that the dependence of lightning on cloud altitude (after a certain threshold is reached) is quite weak. There has been much interest by the SONEX science team in both the meteorological satellite data and the convective influence diagrams and approach. Arguably, SONEX is the first atmospheric chemistry experiment where a systematic effort has been made to recognize the link between the chemical observations and cloud information prior to the experiment, and then ensure that the cloud, trajectory, and meteorological information is available to the team in an easy and systematic way.

Work has continued on analysis of lidar data from the Tropical Ozone Transport Experiment. This work demonstrates the following: (1) subvisible cirrus clouds in the tropics are of two types—those formed in situ and those that are convective outflow; (2) back trajectories in the tropics are good enough to be able to explain the origin of both types—that is, the edges of convective outflow subvisible cirrus are well predicted by trajectory analysis; (3) subvisible cirrus formed in situ can be produced by inertia-gravity waves. With regard to the latter, three different gravity and inertia-gravity wave modes have been isolated in subvisible cirrus case studies with periods ranging from 12 to 48 hours. These periods are long enough to allow these clouds to form particles that are large enough to dehydrate the tropical tropopause region.

Henry Selkirk of the Space Physics Research Institute collaborated with Ames in this research.

Point of Contact: L. Pfister
(650) 604-3183
pfister@telsci.arc.nasa.gov

Atmospheric Physics

Analysis and Modeling of the Upper Atmospheric Research Satellite Data

Azadeh Tabazadeh, Eric J. Jensen

Active chlorine production and denitrification are the two major processes that lead to the formation of the Antarctic ozone hole. Similar levels of active chlorine concentrations have been measured in both polar vortices, an indication that the lack of denitrification may be one of the main factors currently preventing the formation of an Arctic ozone hole. Despite the fact that the importance of denitrification to the formation of the ozone hole has been recognized for many years, the details of polar vortex denitrification have not yet been resolved. The intent is to define the necessary meteorological conditions under which extensive denitrification can occur by analyzing the Upper Atmospheric Research Satellite (UARS) data.

It is well known that polar stratospheric clouds (PSCs) play an important role in the formation of the austral springtime Antarctic "ozone hole" by activating chlorine and denitrifying the stratosphere. Historically, spaceborne PSC observations have been acquired by occultation instruments such as the Stratospheric Aerosol Measurement II or versions of the Stratospheric Aerosol and Gas Experiment. Such observations exclude the polar night during which denitrification occurs, when PSCs are the thickest and most widely distributed. On the other hand, passive remote-sensing instruments, such as the Cryogenic Limb Array Etalon Spectrometer (CLAES) and Microwave Limb Sounder (MLS) onboard the UARS, are able to scan through the polar night and thus provide valuable information with regard to denitrification and dehydration processes. The plan in this project is to examine both denitrification and dehydration of the Antarctic polar vortex in 1992 by correlating the depletion in the nitric acid (HNO_3) and H_2O gas-phase concentrations, as measured by MLS, with the increase in the aerosol extinction, as measured by CLAES.

To identify the onset and duration of both denitrification and dehydration during the 1992 Antarctic winter, daily maps have been generated of gas-phase HNO_3, gas-phase H_2O, and aerosol extinction at 12.82 micrometers for different potential temperature surfaces from early May through November. A denitrified or dehydrated region is defined as an area in which HNO_3 or H_2O vapor-mixing ratios, as seen by MLS, are considerably depleted without a significant corresponding increase in the CLAES aerosol extinction, indicating the absence of Type I or Type II PSCs (ice clouds), respectively. Figure 1 illustrates daily polar maps of HNO_3, H_2O, and aerosol extinction for particular dates during the Antarctic winter of 1992 interpolated onto the 450 degrees kelvin (K) potential temperature surface. Overall similar variations in the gas and aerosol phase concentrations are apparent in the data for potential temperature surfaces ranging from 420 to 650 K, indicating that the loss in gas-phase HNO_3 and H_2O occurred over an altitude range of about 16 to 24 kilometers.

Climate model calculations in general predict a significant cooling of the lower stratosphere in the next century as a result of greenhouse gas buildup in the atmosphere. The results of the UARS data analysis on denitrification will be combined with climate model calculations to explore the possibility of the occurrence of massive Arctic denitrification in a future colder stratosphere, which may have important implications for accurate predictions of Arctic ozone loss in the next century. Patrick Hamill of San Jose State University collaborated with Ames in this research.

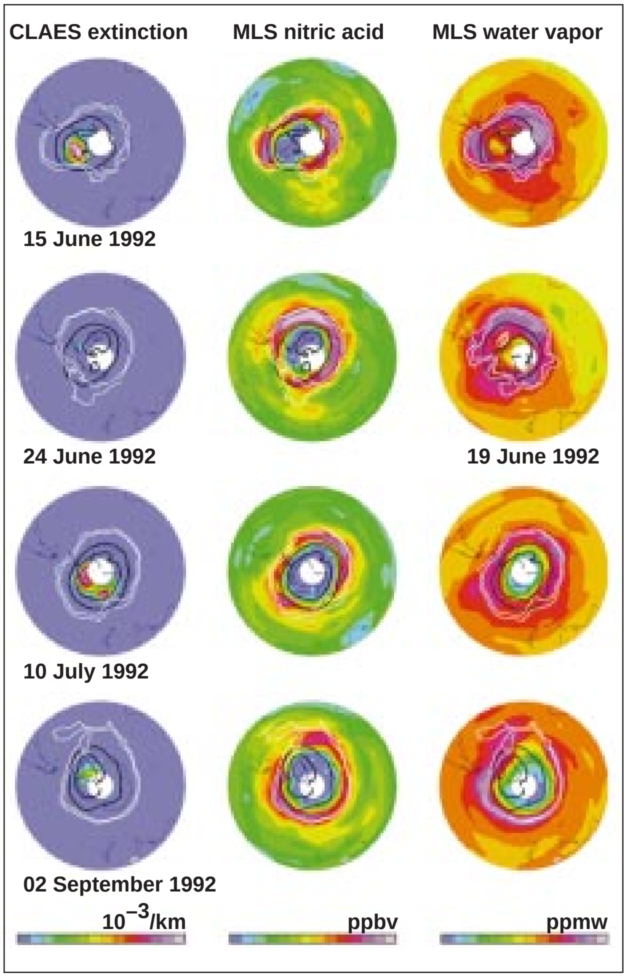

Fig. 1. Maps of CLAES aerosol extinction (at 12.82 micrometers) and MLS HNO_3 and H_2O vapor data for selected days during the 1992 Antarctic winter, interpolated onto the 450 K potential temperature surface using United Kingdom Meteorological Organization (UKMO) temperatures. The thick black contours show UKMO temperatures at 195 and 188 K (the thin black contour is at 185 K). Also superimposed (in white) on each of the maps are two contours of potential vorticity, calculated from UKMO temperature and geopotential height fields to show the boundaries of the Arctic vortex. The data versions used in this figure are V8, V4, and prototype V104 for CLAES, MLS HNO_3, and MLS H_2O, respectively. The MLS radiometer used to measure H_2O vapor was not operational on June 24, 1992. Instead, the H_2O vapor map shown is for June 19, the last day in June for which water-vapor data are available. The change in CLAES aerosol extinction at the 450 K level due to background sulfate hydroscopic growth is near 1 and 2 x 10^{-3} per kilometer at 195 and 190 K, respectively. The CLAES aerosol extinction scale has been chosen to highlight the regions where PSCs are present above the background sulfate levels (shown in purple) during this post-volcanic year. Temperature fields shown may be negatively biased by a few degrees.

Point of Contact: A. Tabazadeh
(650) 604-1096
atabazadeh@mail.arc.nasa.gov

Carbonaceous Aerosol (Soot) Measured in the Lower Stratosphere during POLARIS and Their Role in Stratospheric Photochemistry

Anthony W. Strawa, Katja Drdla, Rudolf F. Pueschel, Sunita Verma, Guy V. Ferry

Recently, modeling studies have suggested a link between black carbon aerosol (BCA) and ozone chemistry. These studies suggest that nitric acid (HNO_3), nitrogen dioxide (NO_2), and ozone (O_3) may be reduced heterogeneously on BCA particles. The ozone reaction converts ozone to oxygen molecules, whereas HNO_3 and NO_2 react to form nitrogen oxide (NO_x). Also, a buildup of BCA could reduce the single-scatter albedo of aerosol below a value of 0.98, a critical value that has been postulated to change the effect of stratospheric aerosol from cooling to warming. Correlations between measured BCA amounts and aircraft usage have been reported. Attempts to link BCA to ozone chemistry and other stratospheric processes have been hindered by questions concerning the amount of BCA that exists in the stratosphere, the magnitude of reaction probabilities, and the scarcity of BCA measurements.

The Photochemistry of Ozone Loss in the Arctic in Summer (POLARIS), a flight mission to study ozone-depletion mechanisms in the Arctic summer, was completed in Alaska in FY97. The Ames Wire Impactors (AWI) participated in this mission as part of the complement of experiments on the NASA ER-2 aircraft, with the objective of measuring the character of the stratospheric aerosol during POLARIS and providing this information to the scientific community. One main objective was to determine the amount of aerosol surface area, particularly BCA, available for reaction with stratospheric constituents and assess, if possible, the importance of these reactions. The AWI collects aerosol and BCA particles (see the figure) on thin palladium wires that are exposed to the ambient air in a controlled manner. The samples were returned to the laboratory for subsequent analysis, which was done in FY98. The product of the AWI analysis is the size, surface area, and volume distributions, morphology, and elemental composition of aerosol and BCA. A modification to the AWI data-analysis procedures was required in which the collection of BCA is modeled as a fractal aggregate. The new method resulted in a 20-fold increase in the measured BCA surface area and a fivefold increase in soot loading over the previously used approach. Despite this increase, BCA surface area is only about 10 percent of the measured sulfuric-acid aerosol surface area. Including heterogeneous reactions on BCA in a photochemical model can have profound effects on photochemistry, leading to renoxification and increased ozone depletion. However, these predicted effects are not supported by the POLARIS observations, in particular, the NO_x/NO_y ratios. Including BCA reactions does not statistically improve the agreement between model and measurement in any of the several

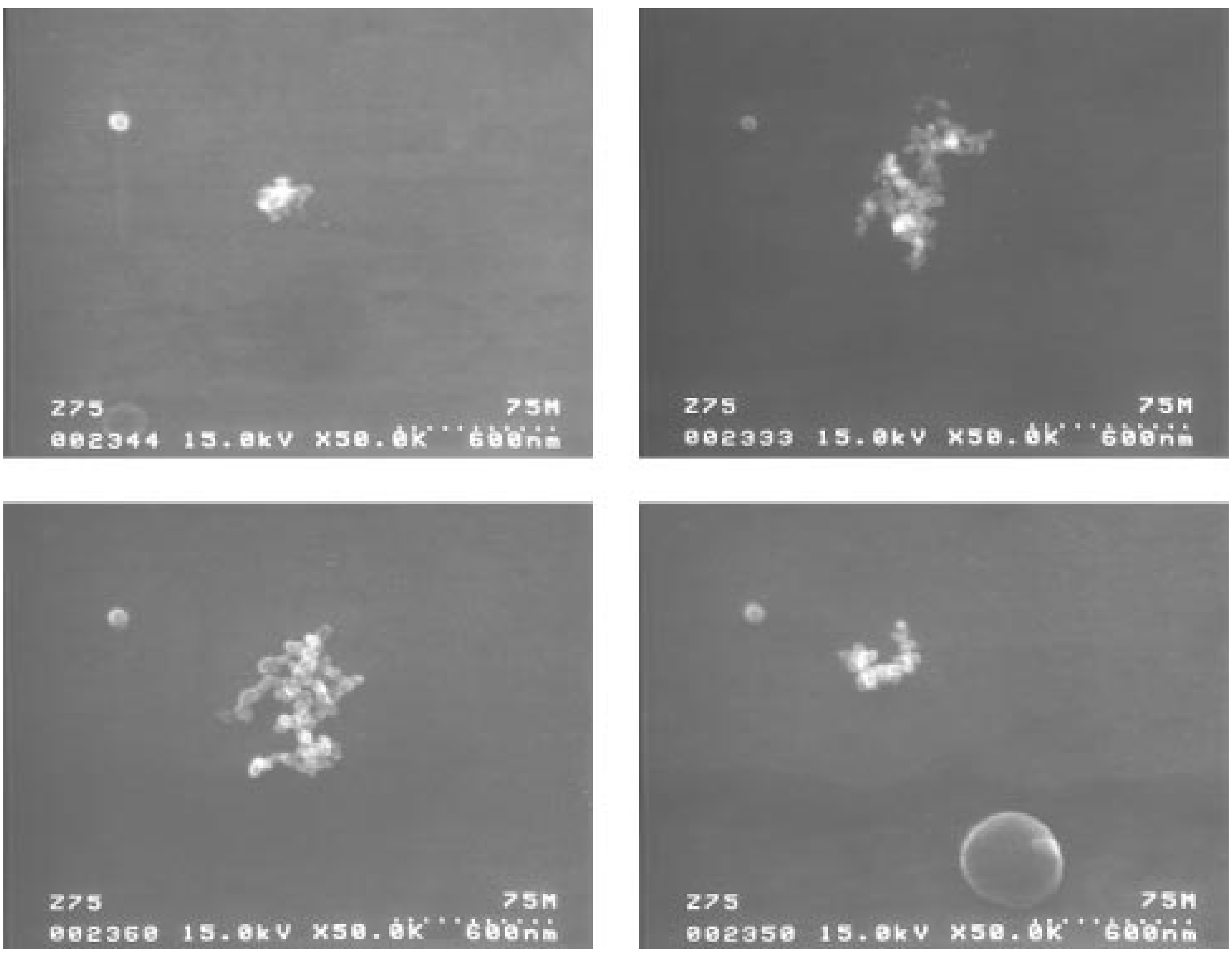

Fig. 1. Electron micrographs of soot particles collected during POLARIS 970921.6.z75.

scenarios considered. Further, consideration of the reaction pathways suggests that these reactions are not important. Laboratory data suggest that BCA reactions are not purely catalytic and they result in the consumption of the BCA at a rate that is inconsistent with observations of BCA in the stratosphere. It may be that stratospheric BCA surfaces are coated or otherwise modified so that they no longer resemble those used in the laboratory studies and have different reactivates.

Collaborators in this study include R. J. Salawitch of the NASA Jet Propulsion Laboratory; Steve Howard of Symtech; M. Yasuda of San Jose State University; R. S. Gao and J. W. Elkins of the National Oceanic and Atmospheric Administration (NOAA); and P. T. Bui and M. Loewenstein of Ames Research Center.

Point of Contact: A. Strawa
(650) 604-3437
astrawa@mail.arc.nasa.gov

Hurricane Microphysical Characteristics

Rudolf F. Pueschel, Guy V. Ferry, Anthony W. Strawa, Duane A. Allen, Rene C. Castaneda

The Ames staff participated in the Convective and Atmospheric Moisture Experiment Mark 3 to determine sizes between 0.3 micrometer and 6.4 millimeters, and concentrations of cloud particles as a function of size at DC-8 flight levels up to FL390. The condensate mass that can be derived from these microphysical characteristics determines the release and distribution of latent heat in the atmosphere, which is the driving force of tropical storms. The microphysical data also permit validation of algorithms that are being developed for remote-sensing instruments flying aboard the aircraft simultaneously with the microphysical sensors, and aboard the Tropical Rainfall Measuring Mission (TRMM) satellite. In addition, the radiative aspects and the heat budgets of tropical storms are determined by the distribution of the condensate over ice crystal size.

Raw data are asymmetric (in the case of ice particles) images, size-classified into 32 bins, from electro-optical sensors. Those 32 linear size bins are converted into 10 equal-logarithmic size intervals. Final products are the distribution of ice-crystal concentration, surface area, and volume as functions of both the horizontal and vertical dimensions of the particle images. Typical results for eyewall penetrations of Hurricane Bonnie in August 1998 follow: cloud particle concentrations of between 1.e-2 and 4.e-1 per cubic centimeter (cm^3) (10 to 400 per liter); particle surface areas of between 6.e3 and 8.e4 square micrometers per cubic centimeter ($\mu m^2\ cm^{-3}$) (6.e2 to 8.e2 $cm^2\ m^{-3}$); and particle volumes of between 3.e4 and 7.e5 $\mu m^3\ cm^{-3}$ (3.e-2 to 7.e-1 $cm^3\ m^{-3}$). With an ice-particle density of 0.7 grams per cubic centimeter ($g\ cm^{-3}$), derived in situ from measured evaporation rates of the ice crystals, the condensate mass in the eyewall amounted to 0.02 to 0.5 $g\ m^{-3}$, which is typical for tropical storms.

Independent of this data analysis, algorithms have been developed that take advantage of the shape information obtained with the electro-optical cloud-particle probes to compute the condensate mass. These data also can be compared with results from microwave sensors on the aircraft and on the TRMM satellite. Follow-on results include vertical and horizontal mass fluxes within a storm utilizing wind data from the Ames Meteorological Measurement System.

Collaborators in this research include John Hallett of the Desert Research Institute; Paul Willis of the National Oceanic and Atmospheric Administration (NOAA); and Steve Howard of Symtech.

Point of Contact: R. Pueschel
(650) 604-5254
rpueschel@mail.arc.nasa.gov

Laboratory Spectroscopy of Carbon Dioxide in Support of Planetary Atmospheres Research

Lawrence P. Giver, Charles Chackerian, Jr.

Spectra of planets have absorption bands caused by the molecules in their atmospheres. Measurements of these spectral features can yield information about these planetary atmospheres, such as the abundance of the absorbing molecules and the pressure and temperature of the gas. This measurement requires knowledge of absorption-band absolute intensities, line positions, pressure-broadening parameters, and temperature dependencies. Over the past 30 years, measurements of these parameters have been made on absorption bands that are relevant for planetary spectra in the High-Resolution Spectroscopy Laboratory at Ames Research Center.

Recent work has emphasized intensity measurements of very weak near-infrared (IR) carbon dioxide (CO_2) bands that are important for understanding the spectrum of the night side of Venus, which has a massive CO_2 atmosphere. An extensive set of CO_2 spectra from 4500 to 12,000 centimeters^{-1} (cm^{-1}) was obtained with the 25-meter base-path White cell and BOMEM DA8 Fourier Transform Spectrometer; the set includes some bands measured with substantial uncertainties about 30 years ago, and many weaker bands never previously measured. Using this database, the first intensity measurements were made of the four bands surrounding the emission window at 5800–5900 cm^{-1} in the night-side spectrum of Venus. The intensity measurement of the 00021–00001 band of $^{12}C^{16}O^{18}O$ at 4639 cm^{-1} was also improved, and found to be 16% higher than the current value on the high-resolution transmission molecular absorption database (HITRAN) compilation of molecular-absorption line intensities. Particularly interesting is the weak Q branch of the 31103–00001 band at 4591 cm^{-1} which has not been previously resolved in laboratory spectra. Lines Q8 through Q44 are identified in figure 1, which shows a 3 cm^{-1} segment of the spectrum obtained with a path length of 1507 meters and a pressure of 60 torr. The other features in this spectrum are lines of other CO_2 bands; the P48 line of the 00021–00001 band of $^{12}C^{16}O^{18}O$ obscures the smaller Q2, Q4, and Q6 lines. With the position measurements for Q branch lines, the rotational constants of the 31103f vibrational level were corrected for the HITRAN tabulation.

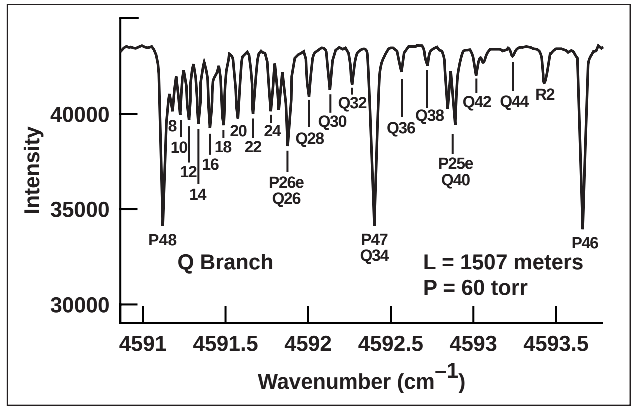

Fig. 1. Q branch of the carbon dioxide band at 4591 cm^{-1}.

These new spectra are being used to complete the measurements of the 21122-00001 CO_2 band at 7901 cm^{-1}. This band is particularly significant in Venus' night-side spectrum, since it is in the emission window at 1.27 meters. With the higher signal/noise on the new spectra, it is now possible to extend measurements to the very weak P branch of this band. Also identified are some high-J Q and R branch lines of the nearby 32211–00001 band, which perturbs the 21122–00001 band, and "borrows" some intensity from it.

L. R. Brown of the NASA Jet Propulsion Laboratory; R. J. Kshirsagar of the National Research Council; and R. B. Wattson of Utah State University collaborated with Ames in this research.

Point of Contact: L. Giver
(650) 604-5231
lgiver@mail.arc.nasa.gov

Microphysics and Chemistry of Sulfate Aerosols at Warm Stratospheric Temperatures

K. Drdla, Rudolf F. Pueschel, Anthony W. Strawa

The Photochemistry of Ozone Loss in the Arctic in Summer (POLARIS) ER-2 measurement campaign in 1997 provided the first comprehensive in situ measurements of the polar summer stratosphere. The warm summer temperatures (up to 235 degrees kelvin (K)) imply that the stratospheric aerosol particles, known to be composed of sulfuric acid solutions, should be very concentrated (up to 80 wt %). Research has focused on the effect of such high acidity on the aerosol chemistry, and the resulting modeled impact on gas-phase chemistry, using the Integrated MicroPhysics and Aerosol Chemistry on Trajectories model. An additional motivation for the research was the observations of high nitrogen oxide/reactive nitrogen (NO_x/NO_y) ratios (overall 35% larger than modeled values) during the POLARIS campaign, raising the possibility that aerosol chemistry is leading to perturbations of the NO_x/NO_y ratio.

The first potential effect of high acidity is that sulfate aerosols are more likely to freeze, into sulfuric acid monohydrate (SAM). This process reduces the efficiency of the important nitrogen pentoxide (N_2O_5) hydrolysis reaction, thus increasing NO_x/NO_y ratios. Model calculations confirmed that this process could occur during polar summer, and could double predicted NO_x/NO_y ratios. However, model/measurement agreement was not improved overall, because SAM formation tends to cause model overprediction in polar spring, but still is not efficient during the continuous solar exposure of polar summer.

Second, if sulfate aerosols remain liquid, the high acidity may promote acid-catalyzed reactions. The most important reaction is:

$$CH_2O(aq) + HNO_3(g) \rightarrow HONO(aq) + CHOOH(aq)$$

This study demonstrated that this reaction effectively increases NO_x/NO_y ratios across a wide range of conditions, improving agreement with measurements. Furthermore, the production of HONO can promote secondary liquid reactions, including:

$$HONO(aq) + HNO_3(g) \rightarrow 2NO_2(g) + H_2O(aq)$$

$$HONO(aq) + HCl(g) \rightarrow ClNO(g) + H_2O(aq)$$

which amplify the predicted effects. Primary uncertainties include the uptake coefficient of formaldehyde (CH_2O) relevant to reaction with nitric acid (HNO_3), the fate of the formic acid (CHOOH) product, the amount of HONO available for secondary reaction, and the relative rates of HONO reaction with HNO_3 and hydrogen chloride (HCl). Uncertainties in these factors allow the predicted increase in the NO_x/NO_y ratio to vary from 8 to 80%.

This research has demonstrated that heterogeneous reaction rates and gas-phase chemical composition can be sensitive to details of the aerosol composition, even during warm, polar summer conditions. However, more laboratory data are clearly needed to reduce the uncertainties in the reaction rates. Further stratospheric measurements, including CH_2O and CHOOH, would also be useful as well as determination of the phase of stratospheric aerosols.

Collaborators in this research include R. C. Cohen of the University of California, Berkeley; T. F. Hanisco of Harvard University; and R. J. Salawitch of the NASA Jet Propulsion Laboratory.

Point of contact: K. Drdla
(650) 604-5663
katja@aerosol.arc.nasa.gov

Principal Component Analysis of Solar Spectral Irradiance Measurements

Maura Rabbette, Peter Pilewskie, Warren Gore, Larry Pezzolo

The Atmospheric Radiation Group deployed a solar spectral flux radiometer (SSFR) at the Atmospheric Radiation Measurement Southern Great Plains Cloud and Radiation Testbed facility during the 1997 Shortwave-Intensive Operating Period. It measured the downwelling solar irradiance in the 360–2500 nanometer (nm) solar spectral region. Several thousand spectra were acquired between September 17 and October 5 in atmospheric conditions that varied from pristine clear to very thick cloud, accompanied by a fivefold change in column integrated water vapor (1–5 centimeters). Figure 1 is a three-dimensional (3-D) surface plot (380–1000 nm) for "clear sky" conditions during the entire 18-day experiment. The oxygen band at 762 nm is evident, as well as several water-vapor bands in the visible and near-infrared, including the σ bands at 942 nm. Structure due to Fraunhofer lines in the solar atmosphere can be seen at shorter wavelengths (<400 nm). The daily repeatability of the maximum irradiance level near 500 nm is evidence of the stability of the instrument.

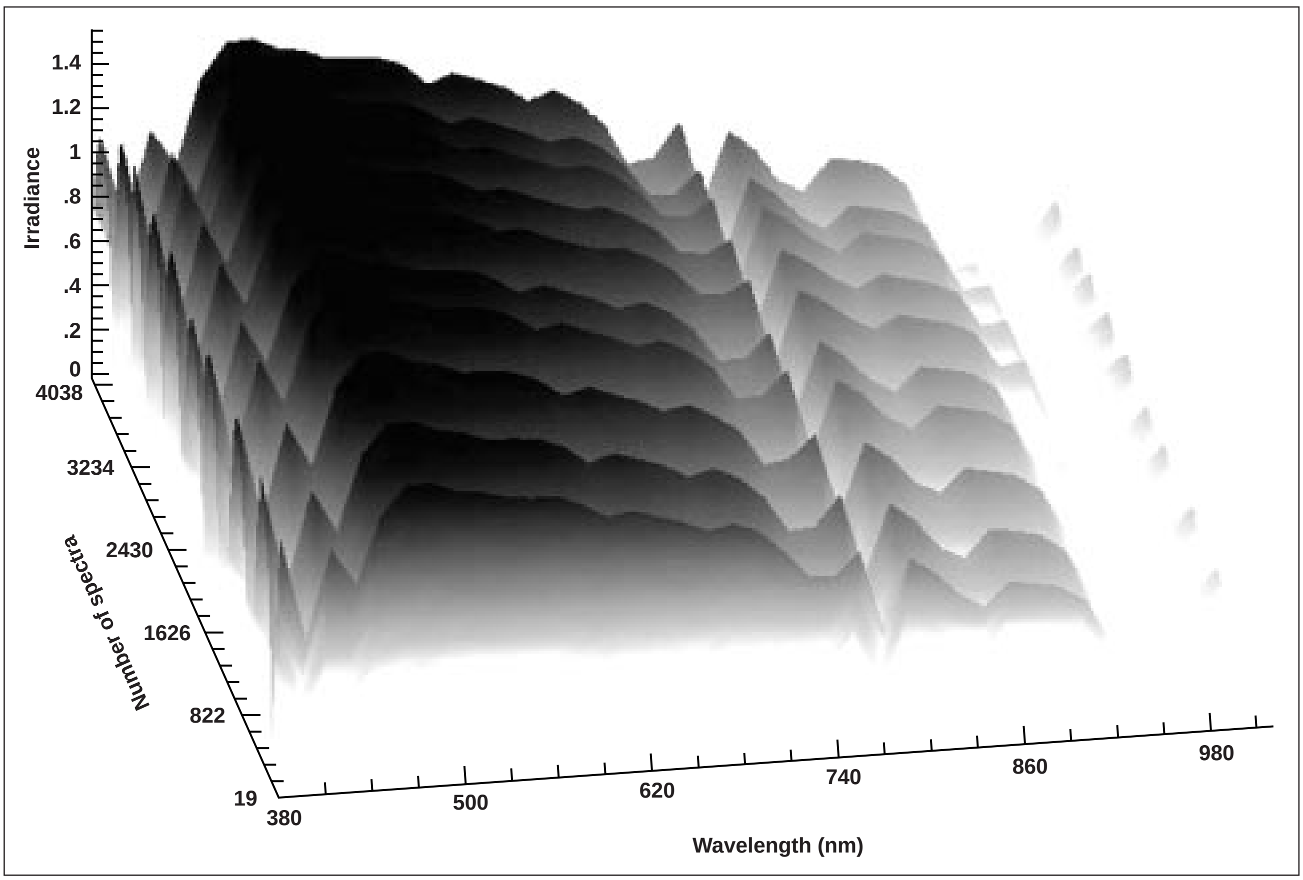

Fig. 1. Three-dimensional surface (380–1000 nm) for clear-sky conditions during the entire 18-day experiment.

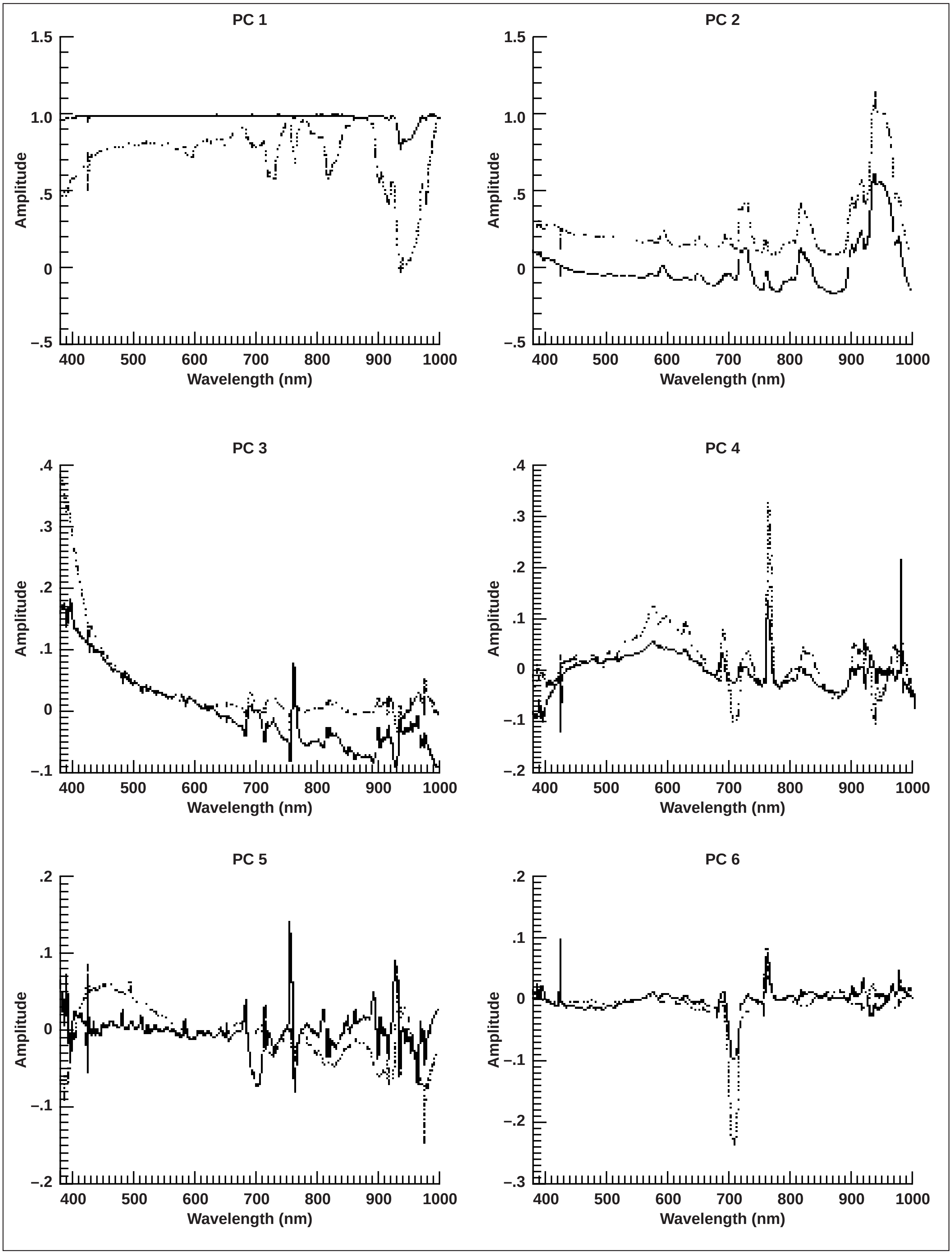
PC 1
1.5
1.0
.5
0
−.5
Amplitude
400 500 600 700 800 900 1000
Wavelength (nm)
PC 2
1.5
1.0
.5
0
−.5
Amplitude
400 500 600 700 800 900 1000
Wavelength (nm)
PC 3
.4
.3
.2
.1
0
−.1
Amplitude
400 500 600 700 800 900 1000
Wavelength (nm)
PC 4
.4
.3
.2
.1
0
−.1
−.2
Amplitude
400 500 600 700 800 900 1000
Wavelength (nm)
PC 5
.2
.1
0
−.1
−.2
Amplitude
400 500 600 700 800 900 1000
Wavelength (nm)
PC 6
.2
.1
0
−.1
−.2
−.3
Amplitude
400 500 600 700 800 900 1000
Wavelength (nm)

Even though each solar irradiance spectrum may contain a thousand or more variables (flux at a particular wavelength), this does not mean there are a thousand pieces of information per spectrum. The principal-component analysis (PCA) technique is used to determine the number of independent pieces of information (independent variables) that exist in a spectrum and to establish the regions of the spectrum in which these variables are strongest; that is, it is used to characterize the 6870 visible *downwelling* solar irradiance spectra. The central step of PCA is to derive a set of variables, which are mutually orthogonal *linear* combinations of the observed variables (flux at wavelengths 380–1000 nm). The aim is to derive *easily interpretable* independent variables (principal components). The application of a *simple structure rotation* to the principal-component (PC) output-loading matrix uniquely clusters and simplifies the variables in the PC loading matrix. For this particular data set, well over 99% of the spectral information is contained in the first six principal components (fig. 2). The solid lines are the unrotated PCs and the dotted lines are the PCs after an oblique promax (k = 3) rotation. Each extracted PC is orthogonal to all previously extracted PCs and, therefore, is independent, in a least-squares sense, of the variability due to the features accounted for in all previous PCs. The first component, PC1, is the overall average variance; it includes such parameters as the systematic instrument noise. The second component, PC2, has absolute amplitude maxima in the water-absorption bands, while PC3 has a broad spectral feature heavily weighted in the visible region. PC4 displays a broad, midvisible feature correlated with the oxygen at 762 nm. The rotated PC5 coefficients display a large weighting in the visible (400–550 nm) and a peak near 940 nm. PC6 proved to be a good diagnostic tool for these SSFR spectra. The relatively large weighting at 700 nm was the result of instrumental saturation in just a few of the 6870 sample spectra. Without the PC analysis, isolating the spectra with the saturated channels would have proven very difficult.

Finally, PCA is also being carried out on several tens of thousands of downwelling *and* upwelling solar irradiance spectra retrieved during the First International Satellite Cloud Climatology Project Regional Experiment, Phase III Arctic Cloud Experiment and coincident Surface Heat Budget of the Arctic Ocean (SHEBA) experiment in Alaska (FY98). Three SSFRs were deployed, two with both zenith and nadir viewing on airborne platforms (the NASA ER-2 and the University of Washington CV-580). A third SSFR was deployed at the SHEBA ice camp.

Point of Contact: M. Rabbette
(650) 604-0128
mrabbette@mail.arc.nasa.gov

Fig. 2. The first six principal components of the SSFR data array (solid lines = unrotated components; dotted lines = rotated components).

Quantitative Infrared Spectroscopy of Minor Constituents of the Earth's Atmosphere

Charles Chackerian, Jr., Lawrence P. Giver

Infrared spectroscopic techniques have become extremely powerful for numerous observational objectives in understanding and monitoring the "health" of the Earth's atmosphere. Prior to designing appropriate instruments, as well as interpreting the observations that monitor the important molecular species, quantitative laboratory spectroscopic measurements must be done. These measurements provide: (1) line and band intensity values that are needed both to establish limits of detectability for as-yet-unobserved species and to quantify the abundance of those species that are observed; (2) line positions, half widths, and pressure-induced shifts, which are all needed for remote and in situ sensing techniques; and (3) data on these basic molecular parameters at temperatures and pressures appropriate to the real atmosphere.

Ames operates a complement of instruments used to obtain the spectral measurements. These instruments include a BOMEM DA8 interferometer; a 25-meter, base-path, multiple-reflection absorption cell; and 30-, 10-, and 5-centimeter absorption cells coolable to about 60–77 kelvin. Also used is the Fourier transform spectroscopy interferometer at the Kitt Peak National Solar Observatory to make laboratory spectral measurements. In addition, a magnetic-rotation spectrometer Herriott-cell combination has been built that can detect numerous free radical species at the parts-per-trillion-by-volume (pptv) level.

Ongoing work includes determining intensity parameters from the emission spectra of hydroxyl radical (OH) molecules, absolute line-intensity parameters for nitric-acid infrared bands, and improved dipole-moment parameters for carbon monoxide.

Collaborators in this research include Linda Brown of the NASA Jet Propulsion Laboratory/ California Institute of Technology; Mike Dulick of the National Solar Observatory; Guy Guelachvili, Ginette Tarrago, and Nelly Lacome of the University of Paris XI; Sumner Davis of the University of California, Berkeley; Aaron Goldman of the University of Denver; Tom Blake of the Battelle Pacific Northwest Laboratory; and Chris Mahon of the Space Physics Research Institute.

Point of Contact: C. Chackerian, Jr.
(650) 604-6300
cchackerian@mail.arc.nasa.gov

Solar Spectral Flux Radiometer

Warren Gore, Peter Pilewskie, Larry Pezzolo, William Chun

In FY98, the design and development was completed of an all-new solar spectral flux radiometer (SSFR) to measure spectral solar irradiance at moderate resolution to determine the radiative impact of clouds, aerosols, and gases on climate, and also to infer the physical properties of aerosols and clouds. Two instruments were built and successfully used in the NASA Arctic Cloud Experiment during May and June, 1998. One was integrated on the NASA ER-2 and the other was flown aboard the University of Washington CV-580 research aircraft.

The SSFR makes spectral flux measurements (300 to 2200 nanometers (nm)) with a zenith-viewing hemispherical field-of-view light collector and a

Fig. 1. The SSFR instrument on a laboratory bench.

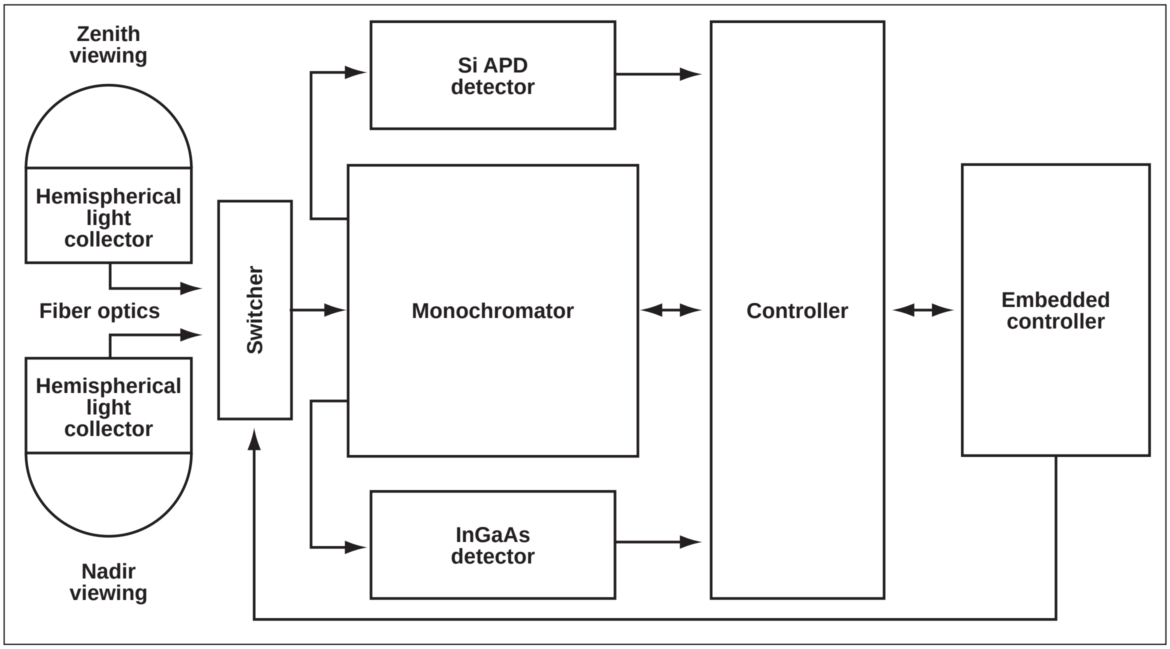

Fig. 2. Schematic of the SSFR instrument.

nadir-viewing hemispherical field-of-view light collector. (See figures 1 and 2.) The signal is transmitted with a high-grade fiber-optic cable to the rack-mounted instrument system. The direction of the field of view is switchable with a specially designed fiber-optic cable switcher. The heart of the instrument is a unique two-spectrum scanning monochromator that uses two continuously spinning diffraction gratings (visible and near infrared) driven by an electronically controlled direct-current motor. Light incident on the input slit is dispersed into its component wavelengths by the diffraction grating. It is then sequentially swept past the output slit, where the detector (silicon avalanche photodiode (Si APD) or indium gallium arsenide (InGaAs)) converts the optical signal into a corresponding electrical signal. This signal is amplified and output to the controller electronics. The data-acquisition and control system is a 100-megahertz 486 embedded controller in a PC104 format. Data are recorded on a compact 175-megabyte PC Flash memory card.

NASA ER-2 SSFR specifications follow:

- 300–2200-nm spectral range
- Spinning (12 hertz) grating monochromator
- Thermoelectrically cooled solid-state detectors
- Hemispheric (cosine response diffuser) field of view
- 5–10-nm resolution (variable with slit width)
- 1-hertz spectral sampling rate for flight observations
- Volume: 0.84 cubic feet; weight: 30 pounds

The compactness of the new NASA ER-2 SSFR makes it suitable for integration in the General Atomics Altus Remotely Piloted Aircraft payload.

The SSFR flown on the University of Washington CV-580 aircraft is functionally similar to the NASA ER-2 instrument with an added operator-interface feature. Instrument performance and data can be monitored in flight by an operator. This system can be easily integrated on the NASA DC-8, Department of Energy (DOE) Twin Otter, or other similar airborne platform.

Lawrence Ng of Sverdrup Technology collaborated in this research.

Point of Contact: W. Gore
(650) 604-5533
wgore@mail.arc.nasa.gov

Sulfuric Acid and Soot Aerosol Measurements

Rudolf F. Pueschel, Anthony W. Strawa, Guy V. Ferry, Duane A. Allen

In FY98, assessment continued of the effect of aircraft operations on the atmospheric sulfuric acid and soot aerosol started during the Subsonic Assessment Ozone and Nitrogen Oxides Experiment field program in FY97.

The Ames Meteorological Measurement System determined a subadiabatic lapse rate, amplified by several inversion layers at various altitudes, that prevented vertical exchange of air masses during a cross-corridor flight out of Shannon, Ireland, on October 23, 1997. Air-mass back trajectories showed that air parcels reaching the aircraft had been exclusively over the Atlantic Ocean for five days prior to sampling. In spite of this inhibited vertical and horizontal transport, a drastic (up to tenfold) enhancement of fine-particle concentration was detected above a pressure altitude of 10 kilometers. Aircraft operated in flight corridors above 10 kilometers were a likely source of this fine-particle abundance.

Volatility measurements identified sulfuric acid contributing 75% to the aircraft-generated aerosol. The rest was equally divided between ammonium sulfate and a nonvolatile component. In contrast, sulfuric acid amounted to only 25% in the air mass below a pressure altitude of 10 kilometers, and this level was not affected by aircraft.

Ames Wire Impactor samples, collected concurrently with the fine-particle measurements, showed that only particle concentration was influenced by aircraft. Neither the particle surface area nor the volume were affected because of the small size (<0.05 millimeters) of the aircraft-generated particles. However, coagulation with the aircraft-generated sulfuric particles could render hydrophobic aerosols, such as soot, to become cloud-condensation nuclei and thereby constitute an indirect effect.

From the impactor samples, it was possible to morphologically identify the fraction of the aerosol that was soot particles. Soot contributed only 4% and 0.2% by number, respectively, to the aerosol below and above a pressure altitude of 10 kilometers. Thus, in contrast to sulfuric-acid fine particles, aircraft had no measurable effect on soot-aerosol concentration. Soot particles, however, are subject to radiometric forces because of their high absorptivity of solar radiation and asymmetric shape. As a consequence, their atmospheric residence time is longer than that of other aerosols, and they can be transported against gravity up to 80 kilometers, where they might affect mesospheric physics.

A discrepancy exists between a nonvolatile aerosol component determined by condensation nuclei (CN) counters, the conventional method to detect soot in the atmosphere, and soot aerosol identified morphologically by impactor samples. To resolve this discrepancy, it is assumed that either the CN counter-determined nonvolatile aerosol is composed of more compounds than only soot, or most of the soot particles that are detected by CN counters are too small to be collected efficiently by wire impactors.

Sunita Verma of Science Systems & Applications, Inc.; Steve Howard of Symtech; and Jindra Goodman of San Jose State University collaborated in this research.

Point of Contact: R. Pueschel
(650) 604-5254
rpueschel@mail.arc.nasa.gov

The Importance of Hypervalent Bromine Compounds to Stratospheric Chemistry

Timothy J. Lee, Srinivasan Parthiban

A previous study in this series pointed out that stratospheric ozone depletion due to bromine is currently believed to be about as important as that due to chlorine, although *much less* is known about stratospheric bromine chemistry. It is, therefore, important to gain a better understanding of stratospheric bromine chemistry. Although the production of man-made chlorine compounds has been either limited or eliminated over the past several years, there is still at least one important man-made bromine source, methyl bromide (CH_3Br), which is used in the agriculture industry. The effectiveness of bromine in promoting ozone loss in the lower stratosphere is related to the fact that most bromine resides in more labile forms, relative to chlorine, capable of taking part in the ozone-removal cycles. In fact, there are no known stable reservoir species for bromine. Unlike chlorine, where hydrogen chloride and chlorine nitrate are relatively stable reservoir compounds under most stratospheric conditions, hydrogen bromide and bromine nitrate are susceptible to destruction mechanisms involving ultraviolet (UV) radiation, hydrolysis reactions, and heterogeneous chemical reactions.

Using the tools of computational quantum chemistry, the previous study showed that hypervalent bromine compounds such as $HBrO_2$ or bromyl nitrate (O_2BrONO_2) are thermodynamically very stable. Previous laboratory experiments also suggested that bromine nitrate itself reacts directly with ozone, and thus may actually be involved in catalytic ozone-depleting reaction cycles. In FY98, this study showed that the critical reactions:

$$BrONO_2 + O_3 \rightarrow OBrNO_2 + O_2 \qquad (1)$$

$$OBrONO_2 + O_3 \rightarrow O_2BrONO_2 + O_2 \qquad (2)$$

will not occur in the gas phase because the products are not thermodynamically favored. Experimental studies by the National Oceanic and Atmospheric Administration (NOAA) group at Boulder, Colorado, support the Ames assessment. However, observational studies were reported in FY98 for the first time indicating that OBrO exists in measurable quantities in the stratosphere, opening significant new pathways in which many $XBrO_2$ compounds may be formed. For example:

$$OBrO + NO_3 \rightarrow O_2BrONO_2 \qquad (3)$$

$$OBrO + OH \rightarrow HOBrO_2 \qquad (4)$$

This study extended the characterization studies of hypervalent bromine oxygen compounds and showed for the first time that not only are $XBrO_2$ compounds thermodynamically very stable, but that they are also stable with respect to photodissociation in the lower stratosphere. That is, the computational chemistry research has shown that the excited electronic states of $XBrO_2$ compounds are shifted to higher energy relative to normal valent bromine compounds. Furthermore, this shift is large enough that the radiation that penetrates to the lower stratosphere, referred to as the actinic flux, is not energetic enough to photodissociate the $XBrO_2$ compounds.

A detailed analysis of the bonding of bromine and chlorine hypervalent compounds has been presented in which a model of this hypervalent bonding is developed to explain the results of the calculations. The results of these studies lead to several important conclusions: (1) hypervalent bromine compounds of the $XBrO_2$ type may be the only stable bromine reservoir species in the stratosphere; (2) several other hypervalent bromine compounds should be characterized, such as $HOBrO_2$, $ClOBrO_2$, and $FBrO_2$; (3) further work on their potential formation and destruction mechanisms should be performed; and (4) laboratory studies of hypervalent bromine compounds should be initiated.

The implications of this work in progress are significant because the knowledge of stratospheric bromine chemistry is severely lacking, and these studies strongly suggest that hypervalent compounds may very well be the only stable bromine reservoir species.

Point of Contact: T. Lee
(650) 604-5208
tlee@mail.arc.nasa.gov

REPORT DOCUMENTATION PAGE

Form Approved
OMB No. 0704-0188

1. AGENCY USE ONLY *(Leave blank)*

2. REPORT DATE
August 1999

3. REPORT TYPE AND DATES COVERED
Technical Memorandum

4. TITLE AND SUBTITLE
Research and Technology 1998

5. FUNDING NUMBERS

6. AUTHOR(S)
Ames Investigators

7. PERFORMING ORGANIZATION NAME(S) AND ADDRESS(ES)
Ames Research Center
Moffett Field, CA 94035-1000

8. PERFORMING ORGANIZATION REPORT NUMBER
A-9900432

9. SPONSORING/MONITORING AGENCY NAME(S) AND ADDRESS(ES)
National Aeronautics and Space Administration
Washington, DC 20546-0001

10. SPONSORING/MONITORING AGENCY REPORT NUMBER
NASA/TM–1999-208768

11. SUPPLEMENTARY NOTES
Point of Contact: Dr. Stephanie Langhoff, Chief Scientist, Ames Research Center, MS 230-3, Moffett Field, CA 94035-1000 (650) 604-6213 or contact the person(s) designated as the point of contact at the end of each article

12a. DISTRIBUTION/AVAILABILITY STATEMENT
Unclassified — Unlimited
Subject Category 99

12b. DISTRIBUTION CODE

13. ABSTRACT *(Maximum 200 words)*

This report highlights the challenging work accomplished during fiscal year 1998 by Ames research scientists, engineers, and technologists. It discusses research and technologies that enable the Information Age, that expand the frontiers of knowledge for aeronautics and space, and that help to maintain U.S. leadership in aeronautics and space research and technology development. The accomplishments are grouped into four categories based on NASA's four Strategic Enterprises: Aero-Space Technology, Space Science, Human Exploration and Development of Space, and Earth Science.

The primary purpose of this report is to communicate knowledge—to inform our stakeholders, customers, and partners, and the people of the United States about the scope and diversity of Ames' mission, the nature of Ames' research and technology activities, and the stimulating challenges ahead. The accomplishments cited illustrate the contributions that Ames is making to improve the quality of life for our citizens and the economic position of the United States in the world marketplace.

14. SUBJECT TERMS
Aeronautics, Space transportation, Space sciences, Earth sciences, Life sciences, Information technology, Research and technology

15. NUMBER OF PAGES
228

16. PRICE CODE
A11

17. SECURITY CLASSIFICATION OF REPORT	18. SECURITY CLASSIFICATION OF THIS PAGE	19. SECURITY CLASSIFICATION OF ABSTRACT	20. LIMITATION OF ABSTRACT
Unclassified	Unclassified		